

# **Predicting and optimising the postoperative outcomes of sagittal craniosynostosis correction**

A thesis submitted in fulfilment for the  
requirements of the degree of Doctor of Philosophy

By  
Connor Charles James Cross

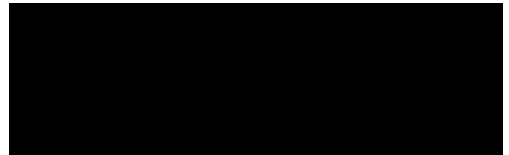
Department of Mechanical Engineering  
University College London

2022

## Declaration

I, Connor Charles James Cross, declare that all material and work presented within this thesis to be my own. Information retrieved from additional literature has been referenced, in which I (unless otherwise stated) declare no ownership of such material.

Signature:

A solid black rectangular box used to redact the signature.

Date:

5<sup>th</sup> December 2022

This work is wholeheartedly dedicated to the loving memory of both **Ron Stock & Linda Cross**, who I miss deeply. It is also dedicated to my fiancé, **Jennie May Oliver**, who gave me the strength and confidence that I needed throughout this PhD. I also extend my heartfelt regards and gratitude to my family (Mother: **Sharon Presley**; Father: **Terry Cross**; Siblings: **Kelly Cross, Shannon Cross, Jordan Cross, Tegan Presley**) as well as many of my close friends and family who I've not mentioned here.

## Abstract

The neonate skull consists of several flat bones, connected by fibrous joints called sutures. Sutures regulate the bone formation along their adjoining edges, while providing malleability to assist with the early phases of rapid brain growth and passing through the birth canal with minimal restriction. By adolescents, these sutures fuse into solid bone, protecting the brain from impacts. The premature fusion of one or more of these sutures is a medical condition known as craniosynostosis, with its most common form being sagittal craniosynostosis (fusion of the midline suture). The condition results in compensatory overgrowth perpendicular to the fused suture, leading to calvarial deformation and possible neurofunctional defects. Surgeons have developed several surgical techniques to restore the normative shape. This has led to debates as to which surgical option provides the most beneficial long term outcome.

The overall aim of this thesis was to develop a computational approach using the finite element (FE) method capable of predicting and optimising the long term outcomes for treating sagittal craniosynostosis. A generic 3D pre-operative FE model was developed using patient specific CT data. The FE model was parameterised to predict the long term calvarial growth, the pattern of suture and bone formation, the pattern of bone healing across the replicated surgical techniques, and the changes in contact pressure levels across the modelled brain. All techniques underwent simulated growth up to the maximum age of 76 months. Morphological results were compared against the patient specific CT data at the same age. Where absent, technique specific follow up CT data were used instead.

Results highlighted a good morphological agreement between the predicted models and their comparative CT data. The FE model was highly sensitive to the choice of input parameters. Based on the findings of this thesis, the \*\*\* approach proved the most optimal across the predicted outcomes. The novel methodology and platform developed here has huge potential to better inform surgeons of the impact various techniques could have on long term outcomes and continue to improve the quality of care for patients undergoing corrective surgery.



## Impact statement

In this work, a new framework was introduced to predict and optimise the postoperative outcomes for sagittal craniosynostosis using a computational approach. This method was adopted and modified from a previously undertaken study in wild and mutant type mice models, which was expanded to model human skull growth whilst undergoing treatment for sagittal craniosynostosis.

The work presented here was submitted and discussed at several inter/national meetings. In 2021, an informative poster was presented at the Anatomical Society Virtual Winter Meeting – Vision and Visualization, whilst oral presentations were delivered at the 26<sup>th</sup> Congress of the European Society of Biomechanics, the annual BioMedEng21 meeting (Sheffield, UK) and The XVI International Conference on Computational Plasticity, Fundamentals and Applications. In 2022, Chapters 3, 4, and 6 of this thesis were published in four well respected journals. Entitled: *Frontiers in Cell and Developmental Biology*, *Scientific Reports*, and *Frontiers in Bioengineering and Biotechnology*. The final chapter of this thesis was further highlighted at three national and international conference events; the 27<sup>th</sup> Congress of the European Society of Biomechanics, BioMedEng22, and the European Society of Craniofacial Surgery 2022, Oxford.

Further, additional funding was provided from the charity foundation The Rosetrees Trust to extend the project detailed here for an additional year of study. This resulted in preparation of a fourth journal article for *The Journal of Plastic, Reconstructive and Aesthetic Surgery*. The work here also achieved a finalist position for the 2022 27<sup>th</sup> Congress of the European Society of Biomechanics student awards located in Porto, Portugal.

The work shown here has formed the bases of another PhD study. At the time of writing, a new student is currently investigating the impacts facial growth could have on the morphological predictions shown here. The student is using the frameworks discussed in this thesis as a foundation for their work.

# Acknowledgements

First and foremost, I would like to thank Prof. Mehran Moazen. I am forever grateful for his kindness, patience, encouragement, and motivation throughout this project, and for trusting me with this project. I would also like to thank Prof. Yiannis Ventikos, Prof. Roman H Khonsari, Dr. Giovanna Patermoster, Dr. David Johnson, Prof. Dawid Larysz, Prof. Lars Kölby, Prof. Eric Arnaud, and Dr. Hans Delye, whose knowledge and insights has been invaluable throughout the thesis.

My deepest gratitude goes to The Department of Mechanical Engineering, University College London, and all members of The Moazen Lab, whose motivation and experiences have propelled the project forward. These include Dr. Arsalan Marghoub, Dr. Katherine Wang, Mahbubeh Hejazi, Ce Liang, Hastya Shadlou, Maurice Leslie, Louise Souquet, Leila Galiey and many others who are not mentioned here.

I would like to give my heartfelt thanks to the following individuals: Sue Oliver, Paul Burlison, Beth Oliver, Ben Roberts, Charlotte Formby, Abby Munro, Sujith and Anna Sudhakar, Loic Seneron, Melissa-Sue Anderson, Mohammed-Rashid Patel, Yousuf Syed, Fadi Salmoon, Brett Long, Anisa Guhad, Jacob Sant, and many others who gave me their support, confidence, and time when I needed it the most.

Finally, I would like to take the opportunity to thank the sponsors of this project. Namely Prof. Mehran Moazen, The Department of Mechanical Engineering, University College London, and The Rosetrees Trust UK Charity (through the PhD research project [A1899], PhD Plus project [PhD2021\100017]), whose funding allowed me to continue this work for an additional year and allow for the attendance to an international conference located in Porto, Portugal.

# List of abbreviations

In order of appearance:

|  |                               |
|--|-------------------------------|
| AF: Anterior fontanelle                  | CI: Cephalic index            |
| PF: Posterior fontanelle                 | FM: Foramen magnum            |
| CS: Craniosynostosis                     | PB: Pars basillaris           |
| ICP: Intracranial pressure               | PL: Pars lateralis            |
| CT: Computational tomography             | PT: Petrous temporal          |
| MRI: Magnetic resonance imaging          | OC: Occipital condyle         |
| 2D: Two dimensional                      | ml: Milliliters               |
| 3D: Three dimensional                    | mm: Millimeters               |
| SCS: Sagittal craniosynostosis           | mmHg: Millimeters of mercury  |
| FE: Finite element                       | FGF: Fibroblast growth factor |
| CSF: Cerebral spinal fluid               | LS: Lambdoid synostosis       |
| ICV: Intracranial volume                 |                               |
| FGFR: Fibroblast growth factor receptors |                               |
| TCR: Total calvarial remodelling         |                               |
| MPa: Megapascal                          |                               |
| SAC: Spring assisted cranioplasty        |                               |
| ESC: Extended strip craniotomy           |                               |
| FBR: Frontal biparietal remodelling      |                               |
| OFC: Occipitofrontal circumference       |                               |
| EAC: Endoscopic assisted cranioplasty    |                               |
| GPa: Gigapascal                          |                               |
| mN/min: milliNewtons per minute          |                               |
| kPa: Kilopascal                          |                               |
| Pa: Pascal                               |                               |
| Kg: Kilograms                            |                               |
| m/sec: meters per second                 |                               |
| FEA: Finite element analysis             |                               |
| FOA: Frontal orbital advancement         |                               |

# List of content

|  |            |
|--|------------|
| <b>Chapter 1: Introduction.....</b>  | <b>11</b>  |
| 1.1 Overview .....   | 12         |
| 1.2 Aims and objectives .....  | 15         |
| 1.3 Methodology.....   | 17         |
| 1.4 Chapter organisation .....   | 19         |
| <b>Chapter 2: Literature review.....</b>   | <b>21</b>  |
| 2.1 Anatomy and physiology .....   | 22         |
| 2.1.1 External calvarial structure.....  | 22         |
| 2.1.2 Internal calvarial structure.....  | 25         |
| 2.1.3 Craniofacial system.....   | 27         |
| 2.1.4 Calvarial sutures.....   | 28         |
| 2.1.5 Mechanobiology .....   | 31         |
| 2.1.6 Suture closure rates .....   | 35         |
| 2.1.7 Neurofunctional development .....  | 35         |
| 2.1.8 Natural calvarial growth .....   | 38         |
| 2.2 Craniosynostosis .....   | 44         |
| 2.2.1 Variations of Craniosynostosis.....  | 44         |
| 2.2.2 Methods of diagnostics.....  | 46         |
| 2.2.3 Surgical options for sagittal Craniosynostosis .....   | 47         |
| 2.2.4 Postoperative management.....  | 53         |
| 2.2.5 Comparative studies for optimising sagittal Craniosynostosis .....                                     | 58         |
| 2.3 Properties of biological tissues .....   | 65         |
| 2.3.1 Cranial bones.....   | 65         |
| 2.3.2 Cranial sutures .....  | 73         |
| 2.3.3 Brain .....  | 77         |
| 2.4 Computational studies of the craniofacial system.....  | 80         |
| 2.4.1 Impact trauma .....  | 80         |
| 2.4.2 Simulating suture morphogenesis and ossification.....  | 82         |
| 2.4.3 Computational studies of Craniosynostosis and skull growth .....                                       | 99         |
| 2.5 Discussion and summary.....  | 112        |
| <b>Chapter 3: Development and validation of a patient-specific sagittal<br/>craniosynostosis model .....</b> | <b>114</b> |

|  |            |
|--|------------|
| <b>3.1 Introduction .....</b>  | <b>115</b> |
| <b>3.2 Materials and methods .....</b>   | <b>115</b> |
| 3.2.1 Model development .....  | 115        |
| 3.2.2 Finite element method.....   | 118        |
| 3.2.3 Material properties and boundary conditions .....  | 118        |
| 3.2.4 Sensitivity studies .....  | 122        |
| <b>3.3 Results .....</b>   | <b>128</b> |
| <b>3.4 Discussion .....</b>  | <b>138</b> |
| <b>3.5 Summary.....</b>  | <b>140</b> |
| <b>Chapter 4: Predicting the postoperative outcomes of three surgical techniques .....</b>             | <b>142</b> |
| <b>4.1 Introduction .....</b>  | <b>143</b> |
| <b>4.2 Materials and methods .....</b>   | <b>143</b> |
| 4.2.1 <i>In vivo</i> CT and literature data.....   | 143        |
| 4.2.2 Finite element method .....  | 146        |
| 4.2.3 Sensitivity studies .....  | 147        |
| <b>4.3 Results .....</b>   | <b>152</b> |
| <b>4.4 Discussion .....</b>  | <b>168</b> |
| <b>4.5 Summary.....</b>  | <b>172</b> |
| <b>Chapter 5: A new approach for modelling the bone formation during calvarial growth .....</b>        | <b>173</b> |
| <b>5.1 Introduction .....</b>  | <b>174</b> |
| <b>5.2 Materials and methods .....</b>   | <b>174</b> |
| 5.2.1 Bone formation methods.....  | 174        |
| 5.2.2 Sensitivity study .....  | 176        |
| <b>5.3 Results .....</b>   | <b>177</b> |
| 5.3.1 Sensitivity study .....  | 177        |
| 5.3.2 Bone formation methods.....  | 180        |
| <b>5.4 Discussion .....</b>  | <b>184</b> |
| <b>5.5 Summary.....</b>  | <b>187</b> |
| <b>Chapter 6: Comparative analysis of ten corrective techniques for sagittal craniosynostosis.....</b> | <b>189</b> |

|  |            |
|--|------------|
| <b>6.1 Introduction .....</b>  | <b>190</b> |
| <b>6.2 Materials and methods .....</b>   | <b>190</b> |
| 6.2.1 Model development .....  | 190        |
| 6.2.2 Bone formation algorithm.....  | 190        |
| 6.2.3 Replicated techniques .....  | 191        |
| 6.2.3 'non-operation' scenario .....   | 195        |
| 6.2.4 Sensitivity studies .....  | 196        |
| 6.2.6 Measurements and comparisons.....  | 197        |
| <b>6.3 Results .....</b>   | <b>197</b> |
| <b>6.4 Discussion .....</b>  | <b>223</b> |
| <b>6.5 Summary.....</b>  | <b>228</b> |
| <b>Chapter 7: Discussion .....</b>   | <b>229</b> |
| 7.1 Introduction .....   | 230        |
| 7.2 Morphological validation and sensitivity of the finite element model...            | 231        |
| 7.3 Predicting the pattern of contact pressure .....                                   | 232        |
| 7.4 Material properties of biological tissues.....                                     | 233        |
| 7.5 Replicating the calvarial growth .....   | 234        |
| 7.6 Modelling of the bone formation.....   | 234        |
| 7.7 Comparison of surgical techniques .....  | 235        |
| <b>Chapter 8: Conclusions and future work .....</b>                                    | <b>238</b> |
| 8.1 Conclusions.....   | 239        |
| 8.2 Future work.....   | 240        |
| <b>References:.....</b>  | <b>242</b> |
| <b>Appendix I: Contact interface .....</b>   | <b>264</b> |
| <b>Appendix II: Measurement of clinically used spring devices.....</b>                 | <b>267</b> |
| <b>Appendix III: Parameters for modelling the <i>in silico</i> helmet device .....</b> | <b>269</b> |
| <b>Appendix IV: List of publications .....</b>   | <b>272</b> |
| <b>Appendix V: Published papers .....</b>  | <b>275</b> |

# Chapter 1: Introduction

## 1.1 Overview

**Infant skull:** During the embryonic and neonatal periods of biological development, the human calvaria consists of five primary bony plates. Two bony plates (frontal bones) form the forehead region of the skull, while two other bony plates form the sides and 'roof' of the skull (parietal bones) and a single substantial portion across the posterior part of the skull (occipital bone). The bony plates are connected at their borders by fibrous tissues, known as sutures (Morriss-Kay & Wilkie, 2005). These sutures are interconnected with each other, providing the structural skull shape. The metopic suture is located between the two frontal bones. The two coronal sutures connect the frontal and parietal bones laterally and are split by a large, patterned region known as the anterior fontanelle. The sagittal suture connects both parietal bones dorsally from the anterior fontanelle to the posterior fontanelle. The temporal sutures, which link with the coronal and lambdoid sutures, are located across the most lateral point of both parietal bones and the bony plates leading to the underside of the skull. The lambdoid suture extends laterally across the occipital region and connects the occipital and parietal bones (Cunningham & Heike, 2007). These sutures have many pivotal roles.

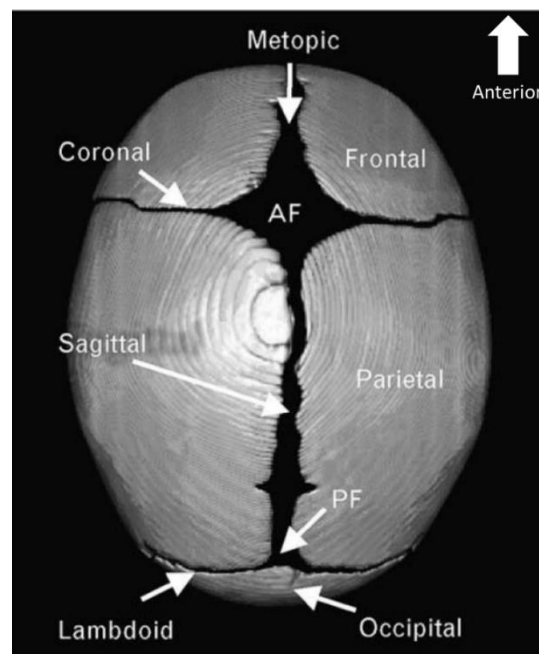


**Figure 1.1:** The calvarial during infancy. Bony plates (Grey) are held in position by sutures (Black) across all regions. Note that AF and PF refer to the anterior and posterior fontanelles, respectively (Adopted from Cunningham & Heike, 2007).



The most notable being the development of new bone along the edges of the existing calvaria, dictating the direction of growth and morphology during the rapid increase in brain growth during early childhood. Further to this, the malleability of these sutures allows for them to function as a form of shock absorbance during birth (Courchesne *et al.*, 2000; Rasmussen *et al.*, 2008). By adolescence, the opening of these sutures is reduced to near-microscopic levels of continuous patency. Bone forms at the sutures at various rates. The only suture which fully fuses prior to adolescence is the metopic, with all others remaining patent. The metopic suture may close as early as 8-months of age, with little patency identified by 14-months (Teager *et al.*, 2019). The sagittal and coronal sutures undergo a rapid reduction in width from birth to the 1<sup>st</sup> month of age and remain partially patent until 21-30 and 24 years of age, respectively (Idriz *et al.*, 2015; Mitchell *et al.*, 2011). The lambdoid and squamosal sutures are typically the last to close, at 26 and 60 years of age, respectively (Idriz *et al.*, 2015).

**Craniosynostosis:** The premature closure of one or more of the sutures is a medical condition known as craniosynostosis (CS). CS has a wide prevalence in newborns, with an occurrence rate of 1 in every 2,000 live births (Kimonis *et al.*, 2007). Most CS cases are non-syndromic, in which only a single suture is affected. The alternative cases are known as syndromic, in which several sutures have undergone fusion. Non-syndromic cases are categorised based on the suture in question. Examples are sagittal, uni (single) or bi (both) coronal and lambdoid synostosis. The incidence rate of each type of synostosis varies, with the most prominent form reported to be sagittal synostosis (3 in 10,000) and lambdoid synostosis being the least common form (1 in 33,000 births - Morriss-Kay & Wilkie, 2005; Greenwood *et al.*, 2014). The resulting condition promotes a series of characteristic deformations and the possible increase in intracranial pressure (ICP), leading to defects in neurofunctional characteristics later in life (Thompson *et al.*, 1995). Molecular biologists have continued to work on understand the genetic mutations and impacts which lead to non-syndromic (sporadic generic mutation) and syndromic (genetically inherited) forms of CS (Alamer *et al.*, 2021; Shim *et al.*, 2016). Several studies suggest that disruptions to various mechanisms and signalling pathways can result in CS.

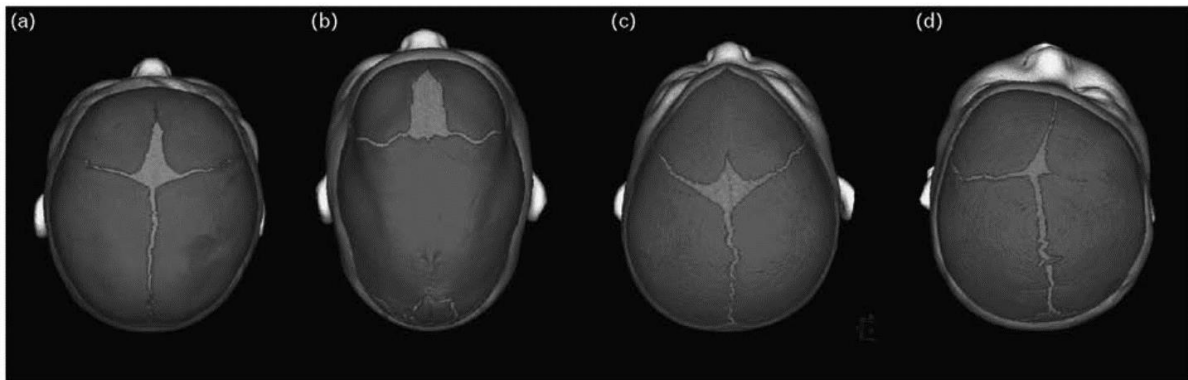


**Figure 1.2:** The normative and various forms of nonsyndromic CS observed at birth. (a) A normocephalic skull lacking any form of synostosis. (b) Anteroposterior expansion and lateral narrowing caused by sagittal synostosis. (c) Frontal bones producing a distinct triangular shape caused by metopic synostosis. (d) Unicoronal synostosis causes orbital and forehead flattening, producing a 'budge' across the opposite frontal region for compensation (Adopted from Cunningham & Heike, 2007).

Restoring the normative shape involves an invasive surgical procedure, where the surgical team remove segments of bone (i.e. craniotomies) allowing for reconstruction of the calvaria. Concerning sagittal synostosis, different surgical procedures have been developed since the early 19<sup>th</sup> century. The earliest attempts involve a simple rectangular extraction of the fused sagittal suture, resulting in limited improvements to the postoperative shape (Otto, 1830). These procedures are categorised into two groups. The first includes less invasive approaches, such as a strip craniotomy, involving the removal or division of the fused sagittal suture with the addition of other craniotomies, thereby taking advantage of the postoperative skull growth after the initial procedure. The second involves more invasive methods, such total calvarial remodelling: this technique involves the rotation, reorganisation or flaring of calvarial bones followed by introducing absorbable fixators to correct the skull shape *in situ* (during surgery). Owing to recent technological advances in medical imaging, computational tomographic (CT) and magnetic resonance imaging (MRI) allow for many long-term surgical comparative studies to be undertaken. These studies debate the alternative methods for correcting sagittal synostosis in relation to the morphological outcomes. These studies also expand and discuss the timings of intervention, by analysing and measuring medical data during follow up examinations (Gewalli *et al.*, 2001; Hashim *et al.*, 2014; Thomas *et al.*, 2015). As an accurate postoperative outcome cannot be determined before surgery, craniofacial surgeons rely on these studies and their previous experiences to manage the corrective process.

**Computational modelling:** Due to the problematic and ethical circumstances surrounding corrective treatments for CS, studies have turned to the use of computational and mathematical programs to answer vital questions. Computationally, two-dimensional (2D) and three-dimensional (3D) geometric models have been previously developed to assist with such questions by mimicking the biological and biomechanical behaviours of human skeletal systems (Malde *et al.*, 2019). Using these, renderings of the neonatal skull have allowed craniofacial surgeons to replicate techniques prior to surgery (relative to computer simulations - Figure 1.3). To answer key biomechanical questions, the finite element method (FEM), first introduced in the 1950s, was developed to predict and assist with an array of engineering applications and problems (Fagan, 1992). Relating to CS, the FEM can be used to replicate and predict the calvarial growth (You *et al.*, 2010; Burgos-Flórez *et al.*, 2016; Li *et al.*, 2017; Malde *et al.*, 2019). Yet, as of the writing of this thesis, no studies have used such a method to compare different reconstruction options for the management of sagittal craniosynostosis. Such investigations may uncover the possible impact different treatment options could have on the resulting brain growth and the skull morphology, leading to greater optimisation.

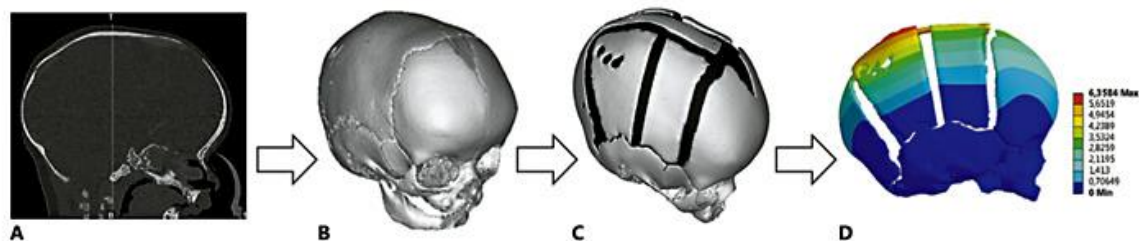


**Figure 1.3:** The process of rendering a 3D geometry of the neonatal skull for CS correction. 2D CT data (A) is used for the segmentation of the calvarial bone (B) for a patient-specific corrective process. Craniotomies are made across the model (C) which is then exported into the FE program for assessment, with the contour plot predicting the level of bone displacement (D) (Adopted from Malde *et al.*, 2019).

## 1.2 Aims and objectives

It is known that various corrective techniques provide a level of improvement in the skull's long-term aesthetic shape and, potentially, neurofunctional characteristics years after the surgery. However, there are limited computational observations on the

impact of suture closure and morphology, the rate of calvarial healing, and the potential detrimental impacts on neurocognitive abilities after surgery has been performed. As the corrective treatment is irreversible once performed, investigating the biomechanics of craniosynostosis from a mechanical perspective could prove highly beneficial for clinicians and surgeons in optimising the management of this condition.

The overall aim of this thesis was to advance our understanding of the biomechanics of various corrective techniques used for the management of sagittal craniosynostosis, with the ambition of optimising the postoperative outcomes years after surgery. The study's long term goal is to provide critical information for surgeons in determining which techniques may provide the most effective outcome for patients and how to improve the pre-operative management from a mechanical point of view. Such observations could give greater clarity for parents and reduce the costs of hospital facilities.

The specific objectives of this thesis were the following: (1) To develop and optimise a generic pre-operative sagittal synostosis model for the purposes of replicating various corrective techniques; (2) To develop a computational framework using the FEM in replicating calvarial growth and bone formation during the postoperative timeframe; (3) To analyse the qualitative and quantitative predictions of the morphological shape, patterns of bone formation, cephalometric measurements, and the changing levels of contact pressure across the modelled brain. A level of validation of the generic model is crucial for building confidence in these predicted outcomes. Hence, the results were morphologically compared against patient-specific follow up CT data throughout the thesis. When comparing various other techniques replicated across the generic model, “technique-specific” CT data was used for the same purposes. In short:

- 1) Patient-specific CT images at pre-operative (4-months of age), postoperative (4-months of age) and follow up (36 and 76 months of age) time points were obtained from the Necker–Enfants Malades Hospital (France, Paris).

2) A 3D FE model was developed using the pre-operative CT image, consisting of the complete internal and external calvarial morphologies.

3) The developed FE model was used to predict the calvarial growth, bone formation across the cranial sutures/replicated craniotomies, and levels of contact pressure across the brain from 4-months to 76-months of age.

4) The predicted morphological data were validated against the patient-specific CT data at 36 and 76 months of age.

5) A total of ten surgical techniques were replicated across the calvaria (of the patient-specific model) at alternating ages of intervention and morphologically compared against technique-specific follow up CT data from a cohort of patients at similar ages.

## 1.3 Methodology

Figure 1.4 presents an overview of the research methodology and the steps to address the aims and objectives of section 1.2. The patient-specific pre-operative CT at 4-months of age was imported into the chosen image processing software. Segmentation of the necessary calvarial components allowed for the development of a 3D computational model. The model was then imported into our chosen FE program. Initial material properties were obtained from various literature sources and studies and are noted accordingly. A thermal expansion analogy established across the segmented brain replicated the effects of brain growth across several load steps. The method of simulating the bone formation was performed based on a radial selection approach. Elements associated with the sutures and craniotomy were highlighted if they were found to be within this selected radius measuring from the bony borders. These highlighted elements then had their elastic modulus updated to represent the new bone growth. Once the target follow up age had been achieved, the predicted morphological shapes were then validated against the patient-specific CT data at 76 months. Several sensitivity studies were conducted to evaluate the impact key parameters could have on predicted outcomes. These, most notably, include alterations to the initial material properties, incorporation of a variable form of

cerebrospinal fluid (CSF), as well as modifications to the algorithm which represents the bone formation during simulated growth. Additional sensitivities included considering the level of strain generated across the model to determine the rate and location of bone formation, expanding on the former modelling premise. Once the model was optimised, a total of ten corrective techniques were replicated across the skull. As the timing of these techniques differ from the original pre-operative age, a controlled growth under no corrective method was undertaken.

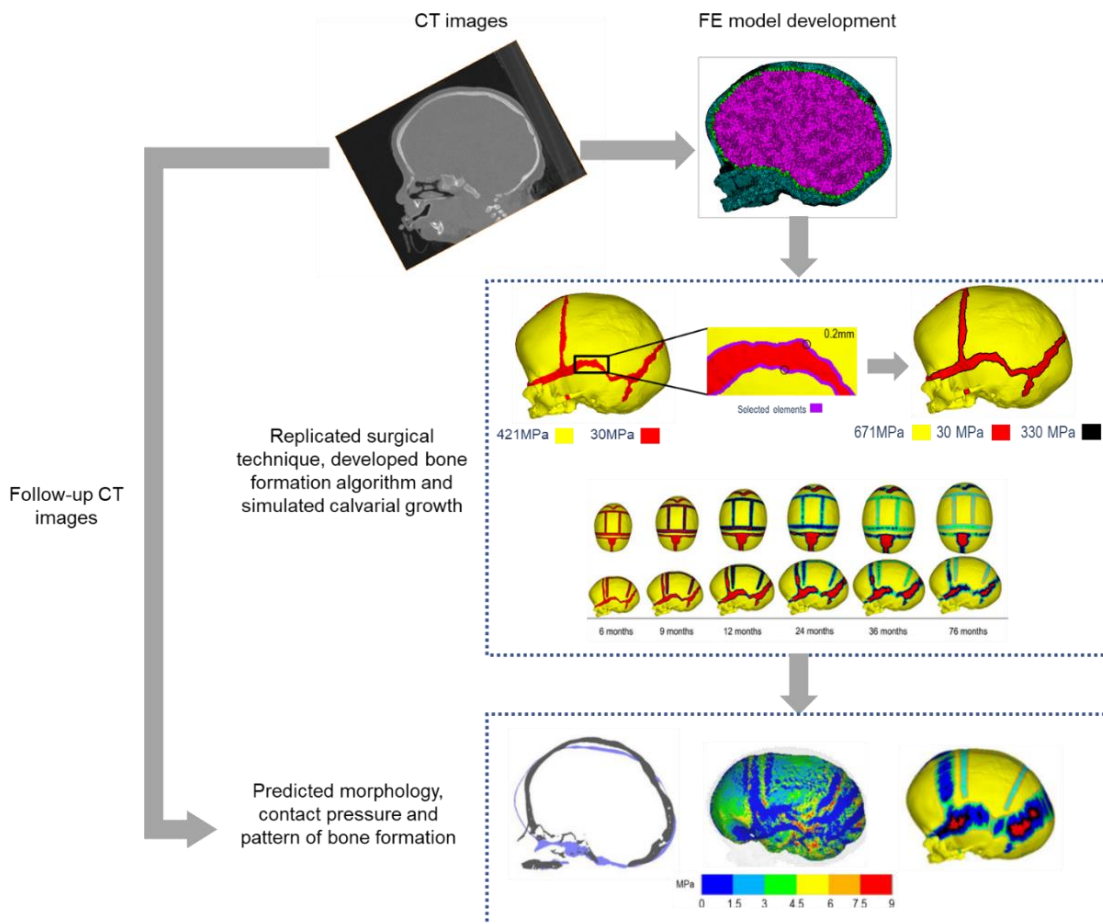


**Figure 1.4:** Overview of the thesis methodology. Pre-operative CT image at 4-months of age was used for model development. During the FE stage, the surgical technique was replicated and an algorithm for predicting bone formation and calvarial growth undertaken (from 4 to 76 months). Morphological predictions were validated against patient-specific CT images at follow up. Further CT images from additional sources were used for comparison of morphology under various replicated techniques.

All findings reported in this thesis, most notably the patterns of bone formation, predicted levels of contact pressure, morphological shape, cephalometric measurements of the length, width, cephalic index (CI), and regional volume changes were recorded and compared where applicable. In addition, relevant technique-

specific CT data was used, where possible, for comparison. This was opted over comparing against normocephalic CT data to capture any predicted shortcomings that may also be seen in the follow up technique-specific CT data.

## 1.4 Chapter organisation

The chapters of this thesis are as follows:

**Chapter 2:** Provides an overview of the literature from previous studies relative to the project in question. Four subsections are introduced. The first expands on the anatomical and physiological fundamentals of the infant calvaria. The second provides an overview of Craniosynostosis, the process of treatment, and the studies providing a comparative analysis of different corrective options. The third details the material properties and mechanical behaviours of relevant biological tissues across human and animal specimen studies relative to various age points. The fourth section highlights the computational studies relative to predicting suture morphogenesis, calvarial ossification, and assisting with Craniosynostosis correction. A summary of the key findings was then discussed.

**Chapter 3:** Details the methodology behind the developed 4-month-old pre-operative FE model and the various sensitivity tests undertaken. These investigate how the method of bone formation, the impacts of incorporating the cerebral spinal fluid, and the impacts of changing material properties could alter the overall predicted outcomes. The morphological predictions (i.e., length, width, height, CI) were validated against patient-specific CT data at 76 months of age across all sensitivity approaches.

**Chapter 4:** Builds on Chapter 3 by providing a preliminary comparison of three different treatment options using the generic FE model. The techniques, adopted from two craniofacial centres, were replicated *in silico* and the impact on the morphology, bone formation and contact pressure predictions were analysed. Additional sensitivity scenarios were examined to optimise the method of implementing distractor devices (Here, springs), the impact differing material properties had on such distractors, the displacement across calvarial morphology under differing distractor forces, and the

## Chapter 1: Introduction

rate of ossification to reflect the calvarial healing. Morphological outcomes were compared against 'technique-specific' patient data provided by the University of Gothenburg (Gothenburg, Sweden) or, where possible, previously published data sets.

**Chapter 5:** Continues to optimise the methodologies discussed in Chapters 3 and 4, by incorporating a level of mechanobiological behaviour in dictating the location and rate of bone formation across our FE model to better resemble the *in vivo* conditions. An additional two methods, with the approach adopted from Chapter 3 used as a baseline here, replicated the formation across the sutures and craniotomy. The previously used patient-specific data and corrective option from Chapter 3 were used here, to compare the suture and craniotomy rate of closure and validate the morphological shape.

**Chapter 6:** Adopts the optimal approaches and parameters (i.e., conclusions from Chapters 3 and 5) to replicate a total of ten techniques across the generic FE model. The natural calvarial shape (i.e., no corrective technique) was grown to 6, 9 and 12 months of age to accommodate techniques performed later than 4 months. All techniques underwent growth up to the age of 76 months. By default, the morphological shape, bone formation and contact pressure across each technique were compared. An additional observation into the predicted changes in the regional volume distributions was further examined here. Compared to the approach in Chapter 4, technique-specific patient data was used at various time points to compare the morphological shape against our predictive data.

**Chapter 7:** Summarises the overall findings of this thesis with further discussion.

**Chapter 8:** Concludes with potential future work to be performed based on the findings reported across the thesis.



## **Chapter 2: Literature review**

**Overview:** The infant calvaria is a highly investigated area within anatomical and physiological literature. Studies exploring the properties, forces and biological characteristics of the skull have noted the overall changes seen from birth to death, despite the difficulties in acquiring suitable samples for analysis. In the absence of *Homo sapiens* specimens, published works opt to use rodent, swine, or relatable mammalian cadavers as a reliable alternative. Therefore, the premise of this chapter was to provide an overview of the core understanding concerning the literature for this thesis. Four subsections are presented here. The first summarises the anatomical and physiological aspects of the infant skull, including the bone structure, sutures, calvarial growth, mechanobiology, brain development, and the changes in morphology during the first year of life. The second investigates the mechanical properties of hard and soft biological tissues. Studies using material characterisation techniques for examining the properties of bone, suture, and the brain were reported here. The third discusses the fundamentals of craniosynostosis, with an emphasis on sagittal craniosynostosis. The distinct types of craniosynostosis, method of diagnosis, various corrective techniques, the standards for postoperative monitoring, and ongoing debates between treatment options were explored here. The fourth section highlights the various computational modelling approaches in suture morphology, calvarial growth and assisting with craniosynostosis correction, with an emphasis on the finite element method. The chapter then concludes with a summary of all findings.

## 2.1 Anatomy and physiology

### 2.1.1 External calvarial structure

The neonatal cranium is a complex structure with many functionalities. The flat bones of the skull are set apart by open joints named sutures. Their structural and malleable characteristics are a fundamental premise in assisting with the birthing process, allowing for the flexibility required to pass through the birth canal (Anatole & Dekaban, 1977; Hegazy & Hegazy, 2018). Post-birth, the flat bones protect the inner brain and adapt to the accelerated shape changes seen in the first year of life. Figure 2.1 illustrates the structure of the neonate skull at birth. The following bones and their functions are as follows:

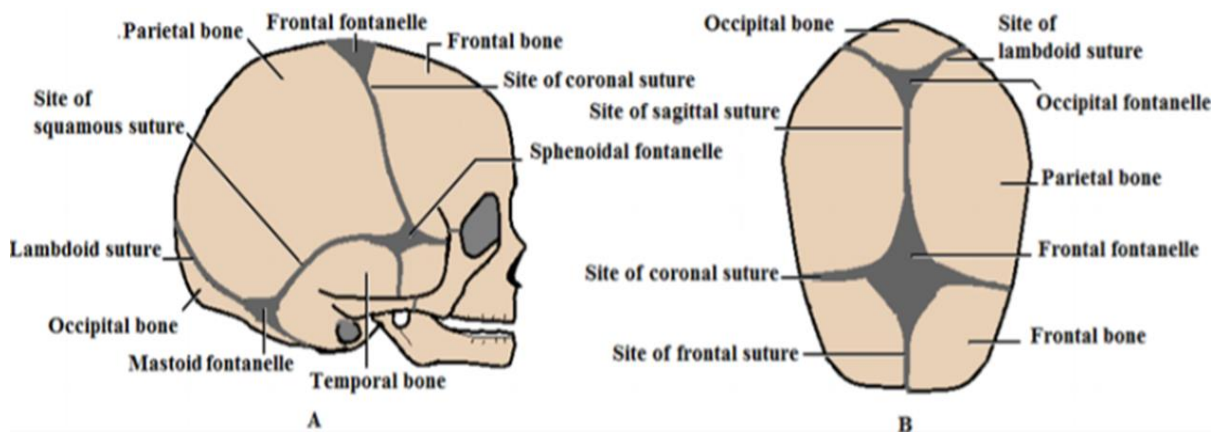


**Figure 2.1:** Diagram of the neonatal skull. Displaying lateral (A) and dorsal (B) views (Adopted from Hegazy & Hegazy, 2018).

**Frontal bones:** The frontal bones consist of two segments, divided by the frontal suture (i.e., metopic). These border superior-inferior from the coronal suture to the orbits and mediolaterally from the metopic suture to the lateral coronal sutures and sphenoidal fontanelle. The bones play a key role in forming the supraorbital foramen, allowing for the arching of the eye sockets (Scheuer & Black, 2004). Upon fusion of the metopic suture, the bones merge into a single structure. Previous studies suggest an average thickness of 8 mm across the frontal bones by late adulthood, however, due to the material behaviour of bone, this is not uniform (Mahinda & Murty, 2009).

**Parietal bones:** Similar to the frontal bones, the parietal bones envelop the lateral and dorsal regions of the skull and represent the largest cranial structures. The sagittal suture connects the two separated bones from the anterior fontanelle to the lambdoid sutures. The bones are connected laterally to the temporal bones by the squamosal sutures. The structural thickness is reportedly lower than that of occipital and temporal bones (Mahinda & Murty, 2009). The porosity of the bone by adulthood can reach as high as 80%, allowing the bone itself to be susceptible to fracturing (Alexander *et al.*, 2019).

**Occipital bone:** During the earlier stages of development, the occipital bone consists of many separate components, which range in size and span across the complete posterior region of the brain. An additional substructure connects across the interior region of the bone, known as the foramen magnum, which supports and develops the

structure of the neck (Figure 2.2). These consist of the sutura intra-occipital, two wing-shaped portions that make up the lateral walls of the foramen magnum, which rapidly form together during gestation (White *et al.*, 2011). At the anterior end, the pars Basiliaris joins with boney lateral portions of the petrous temporal and the posterior part of the sphenoid bone. By the second year of life, this structure has completely formed. With the pars Basiliaris experiencing greater widening post-birth (Scheuer & Maclaughlin-Black, 1994).

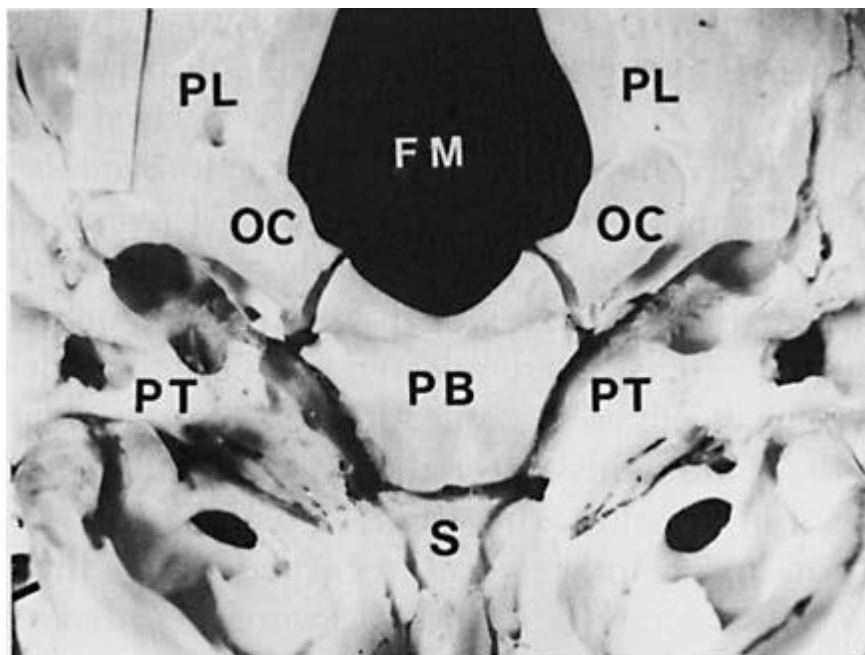


**Figure 2.2:** Depiction of the foramen magnum by the second year of life. (**FM**), Foramen magnum; (**PB**), pars Basiliaris; (**PL**), pars lateralis; (**PT**), petrous temporal; (**S**), body of sphenoid; (**OC**), occipital condyle (Adopted from Scheuer & Maclaughlin-Black, 1994).

**Temporal bones:** Located bilaterally from the foramen magnum are the temporal bones. As well as protecting the temporal regions of the brain, the bones are the main site of the development of the zygomatic process, which connects the upper mandible to the main temporal bone structure (White *et al.*, 2011). Both bones are also the site of the external acoustic meatus, the passage leading to the ear drum, below the zygomatic process.

### **2.1.2 Internal calvarial structure**

Surrounding the calvarial bones are five layers of connective soft tissue, each supporting the homeostasis of the cranium (Figure 2.3). The outermost layer, the epidermis, consists of millions of hair follicles. This layer undergoes significant changes in properties with age, sex, and water content, showing that all have a significant impact on the overall tensile strength (Falland-Cheung *et al.*, 2018). The connective tissue deep to the epidermis maintains the supply of enriched blood to the epidermis and mostly consists of fat lobules bound in fibrous septa (Ellis & Mahadevan, 2014). The aponeurosis acts as the 'anchor' between the connective tissue and muscle systems across the skull. This layer undergoes elevated levels of tension and exists as a thin 'sheet' across the vertex of the skull, extending towards the regions of the eyebrows and bridge of the nose. Loose connective (areolar) tissue underlining the aponeurosis provides the mobility of the skin when under force. This layer provides the surgeons with the ability to create 'scalp flaps' (i.e., foldable incisions allowing access to the calvarial bone) during cranial related surgical procedures (Ellis & Mahadevan, 2014). The periosteum is a layer of soft tissue which tightly connected to the outer cortical layer of the calvarial bone (and bone in general). The outer/cortical layer of calvarial bone is a much more compact structure compared to its central layer (i.e., Diploë) that is made up of trabecular bone. The inner surface of the calvarial bones is tightly interconnected to another layer of soft tissue called the dura mater, which encapsulates the intracranial volume (i.e., the brain and cerebrospinal fluid).

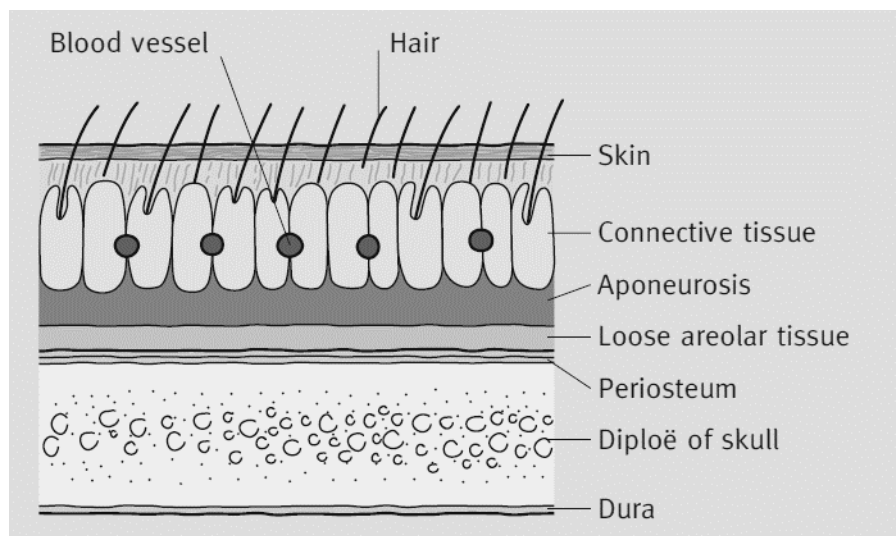


**Figure 2.3:** The surrounding layers between the skin and arachnoid mater (Adopted from Ellis & Mahadevan, 2014).

An integral function of the dura is providing continuous blood supply through the external carotid artery, extending from the occipital region towards the zygomatic arch (Ellis & Mahadevan, 2014). The space between the two membranes (i.e., the periosteum and brain) is known as the subarachnoid space and consists of the cerebral spinal fluid (CSF), along with arachnoid mater (above layer) and the pia mater (below layer). The CSF surrounds the entire brain and filters down to the foramen magnum along the spinal cord. Although the distribution of the fluid is uneven, collectively, 150 ml resides within the human body, with 25 ml residing within the spinal region (Sakka *et al.*, 2011). The CSF has two purposes. The first is supplying the required nutrients for the homeostasis of the brain. The second is providing a cushioning between external impacts and the brain (Couper & Albermani, 2009). CSF flow within the subarachnoid space has an average thickness of 2-3 mm (Lam *et al.*, 2001; Clouchoux *et al.*, 2012). It is worth highlighting that maintaining the intracranial pressure (ICP) is vital for human life and neural development, with the average pressure previously measured between 3-4 mmHg and 10-15 mmHg in neonates and adults, respectively (Sakka *et al.*, 2011).

### 2.1.3 Craniofacial system

The facial bones develop at a separate rate to that of the calvarial bones, responsible for supporting, developing, and protecting the vision, hearing, feeding, and respiratory functions. The nasal cavity makes up the greatest area of the facial region. Although not strictly part of this system, the zygomatic and mandible interconnect with the nasal region and provide important mechanical functions and facial characteristics. These three areas will be discussed.

The nasal cavity plays a vital role in completing the link between the respiratory system and the facial skeleton (Bastir & Rosas, 2013). Due to various syndromic conditions, obstructions in the size and shape of the nasal passage can have detrimental impacts on the quality of life, such as nasal clefts, excessive tissue development and unilateral hypoplastic maxilla (Funamura & Tollefson, 2016).

The zygomatic acts as the bridge between the main neurocranial base and the craniofacial system. The bone is separated across the lateral regions of the facial structure. These bones can act independently from one another during development, leading to substantial changes in the cheek bone structure (Heuzé *et al.*, 2016). The two bones work closely during mastication, with the temporalis and masseter muscles providing the necessary forces required for this function (Yu & Wang, 2021).

The mandible (Figure 2.4) extends across the width of the human facial skeleton, connecting close to the zygomatic process via the rami, which extends downwards towards the main structural body (corpus). The mandible functions as a mechanical 'lever', allowing for mastication and the passage of air to move from the airways to the external environment. The large levels of loading during biting have been seen to lead to large regions of compact bone development across the mandible-hyoid line regions (Lipski *et al.*, 2013). It is known that the characteristic shape of the mandible is morphed by the connected muscles and ligaments attached to it prenatally (Radlanski *et al.*, 2003).

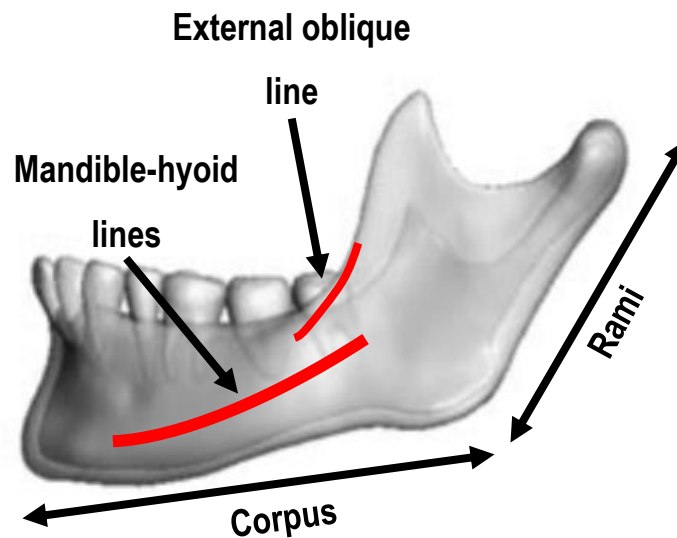


**Figure 2.4:** Anatomical layout of the mandible (Adopted from Ichim *et al.*, 2006).

#### 2.1.4 Calvarial sutures

The pattern of bone formation across the sutures goes hand in hand with brain growth (Richtsmeier & Flaherty, 2013). While representing the site for intramembranous ossification, the objective of sutures is to accommodate the developing brain and to ensure that the natural skull shape (i.e., normocephalic) is achieved (Beederman *et al.*, 2014). Interruptions at the suture sites have the potential to lead to serious morphological changes across the skull and intracranial pressure alterations, resulting in several medical complications (Kim *et al.*, 2019). To ensure morphological stability, the biological and mechanical attributes of the sutures allow for independent timings of closure from one another during human life. Although still under investigation, literature has determined the timing of these closures and aspects that could dictate these timings.

**Biological development:** Two methods of ossification are present in the human body, endochondral and intramembranous processes. The appendicular skeleton, consisting of the long bones, undergoes a method of endochondral ossification, such examples are the femur and tibia, where a cartilage matrix is developed and osteoblast-driven ossification is undertaken (Beederman *et al.*, 2014). This cartilage



process is absent from the flat bones of the calvaria, where intramembranous development (Figure 2.5) occurs (Beederman *et al.*, 2014).

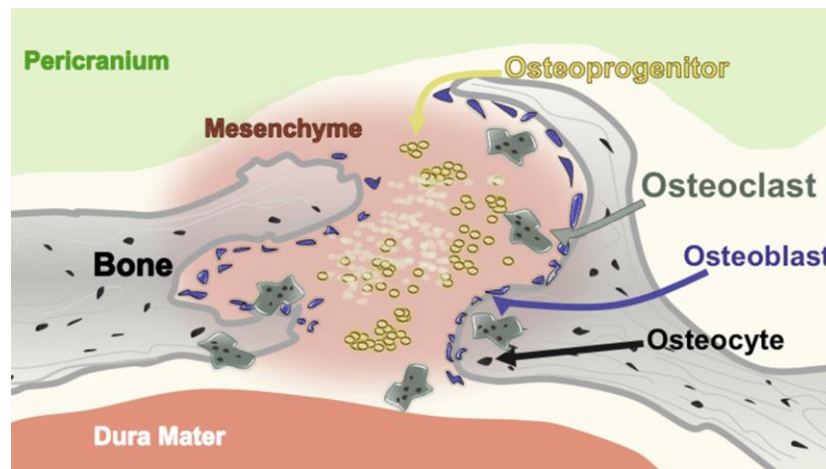


**Figure 2.5:** Illustration showing the biological process to form cranial bone during the ‘open’ cycle of the sutures. Where osteoblast cells develop to create new bone along the existing bone lining (Adopted from Beederman *et al.*, 2014).

Intramembranous bone formation begins at the embryonic stages with the differentiation of the mesenchymal cells, while other cells, known as osteogenic cells, begin to form in the central region known as the ossification centre. Clusters of osteoblasts (i.e., responsible for new bone development) begin to secrete osteoid, leading to a calcified matrix (Opperman, 2000). The surrounding osteogenic cells within this matrix then develop into osteoblast cells (responsible for bone maintenance). Unmineralised osteoid cells result in a trabecular (cancellous bone) matrix eventually consisting of red bone marrow and bone vessels, while osteoblast cells maintained on the cells surface form a protective superficial layer of compact bone (Opperman, 2000).

The structure of overlaying sutures around the cranial vault remains unchanged during the life span of human development. The process of ossification occurs at the two bone fronts of sutures with the mesenchymal tissue maintaining cell differentiation. Osteoclast cells maintain a constant front of bone regulation while osteoblast cells produce new bone across the mesenchymal tissue. Additional membranous tissues are also responsible for maintaining suture patency such as the dura mater, in which spontaneous closure has also been recorded due to its effects on various isoforms (Slater *et al.*, 2009). These isoforms, particularly fibroblast growth factor (FGF)

proteins, have been seen to mutate., leading to the prevalence of severe and rarer forms of craniosynostosis such as apert and crouzon syndrome (Wilkie *et al.*, 2002).

**Suture anatomy:** As previously mentioned, sutures are positioned in a coordinated fashion to enable a natural growth cycle and morphological characteristics within the first years of life (Figure 2.1). To verify the modelling approach in replicating the *in vivo* environment, the rate and timing of suture closure required investigation.

**Metopic:** The metopic suture runs along the frontal bone, forming the forehead and providing room for the frontal lobe during growth. Reports examine various timings of closure. For example, Vu *et al.*, (2001) reported metopic fusion as early as 3 months of age, while estimations from Teager *et al.*, (2018) suggested fusion as late as 19 months of age. However, such sources agreed that complete fusion was achieved by 24 months of age.

**Coronal:** The coronal suture runs parallel along the posterior margin of the frontal bones and intersects with the squamosal sutures at the sphenoparietal suture. The suture remains patent during the neonatal period and reaches a width of micrometres by adulthood. Reports have documented fusion by 24 years of age (Melott, 1999).

**Sagittal:** The sagittal suture separates the parietal bone into two separate segments and joins with the coronal and lambdoid sutures at the anterior and posterior fontanelles. Typical fusion occurs by 22 years of age (Melott, 1999). Unlike other sutures, the sagittal runs the length of the superior sagittal sinus. Due to the location and anatomical deviations of the sinus, surgeons take precautionary measures when removing the adjacent parietal bones (Samadian *et al.*, 2011).

**Lambdoid:** Joining the occipital bone with the parietal and sphenoidal bone, the lambdoid suture runs along the superior margin of the occipital bone towards the squamosal suture and connects with the sagittal suture along the mid-section. Fusion occurs by 26 years of age, the last suture to fuse (Melott, 1999).

**Fontanelles:** Acting as an intersection between the coronal, metopic, and sagittal sutures, the anterior and posterior fontanelles appear as a hollow 'gap' within the skull. As the parietal and frontal bones commence ossification, the fontanelles begin to reduce in size. During the gestation phase, the diameter of the fontanelle remains remarkably constant, measuring on average 40 mm by gestation week 42 (Adeyemo & Omotade, 1999). Typical fusion is estimated to be by 24 months after birth (Pindrik *et al.*, 2014).

### 2.1.5 Mechanobiology

Due to the morphology and malleable nature of the skull at early stage of the life, cranial sutures are subject to high levels of mechanical strain due to the rapid changes within the intracranial volume (Moazen *et al.*, 2015; Weickenmeier *et al.*, 2017). It is widely accepted that at the preliminary stages of the postnatal development the majority of the sutures experience tension and/or shear stresses. This changes as bone gradually forms at the suture where, pending their overall morphology and anatomical position, they can also experience compression. As a result, the mechanobiological anabolic stimulus nature of sutures responds accordingly, more so during the early stage of development. Theories of the behaviour behind cellular activities during loading have been discussed for years (e.g., Herring, 2008; Moazen *et al.*, 2015). Many studies have analysed *ex vivo* mice and rabbit calvarial specimens' and captured their responses to external repeated/cycle loading conditions (Rafferty *et al.*, 2019; Main *et al.*, 2014). However, mechanical loading across the craniofacial sutures under natural brain growth is far less documented (Herring, 2008).

The appendicular skeletons of various species have been studied for many decades, as orthopaedic forces have been seen to affect skeletal growth and structure (Wagemans *et al.*, 1988). Because limitations and ethical considerations remain for examining responses in humans, researchers opt to correlate long-bone loading and the mechanobiological responses as a suitable alternative. Note that due to the lack of published data, this section will focus on both human and animal specimens.

Some of the earliest studies from Frost (1982) pioneered the knowledge of stress-strain relations to the architectural formation of bone in children. It was established

that progressive osteoclastic and osteoblastic drifts allow for bone erosion from one surface and developing bone across another, respectively. It was found that these responses are directly 'one-to-one' with dynamic flexural strain magnitudes, which was observed across the femur bone under loading (Figure 2.6).

Over a decade later, Carter *et al.*, (1998) investigated the changes in compression and tension in long bones and their impacts on tissue differentials into cartilage, bone or fibrous tissue. From a mechanical point of view, materials investigated are seen as a constant material property, allowing for the characterisation of quantitative stress and strain. These values are then relayed to differentiate how tissue forms at a cellular level and alter the shape and pressure of cells.

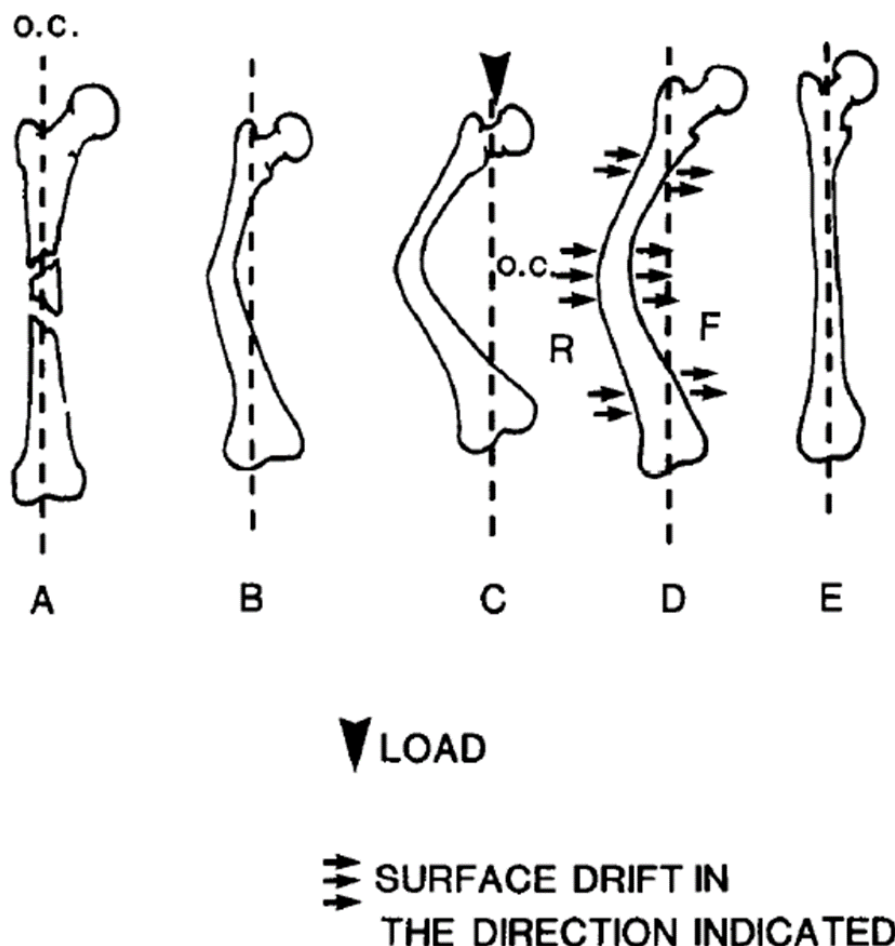


**Figure 2.6:** Angular deformity of a femoral bone in a young child. A fracture occurs across the femur (A). As the healing progresses, angular malformations become evident (B). While loading is present in the transverse, angulation increased (C). The osteoclast and blast drift acts accordingly to realign the bone (D), until its original configuration was reached (E) (Adopted from Frost, 1982).

As such, a finite element approach has been used to investigate these regions of tissue differentiation under fracture healing (Claes & Heigele, 1999). It has been found that, while under hydrostatic compression, the location of the fracture gap experienced the highest level, indicating fibrocartilage formation during the first stages of healing (Figure 2.7). This observation indicated that intramembranous ossification would be permitted on endosteal surfaces. Although the study provides a strong mechanical point of view for ossification healing in human skeletal tissues, quantitative clarification between tissue differentiation occurrence was not specified.

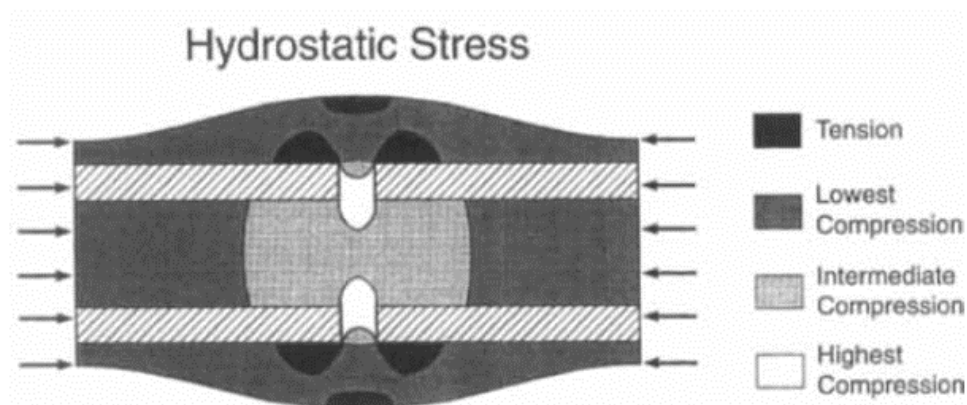


**Figure 2.7:** FE outcomes of patterns of maximum hydrostatic stress in regenerating tissue under axial compression forces (Adopted from Carter *et al.*, 1998)

Claes & Heigele (1999), investigated the local stress/strain along skeletal bones to observe the levels seen across fracture surfaces, implying that a majority of newly formed bone occurs at the existing surfaces. Their study suggests that intramembranous and endochondral ossification occurs under strain values of 5% and 15% while under compression, respectively (Figure 2.8).

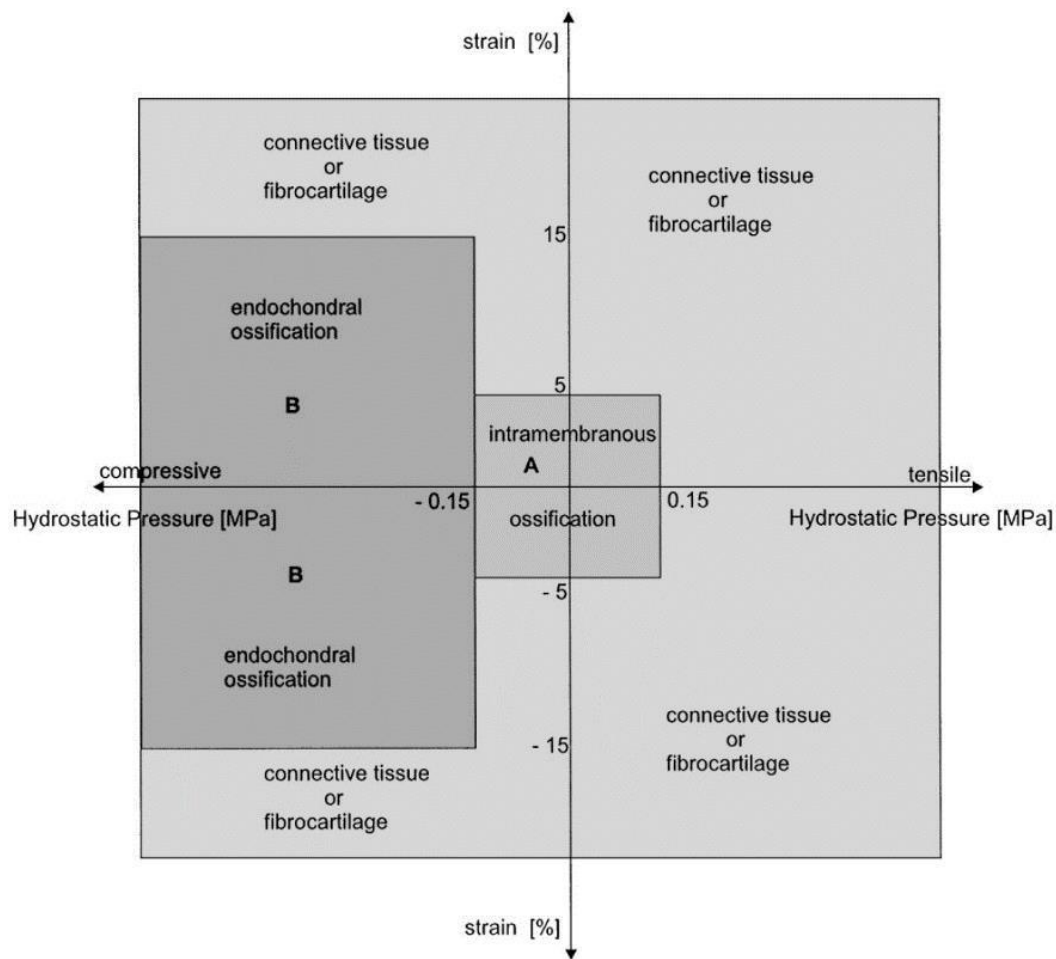


**Figure 2.8:** The hypothesised correlation between mechanical loadings and tissue differentiation during fracture healing (Adopted from Claes & Heigele, 1999).

Although advancements have been made to discover the link between mechanical loading and tissue differentiation, a recent review from Pivonka *et al.*, (2018) highlighted the fundamentals requiring further investigation to fully understand and simulate the ossification and tissue differentiation responses to mechanical loading and across various biological tissues. It should be further noted that the behaviour of bone tissue remodelling has been highly studied and that there are ongoing debates in determining the mechanical behaviour. For example, many studies compare the function of tension or compressive loading, with both maintaining their respective outcomes (Nyman *et al.*, 2009).

### **2.1.6 Suture closure rates**

Although modern technology allows for microscopic measurement in bone deposition, such ambitious studies require time and money for fruition. For clinicians, a suitable alternative comes in the form of CT and MRI data for measuring the rates of suture bone formation. Note that the following studies rational for undertaking their respective CT scans lay in additional medical conditions unrelated to craniosynostosis or conditions affecting suture morphology/fusion.

One such study from Soboleski *et al.*, (1997) examined 50 neonates via sonography over the course of birth to five months of age, where the width and thickness of each major cranial suture were measured. Although the exact quantitative results were not reported, the majority of the sutures were estimated to have a width of less than 1 mm by 5 months of age.

Mitchell *et al.*, (2011) explored CT data of 483 infants' cranial sutures over the first year of life. The proximal width of all sutures upon birth were  $5.0 \pm 0.1$  mm, which drastically narrowed by 12 months reaching  $2.4 \pm 0.1$  mm and  $1.3 \pm 0.1$  mm across the sagittal and coronal sutures, respectively. Although the population size was substantially larger than from the previous study, the observational time points were highly limited.

Recently, Riahiinezhad *et al.*, (2019) performed an extensive examination across all major sutures between the ages of zero to 12 months of age using 302 infants. The study benefited from categorising data into age groups, highlighting the rate of bone formation across each cohort. Using this, an average suture closure rate was calculated to be 0.1-0.2 mm for each month of growth (2.76 mm and 2.52 mm from 2 to 3-4 months of age, respectively).

### **2.1.7 Neurofunctional development**

The human cerebrum is the most complex organ within the human body, with specified areas mapped and based on their positions and relative functions (Figure 2.9). Ongoing research aims to understand the networking responsible for conscious and

unconscious functions (Buckner & DiNicola, 2019; Alvarez & Emory, 2006). The use of magnetic resonance imaging (MRI) over recent years has allowed for high-quality quantification of brain activity during undertaken tasks (Chen & Cohen-adad, 2018) allowing for greater research in the diagnostics of functional illnesses and diseases. During the first year of life, neonatal neurology is primarily responsible for the control of the proximal body (i.e., head and chest) until the development of distal muscle controls (i.e., arms, hands, legs, feet and spine). Development during this period is as follows:

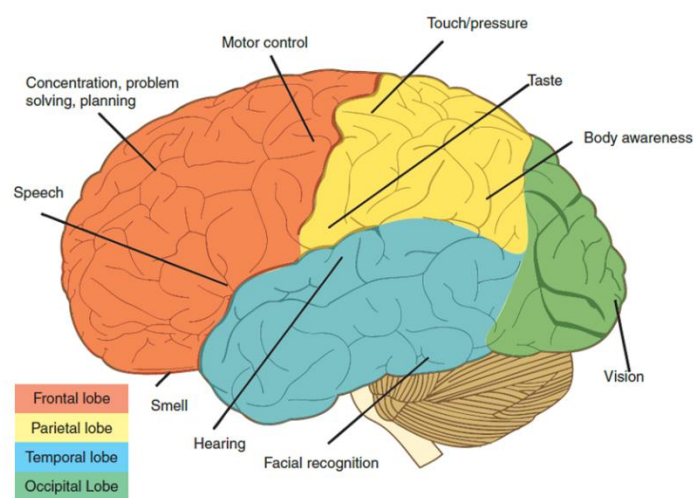


**Figure 2.9:** The human cerebrum's various regions with indications of typical neurofunctional activity locations (Adopted from Obenaus, 2016).

**Birth to 1<sup>st</sup> month:** The visual systems during this period are very immature in contrast to adulthood, with a focal distance of only 21 cm (Law *et al.*, 2011). Unlike the sensory functions, motor functions are highly immature. The movement of feet and toes during this phase is more related to the muscular responses as opposed to mature loco-motor functionality (Sheridan, 1973).

**1 to 2 months:** Visual focus continues to develop with the development of colour distinction. Key cognitive abilities such as memory, and motor processing have yet to form. Full memory retention is not yet exhibited during this period (Rovee-Collier *et al.*, 1980).



**2 to 3 months:** The ability to track depth perception continues to improve with age (Law *et al.*, 2011). Limbs now have greater coordination and the ability to grasp distant objects, although this varies wildly (Sheridan, 1973).

**3 to 5 months:** Facial recognition begins to be retained at approximately 10-15 weeks of age. As these higher levels of visual abilities develop, major anatomical changes have been observed across the cortical regions of the cerebrum (Cocker *et al.*, 1998). This phase of visual development is linked to major processes being developed at a neural level, including attention capabilities, memory development and learning behaviours (Nelson & Collins, 1991).

**5 to 6 months:** Attention retention, hand-eye coordination, and the ability to detect sources of auditorial stimuli are more evident by 36 weeks of age (Sheridan, 1973).

**6 to 12 months:** Associative control over limbs has been fully achieved by this age. Balancing has improved, allowing for voluntary movements for travel (i.e., crawling) (Sheridan, 1973). Significant changes in the loco-motor development begin, allowing for perceptual explorative activities (Adolph & Eppler, 1998).

The developmental changes in neonate perceptions and brain development are still under investigation. The structure of the brain is anatomically universal and is as follows:

**Frontal lobe:** The frontal lobe is the largest of the cerebrum, shielded by the frontal bones. Action retention processes relative to work and language comprehension have been found to originate here (Grisoni *et al.*, 2017). Associations of memory are divided across the pre-frontal area, with the left portion responsible for memory information processes and retrieval of information present in the right (García-Lázaro *et al.*, 2012). Social personality and personal reasoning behaviours are also calculated across the entire lobe (Firat, 2019).

**Parietal lobe:** The parietal lobe is primarily responsible for a majority of the sensory and motor functions, overlined by the parietal and temporal bones. The control of large physical actions such as walking, running, and jumping are found to be active across

this region (Godde & Voelcker-Rehage, 2010) as well as sensory-muscular coordination such as writing and speaking abilities (Brownsett & Wise, 2010). The processing of numerical calculations is also processed in this region (Cappelletti *et al*, 2010).

**Temporal lobe:** Accounting for only 17% of the cerebral volume, the temporal lobe is the sight of major sensory functions, such as visual, auditory, and linguistic processes (Kiernan, 2012). The temporal lobe is also known to contain pathways that connect and assist in the functions of memory with the frontal cortex (Gaffan, 1994).

**Occipital lobe:** The occipital lobe has been regarded as the main region for visual input processing (Schotten *et al.*, 2014). Pathways consisting of white matter create a circuitry system communicating across all other lobes for the processing of functions based on the visual stimuli received from the occipital lobe (Takemura *et al.*, 2015).

During these stages of neurodevelopment, brain growth must be accommodated with minimal restriction caused by the skull. As such, a fundamental understanding must be known of how the morphology and volumetrics of the skull change during the early years of life.

### 2.1.8 Natural calvarial growth

Although sutures play a vital role in the calvarial shape, the expansion of the intracranial volume (ICV) drives the growth of the skull. The most rapid phase of expansion is seen in the first year of life, achieving 60 % and 90 % of the adolescent volume by birth and age of two to three years, respectively (Sperber, 1989). In turn, the changes in morphological measurements (length, width, and height) also rapidly change.

**Volumetric growth:** By the 21<sup>st</sup> century, the foundations of how the growth rate of the internal volume of the skull expands during human development was well understood. Sgouros *et al.*, (1999) explored a large study of infant intracranial volume changes from 7 days to 15 years of age using MRI data. They compared genders and found males to possess an overall mean intracranial volume of 900 ml vs. females 600 ml

## Chapter 2: Literature review

during the first months of life (Figure 2.10). Later, rapid development was seen in both until the growth slowed down after the first year. An average value of 1300 ml by 72

| Age (months): | No: | Male –Mean intracranial volume (ml): | No: | Female –Mean intracranial volume (ml): |
|---------------|-----|--------------------------------------|-----|--|
| 1-2           | 1   | 465                                  | 3   | 423.6                                  |
| 3-4           | -   | -                                    | 1   | 469                                    |
| 5-6           | 1   | 765                                  | 2   | 810                                    |
| 6-12          | 2   | 895.5                                | 3   | 880.6                                  |
| 12-24         | 3   | 1162                                 | 5   | 929.4                                  |
| 24-36         | 5   | 1325                                 | 2   | 1138.5                                 |
| 36-72         | 6   | 1371                                 | 6   | 1207.1                                 |

months of age was observed when all genders were considered (Table 2.1).

**Table 2.1:** Normal ICV changes in children: Data distributed between genders (Data extracted from Sgouros *et al.*, 1999).

Such observations agree with a report from Kamdar *et al.*, (2009) a decade later. The ICV from birth to 9 months was seen to double and afterwards slowed down.

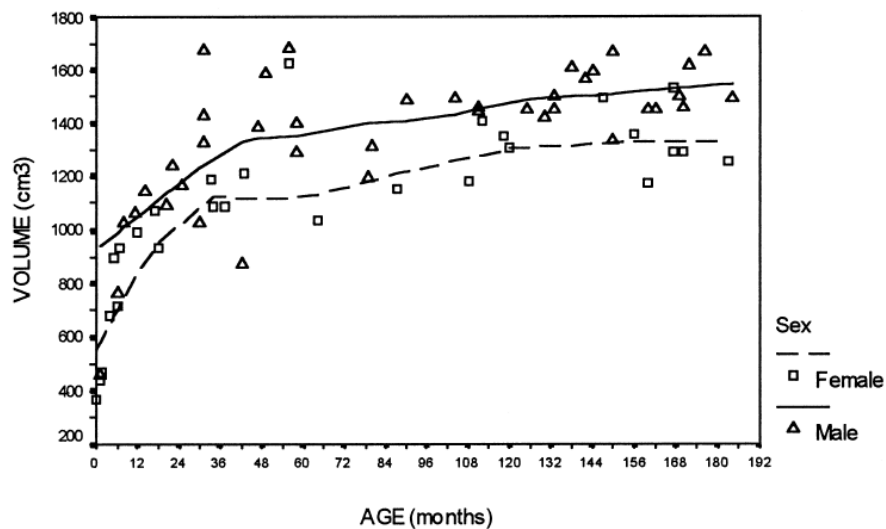


**Figure 2.10:** Scatter plot curvatures of changes in volume during development (Adopted from Sgouros *et al.*, 1999).

Additional studies have compartmentalised the individual volume changes seen in the biological tissues and fluids originating within the ICV. A study from Matsuzawa *et al.*, (2001) compartmentalised the various soft tissues of the brain as well as the CSF from 1 month to 10 years of age using detailed MRI data. A cohort of 28 normal infants were recruited to examine the volume changes of these tissues across the complete compartmental volume, the frontal, and the temporal lobes. The anatomical nature of the brain and quality of the data allowed for further segmentation between left and right hemispheres to evaluate potential asymmetry of tissue distribution. Of all biological tissues, the grey and white matter were seen to rapidly develop during the first 2 years of life, while the CSF stabilised throughout the whole observational period (Figure 2.11 – A.) It was of interest to the authors that an asymmetric behaviour was seen regarding matter distribution. The right hemispheres displayed a greater volume vs. the left (Figure 2.11 – B.) Further, the largest region of growth was seen across both the frontal and temporal regions when considering the whole brain volume.

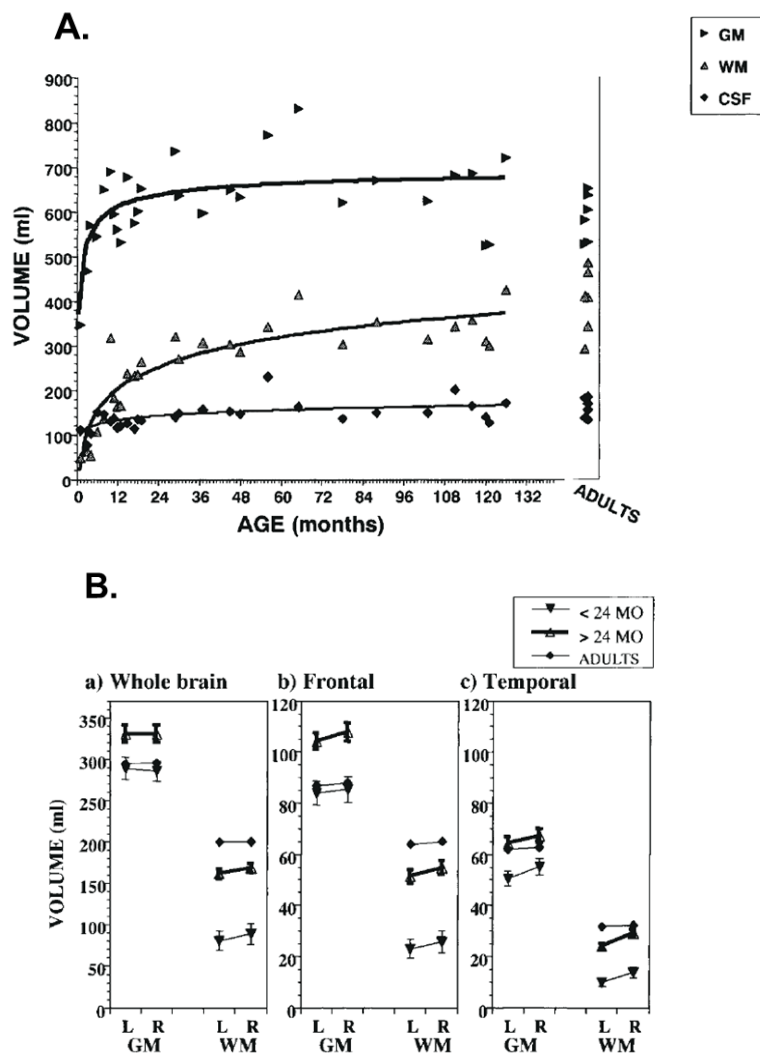


**Figure 2.11:** Age-related changes in grey matter (GM), white matter (WM) and cerebral spinal fluid (CSF) (A). Mean compartmental volume changes across left and right hemispheres of the whole brain, frontal, and temporal lobes (B) (Adopted from Matsuzawa *et al.*, 2001).

**Cephalometric measurements:** The normocephalic skull is designed to accommodate the changes of the ICV. To quantify this from patient to patient in a repeatable manner, clinicians have developed a universal anatomical methodology to characterise the quality of skull shaping. To obtain an accurate measurement of the skull shape, reference planes (Figure 2.12) and anatomical landmarks are used.

These planes, known as the Frankfort (horizontal plane; passes through the infraorbital and triagon, anterior to the ear) and mid sagittal planes (divides left and right of the skull), coordinate the alignment of the skull to an anatomical reference

position, allowing for length, width and circumference measurements to be undertaken uniformly. Such measurements have been reported by e.g., Schneider *et al.*, (1986) across a cohort of normative patients between 0 and 48 months of age. An overall greater length measurement was observed (Range: 149-176 mm) compared to the width (Range: 115 - 134 mm) by the age of 10-12 months.

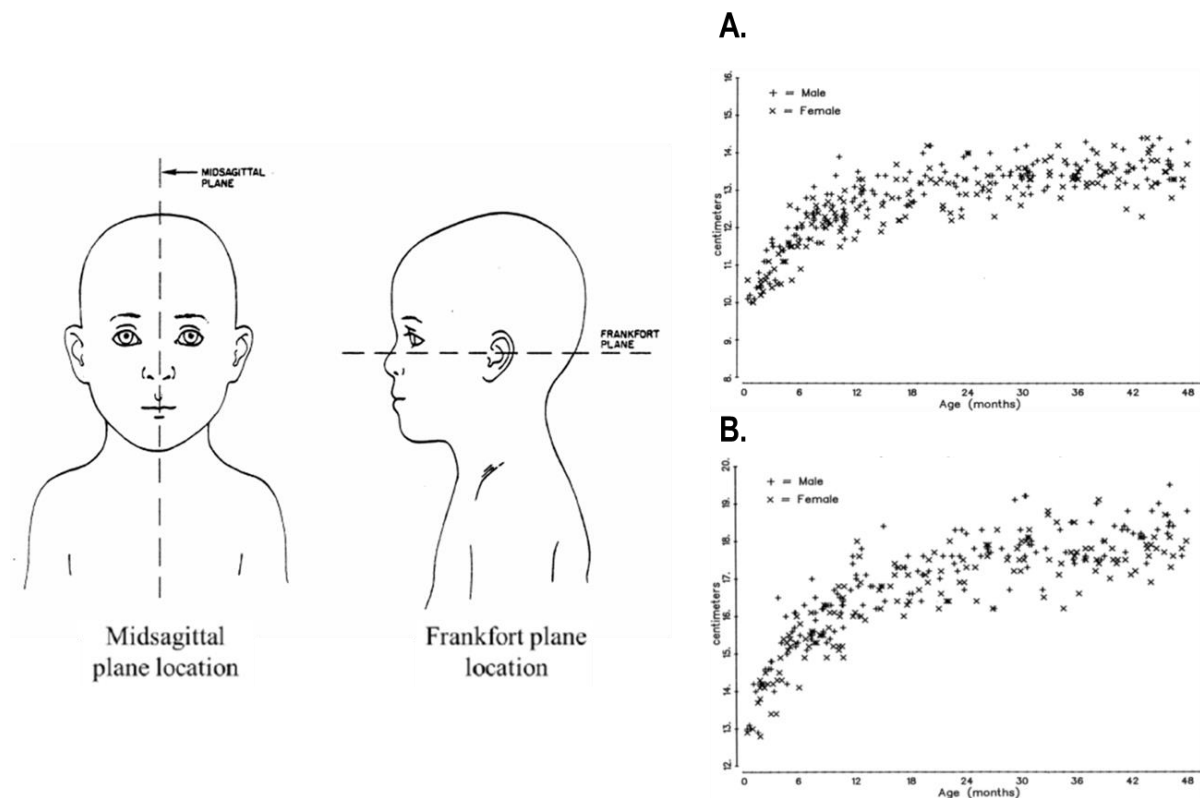


**Figure 2.12:** Reference planes for cephalometric measurements showing the midsagittal and Frankfort planes. Further measurements conducted across the width (from left to right bitemporal - **A**) and length (from most anterior to posterior points - **B**) with age (Adopted from Schneider *et al.*, 1986).

The biology, physiology and morphometric shape of the normative infant skull have been studied extensively (Beederman *et al.*, 2014). This has allowed clinicians to identify craniofacial abnormalities in the skull shape because of mechanical loading or genetic mutations. A major condition affecting the craniofacial system is craniosynostosis, caused by early fusion of cranial sutures (Cunningham & Heike, 2007).

In summary, key physiological parameters will be taken forwards to be implemented in the overall modelling framework of this thesis. This includes the rate of suture closure, the rate of bone healing, and the rate of intracranial volume expansion and how these will be simulated in the model.

## 2.2 Craniosynostosis

Craniosynostosis, defined by the premature closure of one (nonsyndromic) or multiple (syndromic) sutures, leads to compensatory growth perpendicular to the closed suture (Cunningham & Heike, 2007). To broadly examine the extent of Craniosynostosis, a summary of the categories of craniosynostosis will be discussed (Figure 2.13). In addition, with an emphasis on sagittal craniosynostosis, the method of diagnosis, surgical options, postoperative management, and comparative studies will also be explored.

### 2.2.1 Variations of Craniosynostosis

**Metopic Craniosynostosis (trigonocephaly):** Premature metopic fusion presents a distinct triangular shape forehead as the frontal bones undertake an angular malformation with an apexed intersection across the fused suture, forming a “quizzical” appearance across the orbits. Its occurrence rate is minimal to that of other forms, representing less than 10% of all diagnosed cases (Blaser, 2008).

**Sagittal Craniosynostosis (scaphocephaly):** As the most prevalent form of craniosynostosis, representing 40-60% of cases (Blaser, 2008), sagittal craniosynostosis develops a frontal bossing and occipital bulging, due to the patent metopic and lambdoid sutures. A severe cranial width reduction occurs, which is accommodated by a flat vertex surface. When amalgamated, the compensatory growth creates a distinct ‘boat-shaped’ appearance. Most cases are diagnosed as nonsyndromic (Blaser, 2008).

**Unicoronal Craniosynostosis (anterior Plagiocephaly):** Coronal craniosynostosis results in larger craniofacial distortion than the former variations due to the retrusion across the superior orbital region. For compensation, a distinct bulge is present across the opposite coronal suture, leading to an asymmetry of the forehead. Its prevalence is higher than that of metopic craniosynostosis, accounting for 20-30% of cases (Blaser, 2008).



**Bicoronal Craniosynostosis:** While unicoronal cases are typically nonsyndromic, bicoronal craniosynostosis is more common in syndromic patients. As frontal growth is almost completely restricted, the forehead appears to protrude excessively.

**Lambdoid Craniosynostosis (posterior Plagiocephaly):** As occipital growth is restricted to a single lateral region, a “mastoid lump” compensates for this lack of volume. Frontal flattening has been observed in cases of lambdoid synostosis (Blaser, 2008). As the least common form, representing less than 5%, bilateral lambdoid craniosynostosis (i.e., both lambdoid sutures) is rarely seen. Further, it has been reported to result in extreme syndromic deformations, such as that of rhombencephalosynapsis (Blaser, 2008).

Although distinct morphological characteristics can commonly be identified at birth, radiological imaging and genetic testing may be required to fully diagnose a patient’s form of craniosynostosis.

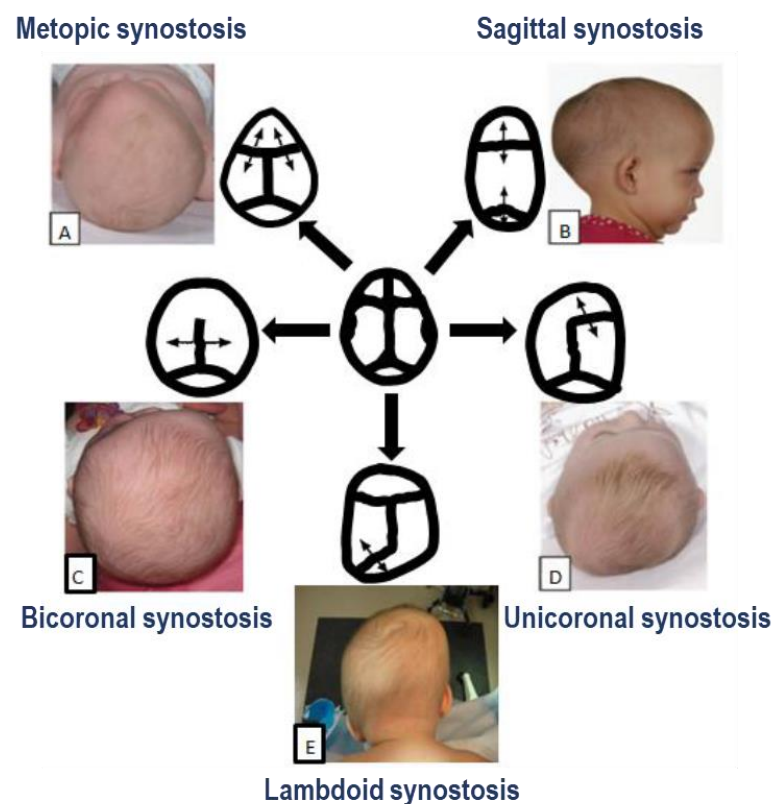


**Figure 2.13:** Variations of Craniosynostosis deformations (Adopted from Johnson & Wilkie, 2011).

### 2.2.2 Methods of diagnostics

Craniosynostosis patients usually display head shape abnormality around 3 months of age if not earlier. Nonetheless, they usually undergo medical imaging assessment (i.e., CT, MRI) to confirm the type and severity of the condition. Further to this, upon the suspect of multiple fusions, modern technological advancements in genetic testing can accurately identify syndromic forms of this condition. These advancements have aided in identifying more cases of craniosynostosis although it is unknown if the increase in prevalence is a result of such advancements or other factors (Cornelissen *et al.*, 2016).

**Medical imaging:** The most common standard of care for identifying the extent and presence of suture fusion is through computed tomographic (CT) imaging, as partial patency could still be presented across the closed suture, warranting such an approach for full diagnosis (Calandrelli *et al.*, 2014). Radiological 'slice' images are performed across the bilateral, transverse, and anteroposterior planes with millimetres separating the distance between image slices. The quality of these images can vary depending on the scanners and can be measured as the size and quantity of pixels (known as voxel size). Although the detail and quality of CT imaging have improved, others advocate ascertaining the diagnosis using less invasive options. Some perform simple physical examinations (i.e., based on feeling across the suspected fused suture) over CT imaging, arguing a cost reduction, ionizing radiological effects and sedation needed for the latter method (Fearon *et al.*, 2007).

**Genetic identification:** Various genes have been identified to be responsible for craniosynostosis. Genetic tests are usually carried out to determine if the condition is syndromic or non-syndromic.

Syndromic craniosynostosis stems from an inherent generic mutation that is passed down from generation to generation. Cases of syndromic craniosynostosis results in additional ligament dysmorphology and craniofacial abnormalities as well as calvarial deformation

Non-syndromic craniosynostosis is caused by a sporadic generic mutation with no links to have inherited the condition from a previous generation. Typically, such cases only impact the morphology of the skull.

A majority of syndromic craniosynostosis cases are associated with mutations of the fibroblast growth factor (FGF) pathway, modulated by twenty-two signalling molecular cells associated with bone growth (Kimonis *et al.*, 2007). Each FGF is represented by several receptors (FGFR), in which FGFR1 to 3 have been associated with severe forms of craniosynostosis, known as Pfeiffer, Apert, Crouzon, and Muenke syndromes. Non-activating FGFR have been further linked to the TWIST 1 genes, a transcription factor that aids in the activation process of receptors (Kimonis *et al.*, 2007). Although 180 different forms of syndromic craniosynostosis exist within genetic identification, these advancements allow for the separation of syndromic and non-syndromic patients (Wilkie *et al.*, 2000).

Once the diagnosis for craniosynostosis has been performed, surgical correction is recommended. The surgeon's option for correction is determined by several factors, including the age of presentation, level of deformation, and whether the case is syndromic or non-syndromic. For non-syndromic sagittal craniosynostosis, many surgical methods have been developed and are used clinically in today's craniofacial centres.

### **2.2.3 Surgical options for sagittal Craniosynostosis**

The primary cosmetic goal for all forms of sagittal synostosis correction is to reduce the anteroposterior overgrowth and allow for bilateral and vertex widening. Individual craniofacial centres have adopted a previously used surgical corrective method or developed their own approach. Nonetheless, these techniques fall into two common corrective groups: invasive and minimally invasive techniques. An example of invasive techniques includes total calvarial remodelling, while examples of minimally invasive techniques include strip craniotomy and spring-assisted cranioplasty (e.g., Simpson *et al.*, 2017; Mathijssen, 2015 - Figure 2.14). The following sections provide an overview of some of the main techniques currently used for the management of sagittal synostosis.

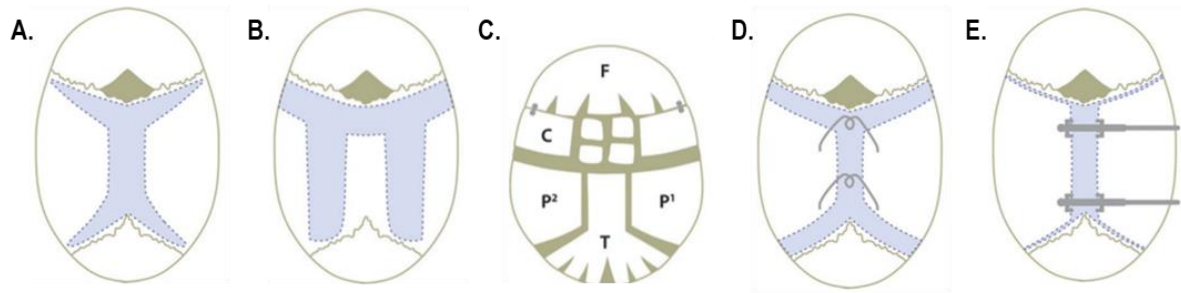


**Figure 2.14:** Compilation of various surgical methods for sagittal synostosis. Renier's 'H' technique (A), Pi-plasty (B), The Melbourne technique (C), Spring assisted craniectomy (D), Distraction osteogenesis (E) (Adopted from Simpson *et al.*, 2017).

**Strip craniectomy:** First developed by Lane in 1892, the strip craniectomy (removal of the fused suture) is widely recognised as the first surgical option for scaphocephaly (Faber & Lane, 1962). Simple extraction of the fused sagittal suture from bregma to lambda is performed, with diverse cosmetic outcomes. Due to the advantages of rapid growth and accelerated bone regenerative abilities, many craniofacial centres now adopt the strip craniectomy approach, with several modifications made.

**Renier's H technique:** An example developed by Renier in 1980 (Rocco *et al.*, 2012) is dubbed the 'H' technique, named after the distinctive shape, made by the excised bone. Much like the Lane technique, a wedge of bone, measuring approximately 4 cm in width, is removed across the sagittal suture. The removed rectangular wedge is then shortened and then replaced in the skull. Four wedges of triangular bone are then removed bilaterally across the parietal bone, two posterior to the coronal suture and two anterior to the lambdoid, creating a rectangular 'flap' to encourage skull widening. Patients then remain in hospital 2 days post-surgery. The surgery is hailed for its immediate cosmetic improvement and the lack of required helmet treatment to assist with postoperative morphology. The risk of this technique involves the need to perform at a relatively young age (less than 6 months) for optimal long term outcomes (Rocco *et al.*, 2012). However, a younger intervention age has reportedly led to higher levels of blood loss and, potentially, secondary closure of the coronal suture (Melo *et al.*, 2013).

**Modified 'H' Technique:** Micovic *et al.*, (2016) built on the premise of Renier's method using a more invasive triple square extended osteotomies approach. Three-square fragments of removed sagittal bone form over the under-sinus without dissection of the bone itself from the underlining dura. The number of triangular wedges created bilaterally from the removed sagittal bone varies between two or more. In severe deformities, to promote anteroposterior reduction, the excision of the coronal suture is also performed to further counter the restenosis (i.e., re-fusion) of the respective sutures. The procedure also benefits from a lack of required fixators, so that no postoperative intervention is needed.

**Pi-plasty:** Developed in the early 21<sup>st</sup> century, the pi-plasty procedure described by Guimarães-Ferreira *et al.*, (2001) further elaborates on the Lane premise. Extensive extraction of the coronal and lambdoid sutures is performed towards the squamosal parietal bones, creating a large bony flap on either side. Rectangular bone strips extending anteroposterior across the vertex are created on either side of the closed sagittal suture, leaving a 10-20 cm strip of bone across the sagittal sinus. In modified cases, additional 'flaring' (bending of bone) across the occipital and frontal bones may be performed, to rectify the overgrowth of scaphocephaly (Guimarães-Ferreira *et al.*, 2001). An acceptable level of changes to the cephalic index (achieved by calculating the width divided by the length and multiplying by a hundred) was also captured from pre-operative (~ 65) to 3 years postoperative (~ 72), however, did not achieve normal mean cephalic index values at the same age range ( $79.76 \pm 5.56$ ), as reported by Likus *et al.*, (2014).

**Endoscopic strip craniectomy:** Although improvements in the skull shaping are seen between techniques, surgeons remain concerned about the level of blood loss across these approaches. To improve this, a minimally invasive endoscopic approach, detailed by Dr. Jimenez and Dr. Barone in the 1990s and described by Proctor (2014), utilised the method of keyhole surgery (i.e., minimal incision across the scalp to reach the calvarial bone) to perform small scale osteotomies. Although the level of biparietal barrel staving osteotomies may vary from centre to centre, it is standard procedure to remove 1 cm of bone across the sagittal suture.

**Spring-assisted cranioplasty:** Lauritzen *et al.*, (1998) described an alternative method using distractor instrumentation to promote bilateral widening. Steel springs were placed within the craniotomy or placed within burr holes across the parietal bone. After full healing is achieved, typically by 3-5 months postoperative, the springs are removed in a secondary procedure. As the springs can be compared and created during the surgical procedure, differing levels of stiffness are optional and decided on the expertise of the surgeons (Borghi *et al.*, 2017). In addition, more extensive deformation results in more than the standardised two spring approach (Fischer *et al.*, 2021).

**Total calvarial remodelling:** Total calvarial remodelling is the most invasive method of correcting craniofacial abnormalities. Many variations exist for the management of sagittal craniosynostosis, and all follow the process of bone remodelling, bone rotation, and in some cases, the use of bioabsorbable fixators. Due to the invasiveness of these techniques and the high volumes of blood loss, it is advocated that such procedures be performed later than 6 months of age (e.g., Greensmith *et al.*, 2008).

Although the method of correction and level of invasiveness in bone extraction is highly determined by the surgeon's judgment, literature has discussed a parameterised approach. One such method, known as the Melbourne technique, documented by Greensmith *et al.*, (2008), involves an extensive rotation-based approach to bone remodelling performed in a single surgical phase. A 180- and 90-degree rotation of the coronal and occiput flaps are performed, respectively. Due to the extent of correction, a noticeable correction of the skull shape is seen postoperatively and near normalisation of the cranium has been reported (Greensmith *et al.*, 2008). Instances of postoperative elevated intracranial pressure (ICP) have also been seen when undertaking TCR, although it is uncommon (Thomas *et al.*, 2015). Surgeons also argue the benefits between cosmetic appeasement and the higher costs of surgery (Jivraj *et al.*, 2019).

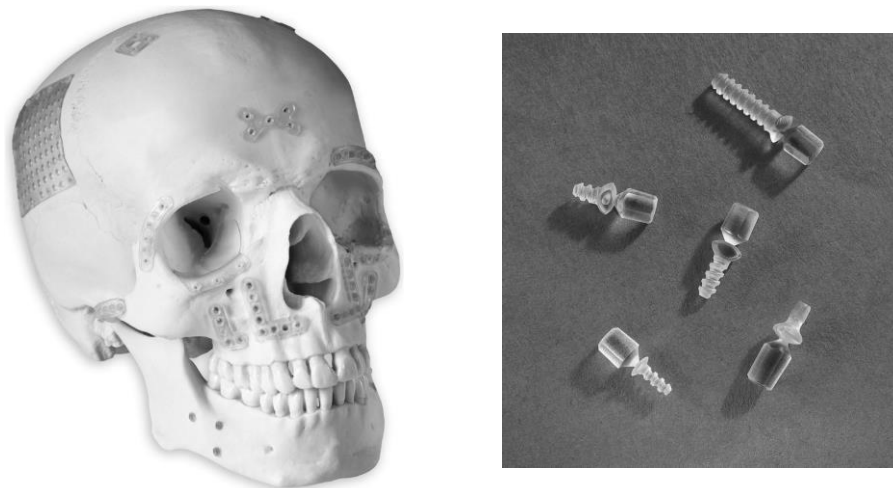


**Figure 2.15:** An example of various geometric bio fixator shapes used during calvarial reshaping and craniofacial surgery (left). A close-up of the absorbable screws used to constrain the plates into position (right) (Adopted from Ahmad *et al.*, 2008).

The addition of self-reinforced bioabsorbable fixators aids to constrain the bony elements after surgery (Figure 2.15). Such devices retain a high level of structural stiffness upon insertion, approximately 2000 MPa (Landes *et al.*, 2006). Suitable biocompatibility and natural progressive degradation have made fixators a favourable alternative to titanium plating and wiring methods, as no secondary procedure is necessary (Ashammakhi *et al.*, 2004). Although the rate in which degradation varies from case to case, partial resorption is noted 3 months after insertion (Ashammakhi *et al.*, 2004).

**Helmet therapy:** In the early 1990s, the prospect of supplementing a helmet-based approach for assisting postoperative growth was introduced in addition to endoscopic surgery (Jimenez and Barone, 1998). Devices range in appearance, constraints, and quantity following the severity of the patient's deformation (Figure 2.16).



**Figure 2.16:** Moulded helmets for Craniosynostosis patients. Used for the correction of trigonocephaly (left) and sagittal Craniosynostosis (right) (Adopted from Delye *et al.*, 2018).

As described by Delye *et al.*, (2018), the technique's levels of corrective success stem from the postoperative helmeting than the surgical craniotomy performed, constraining the frontal and occipital bossing while encouraging bitemporal widening. To enhance the surgical goals, advocacy for surgery is noted as early as 3 months of age. The patient's helmet therapy (post-modelling of the device) traditionally begins within two weeks post-surgery, wearing the device for 23 hours and continues until the age of 1 to 1.5 years, maintaining an average length of 10 months in total (Delye *et al.*, 2016). Although other centres have maintained an earlier removal time of 5 to 6 months after surgery (Proctor, 2014) as the surgical teams must consider the rapid changes in skull and brain volume, it is common practice for patients to alternate helmet sizes as they grow older. The quantity can vary but maintains between 1 to 3 various helmet sizes being required throughout treatment (Delye *et al.*, 2018).

Considerations of the hospital and patient treatment costs have been reported (Chan *et al.*, 2013). The mean costs of performing the endoscopic procedure, coupled with the utility costs of helmet production range in the value to \$4200 per patient. This was compared to the costs of performing TCR procedures, reported to be overall more expensive than helmet treatment (Chan *et al.*, 2013).



## 2.2.4 Postoperative management

As the level of corrective achievement can differ, a universal method for evaluating the changes in morphology and neurofunctional is essential to estimate the level of postoperative success. Studies have suggested several methods to assist surgeons in correctly identifying complications early, to minimise the risk and need for reoperation.

**Cephalometric measurements:** The most consistent and basic method of assessing cephalic changes is measuring the length and width of the skull during growth. These measurements allow surgeons to parameterise and track the normalisation of the shape using the cephalic index, a method first adopted by Andres Retzius (1796-1860) and calculated by dividing the width by the length, then multiplied by a hundred. Clinicians have used this approach to assess the overall average values within the normal population, allowing craniofacial surgeons to estimate the effectiveness of the corrective process. Likus *et al.*, (2014) performed a clarification study on 180 healthy individuals to access this normocephalic range in the first three years of life. The average cephalic index value was  $81.45 \pm 7.06$ , although interestingly, between the period of two and three years, this value was seen to relapse to 79.76.

**Neurofunctional attainment:** Although the purpose of sagittal craniosynostosis correction is primarily cosmetic adjustment, studies have reported the impacts surgery can have on neurofunctional aspects later in life (Gewalli *et al.*, 2001; Bellew *et al.*, 2011). Currently, centres investigate the impacts of their preferred methods on functional outcomes. Extending from this, others perform comparative assessments against the normal population's functionality. Although not every centre may track these outcomes, this is an ongoing debatable area among the craniofacial community and of high interest to the parents of children affected by craniosynostosis.

The assessment of evaluating developmental attainment falls into various analysing methods. A number of studies compare outcomes against a normal population while others opt for a pre vs. postoperative comparative approach (Bellew *et al.*, 2005; Bellew *et al.*, 2011; Speltz *et al.*, 2007). In either circumstance, there are focal regions of interest across these studies.

Due to the complexities of corrective techniques and the natural responses human cerebellums incur, the risks of developing one type of functional defect may be higher than others. This was assessed by Becker *et al.*, (2005), by evaluating 214 patients across a timeline of 18 years after corrective surgery. Their interest was within patients' postoperative speech, psychological and school performance attainment and whether the abnormalities could progress with age. Their observations, shown in Figure 2.17, showed that 39 % of patients (27 out of 70) treated for scaphocephaly experienced greater abnormalities when compared with other forms of craniosynostosis (i.e., unilateral, and bilateral coronal and lambdoid synostosis). Such data was, however, not compared to the normal control population.

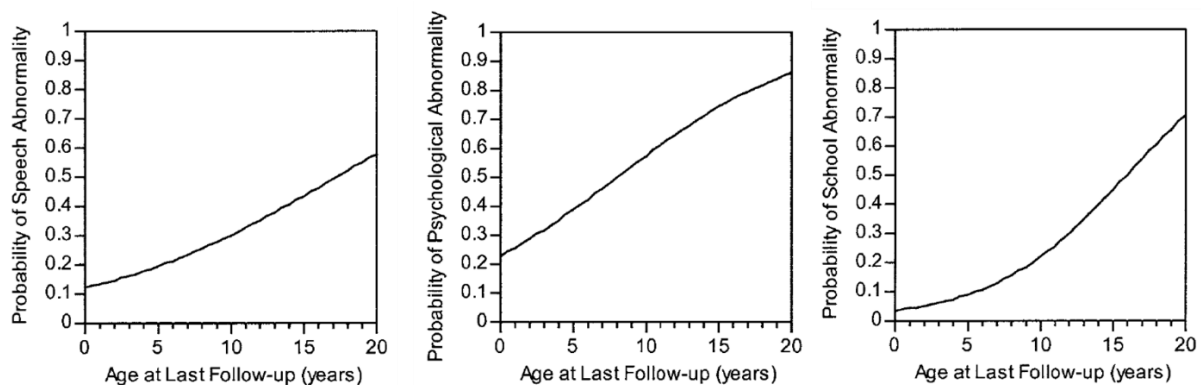


**Figure 2.17:** Logistics graph showing the probability of defects occurring overtime within a region of functionality or 214 postoperative patients (Adopted from Becker *et al.*, 2005).

Contrarily, other studies report improvements with age. The study by Bellew *et al.*, (2011), investigated aspects of locomotor functionality, speech and hearing, hand-eye coordination, and general school performance across a 5-year follow up timeline. Improvements in locomotor functionality were seen after surgery and continued into the follow up observational period. However, areas of developmental attainment were lower than comparative normal population readings.

These studies highlight the importance of assessing functional capabilities, proving to potentially be a greater issue than the initial calvarial deformities. As such, many

studies demonstrate various outcomes and assessing a wide range of these functionalities is critical.

**Intracranial hypertension:** One of the more life-threatening implications of craniosynostosis is the rise in intracranial pressure that can e.g., impact optic nerve leading to papilledema. Although surgery may avoid such complications, postoperative monitoring is advised in cases of pre-operative papilledema watching whether, in unusual circumstances, these complications may resurface. Thomas *et al.*, (2015) have reported such an instance, where raised intracranial pressure was observed after invasive surgical correction in 1 in 20 patients, 51 months after correction. Although such an occurrence within a cohort of 128 patients is minimal, it is, nonetheless, not be overlooked.

Although monitoring the levels of intracranial pressure is a viable method of surveying patient wellbeing, other studies by Van De Beeten *et al.*, (2019), removed the need for invasive observations by recording the occurrence of postoperative headaches in individuals undergoing one of two surgical techniques via questionnaires.

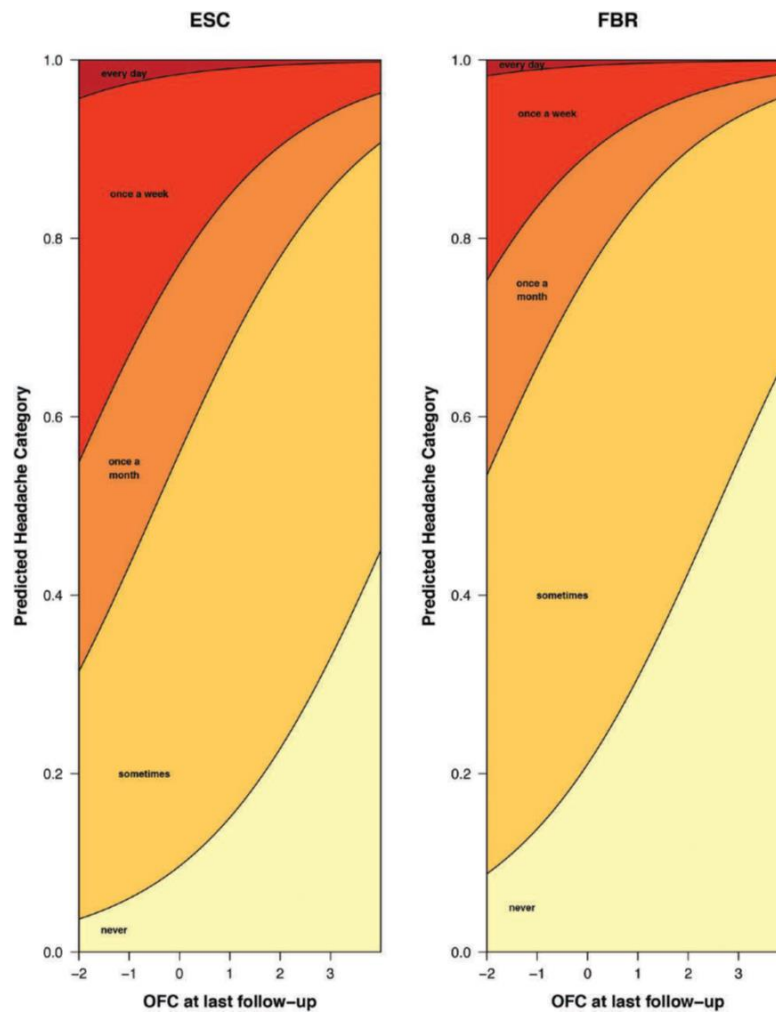


**Figure 2.18:** Occurrence rates of headaches experienced in corrected individuals in sagittal synostosis. Two plots were created which compare the frequency in patients undergoing extended strip craniotomy (ESC – left) and frontobiparietal remodelling (FBR – right). The study further correlates the changes in occipitofrontal head circumference (OFC) with this frequency at each follow up timepoint (Adopted from Van de Beeten *et al.*, 2019).

Although the outcomes found the rate of headaches to be within the “normative” range, they appeared to differ between corrective techniques (Figure 2.18). As such, the clinic maintains that a questionnaire of the patient’s physical and mental condition is an important aspect of postoperative management. Further, the chosen technique could play a role in altering the outcomes of surgery.

**Calvarial defects:** The traumas of surgery across calvarial tissues can lead to profound interruptions of the natural biological processes. These include circumstances of lack of reossification (i.e., bone-forming across exposed surgical areas) after surgery (Figure 2.19). The direct influence that causes such cases is still

unclear. But reports behind such cases attempt to understand what may impact a lack of or delayed healing in postoperative individuals.

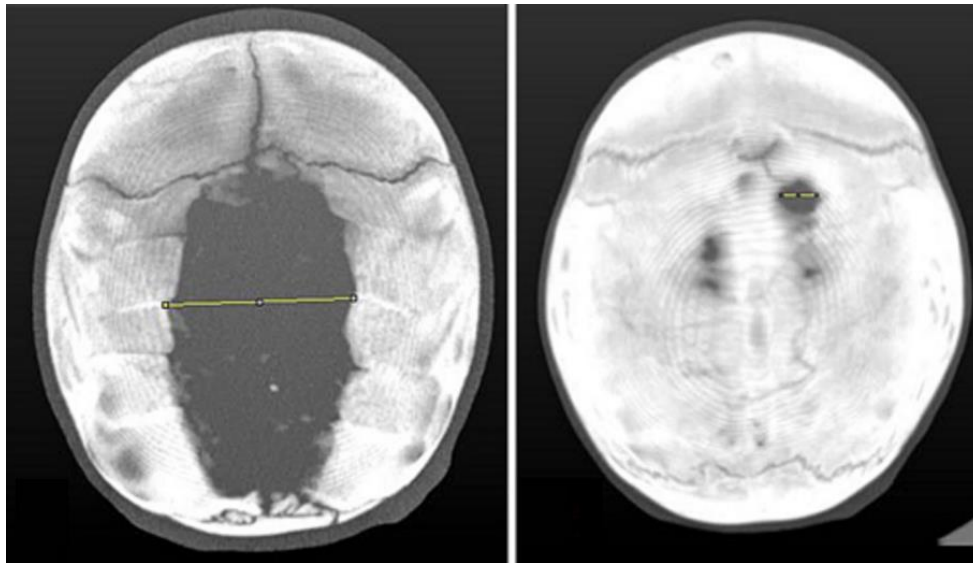


**Figure 2.19:** Comparison of patient-specific defect data undergoing endoscopic assisted suturectomy. A 5 cm craniotomy was created at 4 months of age, to which the bone growth rate was measured under two points across the surface (left). Visible minor defects are still present in the patients 2 years after surgery (right) (Adopted from Thienier-Villa *et al.*, 2018).

Though limited in human studies, Thienier-Villa *et al.*, (2018) attempted to understand the timing of calvarial healing under differing craniotomies. A clinical follow up of endoscopic-assisted suturectomy, open suturectomy (See: Faber & Lane, 1962), and fronto-orbital advancement surgical options were analysed. Out of the 216-patient cohort, 92 (42.5%) achieved complete closure of the created defects, while 12 patients (5.5%) indicated a significant lack of formation. Further, such severe cases were captured in patients in which surgical defects spanning greater than 5 cm, achieving a bone growth rate average of 0.3 to 0.8 mm for every month of age.

Skolnick *et al.*, (2019) continued the study of calvarial defects across both total calvarial remodelling and endoscopic treatments. Defects in patient data were defined as greater than 1 cm<sup>2</sup> in size, which were tracked throughout postoperative recovery. 74 defects, monitored over course of one year after surgery, were seen. A faster rate of closure was recorded across the parietal and frontal bone plates, echoing the findings of Thienier-Villa *et al.*, (2018), 9 cm<sup>2</sup> size defects have only a 10% probability of closing to 2.5 cm<sup>2</sup> by the first postoperative year.

As skeletal maturity is reached, the regenerative bone healing capabilities in mammals begin to wane. Alleyne *et al.*, (2016) investigated the sizes of cranial defects in mature and infant rat specimens. It was seen that defects performed at the age of postnatal day 6 (P6) achieved the highest rate of healing and were seen to regress as defects were performed at a later age (i.e., P20 and P84). The study provided a good understanding of the risks of correction at a later age.

### 2.2.5 Comparative studies for optimising sagittal Craniosynostosis

Reports within this area of literature explore factors considered by surgeons, such as the intervention age, chosen technique, and resulting costs (Chan *et al.*, 2013). Studies prioritise the comparison of the aesthetic outcomes of the skull, while observations in neurofunctionality remain limited. Table 2.2 summarises some of the studies that have compared the clinical outcomes of different surgical techniques for the management of sagittal craniosynostosis.

**Cephalometric comparisons:** Reports examining cosmetic outcomes have been published since the early '90s. A study from Panchal *et al.*, (1999) expressed a lack of literature on the topic of surgical technique comparisons and timing of intervention during this period. A retrospective quantitative analysis involving a total of 40 infants explored the changes in outcomes between TCR and strip craniectomy (Here, the Renier's H or Pi plasty procedure) treated patients. To analyse the timing of intervention, the extended strip group was further subdivided between those undergoing surgery before and later than 4 months of age. Although no statistical significance was found in the cephalic index between the aforementioned groups, both groups did exhibit a relapse in the cephalic index by twelve months follow up. In contrast, TCR showed minor difference by follow up vs. the strip procedures. Improvements in the cephalic index were seen across all groups but did not reach the normative age-matched range. Despite this, the report advocated that TCR procedures provide more reliable cosmetic satisfaction.

More recently, Thomas *et al.*, (2015) compared the clinical outcomes between a modified strip craniectomy, where a 5 cm vertex strip of bone was removed, and a

variation of total calvarial remodelling. The study benefited from an extended follow up period of up to 9 years. Patients undergoing strip at an age older than six months were divided against those performed earlier. Minor difference was seen across the two age groups, in which 15% to 18% reached a cephalic index greater than 75. Overall, 31% of patients undergoing extended strip achieve a greater cephalic index by one year postoperative versus preoperative, while the calvarial remodelling treatment achieved a greater cephalic index in 62% of patients. Such observations agreed well with the findings of Panchal *et al.*, (1999), justifying the centre's choice to favour the latter approach over the former.

A study that rebuts such findings come from Gerety *et al.*, (2015), who suggested less invasive forms of correction can equal the cephalic index seen in TCR. The meta-analysis reported outcomes in spring-assisted cranioplasty (SAC) procedures as well as strip craniectomy for comparison. While poorer outcomes in the strip procedure were seen, the spring technique produced a statistically insignificant difference against the total remodelling procedures. An emphasis on hospital costs, blood loss and length of hospitalisation were further examined, in which all were halved within the spring-mediated group when compared to strip craniotomy.

Continuing from this, Le *et al.*, (2014) further advocated the lack of long-term cephalic differences between minimally invasive and complete remodelling techniques. Endoscopic procedures which included bilateral barrel-staving, as well as postoperative helmeting, were the chosen form of non-invasive correction, allowing minimal blood loss and operation time. The study reported that, by three years postoperative, no significant difference was seen across the measured parameters across both surgical techniques although the study is limited regarding the size of medical data used. Subsequent later studies by Isaac *et al.*, (2018) agreed with such findings, where less invasive methods proved more beneficial than more excessive corrective types.

Recently, Al-shaqsi *et al.*, (2021) expanded on the number of patients used under the previously discussed techniques. The timing of follow up examination differed here, in which endoscopic and total calvarial remodelling patients were observed 5 months and 20 months postoperative, respectively. Despite this shortcoming, both techniques

established a well-rounded cephalic outcome, which was compared to the lay-public and matched or exceeded the 70% satisfaction benchmark.

Although studies have performed a comparative analysis between the low and high invasive options, others have focused on comparisons between the minimally invasive surgical methods. Magge *et al.*, (2019) compared the use of helmet therapy for endoscopic correction against that of the commonly used 'Pi'-Plasty technique. Both techniques' findings suggest greater improvement by three years postoperative but were more in the favour of the helmet therapy technique.

There are also considerations within the use of distractors for spring-mediated procedures. Clinicians have also investigated how greater than two springs, of which is the standardised number to use, can impact the morphology. This was considered by Fischer *et al.*, (2021), who examined a three-year follow up period across 112 patients who differed from being treated with two or three spring distractors. Greater long term improvements to the cephalic index were captured in the 3 spring cases (increasing by a mean of 6.0) compared with the two springs (mean increase: 3.6), which was seen across the complete follow up timeline.

Skolnick *et al.*, (2021) provided an anthropometric analysis of outcomes across both SAC and endoscopic-assisted craniotomy with helmet therapy procedures between two surgical centres. Their collaborative study examined 67 patients and quantified the level of changes in the cephalic index. Under the condition of maintaining helmet therapy for 7.6 months and spring placement for 4.6 months, the former technique provided the greatest cephalic index change (9% improvement) vs. the latter (7% improvement) when quantified at 16.7 and 19.7 months of age, respectively.



**Table 2.2:** Cephalometric measurements reported by each published study.

| Author:                      | Subjects (n): | Surgical option: | Age at surgery (Mean months): | Preoperative CI: | Follow up age (months): | Follow up CI:          |
|------------------------------|---------------|------------------|-------------------------------|------------------|-------------------------|------------------------|
| Panchal <i>et al.</i> , 1998 | 15            | ESC              | 2.9                           | 67               | 12                      | 72                     |
|                              | 13            | ESC              | 7.6                           | 66               | 12                      | 70                     |
|                              | 12            | STC              | 5.2                           | 66               | 12                      | 74                     |
| Taylor & Maugans, 2011       | 7             | SAC              | 3-4                           | 65               | N/A                     | 78                     |
|                              | 7             | SC               | 2-3                           | 65               | N/A                     | 78                     |
| Le <i>et al.</i> , 2014      | 33            | ESC              | 3.3 ± 0.1                     | N/A              | 24                      | 74.4                   |
|                              | 13            | TCR              | 5.1 ± 0.5                     | N/A              | 24                      | 76.4                   |
| Thomas <i>et al.</i> , 2015  | 162           | TCR              | 16.9 (8.0-139.3)              | 66.7 ± 4.3       | 12                      | 76.1 ± 4.1             |
|                              | 41            |                  |                               |                  | 60                      | 75.6 ± 3.4             |
|                              | 17            |                  |                               |                  | 108                     | 76.7 ± 3.4             |
|                              | 34            | MSC              | < 6                           | 65.7 ± 4.7       | 12                      | 73.3 ± 5.2             |
|                              | 24            |                  |                               |                  | 60                      | 71.5 ± 4.3             |
|                              | 17            |                  |                               |                  | 108                     | 71.7 ± 4.8             |
|                              | 28            | MSC              | > 6                           | 68.6 ± 3.5       | 12                      | 72.1 ± 5.2             |
|                              |               |                  |                               |                  | 60                      | 72.5 ± 3.5             |
|                              |               |                  |                               |                  | 108                     | 71.0 ± 3.5             |
| Gerety <i>et al.</i> , 2015  | 187           | TCR              | 8.4                           | N/A              | 28                      | Improved by 8.95 ± 2.8 |

## Chapter 2: Literature review

|                               |     |                 |               |                |                 |                            |
|-------------------------------|-----|-----------------|---------------|----------------|-----------------|----------------------------|
|                               | 299 | SC              | 4.0           | N/A            | 28              | Improved by $6.40 \pm 2.1$ |
|                               | 187 | SAC             | 5.0           | N/A            | 28              | Improved by $6.42 \pm 2.1$ |
| Isaac <i>et al.</i> , 2018    | 187 | ESC             | 2-4           | N/A            | 36              | Improved by $8.5 \pm 0.1$  |
|                               | 20  | CVR             | 11.8-23.8     | N/A            | 45              | Improved by $1.2 \pm 0.1$  |
| Magge <i>et al.</i> , 2019    | 30  | ESC-H           | $3.1 \pm 1.1$ | 68.5           | $23.2 \pm 12.2$ | 76.7                       |
|                               | 21  | PP              | $5.0 \pm 2.6$ | 68.4           | $31.4 \pm 20.1$ | 71.9                       |
| Fischer <i>et al.</i> , 2021  | 55  | SAC (2 springs) | $3.9 \pm 1.1$ | $72.1 \pm 4.1$ | 6.0             | $77.0 \pm 3.5$             |
|                               |     |                 |               |                | 36              | $74.6 \pm 4.3$             |
|                               |     | SAC (3 springs) | $3.7 \pm 1.5$ | $70.7 \pm 4.3$ | 6.0             | $77.0 \pm 4.4$             |
|                               |     |                 |               |                | 36              | $74.8 \pm 3.7$             |
| Sholnick <i>et al.</i> , 2021 | 40  | ESC-H           | $3.0 \pm 0.9$ | $70.1 \pm 3.6$ | $16.7 \pm 2.5$  | $77.0 \pm 3.8$             |
|                               | 27  | SAC (2 springs) | $4.6 \pm 0.9$ | $71.2 \pm 5.2$ | $19.7 \pm 3.4$  | $74.3 \pm 4.2$             |

**ESC:** Extended strip craniectomy; **STC:** Sub-total calvarectomy; **SAC:** Spring-assisted cranioplasty; **SC:** strip craniectomy; **TCR:** total calvarial remodelling;

**ESC-H:** endoscopic strip cranioplasty with helmeting treatment; **PP:** Pi-Plasty.

**Neurofunctional defects:** The number of neurofunctional comparative studies are far fewer than cephalometric observations. Despite this, there remain reports of postoperative functional quality.

One well-known study by Hashim *et al.*, (2014) evaluated aspects of postoperative behavioural, visual motor and reading skills after correction. Two techniques were compared: forty-two patients treated with total calvarial remodelling and thirty treated with strip cranioplasty, a combination of modified 'Pi' and endoscopic strip cranioplasty. To estimate the impact of age on surgical treatment, both techniques were divided between before and after six months of age at the time of intervention. All patients were examined before the age of 10 years. Greater improvements were seen in the TCR cohort before 6 months intervention, with all functions showing improvement against all other surgical options. Patients treated at a later age were seen to lack the same level of improvement. The study illustrated that, in conjunction with the surgical type, the age at intervention may impact clinical outcome.

Care *et al.*, (2019) carried out a multidisciplinary study comparing various functional outcomes of children treatment for craniosynostosis across the UK. Gross motor, and fine motor skills along with behavioural responses were examined across the average age groups at 36, 42 and 48 months of age. Outcomes were determined by a series of questionnaires completed by patient guardians. Shape normalisation was estimated against that of the normal population. Discrepancies were found in four out of five functions, regarding gross motor and fine motor skills by 48 months of age. Behavioural outcomes were shown to be normalised. Importantly, only 51% of questionnaires were complete for analysis. Further, the nature of correction and timings of intervention were unavailable.

Gewalli *et al.*, (2001) assessed the patients treated under the Pi plasty technique by comparing the postoperative outcomes with their pre-operative states. Although there were limitations in sample sizes (twenty-six patients in total), the study benefited by correlating defects in functionality with raised ICP. All patients underwent correction at the mean age of 7 months. Absorbable fixators were used to secure the frontal bones and improve the anteroposterior overgrowth *in situ* (during surgery). By 16 months of age, only two patients were seen to have a 'below average' score across hearing,

## Chapter 2: Literature review

speech, locomotor, and social behavioural assessments. Interestingly, no abnormalities were captured within the ICP analysis, suggesting that neurofunctional defects and raised ICP could be mutually exclusive.

Bellew *et al.*, (2019) used a similar methodology of comparing patients pre-operative and postoperative functional characteristics to examine those treated with a modified version of Renier's 'H' procedure before 7 months, between 7 and 12 months and after 12 months of age. The study further benefited from longitudinal postoperative examination groups at 6-7 months, 5 years, 10 years and 15 years. Locomotor, personal-social behaviour, and visual-motor functions were examined, in which defects in the former and latter observations at 10 years postoperative were detected at later intervention. The reverse was found in earlier treated patients, where functionality was even seen to improve. However, patient numbers treated earlier ( $n = 25$ ) and later ( $n = 8$ ) varied with some significance. Nonetheless, the study correlated well with the author's previous findings (Bellew & Chumas, 2015).

Chieffo *et al.*, (2010) explored the physiological outcomes of sixty-five total calvarial remodelling patients at an average intervention age of 7.2 months, with a monitoring follow up time scale of 12 years. Although fine motor, language and visual-spatial were all examined, the study classified abnormalities under the level of standard deviation, denoting greater than 2 as a 'severe defect' while 1 was classified as a 'mild' defect. Under this method, 14% of cases expressed severe or mild defects in attention maintenance although memory examinations were seen to be within the normative range. Despite no comparison being made to normative data, the report advocates that earlier treated patients displayed overall improved outcomes.

Although each study highlights improvements in functional outcomes, some advocating defects could be eradicated postoperatively. However, it remains unclear as to which technique option is most beneficial. Nonetheless, the studies reviewed here advocate earlier intervention over later for the most optimal outcomes.

In summary, studies which highlight the key postoperative morphological and, where possible, neurofunctional changes will be used for comparison against the model's predicted outcomes. Such studies may also be used in addition to acquired CT data.

## 2.3 Properties of biological tissues

An understanding of the biological mechanical properties around the human calvarial is vital to enable computational modelling of this system. Relative to this, three of the most studied biological tissues are the cranial bones, sutures, and the brain (Coats & Margulies, 2006). Studies attempted to investigate human cadaver samples. However, where limited, researchers refer to the use of animal specimens. This section explores the literature under both these specimen types. Three-point bending, tension, and compression mechanical testing have been undertaken to estimate the mechanical properties of biological tissues. An emphasis on the elastic properties of cranial bones, cranial sutures and brain is reported here, in preparation for finite element simulations that were conducted in this thesis and will be described in the following chapters.

### 2.3.1 Cranial bones

**Human studies:** In human, ossified bone is one of the strongest substances in the body (with enamel in the tooth being stronger). As the structure of bone rapidly changes with age, the properties of adult bone cannot directly correlate to that of human infant bone. Although there is greater availability of adult cadavers, infant cadavers are far less investigated. As such, this section will explore the material properties of both neonatal and adolescent skull properties, with a primary focus on mechanical point bending studies (Figure 2.20). Table 2.3 highlights all numerical values reported across the reviewed studies.

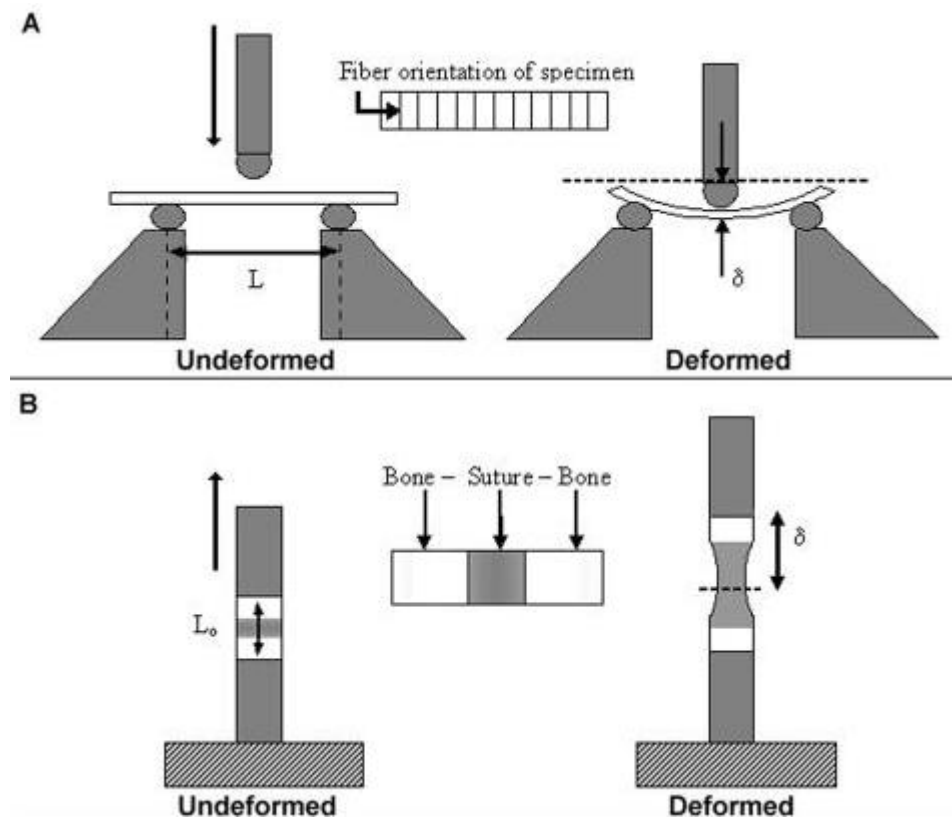


**Figure 2.20:** Schematic of the testing set-up for three-point bending of bone (A) and suture (B) specimens. An applied force was exerted across the samples, in which displacement ( $\delta$ ) occurs, allowing for the elastic modulus of materials to be calculated (Adopted from Coats & Margulies, 2006).

A prominent study in neonatal skull properties by McPherson & Kriewall (1980) investigated the mechanical bone stiffnesses during gestation in humans from 25 to 40 weeks of age. Under a method of three-point bending, the sensitivity of the elastic modulus was examined by alternating the axis in which testing was performed (perpendicular or parallel). It was found that when orientated along the long axis (here, anteroposterior) a higher elastic modulus was seen vs. the samples orientated perpendicular.

To further understand the biomechanics of fetal bone behaviour, the material properties of neonates were analysed by Kriewall *et al.*, (1981). Forty-five specimens ranging from 25-40 weeks gestation underwent three-point bending. For comparison, five specimens aged six years were also examined. Conclusively, a larger stiffness

was seen in six-year vs. 25–40-week samples in which the later age exhibited twice the elastic modulus vs. at gestation.

Marguiles & Thinbault (2000) researched the paediatric bone properties (elastic modulus) in both infants and porcine cadavers under three-point bending. The study extended the age range investigated by Kriewall *et al.*, (1981), where specimens estimated at 1 week post birth and 6 months of age were examined. Although larger sample sizes remained limited in human samples, younger aged samples exhibited an elastic modulus in the low megapascals (71.6 – 95.3 MPa) in contrast to infants at term who showed two orders of magnitude higher (2111.7 – 3582.2 MPa).

A highly cited study by Coats & Margulies (2006) investigated a similar time scale to that of McPherson & Kriewall (1980). Between the ages of 21 weeks of gestation and 12 months post-birth, the elastic modulus and, in addition, the elastic modulus, under the three-point bending methodology, were examined. The similarities in properties between the 28 week-gestation and 12 months samples appeared interchangeable, indicating an elastic modulus of 14.2 MPa and 16.2 MPa, respectively. It should be noted that only eleven samples were examined, potentially contributing to such a minor difference. On the contrary, later reports of bone properties from Wang *et al.*, (2014) would agree with such findings.

Recently, Ajami *et al.*, (2022) characterised the mechanical properties of extracted parietal bone samples across 12 patients undergoing sagittal craniosynostosis correction. Sample age groups between 3 to 8 months were reported using a three-point bending and reference point indentation approach. In conjunction with this, a micro-FE model was used to calibrate the properties of the cortical bone in both trilaminar and diploe structures of the specimens. Although the number of specimens were limited, the study highlighted the differences in the elastic modulus between the cortical bone in trilaminar ( $3973.33 \pm 268.4$  MPa) vs. that of the diploe structures ( $1958.17 \pm 563.79$  MPa). Based on these preliminary findings, it was suggested that routine CT examinations of bone structure be carried out prior to surgery henceforth.

**Animal studies:** While literature on human specimens is limited, animal bone sampling studies remain a favourable alternative. As such, to expand on the reviewed

## Chapter 2: Literature review

human studies, reports considering the rodent and porcine samples will be discussed, with all findings highlighted in Table 2.4.

Marguiles & Thinbault (2000), as stated previously, examined porcine samples in addition to human infants. While limited in reported observation, a sensitivity was undertaken in the loading rates of the 2-to-3-day old samples to assess its capabilities of trauma absorption. As seen in the human samples, values did not achieve the levels of elastic modulus typically seen in adults indicating the lack of the ability to resist large traumatic loads at such an age.

Moazen *et al.*, (2015) examined the property differences between normative and craniosynostosis diseased mice skulls at postnatal ages 10 and 20 days. The report's findings reflected that of human infants at six years of age, ranging between 4000 and 7000 MPa. Further, a large change in properties was captured in a normative or diseased bone in samples extracted from the frontal bones. However, this discrepancy was not captured across parietal bone samples.

Relative to the study published by Ajami *et al.*, (2022), questions have been raised to understand the differences in properties across inner and outer cortical bone regions. Zapata & Wang, (2020) performed a single-subject analysis under primate specimen. The study utilised a modern method of elastic modulus estimation under an ultrasonic technique, maintaining the integrity of samples during and after testing. Results highlighted the sensitivity of testing inner or outer laying in cortical bone, in which the highest levels of elastic modulus would alternate between the two regions.



## Chapter 2: Literature review

**Table 2.3:** Material properties of the biological tissues of cranial bone – Human-focused studies. **E** represents the elastic modulus.

| Author:                        | Method<br>(Load rate): | Specimen<br>type: | Age of sample:               | Region of extraction:          | E:              | Unit: |
|--------------------------------|------------------------|-------------------|------------------------------|--------------------------------|-----------------|-------|
| McPherson <i>et al.</i> , 1980 | Three-point bending    | Human             | 25 Weeks (gestation) $\pm$ 2 | Parallel - Right Parietal      | $1.30 \pm 0.60$ | GPa   |
|                                |                        |                   | 25 Weeks (gestation) $\pm$ 2 | Perpendicular - Left Parietal  | $0.12 \pm 0.01$ | GPa   |
|                                |                        |                   | 27 Weeks (gestation) $\pm$ 2 | Parallel - Right Parietal      | $0.94 \pm 0.41$ | GPa   |
|                                |                        |                   | 27 Weeks (gestation) $\pm$ 2 | Perpendicular - Right Parietal | $0.18 \pm 0.03$ | GPa   |
|                                |                        |                   | 28 Weeks (gestation) $\pm$ 2 | Parallel - Right Parietal      | $3.62 \pm 0.46$ | GPa   |
|                                |                        |                   | 38 Weeks (gestation) $\pm$ 2 | Parallel - Right Parietal      | $4.24 \pm 0.73$ | GPa   |
|                                |                        |                   | 38 Weeks (gestation) $\pm$ 2 | Perpendicular - Right Parietal | $0.84 \pm 0.19$ | GPa   |
|                                |                        |                   | 40 Weeks (gestation) $\pm$ 2 | Parallel - Right Parietal      | $4.01 \pm 1.28$ | GPa   |
|                                |                        |                   | 40 Weeks (gestation) $\pm$ 2 | Perpendicular - Right Parietal | $1.74 \pm 0.59$ | GPa   |
|                                |                        |                   | 40 Weeks (gestation) $\pm$ 2 | Parallel - Left Frontal        | $3.05 \pm 0.88$ | GPa   |
|                                |                        |                   | 40 Weeks (gestation) $\pm$ 2 | Perpendicular - Right Frontal  | $1.70 \pm 0.79$ | GPa   |
| Kirewall <i>et al.</i> , 1981  | Three-point bending    | Human             | 40 $\pm$ 2 Weeks (gestation) | Right Parietal - Left Frontal  | $3627 \pm 0.23$ | MPa   |
|                                |                        |                   | 38 $\pm$ 2 Weeks (gestation) | Right Parietal                 | $4413 \pm 0.67$ | MPa   |

## Chapter 2: Literature review

|                            |                                   |       |                          |                |             |     |
|----------------------------|-----------------------------------|-------|--------------------------|----------------|-------------|-----|
|                            |                                   |       | 27 ± 1 Weeks (gestation) | Left Parietal  | 1145 ± 1.11 | MPa |
|                            |                                   |       | 25 ± 1 Weeks (gestation) | Right Parietal | 1386 ± 3.91 | MPa |
|                            |                                   |       | 28 ± 1 Weeks (gestation) | Right Parietal | 3620 ± 5.04 | MPa |
|                            |                                   |       | 40 ± 2 Weeks (gestation) | Right Parietal | 3723 ± 2.32 | MPa |
|                            |                                   |       | 40 ± 2 Weeks (gestation) | Left Parietal  | 3296 ± 2.29 | MPa |
|                            |                                   |       | 40 ± 2 Weeks (gestation) | Left Frontal   | 3289 ± 1.75 | MPa |
|                            |                                   |       | 40 ± 2 Weeks (gestation) | Right Parietal | 2834 ± 5.14 | MPa |
|                            |                                   |       | 6 years                  | Left Parietal  | 7123 ± 586  | MPa |
| Marguiles & Thibault, 2000 | Three-point bending (2.54 mm/min) | Human | 25 Weeks (gestation)     | Left Parietal  | 71.6        | MPa |
|                            |                                   |       | 30 Weeks (gestation)     | Left parietal  | 95.3        | MPa |
|                            |                                   |       |                          | Right Parietal | 618.8       | MPa |
|                            |                                   |       | 6 Months                 | Left Parietal  | 2111.7      | MPa |
|                            |                                   |       |                          | Right Parietal | 2199.4      | MPa |
|                            | Three-point bending (2540 mm/min) |       | 25 Weeks (gestation)     | Left Parietal  | 43.8        | MPa |
|                            |                                   |       | 30 Weeks (gestation)     | Right Parietal | 444.5       | MPa |
|                            |                                   |       |                          | Right Parietal | 407.7       | MPa |
|                            |                                   |       |                          | Right Parietal | 445.4       | MPa |
|                            |                                   |       | 1 Week                   | Left Parietal  | 820.9       | MPa |
|                            |                                   |       | 6 Months                 | Left Parietal  | 2671.9      | MPa |
|                            |                                   |       |                          | Right Parietal | 3582.2      | MPa |

## Chapter 2: Literature review

|                            |                     |       |                      |  |                  |     |
|----------------------------|---------------------|-------|----------------------|--|------------------|-----|
| Coats & Margulies, 2006    | Three-point bending | Human | 28 Weeks (gestation) | Occipital                              | 14.2             | MPa |
|                            |                     |       |                      | Occipital                              | 13.2             | MPa |
|                            |                     |       | 32 Weeks (gestation) | Occipital                              | 4.3              | MPa |
|                            |                     |       | 34 Weeks (gestation) | Parietal                               | 6.9              | MPa |
|                            |                     |       | 35 Weeks (gestation) | Parietal                               | 8.1              | MPa |
|                            |                     |       | 2 days               | N/A                                    | 3.8              | MPa |
|                            |                     |       | 2 Weeks              | N/A                                    | 6.4              | MPa |
|                            |                     |       |                      | N/A                                    | 3.8              | MPa |
|                            |                     |       | 11 Months            | Occipital                              | 4.2              | MPa |
|                            |                     |       | 12 Months            | Occipital                              | 16.2             | MPa |
| Davis <i>et al.</i> , 2012 | Four-point bending  | Human | 6 years              | Frontal and Parietal bone (cortical)   | 9.87 ± 1.24      | GPa |
|                            |                     |       | 6 years              | Frontal and Parietal bone (Tri-layer)  | 3.69 ± 0.92      | GPa |
| Wang <i>et al.</i> , 2014  | Three-point bending | Human | 1.5 ± 0.5 years      | Frontal                                | 1265.65 ± 120.90 | MPa |
|                            |                     |       | 1.5 ± 0.5 years      | Parietal                               | 1103.01 ± 112.77 | MPa |
| Ajami <i>et al.</i> , 2022 | Three-point bending | Human | 5.2 ± 1.3 Months     | Paritetal - cortical bone (trilaminar) | 3973 ± 268.45    | MPa |
|                            |                     |       |                      | Paritetal - cortical bone (diploe)     | 1958.17 ± 563.79 | MPa |

## Chapter 2: Literature review

**Table 2.4:** Material properties of the biological tissues of cranial bone – Animal-focused studies. **E** represents the elastic modulus.

| Author:                        | Method<br>(Load rate):               | Specimen<br>type: | Age of sample: | Region of extraction: | E:           | Unit: |
|--------------------------------|--------------------------------------|-------------------|----------------|-----------------------|--------------|-------|
| Marguiles &<br>Thibault, 2000  | Three-point bending<br>(2.54 mm/min) | Porcine           | 2-3 days       | Parietal              | 615 ± 96.2   | MPa   |
|                                | Three-point bending<br>(2540 mm/min) |                   |                |                       | 1371 ± 275.8 | MPa   |
| Moazen <i>et al.</i> ,<br>2015 | Nano-indentation                     | Mouse             | 10-20 days     | Frontal               | 5320 ± 680   | MPa   |
|                                |                                      |                   |                |                       | 7140 ± 790   | MPa   |
|                                |                                      |                   | 10-20 days     | Parietal              | 4330 ± 180   | MPa   |
|                                |                                      |                   |                |                       | 6300 ± 470   | MPa   |
| Zapata <i>et al.</i> ,<br>2020 | Ultrasonic system                    | Primate           | 14-years       | Parietal-outer layer  | 16.29 ± 1.07 | GPa   |
|                                |                                      |                   |                |                       | 21.84 ± 1.17 | GPa   |
|                                |                                      |                   |                |                       | 28.05 ± 1.14 | GPa   |
|                                |                                      |                   |                | Parietal-inner layer  | 14.23 ± 1.33 | GPa   |
|                                |                                      |                   |                |                       | 21.22 ± 0.82 | GPa   |
|                                |                                      |                   |                |                       | 24.14 ± 2.03 | GPa   |

### 2.3.2 Cranial sutures

As seen in calvarial bone reports, literature into infant suture properties follow the same trend. As such, both human and animal specimen studies will be considered here. Tables 2.5 and 2.6 highlight all numerical findings.

**Human studies:** One of the most referenced studies regarding suture properties is reported by Coats & Margulies (2006). Previously discussed in section 2.3.1, the study also examined calvarial suture properties. In total, 11 coronal suture samples were examined under three-point bending, in which 10 recorded values were measured. These were seen to fluctuate between the ages of 28 weeks gestation to 12 months of age, in which an elastic modulus of 14.2 MPa and 16.2 MPa was captured, respectively. The study suggests that, while age can impact the properties of these tissues, across the first year of life, these values remain unchanged.

Davis *et al.*, (2012) investigated the properties of a single cranial suture extracted from a six-year-old school-aged specimen. A method of four-point bending was used, resulting in an estimated value of 1.1 GPa. Although the location of extraction was unclear, within the limitations of this report, the elastic stiffness here assumed a higher value when compared with Coats & Margulies (2006) findings.

Wang *et al.*, (2014) examined two 1-year old samples, in which elastic modulus values achieved an order of magnitude greater than that of Coats & Margulies (2006). As only two values were reported across both the sagittal and coronal sutures, the values generated vary by a large margin (See Table 2.5). Further, the method of preparation, extraction and preservation of samples may have impacted these outcomes.

**Animal studies:** A report from Margulies & Thibault (2000), extending from their findings in calvarial bone, investigated the properties of the suture in porcine specimens under the same three-point bending rates reported in Table 2.3. While the lower rates achieved an elastic modulus of 194.2 MPa, the larger rates were seen to triple this estimation (610.3 MPa). The study concluded that, at the time of publication, limited studies of human infant suture properties had been reported. In turn, the authors proclaimed that the findings reported may be similar to that of humans.

Henderson *et al.*, (2004) investigated the properties of rat calvarial sutures during the development under a quasi-static testing approach. The age of the samples was correlated with the age of humans, estimated to be the first four years of life. The study intended to analyse the magnitude of elastic moduli properties during bone deposition, in which a decrease was seen with aging.

Moazen *et al.*, (2015) examined the mechanical properties of both bone and suture in the wild type (i.e., unaffected specimens) and mutant type mice (i.e., those affected by craniosynostosis) at postnatal days 10 to 20. Nano-indentation was used for this study, in which an indentation rate of 120 mN/min was used. No statistical differences across the examined sagittal, coronal, and posterior frontal sutures' elastic modulus were seen between the wild and mutant type specimens, showing an average value of  $30 \pm 0.3$  MPa. Interestingly, a difference was detected across the frontal bones between the two skull variations, suggesting these findings could aid in cosmetic surgical correction for calvarial deformation in humans.

As there are various material property outcomes report here, it is clear a sensitivity study into the impact these various properties could have on the models' predictive outcomes needs to be performed.

## Chapter 2: Literature review

**Table 2.5:** Material properties of the biological tissues of cranial sutures – Human-focused studies. **E** represents the elastic modulus.

| Author:                       | Method<br>(Load rate):         | Specimen<br>type: | Age of sample:       | Region of extraction: | E:             | Unit: |
|-------------------------------|--------------------------------|-------------------|----------------------|-----------------------|----------------|-------|
| Coats <i>et al.</i> ,<br>2006 | Three-point<br>bending/tensile | Human             | 28 Weeks (gestation) | Coronal suture        | 14.2           | MPa   |
|                               |                                |                   |                      | Coronal suture        | 13.2           | MPa   |
|                               |                                |                   | 32 Weeks (gestation) | Coronal suture        | 4.3            | MPa   |
|                               |                                |                   | 34 Weeks (gestation) | Coronal suture        | 6.9            | MPa   |
|                               |                                |                   | 35 Weeks (gestation) | Coronal suture        | 8.1            | MPa   |
|                               |                                |                   | 2 days               | Coronal suture        | 3.8            | MPa   |
|                               |                                |                   | 2 Weeks              | Coronal suture        | 6.4            | MPa   |
|                               |                                |                   |                      | Coronal suture        | 3.8            | MPa   |
|                               |                                |                   | 11 Months            | Coronal suture        | 4.2            | MPa   |
| Davis <i>et al.</i> ,<br>2012 | Four-point bending             | Human             | 6 years              | N/A                   | 1.1 ± 0.53     | GPa   |
| Wang <i>et al.</i> ,<br>2014  | Three-point bending            | Human             | 1.5 ± 0.5 years      | Sagittal suture       | 408.12 ± 59.08 | MPa   |
|                               |                                |                   | 1.5 ± 0.5 years      | Coronal suture        | 354.83±44.86   | MPa   |

## Chapter 2: Literature review

**Table 2.6:** Material properties of the biological tissues of cranial sutures – Animal-focused studies. **E** represents the elastic modulus.

| Author:                           | Method<br>(Load rate):              | Specimen<br>type: | Age of sample: | Region of extraction:                    | E:            | Unit: |
|-----------------------------------|-------------------------------------|-------------------|----------------|--|---------------|-------|
| Margulies <i>et al.</i> ,<br>2000 | Three-point bending<br>(2.54mm/min) | Porcine           | 2-3 days       | Coronal suture                           | 194.2 ± 42.5  | MPa   |
|                                   | Three-point bending<br>(2540mm/min) | Porcine           | 2-3 days       | Coronal suture                           | 610.3 ± 122.6 | MPa   |
| Henderson <i>et al.</i> , 2004    | Tensile test                        | Rat               | 2-60 days      | Sagittal suture                          | 9.517 ± 6.51  | MPa   |
| Moazen <i>et al.</i> ,<br>2015    | Nano-indentation                    | Mouse             | 10-20 days     | Sagittal, coronal &<br>posterior frontal | 32 ± 32       | MPa   |



### 2.3.3 Brain

Here, only relevant animal studies will be discussed. Table 2.7 summarises the properties reported by studies considered in this mini review.

Gefen *et al.*, (2003) highlighted the changes in brain properties using rat samples at different ages. Their study suggested that the elastic modulus decreases with age. An explanation regarding this outcome was potentially related to the characteristic of the brain's stiffness in response to the strain that is experienced with age.

A decade later, Sridharan *et al.*, (2013) explored the mechanical properties of the brain in rodents. While investigating the age-related changes in elastic modulus between 1 day and 6-8 weeks, similar findings to that of Gefen *et al.*, (2003) were found although they recorded higher values that might be due to the differences in the methods of testing and preparation between the two studies.

While the age and location of the samples play a role in outcomes, the brain structure may vary, relative to grey and white matter. Budday *et al.*, (2015) analysed the elastic modulus of bovine brain cadavers at 16 months of age using a nanoindentation approach. Various indenter diameters, loading rates and holding times were compared between white and grey matter samples over 192 various indentation tests. White matter was found to be 39% stiffer than grey matter, with results ranging in the low KPa for both grey and white matter.

Outcomes that contradict findings of Budday *et al.*, (2015) were later reported by Koser *et al.*, (2018), suggesting that grey matter's elastic modulus (159 Pa) provided a higher level than that of white matter (60 Pa). It should be noted that the specimens and method of testing (here, atomic force microscopy) drastically differs from that reported by Budday *et al.*, (2015). Nonetheless, there was a clear difference in properties between the two studies suggesting that specimens used, and method of testing can impact the overall findings.

In summary, there is clearly a large variation in the overall elastic modulus reported across all studies. To understand the impact these large variations could have on

## Chapter 2: Literature review

predicted outcomes, a sensitivity study will be carried out using several of the reported elastic modulus values here.

## Chapter 2: Literature review

**Table 2.7:** Material properties of the biological tissues of cranial brain tissues – Animal focused studies. **E** represents the elastic modulus.

| Author:                           | Method<br>(Load rate):         | Specimen<br>type: | Age of sample:    | Region of extraction: | E:         | Unit: |
|-----------------------------------|--------------------------------|-------------------|-------------------|-----------------------|------------|-------|
| Gefen <i>et al.</i> ,<br>2003     | Indentation (1<br>mm/sec)      | Rat               | 13 - 43 days      | N/A                   | 2 - 1.3    | kPa   |
| Sridharan <i>et al.</i> ,<br>2013 | Chronic force<br>measurement   | Rat               | 1 day             | Somatosensory cortex  | 7.5        | kPa   |
|                                   |                                |                   | 10 days - 2 Weeks | Somatosensory cortex  | 24.6       | kPa   |
|                                   |                                |                   | 4 Weeks           | Somatosensory cortex  | 35.2       | kPa   |
|                                   |                                |                   | 6-8 Weeks         | Somatosensory cortex  | 19.6       | kPa   |
| Budday <i>et al.</i> ,<br>2015    | Nanoindentation                | Bovine            | 16 Months         | Grey matter           | 1.38 ± 0.2 | kPa   |
|                                   |                                |                   |                   | White matter          | 1.89 ± 0.5 | kPa   |
| Koser <i>et al.</i> ,<br>2018     | Anatomical force<br>microscopy | Mice              | 4-7 Weeks         | Grey matter           | 0.159      | kPa   |
|                                   |                                |                   |                   | White matter          | 0.60       | kPa   |

## **2.4 Computational studies of the craniofacial system**

With the advances of computational-based software in the 21<sup>st</sup> century, understandings of the biomechanics of humans and animals' craniofacial system have advanced greatly. Today, 3D geometric models using medical-based images have allowed accurate simulations of real-world mechanics and impacts. For this section, three areas of literature will be covered. The first explores the validation of computational models to examine skull related traumas and their predictive responses. The second is to replicating ossification across the calvarial sutures. The third discusses studies to optimise craniosynostosis treatment.

### **2.4.1 Impact trauma**

There exists a variety of calvarial physiological responses caused by foreign impact. To replicate these impacts, complex and anatomically accurate 3D models have been developed (Figure 2.21). As such, this first section will highlight the studies relative to impact traumas. Note that all studies in this section utilise the finite element method, a program designed to assess the reactions of computational models by assessing the displacement over the force using elements (regions that divide the area of the model) and nodes (connected to the corners of the elements).

Lapeer & Prager (2001) explored the morphological responses of a neonatal skull model during the early stages of birth. Analysis of the cephalometric changes across the model's posterior apex was recorded while under exertion produced by linear intra-uterine pressure and various head-cervix pressure levels. While the method of laser scanning to create the model minimised the overall geometric accuracy, the predictive outcomes did resemble a clear match against clinical photographic data. The measurement of moulding indexes (i.e., changes in morphology before and after exertion presented as a percentage) valued at 6.2 % (predictions) and 4.8 % (clinical data). Further, the morphological appearances of both predicted and clinical data show lifting of the parietal bones across the region of the sagittal suture.

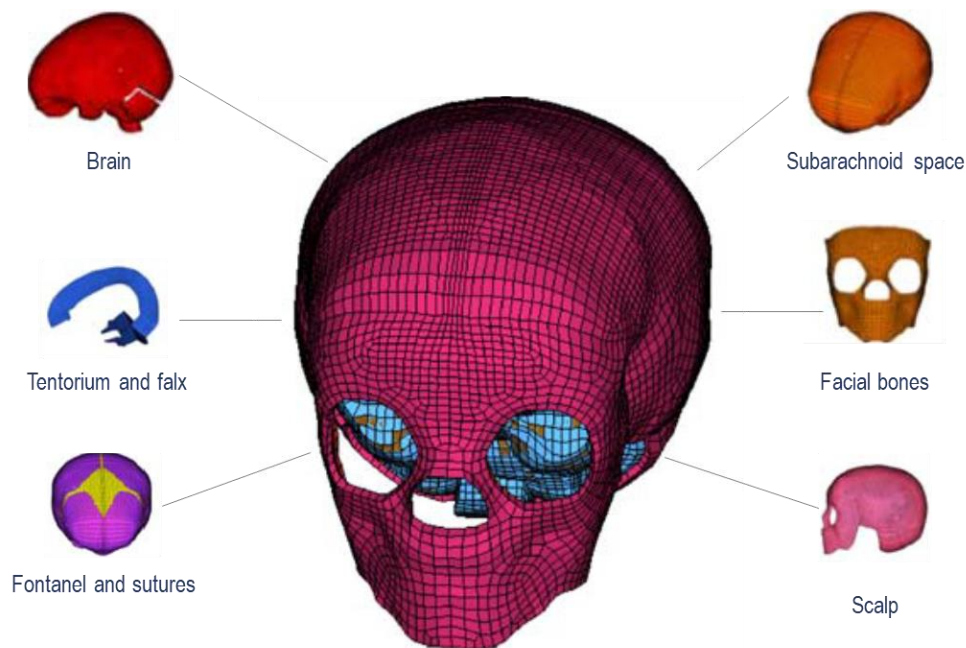


**Figure 2.21:** A developed FE model of a 6-month-old infant head (Adopted from Lapeer & Prager, 2001).

Replicating abnormal impacts and capturing the internal mechanical responses using adolescent skull models has been extensively discussed in the literature. Zhang *et al.*, (2001) investigated various mechanical forces impacting the frontal and parietal regions of an adolescent human skull model to highlight the most probable regions of brain injury. Validation was performed using cadaver specimens' and measuring the pressure, shear stress and shear strain responses while undergoing the same impact conditions (i.e., level of impact, velocity, location etc.). While frontal brain regions were resistant to impact levels of 5.23 kg at an impact speed of 6.33 m/sec, both predictive and *ex-vivo* agreed that the lateral regions of the brain were less resistant to injury. The conclusions of this study suggest that the region of mechanical impact can be just as detrimental to the integrity of the brain as the enforced level of impact.

While the potential damages to the adult calvarial and its internal organs are evident, reports of human inflicted damage to neonatal skulls are limited. Roth *et al.*, (2007) developed a 6-month-old infant model with the intention of replicating the impacts seen in 'Shaking baby' syndrome using the FE method. As a comparative analysis, the level of cerebral pressure changes and shear stress across the brain were investigated when the model was struck against a rigid surface. The report described a highly complex method of reconstructing the internal calvarial components and, in turn,

highlighted the similarities between surface impacts and damage inflicted during 'shaking'. Both pressure and shear stress changes in the model highlighted the possibility of subdural haematoma. Such studies could allow for medical professionals to distinguish between 'accidental' injuries and a lack of care.

For animal-based models, several studies have investigated the biomechanics of craniofacial system in several species, see e.g., review papers by Rayfield (2007) or O'Higgins *et al.*, (2011). Nonetheless, an example study that investigated the impact of cranial sutures was published by Moazen *et al*, (2009). They simulated the impact of sutures during the mastication in a *Uromastyx* lizard using the FE method. The sutures were seen to relieve the localised strain and distribute the strain more evenly across the skull. Relevant to the biological suture abnormalities discussed in the present thesis, a secondary approach consisting of suture fusion supported the aforementioned findings displaying higher regional strains vs. open sutures and leading to the possible progression of irregular bone growth and morphology. Furthermore, the levels of load-bearing for each suture was diverse indicating the frontal-parietal plays a sustainable role in evenly distributing strain. Such findings have brought into question the evolutionary role of sutures and their impact on the mechanics of skull.

The studies investigated here involve large scale and complex modelling parameters. However, many negate or are not required to replicate key biological characteristics seen during cranial development. Although such a process may not apply here, other reports have presented theoretical findings to answer complicated biomechanical and biochemical questions regarding suture and bone formation.

### **2.4.2 Simulating suture morphogenesis and ossification**

The cranial sutures are developed under a complex array of biological and biochemical signals (See: section 2.1.4). To examine the characteristics of sutural morphogenesis at the embryotic macrostructural level, reports have turned to developing complex computational and mathematical modelling approaches, allowing hypotheses of behaviours of the morphological development and ossification of sutures to be tested.

## Chapter 2: Literature review

Such studies are the highlight of this next section, with table 2.8 providing a summary of all studies' aspects.

While it is known that mechanobiological strain impacts the process of ossification, understanding the matrixes of these fibres under natural loads and examining the influence of different morphological characteristics is an area of interest to many within the clinical field of biomechanics. Jasinowski *et al.*, (2010) carried out an in-depth finite element study modelling the orientation of suture fibres and their impact on the pattern of strain and stress within the sutures. Predictions were compared under a compressive and tensile loading between two bone pieces, which varied in the level of morphological interdigitation (i.e., the interlocking of sutures). While accurately establishing the true complex structures of fibre cartilage is beyond today's scopes of computational models, variations in strain energy were seen in orientation changes providing vital understanding as to the interactions between suture construction and strain distributions at a macroscopic level.

Zhang & Yang (2015) complemented the aforementioned study further, by undertaking a similar approach to the understanding dynamics of suture-strain distribution. The study expanded on the findings of Jasinowski *et al.*, (2010), by simulating five orientations (vs. Jasinowski's two orientations) across three complex 2D sutural structures. A greater understanding of fibre orientation was reported here, which agreed well with the previous studies' findings. Stress attenuation and strain energy absorption were greater in fibres with a greater orientation than the control although, due to the simplicity of their modelling approach, a full robust validation was unobtainable. Despite this shortcoming, a greater understanding of bone and suture stress distributions was achieved.

Complementing these findings are studies where the natural responses of mesenchymal cells in developing and absorbing bone are computationally replicated. Zollikofer & Weissmann (2011) expanded on a differentiation methodology using 'finger-like' extrusions, known as the Laplacian approach. The modelled sutures were governed by growth velocities positioned on either side of the suture construct. The study benefited from the little parameterisation required to achieve concise morphogenetic representation, as it was seen that the predictive growth led to various

levels of interdigitation forming. Such modelling abilities lead to questions on how the suture morphology is governed in the long term.

Developing a methodology that considers the properties of elasticity in predicting bone generation and absorption has been reported by Khonsari *et al.*, (2013). ‘Programmed’ mesenchymal cells were instructed to migrate towards the regions of larger principal stresses, observed within the modelled collagen fibres. An interest in the patterning processes was discussed here, which showed greater ossification simulation across the convex of interdigitation. Such findings were supported by studies exploring the morphology of mice embryonic sutures. Conversely, replicating the primary flat-bone development cycle has been an active area for mathematical modelling.

Garzón-Alvarado (2013) parameterised areas of bone ossification with the intention of reconstructing and predicting the human calvarial shape. Expanding on the Turing method (i.e., under an activator-substrate behaviour of bone formation), consistent regulation of the two primary growth factors predicted the surface areas capturing a remarkable resemblance of the two frontal, two parietal, and the single occipital bones when compared with embryonic levels of development.

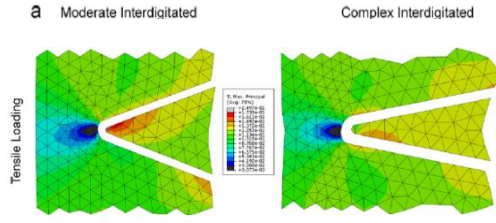
Lee *et al.*, (2015) attempted to replicate the calvarial structure of a mouse model from the earlier (15 days) to later (22 days) stages of embryonic development. The hypothesis of chemical reactions triggering the interaction between molecules was parameterised, allowing for osteoblast and osteoclast characteristics to be represented. Using two initial activators (allowing for bone modelling to initially form), five concentrated regions of bone development are present by embryonic day 22. Again, similar findings were seen by Garzón-Alvarado (2013), where an accurate morphological resemblance to that of mice skulls was seen despite complex parameterization being required.

Burgos-Flórez *et al.*, (2016) attempted to replicate the initial bone formation witnessed in human embryonic stages. Although the two key factors which regulate the production and absorption of bone differ, a consistent and accurate embryonic morphology was predicted across the mathematical model. This approach however was unable to anticipate the development of both the anterior and posterior fontanelles

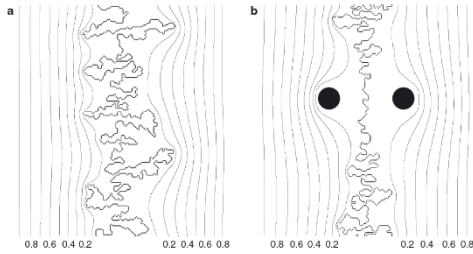


Although such mathematical application has no doubt progressed the understanding of suture biochemical behaviours, the impacts of mechanobiological strain dictating the rate of ossification are limited. Marghoub *et al.*, (2019), using the finite element method, predicted the growth of the mouse skull with the natural stresses from brain expansion governing the rate of ossification across the model's bony linings. The parameterised levels of hydrostatic strain and element distances from the bone allowed for the further modelling of tissue differentiation through the changing of element elastic moduli. The study was further strengthened by validating the predictions qualitatively and quantitatively with later *ex vivo* CT data from the same mouse specimen used for model development. In this thesis I will be using this approach and further translate it to human model and predicting outcomes of different reconstruction techniques for the management of sagittal craniosynostosis.

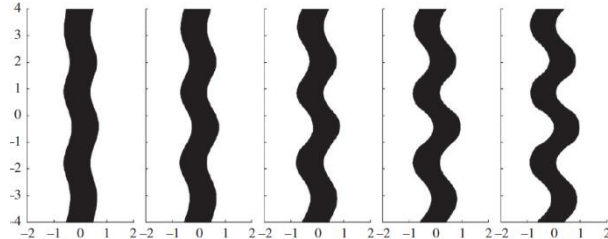
**Table 2.8:** List of studies analysing the process of ossification using various computational approaches.

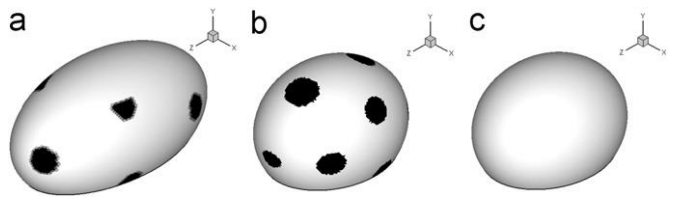
| Authors:                       | Objective:  | Methods:   | Results/conclusions:   | Figure/caption:  |
|--------------------------------|---|--|--|--|
| Jasinoski <i>et al.</i> , 2010 | Investigate the impact of three morphological cranial suture configurations and their mechanical responses under tensile and compressive loads. | A 2D FE model was developed. Various interdigitation indexes (II) were investigated. The sensitivity of the replicated collagen fibres orientation under loading was compared. A static 100 KPa resembled the stresses | A decrease in the II produced higher strain energy levels within the fibres and vice versa. Steeper collagen fibre orientation led to higher strain energy values vs. that of shallower orientation. Validation against miniature pig studies supports the findings. |  <p>Various interdigitation model's strain predictions under tensile loading.</p> |

## Chapter 2: Literature review

|                              |  |   |   |   |
|------------------------------|--|---|---|---|
|                              |  | across the adjoining bones.   |   |   |
| Zollikofer & Weissmann, 2011 | To develop a computational model for evaluating suture growth under strain-mediated morphogenesis. | A Laplacian modelling approach is used, allowing for suture like geometries to arise under various regions of growth velocity. The sensitivity of the positioning of these stress | Characteristic morphologies of cranial sutures were captured here. Consistent representations of a 'horses-shoe' like appearance were apparent across all tested parameter settings. The study demonstrates how strain gradients govern the shapes of developing cranial sutures. |  <p>Predictions of suture formation across the parietal (a), with stress distribution around the suture lines (b – black circles).</p> |

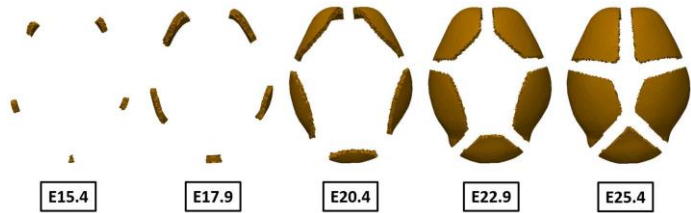
## Chapter 2: Literature review

|                               |   |   |  |  |
|-------------------------------|---|---|--|--|
|                               |   | regions was investigated. The model growth is governed by a disposition-reabsorption interface.   |  |  |
| Khonsari <i>et al.</i> , 2013 | To enhance the modelling approach in complementing the chemical behavioural processes seen in suture morphological instability. | Modelling was validated against that of mice embryo studies. A continuous scale, vs complex biological processes, was chosen for modelling mesenchymal cells. | Simple mechanical processes allowing for the distribution of mechano-transduction were achieved with validity against animal models being achieved. Ossification was seen to accelerate across the convex areas, where collagen fibre migration had taken place. |  <p>The onset of simulated suture morphological instability over 30 days (<i>in silico</i>).</p> |

|                       |  |   |   |   |
|-----------------------|--|---|---|---|
|                       |  | Equations of elasticity were used to distinguish between mesenchymal cells and bony boundaries.   |   |   |
| Garzón-Alvarado, 2013 | Develop a mathematical model of the emergence of ossification centres across the human calvarial, to replicate the primary calvarial bone development. | The Turing space method is adopted here and replicated the activator-substrate behaviour of proteins across the differentiation of the tissue. This was the | The model predicts regions of higher BMP2 demonstrated higher bone growth vs. higher regions of Noggin. The model successfully predicts the primary centres of growth for the two frontal, two parietal and two occipital bones. Using this mathematical approach, maturation centres of the primary bones were predicted |  <p>Regions of predicted ossification (black) across the computational model.</p> |

## Chapter 2: Literature review

|                          |  |   |   |  |
|--------------------------|--|---|---|--|
|                          |  | basis on which predictive formation would be regulated under the mathematical model.  | with consistency to that at an embryotic level of development.  |  |
| Lee <i>et al.</i> , 2015 | To develop a modelling approach for simulating activator-inhibitor osteoblast behaviours during bone growth in mice. | A finite-volume method was used to solve the reaction-inhibitor 3D model and predict the pattern and location of growth. Modelled mesenchymal | Five concentrated regions of growth are evident by E15.4. Primary ossification appears where the concentration of the activator is high. Due to a predicted spatial effect on cell differentiation, the region in which the anterior fontanelle appears does not fully ossify. Locations of |  |

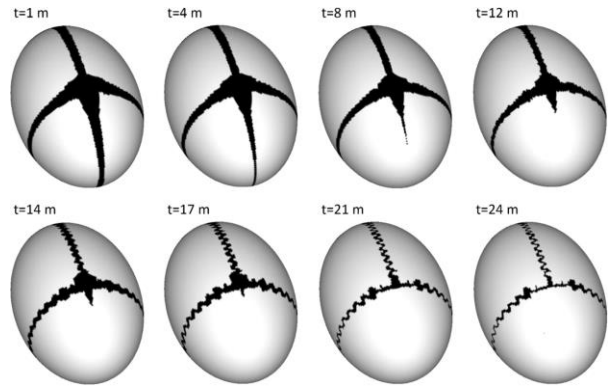
|  |  |   |   |  |
|--|--|---|---|--|
|  |  | <p>cells surround the <i>in-silico</i> brain, where the activator-inhibitor behaviour will take place. Embryotic day 17.5 CT was used to model the brain morphology. Two primary activators were positioned across the orbital of the eyes, in the position of the flat bones</p> | <p>ossification correspond to biological positionings of the flat bones of the skull. Bone growth continues from these centres from E15.4 to E22.9. The posterior end continues to ossify slower.</p> | <p>Changes in predicted regional bone growth under osteoblast concentration and positional suture formation.</p>  |
|--|--|---|---|--|

|                    |  |  |  |  |
|--------------------|--|--|--|--|
|                    |  | to activate the modelled ossification process.   |  |  |
| Zhang & Yang, 2015 | <p>Three morphologies of cranial sutures are studied and their responses to impulsive loading are studied. Additionally, the parameters of Young's modulus and fibre orientation are explored across the modelled sutures and bones.</p> | <p>All models were developed as 2D geometries. The three modelled morphologies were shaped All material properties were treated as isotropic. Sutures were modelled to simulate the random orientational</p> | <p>As the increase in the hierarchal order model was observed, the dynamic strain energy of sutures increased in both isotropic and orthotropic scenarios. The higher-order hierarchical suture was seen to provide a better attenuation of the stresses across the bone-suture complex. Both higher suture elasticity and orientation benefited the energy absorption and stress attenuation.</p> | <p>Von Mises stress fields across each modelled suture morphology. (a) Straight line, (b) pure sinusoidal suture and (c) two-order hierarchical sinusoidal suture.</p> |



## Chapter 2: Literature review

|  |  |  |  |  |
|--|--|--|--|--|
|  |  | nature of the collagen fibres. Values of suture isotropic behaviour were between 50 MPa – 500 MPa. Five orientation (from 15 degrees to 75 degrees) approaches were explored. A loading of 50 KPa was applied along the left edge of the bone-suture |  |  |
|--|--|--|--|--|

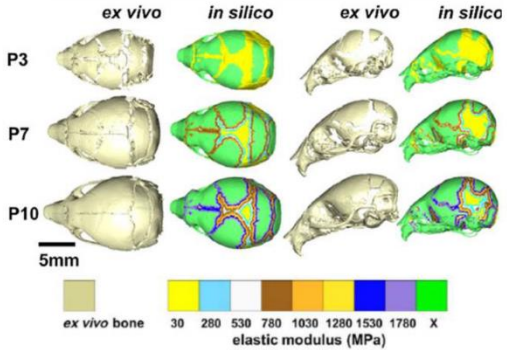
|                                    |  |   |   |   |
|------------------------------------|--|---|---|---|
|                                    |  | complex, applying compression across the suture.  |   |   |
| Burgos-Flórez <i>et al.</i> , 2016 | To model the mechanisms underlying suture formation and how biochemical factors regulate bone formation during prenatal human development. | The work expands on that of Garzon-Alvarado <i>et al.</i> , (2015), in that the modelling approach depends on the changes in the biochemical reaction between two key factors (Here TGF- $\beta$ 2 and TGF- | The model was highly dependent on both TGF-2 and 3 cells concentration for predicted suture and bone development. Suture interdigitation patterning was captured, resembling that of various developmental ages and achieving an agreeable match when compared to normative cranial development. Fusion of the metopic suture and both anterior and posterior fontanelles were seen, suggesting |  <p>Evolution of predicted suture interdigitation across the coronal and sagittal sutures. (m) is expressed as months.</p> |

## Chapter 2: Literature review

|  |  |   |  |  |
|--|--|---|--|--|
|  |  | <p>β3). Where TGF-2 induces bone growth and TGF-3 inhibits. Suture interdigitation seen during embryonic stages was replicated by applying resorption sites across the bone linings. The finite element method with a Newton-Raphson scheme is used here.</p> | <p>that the fate of suture formation appears to be highly dependent on the osteoinhibitory proteins and that such an imbalance could lead to premature suture fusions.</p> |  |
|--|--|---|--|--|

## Chapter 2: Literature review

|  |  |  |  |  |
|--|--|--|--|--|
|  |  | <p>The 3D 14 weeks of gestation model consists of all cranial components, apart from the facial and temporal bones.</p> <p>Results were compared with that of Garzon-Alvarado <i>et al</i>, (2015) and compared at time points 9 months prenatal and 24 months of age.</p> |  |  |
|--|--|--|--|--|

|   |  |  |  |   |
|---|--|--|--|---|
| <p>Marghoub<br/><i>et al.</i>, 2019</p> | <p>To replicate the ossification and changes in elastic magnitudes during skull growth in mice, dictated by the changes in hydrostatic strain.</p> | <p>CT imaging of a neonatal mouse was used for 3D FE modelling. Skull growth was presented by expanding the ICV linearly in all directions. Changes in elastic properties represent the calcification of bone expanding away from the bony linings of the sutures.</p> | <p>The model closely represents the bone formation of the sutures and closely represents <i>in-vivo</i> suture diameters when compared. A good morphological match against <i>in-vivo</i> data is also achieved, allowing potential use for human models in future research.</p> |  <p>Morphological changes and bone formation patterns during ICV expansion. Results are compared against the CT data of the same mouse used for initial modelling.</p> |
|---|--|--|--|---|

|  |  |  |  |  |
|--|--|--|--|--|
|  |  | Elements within the specified radii and strain were selected to have their properties updated. |  |  |
|--|--|--|--|--|

### 2.4.3 Computational studies of Craniosynostosis and skull growth

Through the advancements in understanding craniosynostosis and skull growth, many studies have been able to adopt and develop methodologies to assist with the biomechanics of skull surgery. For such studies, the finite element method is a powerful tool for 3D modelling and simulating the mechanical responses of bone and overall shape changes. One of the earliest reported is that of Hardey & Marcal (1971). Although low-resolution compared to modern-day modelling approaches, possessing only 45 elements (Figure 2.22), it provided a foundation in the possibilities of modelling the biomechanics of the skull. Table 2.9 highlights each study reviewed in the following section.

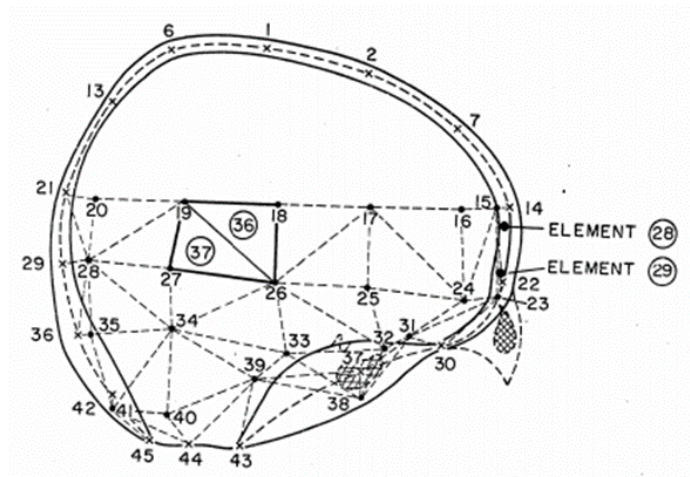


**Figure 2.22:** 2D calvarial model reconstructions. Made up of 45 elements for the simulation of mechanical loading responses (Adopted from Hardy & Marcal, 1971).

The FE approach has been used to optimise pre-existing techniques for sagittal craniosynostosis correction. You *et al.*, (2010) highlighted the predictive impacts on bone displacement across the parietal bone under four modified ‘Pi’ techniques. There was a clear impact on the integrity of the modelled bone. Such studies could lead to optimising the overall approach to correction in the long term.

Wolański *et al.*, (2013) expanded on this approach by incorporating the complete calvarial morphology to capture bone displacements under surgical intervention. It was found that the modelled craniotomies had a profound effect on the frontal bone region, leading to the possibility of an alternative corrective option for the craniofacial centre.

However, the study adopted a simplistic method of simulating the brain growth, which may not resemble real world conditions.

The level of intervention and the number of bioabsorbable materials used for the correction of Craniosynostosis treatment can differ between centres (See: section 2.2.3). Li *et al.*, (2017) attempted to combat the levels of blood loss and operational costs using 3D modelling to simulate total calvarial remodelling. The technique allowed surgeons to plan preoperatively and examine the resulting rigid fixator strain across the corrected bones. In conjunction with this, Chen & Yang (2019) used the FE method in mechanically assessing the impacts across the skull after frontal-orbital remodelling surgery in particular, the responses the replicated craniotomies would have while under loading.

Implications of spring-assisted cranioplasties have further been explored using the FE approach. Borghi *et al.*, (2018) presented a novel method of simulating the impacts of SAC using a pre-operative 3D calvarial model. The method was validated against patient-specific CT data, undergoing the same treatment process for sagittal Craniosynostosis. Predictions coincided with the CT observations, allowing for a comparison of the morphology as well as the level of displacement seen across the springs. A later study (Borghi *et al.*, 2019) assessed 18 patients in optimising and evaluating the kinematics and shape changes under the SAC corrective technique. Using this data, the report validated a modelling approach that aimed to simulate the initial distractors expansion across the craniotomy upon insertion. Although the effects of brain growth were not considered, an agreeable match in the level of spring displacement prediction was seen.

While SAC is a clinical option for sagittal Craniosynostosis correction, these distractors are also used in other patient cases. Bozkurt *et al.*, (2020) built on the premises of the above studies while incorporating the parameters of skull growth for spring assisted lambdoid Craniosynostosis correction. Distractors were used for posterior skull expansion across an improvised craniotomy. The model allowed for surgical teams to alternate the levels of spring forces generated, controlling the level of bone displacement. Once again, an agreeable morphological match was seen, but the premise of postoperative bone healing was not established.

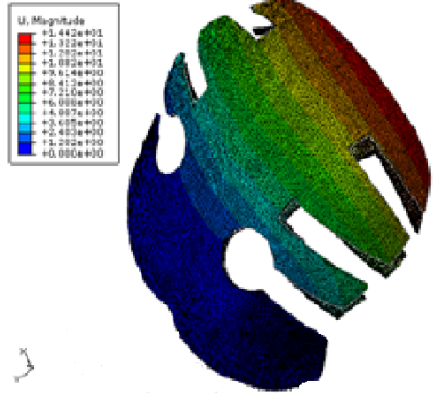


In the area of replicating skull growth, an earlier study by Libby *et al.*, (2017) examined the normative growth of a single predictive model and validated it against a large cohort of CT data. In addition, *in vitro* experimentation was conducted to justify the findings using a 3D printed skull geometry. Overall, by using a thermal analogy approach to replicate the brain expansion, the study yielded a good morphological match across both *in vivo* and *in vitro* data. Building off this study, Marghoub *et al.*, (2018) and Malde *et al.*, (2020) expanded on the use of thermal expansion for skull growth in mice and sagittal Craniosynostosis geometries, respectively. Both presented a good match in morphology, with the former study investigating various material and boundary conditions and the latter study exploring the impacts of suture fusion during corrective growth. As such, this thesis will use the thermal expansion methods described by these studies throughout all generated models.

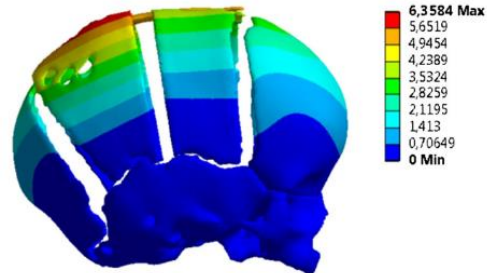
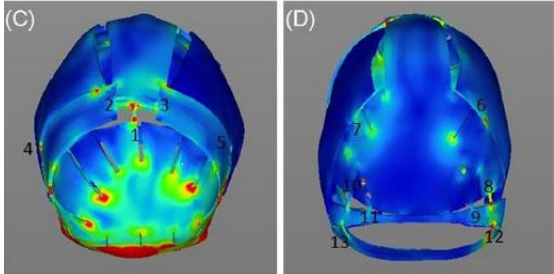
While the thermal expansion approach may not represent the exact anisotropic characteristics of brain growth, other computational studies opt for an alternative to this. Barbeito-Andrés *et al.*, (2020) investigated the use of two morphological approaches to implement skull growth under a linear expansion and geometric morphometric approach. The study found merit in attempting to anticipate the anisotropic characteristics that is brain growth while using a simplistic approach to modelling. Their report found that the modelling approach to brain growth can have profound implications on predictive outcomes.

In summary, previously used computer models have assessed the impacts of craniosynostosis as well as simulated key physiological characteristics seen in human and animal. Most notably, studies from Libby *et al.*, (2017), Marghoub *et al.*, (2018 & 2020), Malde *et al.*, (2020), and Borghi *et al.*, (2019) who's reported methodologies and parameters will be carried forward to be used in the modelling framework throughout this thesis.

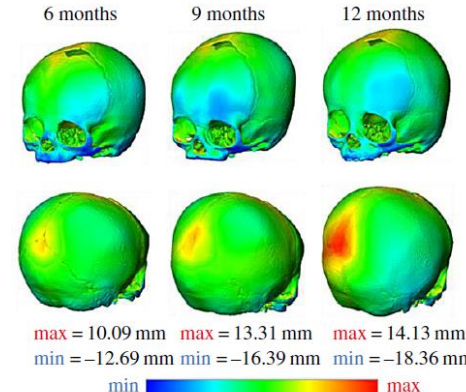
**Table 2.9:** A summary of key studies investigating the biomechanics of Craniosynostosis and skull growth.

| Authors:                 | Objective:   | Methods:   | Results/conclusions:   | Figure/captions:   |
|--------------------------|--|--|--|--|
| You <i>et al.</i> , 2010 | To compare varying surgical techniques concerning bone slots dimensions created in the correction of Craniosynostosis. | Varying bone slots interpreted from a pi procedure are created on a single patient CT model. Constant intracranial pressure is loaded within the endocranium and captures the rigidity of the parietal bone using FEA. | Upon observing varying schematics of bone slot techniques for modifying a pi procedure, the study concludes with the most applicable method for correction while maintaining bone integrity and bone rigidity. |  <p>Distance contour of the most applicable method for scaphocephaly in this chosen patient case.</p> |

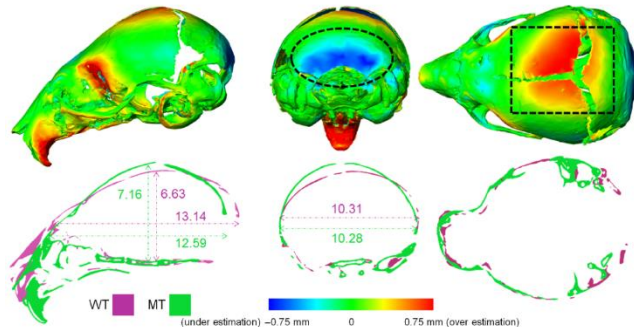
## Chapter 2: Literature review

|                                     |   |  |   |  |
|-------------------------------------|---|--|---|--|
| <p>Wolański <i>et al.</i>, 2013</p> | <p>To aid in pre-operative and post-operative management for the correction of Craniosynostosis by observing the displacement of bone under different surgical methods.</p> | <p>A 3D geometry of patient-specific models was created, and operational procedures were simulated. Constant intracranial pressure was then exerted on the inner cranial base.</p> | <p>The use of FEA allows for pre-operative surgical practice and the ability to observe stresses exerted on the bone when varying the surgical approach for scaphocephaly and trigonocephaly.</p> |  <p>Displacement plot of bone after scaphocephaly.</p>  |
| <p>Li <i>et al.</i>, 2017</p>       | <p>To improve surgical efficiency through biomechanical analysis and 3D calculations on Craniosynostosis patients.</p>  | <p>Two surgical methods were compared within 18 patients. Cranial indexes, blood loss, operation cost, postoperative</p>   | <p>Computer-assisted 3D techniques allow surgeons to plan surgical interventions. The work allows for bone setting positions and fixtures of sutures allowing for less surgical time and</p>      |  <p>Stress-strain graph as force exertion on the skull is increased. Showing the frontal and rear view of the skull.</p> |

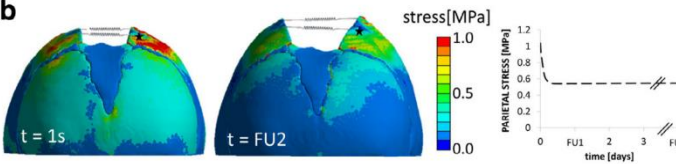
## Chapter 2: Literature review

|                            |  |   |   |   |
|----------------------------|--|---|---|---|
|                            |  | complications and biomechanical analyses were all investigated in TCR cases.  | minimising wastage of materials.  |   |
| Libby <i>et al.</i> , 2017 | Develop a validated computational model in the biomechanics of human skull growth in the early months of life <i>in-vitro</i> and <i>in-silico</i> . | A 3D printed and FEA model is created from CT data to simulate the increase in ICV from 0-12 months of age. The resulting morphological changes were then compared with <i>in-vivo</i> data for validation. | FEA can be utilised to simulate ICV growth in humans and matches well against <i>in-vivo</i> data of the same age. Demonstrating the use in aiding Craniosynostosis management. |  <p>3D Distance plot comparing <i>in-silico</i> with <i>in-vivo</i> morphology at different ages.</p> |

## Chapter 2: Literature review

|                                     |   |   |  |   |
|-------------------------------------|---|---|--|---|
| <p>Marghoub <i>et al.</i>, 2018</p> | <p>Investigate the possibilities of computational models accurately predicting the normative and Craniosynostosis skull growth.</p> | <p>Skull growth is quantified at time points 3, 10 and 20 days of age. 3D modelling was based on a single mouse micro-CT image. Sensitivity of the boundary conditions, properties of the modelled brain and sutures were undertaken.</p> | <p>Both models predicted shape coincided with micro CT data at various time points. The choice of parameters was seen to have a profound effect on skull growth, leading to extreme calvarial displacements.</p> |  <p>3D and 2D morphological predictions between <i>in silico</i> vs. <i>ex vivo</i> mice skulls.</p> <p>The figure displays 3D and 2D morphological predictions of mouse skulls. The top row shows three 3D models of skulls, each with a color-coded surface representing the difference between <i>in silico</i> and <i>ex vivo</i> data. The bottom row shows three 2D cross-sectional views of the skulls, with numerical values indicating the difference in millimeters. A legend at the bottom indicates that blue represents under-estimation (under 0.75 mm) and red represents over-estimation (over 0.75 mm). The values shown are: 7.16, 6.63, 13.14, 12.59, 10.31, and 10.28.</p> |
|-------------------------------------|---|---|--|---|

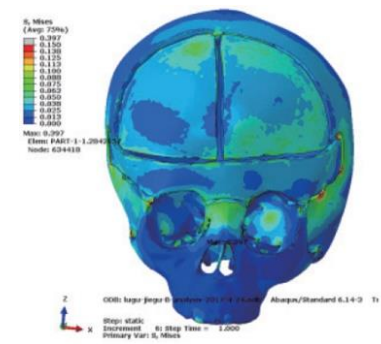
## Chapter 2: Literature review

|                                   |   |   |  |   |
|-----------------------------------|---|---|--|---|
| <p>Borghi <i>et al.</i>, 2018</p> | <p>Develop a patient-specific model undergoing SAC to predict the stresses and head shapes upon placement and by the time of removal.</p> | <p>Patient modelling was based on a single sagittal synostosis child. Model's anatomy included partially the frontal bones and the majority of the parietals. Distractor's parameters were based on in-house experimentation.</p> | <p>The model accurately predicted levels of spring expansion upon placement. An agreeable morphological prediction has also been by spring removal, 22 days later.</p> | <p><b>b</b></p>  <p>Simulated spring opening across the generated FE model. Evaluation of stress distribution from time of placement to time of removal.</p> |
|-----------------------------------|---|---|--|---|

## Chapter 2: Literature review

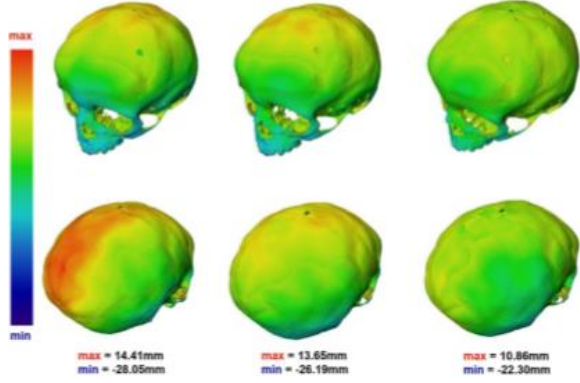
|                                   |  |   |   |   |
|-----------------------------------|--|---|---|---|
| <p>Broghi <i>et al.</i>, 2019</p> | <p>Utilising FEA in observing forces on the parietal bone by altering spring expansion in a spring mediated cranioplasty patient population and adaptations in calvarial morphology.</p> | <p>Pre-operative SMC CT scans of patient data were used to simulate the forces of spring devices later after the procedure. Displacement of the bone and volume of the cranium were then assessed against <i>in-vivo</i> data of the same patients.</p> | <p>The method allows surgeons to have a perspective on the effects spring mediated devices have on the bone during follow up evaluations and improve pre-surgical planning.</p> | <div data-bbox="1291 373 1879 625"> </div> <p>Distance plot of spring expansion from pre-operative to follow up ages.</p> |
|-----------------------------------|--|---|---|---|

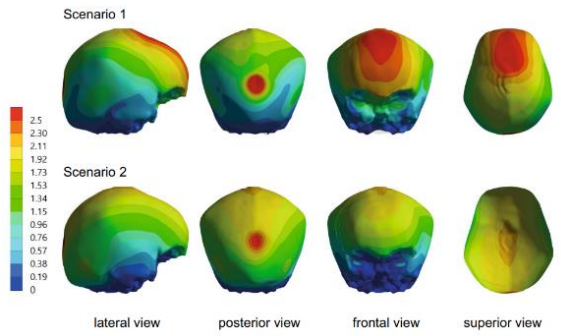
## Chapter 2: Literature review

|                              |  |  |  |  |
|------------------------------|--|--|--|--|
| <p>Chen &amp; Yang, 2019</p> | <p>To utilize FEA in guiding the use of distractors in frontal-orbital advancement and observe the mechanical characteristics of bone.</p> | <p>3D CT images of patients were used to simulate different FOA techniques. Varying forces were then exerted at points along the defects to calculate the stresses observed on the bone and surrounding cranium.</p> | <p>By simulating a distraction operation, areas of concentrated stress on the bone before the correction was found to have dispersed. Allowing surgeons to take further action in lower complications postoperatively.</p> |  <p>Stress distribution map after frontal orbital simulation.</p> |
|------------------------------|--|--|--|--|

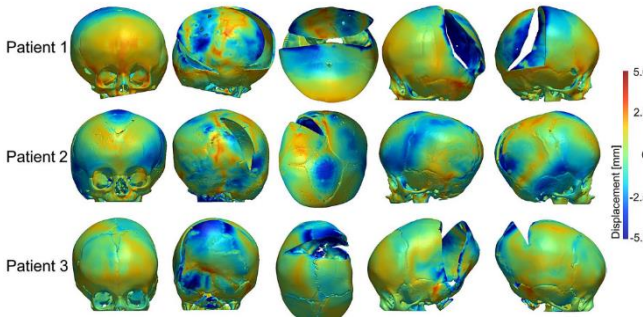


## Chapter 2: Literature review

|                                  |  |  |  |  |
|----------------------------------|--|--|--|--|
| <p>Malde <i>et al.</i>, 2020</p> | <p>Create a validated patient-specific model for predicting calvarial morphology under different hypothetical scenarios.</p> | <p>CT images of a patient model are created, and three scenarios are introduced. 1. All open sutures 2. All closed sutures 3. <i>In-vivo</i> scenario. Models were compared with patient follow up data for validation. Material properties of bone, suture and craniotomies were increased at intervals</p> | <p>Comparing the <i>in-vivo</i> scenario and patient model shows a good <i>in-silico</i> prediction of the skull shape. This leads to the potential of predicting various surgical techniques using a finite element approach.</p> |  <p>3D distance plots of each hypothetical scenario comparing simulated morphology with the <i>in-vivo</i> follow up skull.</p> |
|----------------------------------|--|--|--|--|

|                                      |   |   |  |  |
|--------------------------------------|---|---|--|--|
|                                      |   | during simulation.  |  |  |
| Barbeito-Andrés <i>et al.</i> , 2020 | To model the effects of brain growth using a geometric morphometric approach using the FE method. | Semi-coordinated landmarks are positioned across the 3D skull casing. Two scenarios: 1. Linear growth and 2. Morphometric analysis for brain growth was investigated. | Localisation of suture displacement was seen under a linear growth approach. Displacements under the second approach captured larger displacement across the posterior. The study demonstrates a realistic approach to predicting the various levels of growth across the brain. |  <p>Displacement mapping under two parameterised methods for simulating pressure across the brain.</p> |

## Chapter 2: Literature review

|                                    |   |   |   |  |
|------------------------------------|---|---|---|--|
| <p>Bozkurt <i>et al.</i>, 2020</p> | <p>To develop a parametric FE model for the predictive outcomes of lambdoid synostosis under a spring-assisted technique.</p> | <p>Three individual patients undergoing SAC for LS were modelled for validation. Skull growth was simulated from pre-op to follow up. Linear elastic properties were defined for the materials.</p> | <p>Morphological predictions against each patient's data agreed well. A 5 mm difference was seen between the comparative data sets. The method provides a novel effort in assisting with surgical outcomes.</p> |  <p>3D distance mapping between predictive FE expansion of calvarial bones and resulting CT images.</p> |
|------------------------------------|---|---|---|--|

## 2.5 Discussion and summary

An overview of the key areas of literature related to the main body of work conducted in this thesis was provided in this chapter. This section presents the overall findings of the previous sections.

The human infant craniofacial system is a complex structure, with many biological characteristics that will require consideration. The mechanical properties of various constituents of the craniofacial system vary within and between humans and animals. The method of sample preparation and mechanical testing can influence the measurement of parameters of interest. Although the studies on humans are limited, the literature provides a broad overview of various species. As such, aspects of material properties will also be explored in Chapter 3.

While Craniosynostosis is a widely known medical condition, important questions about how the skull responds to corrective methods remain. These range from the timing of skull healing to the comparative nature of each technique. Such considerations were discussed in section 2.4.3 of this Chapter. However, studies did not provide a contrast of techniques across their modelling approaches. Further, the timing of skull healing can vary dramatically due to the chosen technique by surgeons. As there is no clear methodology for replicating craniotomy healing computationally, Chapter 4 will focus on these areas.

Further to the biological impacts of calvarial growth, the mechanobiological strain has a fundamental part to play in regulating the ossification of the sutures and craniotomies after correction. Although such studies explore, in detail, the morphology and stresses of suture under loads, there is a clear limitation in incorporating the skull growth. While such aspects have been explored in mice models, there is not yet a study that parameterises mechanobiological strain in a human model. This will be the focal point of Chapter 5.

In summary, the option for correcting sagittal Craniosynostosis can perhaps impact the long term well-being of individuals in both aesthetic and functional aspects. The

## Chapter 2: Literature review

investigated computational studies reviewed here consider only one method of treatment, whether that be due to validation rationale or only applicable to the craniofacial centre of interest. A more comprehensive and large-scale observational analysis of predicting skull growth under different techniques could assist with postsurgical optimisation and expand on the biomechanical understanding behind different corrections. This will be the main premise of Chapter 6.

## **Chapter 3: Development and validation of a patient-specific sagittal craniosynostosis model**

## 3.1 Introduction

The overall aim of this chapter was to develop a validated patient-specific model capable of simulating calvarial growth in a sagittal synostosis patient. The CT scans of a child preoperatively were obtained and used to virtually reconstruct the skull. This was then used to predict the skull shape at different time points matching the follow up CT data obtained from the same individual. Here a series of sensitivity studies were performed, investigating the impact of the following parameters on the predictions of growth: methods of bone formation, the elastic modulus of various materials, and the presence or absence of cerebrospinal fluid on the predictive growth.

## 3.2 Materials and methods

This section first details the development of the baseline pre-operative model developed using image processing techniques. Secondly, it describes the choice of initial parameters for the model. Finally, it summarises various sensitivity studies performed.

### 3.2.1 Model development

**Patient-specific data:** Anonymised pre and post-operative CT images of a single patient affected by sagittal craniosynostosis were provided from the Hôpital—Necker Enfants—Malades Cranio-facial Surgery Unit (Paris, France). The patient's gender and previous medical records were unknown. Data was provided at four time points during the treatment process. Both the first (preoperative) and second (immediately postoperative) CT data sets were obtained at the age of 4 months, with only two days separating these two time points. Two further CT data sets were obtained at 36 and 76 months of age, denoted as follow up 1 and 2, respectively. All images were provided in DICOM format. The manufacturer and model version of the CT device used were unknown. The voxel size of all images maintained a resolution of 0.625 by 0.625 mm across all planes.

All images were imported into the image processing software, Avizo (Avizo Lite, FEI, V9.2.0) for component segmentation. 3D rendering of the calvarial structure was performed across all CT images (Figure 3.1). The cephalometric measurements and internal volume (ICV) were recorded before model development, as shown in Table 3.1

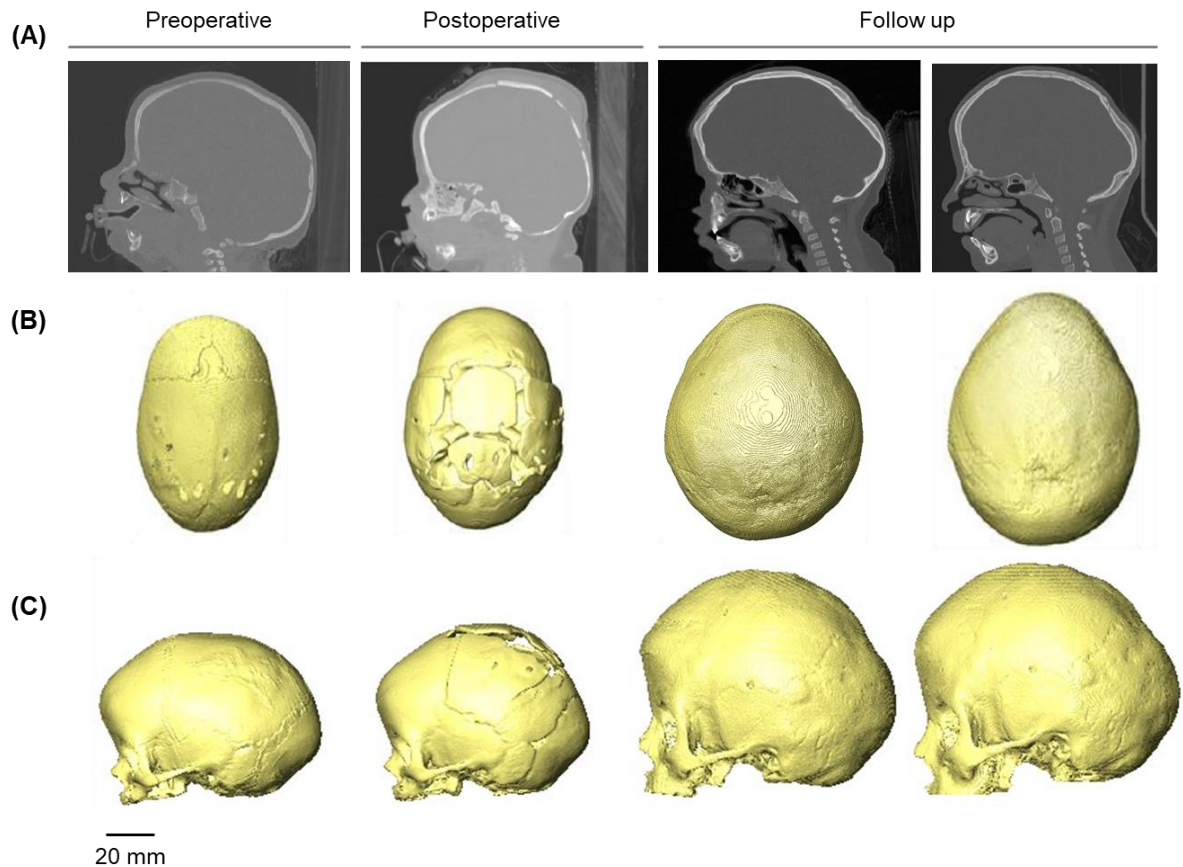


**Figure 3.1:** Imported patient-specific computed tomographic (CT) data undergoing sagittal craniosynostosis correction. Four time-points were provided (A), with the pre-operative providing the geometry of the baseline model. 3D rendering of all CT data was performed, displaying the dorsal (B) and sagittal (C) viewpoints.

**CT segmentation:** The 4-month pre-operative data was used for further compartmentalisation of hard and soft structural tissues (Figure 3.2). The three components consisted of the calvaria bones, (frontal, parietal, occipital temporal, foramen magnum and craniofacial bones), the cranial sutures (metopic, coronal, squamosal, anterior-posterior fontanelles, frontozygomatic and zygomaticotemporal sutures), and the intracranial volume (cerebral spinal fluid [CSF], frontal lobe, temporal lobe, parietal lobe, occipital lobe, and cerebellum).



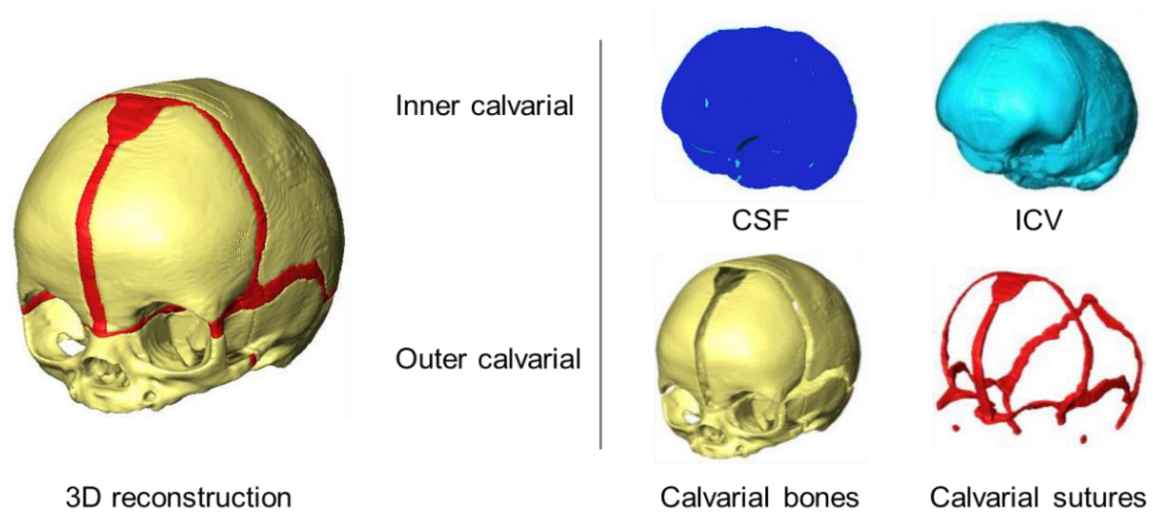


**Figure 3.2:** The pre-operative models segmented 3D components. The CSF was segmented separately from the ICV in an alternative model in preparation for the applicable sensitivity study.

**Table 3.1:** Cephalometric and ICV measurements of all CT data.

| Measurements:       | Preoperative: | Postoperative: | Follow up 1: | Follow up 2: |
|---------------------|---------------|----------------|--------------|--------------|
| Age (months):       | 4             | 4              | 36           | 76           |
| Length (mm):        | 137.2         | 134.3          | 162.1        | 166.2        |
| Width (mm):         | 108.1         | 113.1          | 142.3        | 143.9        |
| Cephalic index:     | 78.8          | 84.2           | 87.7         | 86.6         |
| Circumference (mm): | 396           | 380.9          | 481.6        | 505.5        |
| ICV (ml):           | 659.9         | 662.3          | 1214         | 1245         |

Calvarial bones were segmented based on an automated grey-scale threshold approach, differentiating the soft tissues from the dense. Both the sutures and the ICV were segmented manually, as the program was unable to differentiate between the two tissues. By manually highlighting the sutures, it should be noted that the level of thickness is inconsistent across the calvarial. Nonetheless, to ensure the bone formation can be simulated correctly, the sutures do not maintain a thickness of less than 3 mm. To fully encapsulate the inner calvarial, the nasal openings, eye sockets

and foramen magnum were sealed with the same material as calvarial bone limiting the level of complications during simulated growth.

### 3.2.2 Finite element method

The pre-operative model was imported into the finite element (FE) program, ANSYS (APDL, V19.0, ANSYS Inc., Canonsburg, PA, USA), where the simulated calvarial growth, contact pressure boundary conditions, and the bone formation algorithm were carried out. Quadratic tetrahedral elements (SOLID187), consisting of 10-nodes with quadratic displacement effect, were used to mesh the model. The number of elements was determined on a mesh convergence analysis (Section 3.2.4).

**Surgical intervention:** The surgical technique performed on the patient (Figure 3.1), as well as being described by Melo *et al.*, (2013) and Rocco *et al.*, (2012), were replicated across the calvarial bones of the model, by highlighting the bone elements and altering their elastic modulus to represent the craniotomy (i.e., surgical removal of bone). In short, two bitemporal wedges, extending from the left to right squamosal sutures, were created posterior to the coronal suture and anterior to the lambdoid suture. A 2-3 cm rectangular wedge of bone containing the fused sagittal suture was created by performing two linear segments extending from the anterior bitemporal craniotomy to the posterior.

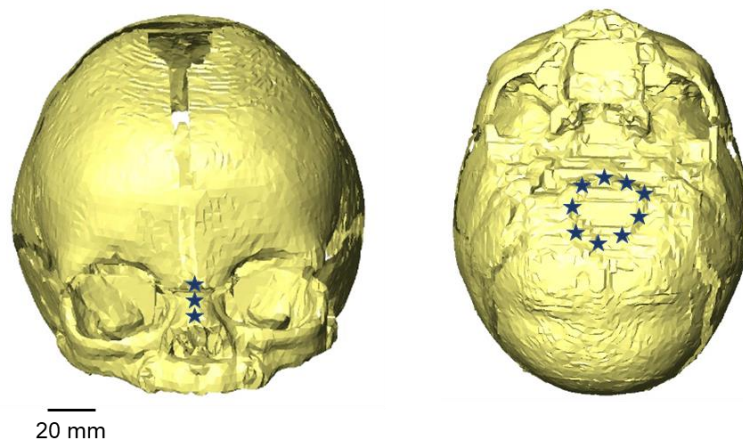
### 3.2.3 Material properties and boundary conditions

**Material properties:** All components were modelled with linear isotropic material properties. Prior to the sensitivity studies, the calvarial bones, sutures, ICV and craniotomies were given an elastic modulus of 3000 MPa, 30 MPa and 100 MPa, and 30 MPa, respectively. A Poisson's ratio of 0.3 was assigned to the calvarial bones, sutures, and craniotomies. A value of 0.48 was assigned to the ICV. Table 3.2 highlights all initial properties and their respective sources. These properties were assigned based on the data in the literature. The model with these properties was denoted as the 'baseline model' for comparison with other models described later as part of the sensitivity studies performed.

**Table 3.2:** Assigned material properties for the baseline FE model.

| Components:        | Elastic modulus (MPa): | Poisson's ratio: | References:                   |
|--------------------|------------------------|------------------|-------------------------------|
| Calvarial bones:   | 3000                   | 0.3              | McPherson & Kriewall, 1980    |
| Calvarial sutures: | 30                     | 0.3              | Moazen <i>et al.</i> , (2015) |
| ICV                | 100                    | 0.48             | Libby <i>et al.</i> , (2017)  |
| CSF:               | 40                     | 0.3              | Convergence test              |
| Craniotomies:      | 30                     | 0.3              | Convergence test              |

**Nodal constraints:** To avoid rigid displacement during simulated growth, a total of eight and three nodal constraints were placed around the foramen magnum and nasal ridge, respectively. These nodes were constrained in all degrees of freedom. The nose constrain was applied due to the facial growth being absent throughout this work, allowing for greater reduction in rigid displacement during simulated growth. Figure 3.3 highlights the precise placement of the nodal constraints.

**Figure 3.3:** Positioned nodal constraint (dark blue) across the models' nasion (left) and foramen magnum (right).

**Contact parameters:** To predict the level of contact pressure at the interface of the segmented intracranial volume and overlying calvarial bones, a surface-to-surface

based contact behaviour was defined. Here, normal and tangential directional movement/sliding between the aforementioned surfaces was granted during the growth of intracranial volume (see below section). The contact surface (here, the ICV) using the element type CONTA174 moves into the target surface (TARGE170), defined as the complete inner calvarial surface. To regulate the penetration between the surfaces, a penalty-based method was parameterised, maintaining the constant values for the friction coefficient (0.1), the penetration-based stiffness (600 N/mm) and the allowable penetration tolerance (0.5 mm). A 'Bonded' contact (no relative movement granted) behaviour was defined between the bones-sutures, sutures-craniotomies, and craniotomies-bone connecting interfaces. Figure 3.4 presents the regions of 'contact' and 'bond' within the model. Note that the entire ICV was assumed to be in initial contact with the inner calvarial interface before growth. Appendix I provides a thorough overview of how the contact interface functions.

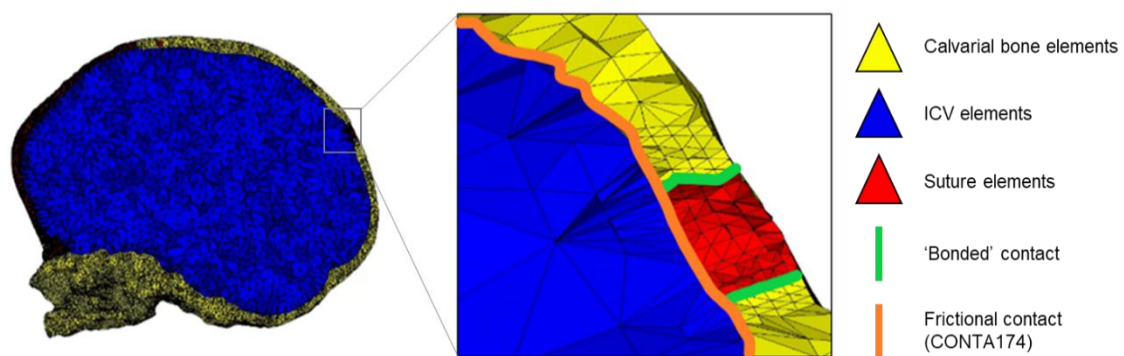


**Figure 3.4:** Enhanced illustration of the contact behaviour between interfaces across the model.

**Calvarial growth:** A thermal expansion analogy was implemented across the ICV component to simulate the calvarial growth. Here the coefficient of thermal expansion was altered by trial and error to generate an expansion of ICV from the pre-operative 4 months (measuring 659 ml) to follow up 76 months (1245 ml) in six load-steps (Table 3.1). As a result, a secant coefficient of 0.00254, a uniform temperature of 100 °C and a reference temperature of 0 °C was used throughout all simulations of this thesis. The estimated ICV at each age was obtained by correlating the predictive volume against data in the literature reporting the normative increase of the ICV (Sgouros *et al.*, 1999). Table 3.3 highlights the comparison between the predictive volumes vs. the literature

data. Further to this, the predictive volumes at 36 and 76 months of age were validated against the patient-specific CT data measurements (Table 3.1), in which a 9.4% volume difference was achieved at 36 months. A difference of less than 1% was then achieved by 76 months. The volume changes and the number of load steps remain consistent throughout all growth simulations. After each load step, the newly deformed calvarial geometry was updated. No computational refinement of the mesh was performed, as this was seen to impede convergence.

**Table 3.3:** Predicted volume at each load step and compared against literature.

| Load-step #: | Predicted volume (ml): | Sgouros <i>et al.</i> , (1999) (ml): | approximate age (months): |
|--------------|------------------------|--------------------------------------|---------------------------|
| 0            | 659                    | -                                    | 4                         |
| 1            | 769                    | 667-901                              | 6                         |
| 2            | 843                    | 719-1026                             | 9                         |
| 3            | 901                    | 990-1143                             | 12                        |
| 4            | 1010                   | 1088-1188                            | 24                        |
| 5            | 1105                   | 1198-1314                            | 36                        |
| 6            | 1245                   | 1258-1666                            | 76                        |

**Bone formation algorithm:** The baseline algorithm to simulate the bone formation across the model was adopted from Marghoub *et al.*, (2020). The global coordinates of all nodes along the bone borders of the sutures and craniotomy components were recorded. Across each node, a radius was used to select suture and craniotomy elements within its range. The range of this radius was determined by the level of volume growth between each load step. Here, a radius of 0.1 mm and 0.8 mm (determined from the literature review) was enforced for each month of growth for the sutures and craniotomy, respectively (Mitchell *et al.*, 2011; Thenier-Villa *et al.*, 2018; Riahihinezhad *et al.*, 2019).

These selected elements had their elastic modulus increased (representing new bone growth) and updated at each load step (representing bone maturity with age). After the initial load step, the next set of elements are selected along the borders of the previously select elements. This pattern continued until the models applicable follow up age was reached.

### 3.2.4 Sensitivity studies

A total of five sensitivity studies were undertaken concerning the geometric parameters, material properties and method of bone formation based on the “baseline model”. Predictions were morphologically validated against the CT data at the follow up age of 76 months where applicable, as discussed in section 3.2.1.

**Mesh convergence:** Mesh convergence was carried out by increasing the number of elements across the entire model from approximately 256,116 to 5,518,454 under five conditions. Specifically, the number of elements across the thickness of the calvarial bones were increased as well as increasing the number of elements across the intracranial volume (to ensure on convergence of the contact pressure values across this volume). Figure 3.5 highlights the five conditions and their numerical values. The first possesses an element count of 256,116, with a consistent ‘single element’ across the thickness of the calvarial bones. The second increases the number of elements from 256,116 (model 1) to 459,635 elements (model 2), whilst maintaining an element thickness of one across the bone and sutures. The third model had 1,148,637 elements, with a minimum of three to four elements across the thickness of the calvarial bones and sutures. The fourth model had 3,535,704 elements, with the number of elements across the ICV surface also increasing. The final model had 5,518,454 elements with a minimum of four elements across the thickness of calvarial bones and refined mesh across the surface of the ICV.

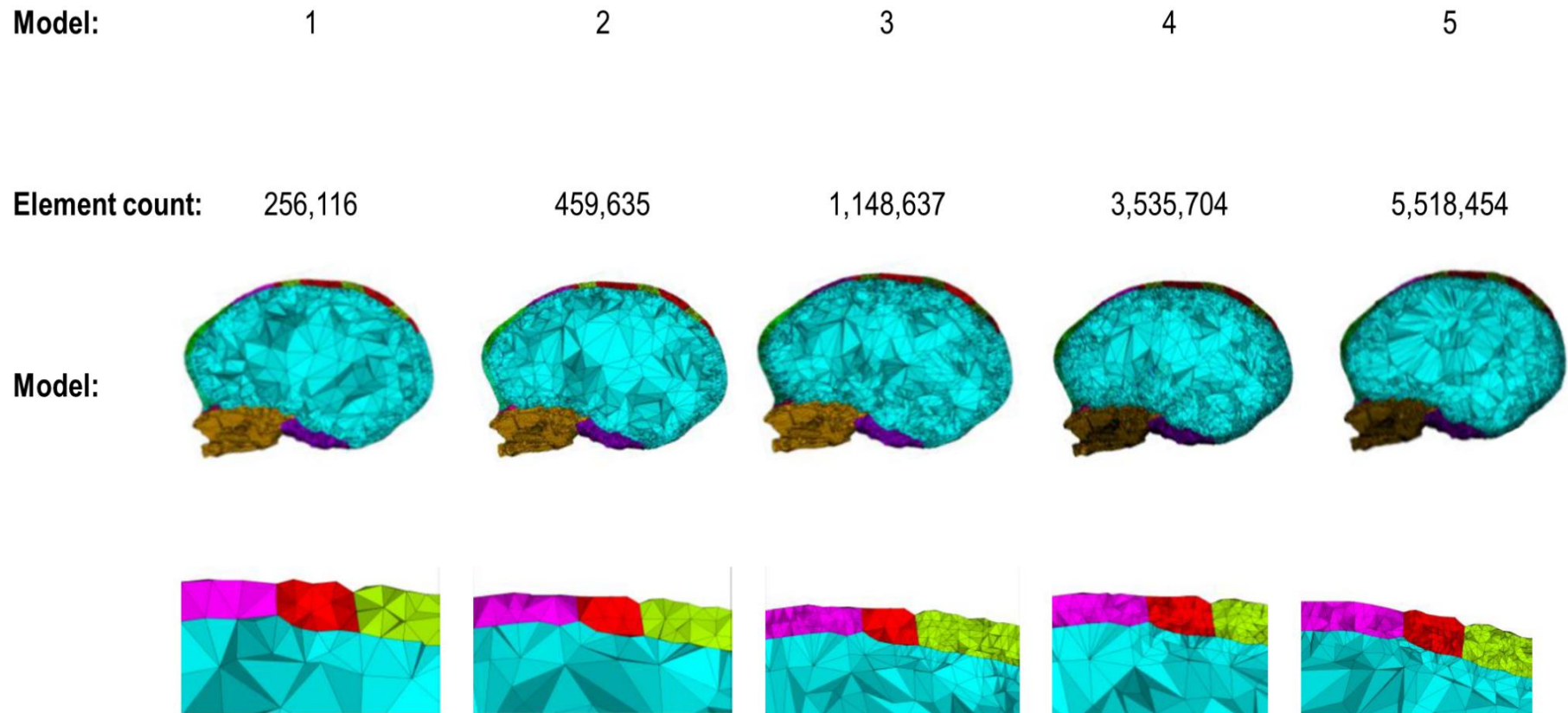


**Figure 3.5:** Mesh convergence analysis. Highlighting the total elements recorded, the internal element structure of the model (sagittal view), and enhanced view of the element structure.



**Intracranial content:** A preliminary investigation was carried out to understand the potential impact of CSF on the predictions of calvarial growth (Figure 3.6). Here CSF was modelled with a thin layer of solid elements to incorporate its impact on the results. It must be noted that CSF is well established to be an incompressible fluid and that here it was modelled with compressible 3D solid elements. While this is a major simplification and does not necessarily represent the nature of this fluid, carrying out a fluid-solid interaction modelling was beyond the scope of this thesis. Nonetheless, this simple approach was adopted to gain some insight into the potential impact of CSF on the growth modelling approach adopted here. In brief, within the “baseline model”, a thin layer of 2-3mm was segmented across the ICV. This level of consistent thickness was chosen, as the CT data was not detailed enough to highlight the CSF accurately. this layer was then meshed with solid elements and imported together with the underlying “brain” in preparation for FE simulations with an elastic modulus of 40 MPa and a Poisson's ratio of 0.3. A ‘bonded’ contact was established between the inner calvarial and the CSF interface. The second (Model II), used as the baseline approach for all forthcoming sensitivity studies, incorporates the CSF and ICV as a single structure, as previously mentioned (section 3.2.1). The impact on the calvarial shape and levels of contact pressure were captured between the two models at 76 months of age. Morphological validations were carried out under a cross-sectional approach between the predictions and the CT data at the same follow up ages.

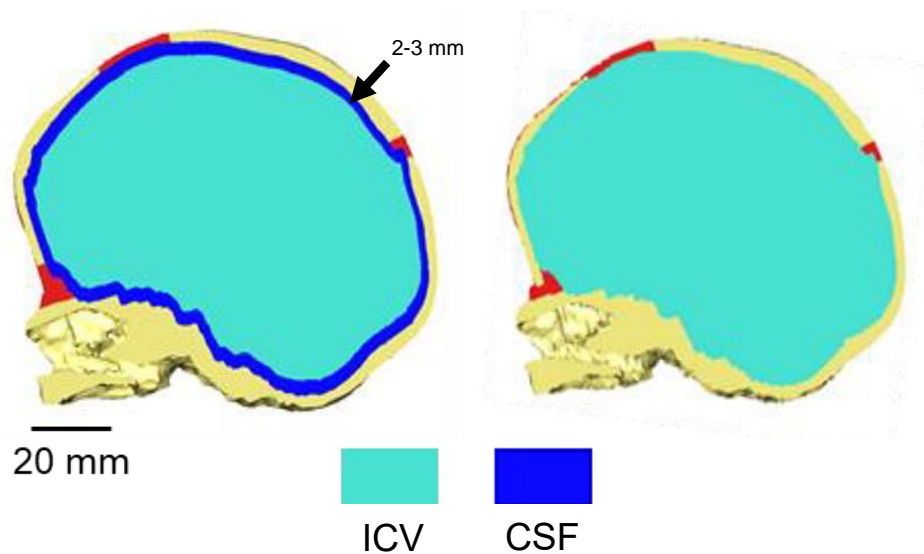


**Figure 3.6:** Sensitivity study of the internal content of the model. Highlighting the newly developed approach (model I-left) and the original baseline approach (model II-right) as seen internally (sagittal view). Abbreviations stand for intracranial volume (ICV) and cerebral spinal fluid (CSF).



**Material properties:** To understand the impact of material properties, changes to the elastic modulus were made under three different scenarios in comparison to the “baseline model”. Table 3.4 summarises the changes and their reference sources. The first scenario reduced the calvarial bone elastic properties from 3000 MPa to 421 MPa, to compare the various values reported across the literature. In the second scenario the elastic modulus of the modelled craniotomies was reduced from 30 MPa to 0.3 MPa. This reduced the resistance of the growth and resemble the ‘gaps’ seen postoperatively although the level of deformation was seen to plateau at 0.3 MPa after a convergence test. The third scenario decreases the rigidity of the ICV by reducing the initial elastic modulus value of 100 MPa to 0.003 MPa. All tests were subjected to morphological comparison against the follow up CT data at 76 months of age to understand the impacts on growth.

**Table 3.4:** Material properties sensitivity. All modelling values and respective reference sources.

| Test #:        | Calvarial bone<br>E (MPa); $\nu$ : | Sutures<br>E (MPa); $\nu$ : | ICV<br>E (MPa); $\nu$ : | Craniotomies<br>E (MPa); $\nu$ : | Sources:                     |
|----------------|------------------------------------|-----------------------------|-------------------------|----------------------------------|------------------------------|
| Baseline model | 3000; 0.3                          | 30; 0.3                     | 100; 0.48               | 30; 0.3                          | See Table 3.2                |
| 1              | 421; 0.22                          | NA                          | NA                      | NA                               | Coats and Margulies, (2006)  |
| 2              | NA                                 | NA                          | NA                      | 0.003; 0.3                       | Convergence test             |
| 3              | NA                                 | NA                          | 0.003; 0.48             | NA                               | Gefen <i>et al.</i> , (2003) |

E: Elastic modulus     $\nu$ : Poisson’s ratio    NA: no change from baseline model values

**Modelling bone growth:** A simplified version of simulated bone formation was compared against the baseline algorithm (See above). Figure 3.7 provides an example of each approach. Designated as “Bulk bone formation”, increased the material properties of all sutures, the craniotomy, and calvarial bone by 100 MPa, 100 MPa, and 125 MPa, respectively, for every month of calvarial growth. These values were taken as an average from calvarial bone and suture studies investigated in mice (Moazen *et al.*, 2015) and the rate of change seen across the ICV (Moazen *et al.*, 2016). The properties of the ICV and CSF remained unchanged throughout.

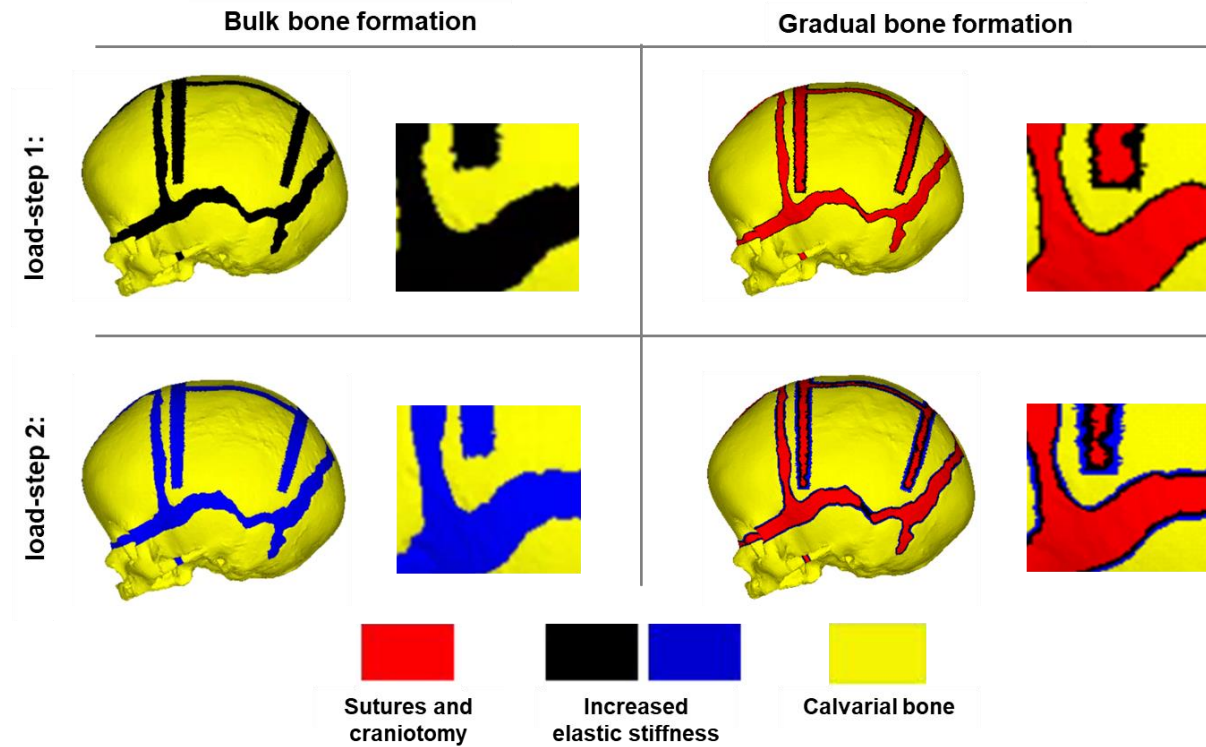


**Figure 3.7:** Illustration of the two approaches to simulating bone formation from the first load-step (6 months) to the second (9 months). “Bulk” bone formation increases the overall stiffness of the segmented components while the baseline bone formation method increases the stiffness from the calvaria bone or newly created bony borders across the sutures and craniotomy. The stiffness changes and distance from the borders were based on the level of growth per month.

To negate the strain affecting the rate or position of bone formation, various thresholds of the hydrostatic strain (i.e., summation of all principal components divided by three) across the suture and craniotomy elements were investigated across the first load-step of simulated growth (4 to 6 months of age), as seen in Figure 3.8. The threshold which highlighted all relevant elements was chosen, this was found to be between 0 - 50% of hydrostatic strain. This allowed both the bulk and baseline formation algorithms to be dictated by simply changing the component's material properties or the specified radii, respectively. The two bone formation approaches were simulated across both models I (with CSF) and II (without CSF) in which the morphological validation was assessed against the CT data at 76 months.

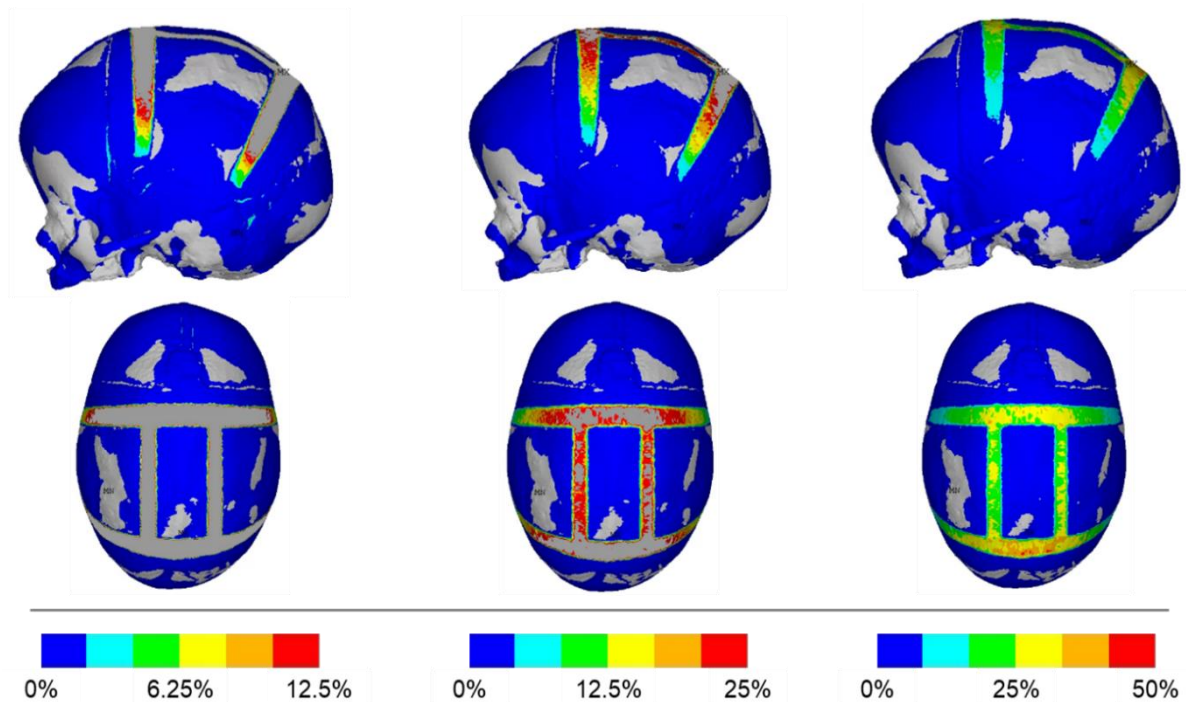


**Figure 3.8:** Qualitative analysis of the different thresholds of the hydrostatic strain seen across the calvarial after the first load-step of simulated growth. Sagittal and dorsal views. The threshold between 0-50% was found to be the most optimal for negating this parameter, as all elements were found to be within this range. Areas in grey represent elements outside of the contour range.

**Rate of bone formation:** Alternating the rates of bone formation across the cranial sutures were carried out across two alternative approaches, using the baseline algorithm model. Table 3.5 details the changes across each approach. The first (noted as approach 1) doubled this rate across all sutures uniformly (from 0.1 mm to 0.2 mm). The second (approach 2) aimed to highlight the natural biological timings of closure across the metopic and anterior fontanelle, where both have been reported to close by 24 months (Pindrik *et al.*, 2014; Teager *et al.*, 2018). To replicate this, the rate of bone formation across these sutures were increased to 0.6 mm/month. The remaining sutures continued to use approach one's value of 0.2 mm/month.

**Table 3.5:** Changes in formation rate values using the baseline formation algorithm under each scenario. Values are for every month of calvarial growth.

| Approach #: | Sutures *<br>(mm/month): | Metopic suture<br>(mm/month): | Anterior fontanelle<br>(mm/month): |
|-------------|--------------------------|-------------------------------|------------------------------------|
| Baseline    | 0.1                      | 0.1                           | 0.1                                |
| 1           | 0.2                      | 0.2                           | 0.2                                |
| 2           | 0.2                      | 0.6                           | 0.6                                |

\*: Incorporating the lambdoid, coronal, squamosal, and craniofacial sutures

### 3.3 Results

**Mesh convergence:** Figures 3.9 and 3.10 highlight the calvarial bone and sutures von mises strain and ICD contact pressure maps across each mesh sensitivity model, respectively. Satisfactory convergence was determined when the overall quantitative values changed by  $\pm 5\%$ . Such satisfaction was achieved in model 3, where a plateau of the strain and pressure commenced. Further, a clear convergence was seen in model 4. From this, the mesh quantity of approximately 3.5 to 4 million elements (900,000 across the ICD) and suitable thickness geometry (i.e., the thickness of 2-4 elements) were used, as the computational cost of model 5 was overwhelming (12-24 hours solving time) while showing little change in overall accuracy.

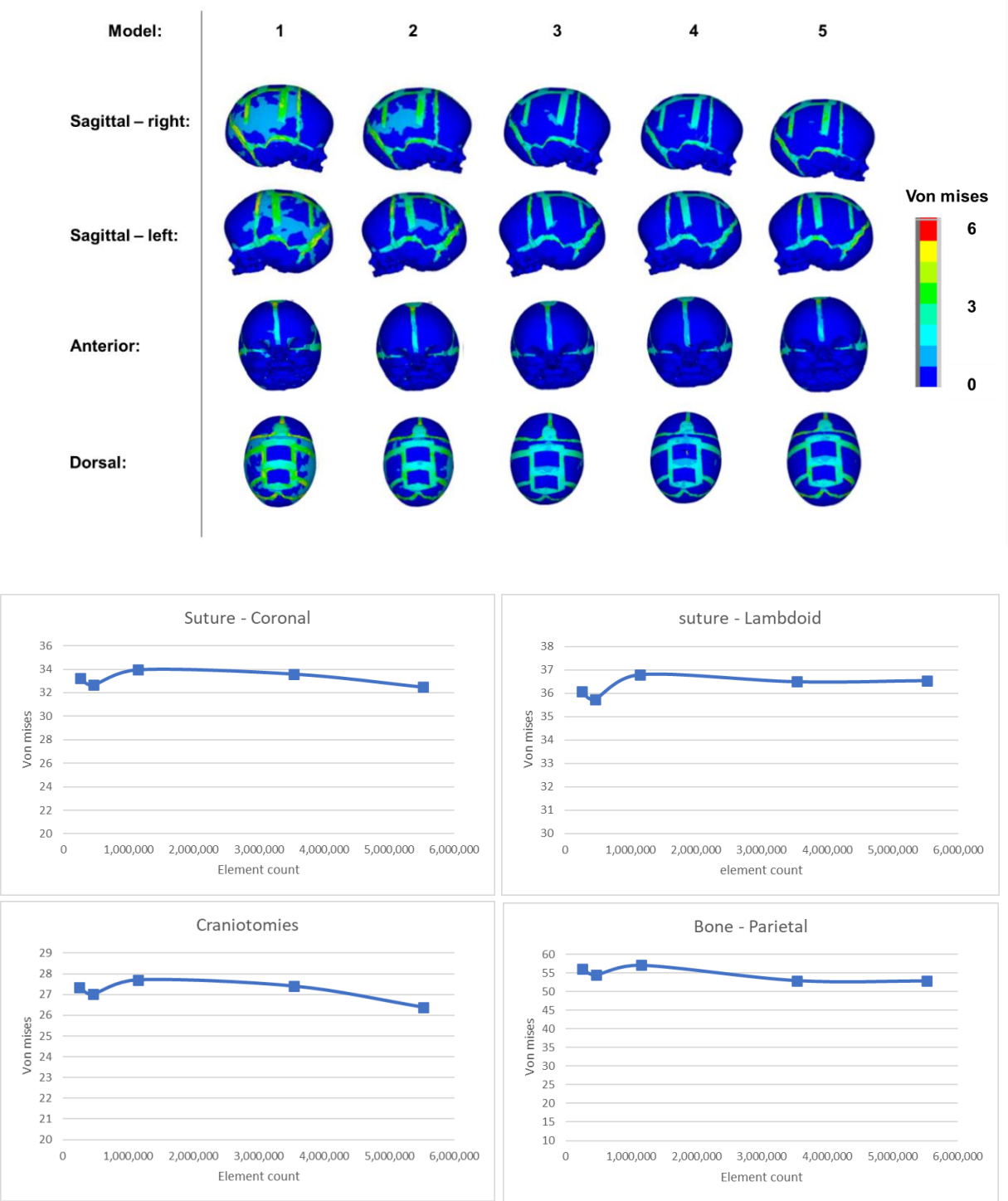


**Figure 3.9:** Observational and quantitative results of calvarial mesh convergence analysis. Displaying each model's von mises strain contour plot after the first load-step of growth (Top) and numerical values across all models (bottom).

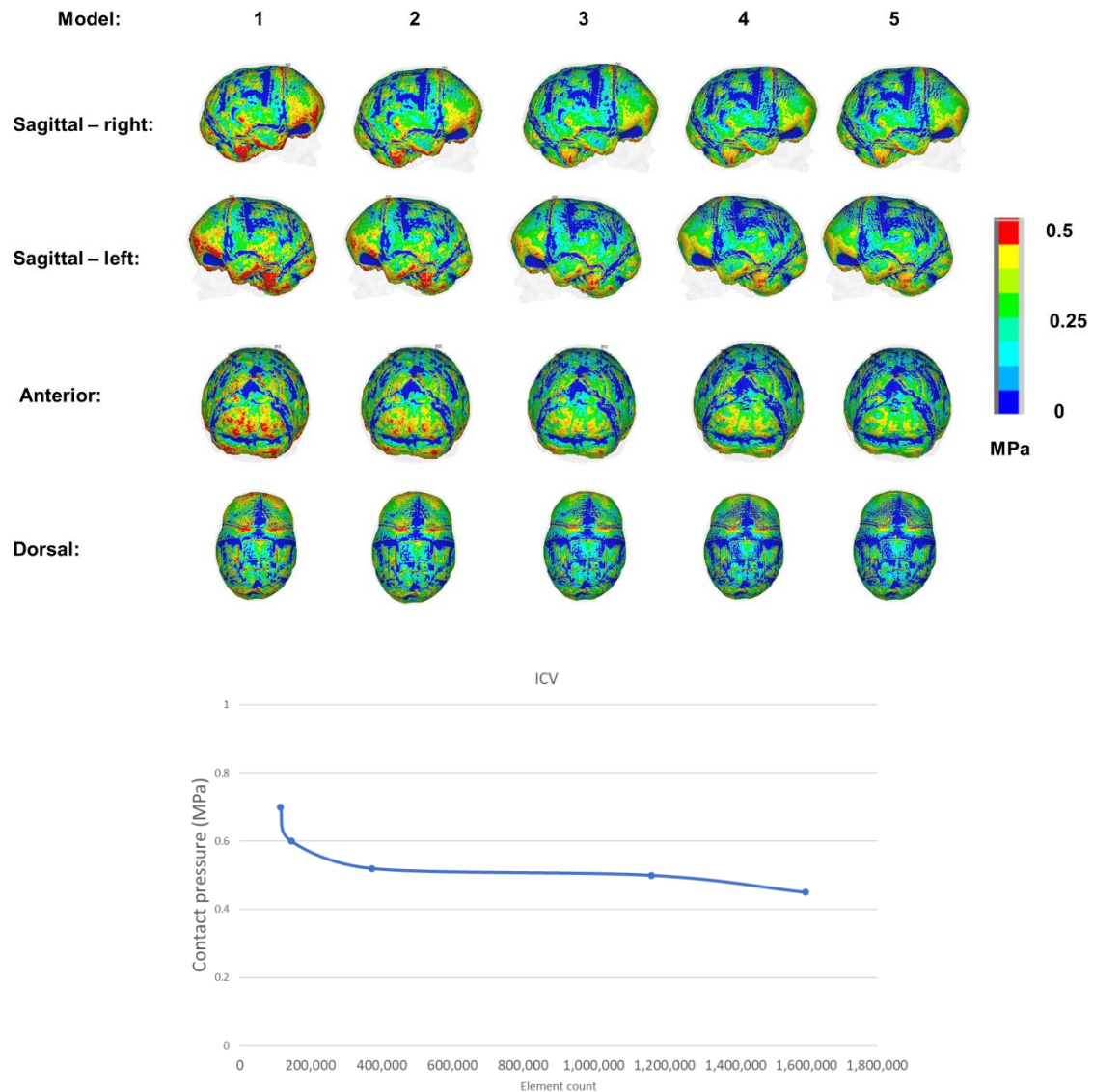


**Figure 3.10:** ICV mesh convergence under contact pressure observations and quantifications across the first load-step for all scenarios.

**Intracranial content and modelling bone growth:** Figures 3.11 validates each morphological prediction across both bone formation methods and intracranial content models using a cross-sectional analysis approach. Table 3.6 further quantifies the cephalometric measurements at 76 months of age. Figure 3.12 displays the level of contact pressure predictions, while Table 3.7 displays how the mean ICV pressure levels vary at alternating regions of interest. Figure 3.13 highlights the growth cycle of both bone formation algorithms introduced.

By 76 months, all modelling approaches demonstrated biparietal underprediction and anteroposterior overprediction when validated against the CT data. This was further accompanied by vertex underpredictions. The model demonstrated no large implications on the morphological shape when CSF was introduced (i.e., model I) vs. the absence of CSF (model II).

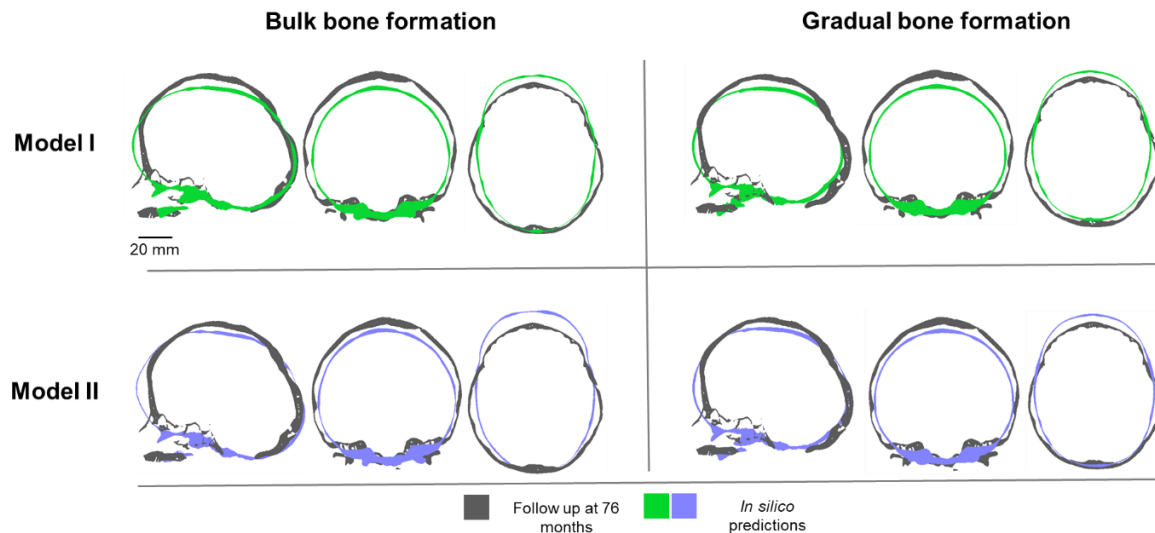


**Figure 3.11:** Comparison of the morphological shape across all possible bone formation and intracranial content scenarios against patient data at 76 months.

Numerically, a more agreeable match was seen across the predictive models undergoing the gradual formation approach. The cephalic index in both models I (83.2) and model II (82.5) were comparable to the CT data (86.6). However, a consistent underprediction was seen for all scenarios in the width (range: 129.4 mm – 132.5 mm) vs. the CT data (143.9 mm). Interestingly, when comparing the method of bone formation, little change was seen between the two approaches. with only a  $\pm 5$  mm and  $\pm 3$  mm in length and width outcomes, respectively. As a result, the cephalic index showed little change between the two scenarios, showing less than a 5 % difference.

Overall, little change was captured across the contact pressure when introducing the variation of CSF, ranging within a value of  $\pm 0.3$  MPa when compared to the absence of CSF. The largest overall changes were seen when altering the method of bone formation, which was seen to double the overall average pressure across all analysed



regions. Visually, all scenarios maintain the largest region of pressure to be across the anterior and temporal regions.

**Table 3.6:** Cephalometric measurements against CT follow up data at 76 months.

| Bone formation method: | Model:   | Length (mm): | Width (mm): | Height (mm): | Cephalic Index: |
|------------------------|----------|--------------|-------------|--------------|-----------------|
| Bulk                   | Model I  | 160.97       | 129.46      | 122.18       | 80.42           |
|                        | Model II | 166.58       | 131.87      | 132.93       | 79.16           |
| Gradual                | Model I  | 155.86       | 129.81      | 128.31       | 83.28           |
|                        | Model II | 160.95       | 132.52      | 132.96       | 82.52           |
| Follow up at 76 months |          | 166.17       | 143.94      | 137.23       | 86.62           |

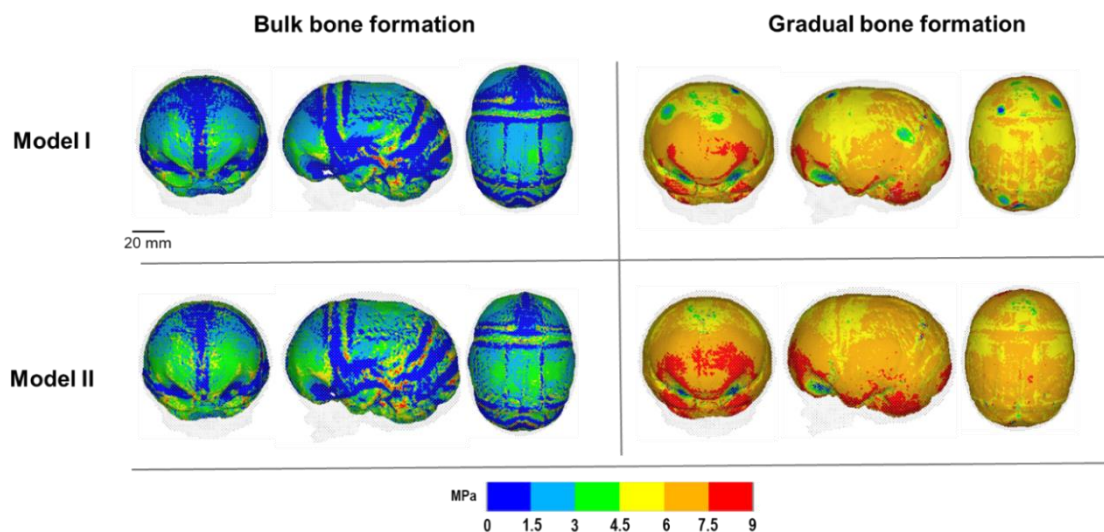


**Figure 3.12:** Comparison of the contact pressure across all possible bone formation and intracranial content scenarios at 76 months.

**Material properties:** The morphological predictions at 76 months across all material property changes and comparison against the follow up CT data are shown in Figure 3.14, with all cephalometric measurements displayed in Table 3.6. All scenarios maintained a good match with the CT data when compared. This was further demonstrated across the cephalic measurements. The most realistic scenario was



seen when lowering the elastic properties of the craniotomy (here, test 2) which demonstrated a characteristic biparietal bulging, matching closely with the cross-sectional data of the CT data when compared. Numerically, all predictions remained within 79 values for the cephalic index, underpredicting the CT follow up value (86.62). All scenarios estimated the overall length changes, whilst underpredicting both the width and height outcomes.

**Table 3.7:** Regional pressure levels across the ICV against all intracranial and bone formation conditions.



| Bone formation method: | Model :  | Frontal lobe |           |            | Parietal lobe |           |            | Temporal lobe |           |            | Occipital lobe |           |            | Cerebellum |           |            |
|------------------------|----------|--------------|-----------|------------|---------------|-----------|------------|---------------|-----------|------------|----------------|-----------|------------|------------|-----------|------------|
|                        |          | Min (MPa)    | Max (MPa) | Mean (MPa) | Min (MPa)     | Max (MPa) | Mean (MPa) | Min (MPa)     | Max (MPa) | Mean (MPa) | Min (MPa)      | Max (MPa) | Mean (MPa) | Min (MPa)  | Max (MPa) | Mean (MPa) |
|                        |          | :            | :         | :          | :             | :         | :          | :             | :         | :          | :              | :         | :          | :          | :         | :          |
| Scenario I             | Model I  | 0            | 17.36     | 1.65       | 0             | 20.82     | 2.19       | 0             | 20.61     | 1.83       | 0              | 22.94     | 1.45       | 0          | 17.49     | 2.17       |
|                        | Model II | 0            | 15.40     | 2.29       | 0             | 18.62     | 2.68       | 0             | 22.63     | 2.33       | 0              | 16.95     | 1.87       | 0          | 20.46     | 2.86       |
| Scenario II            | Model I  | 0            | 8.83      | 5.98       | 0             | 10.97     | 5.69       | 0             | 18.55     | 5.66       | 0              | 11.37     | 5.94       | 0          | 11.61     | 6.64       |
|                        | Model II | 0            | 18.58     | 6.41       | 0             | 23.28     | 6.08       | 0             | 20.82     | 6.06       | 0              | 31.57     | 6.39       | 0          | 31.98     | 6.88       |

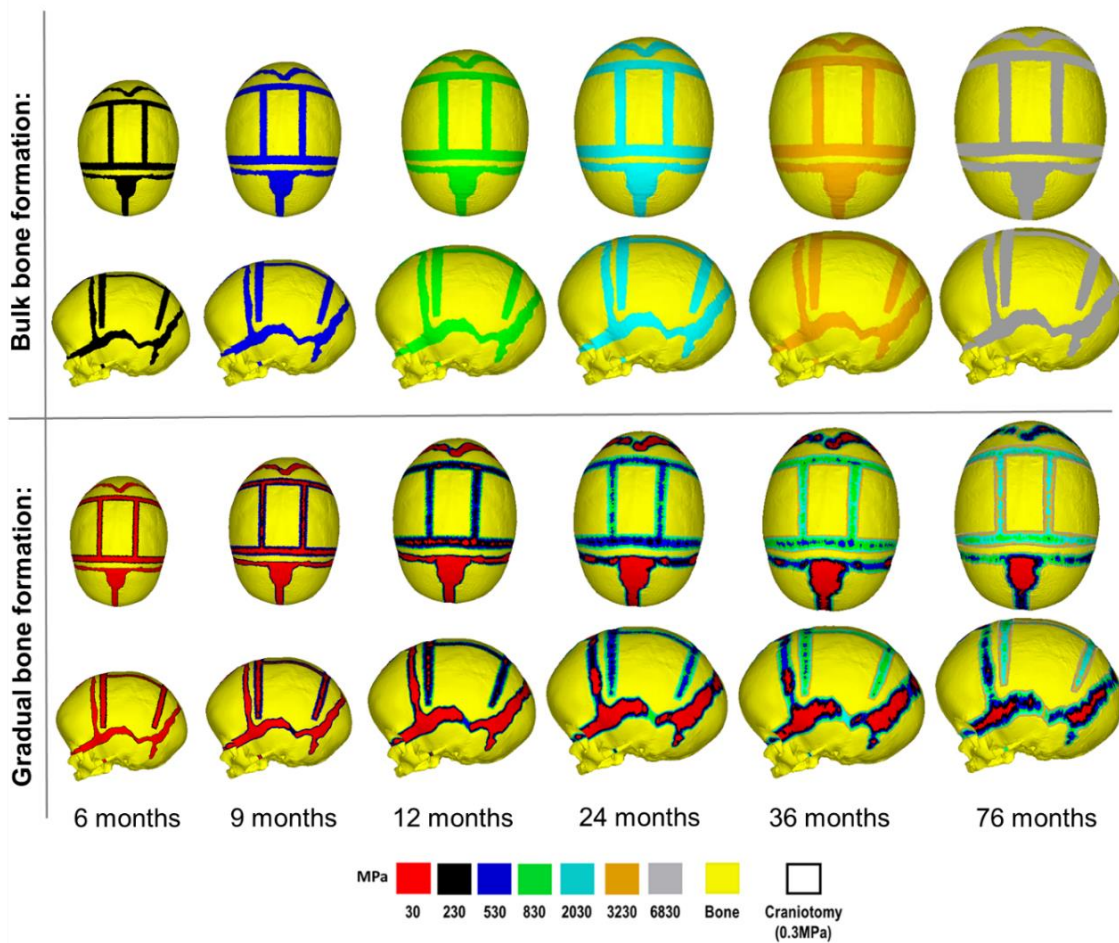


**Figure 3.13:** Predicted outcomes across all load steps for both bone formation methods. All figures are 1:1 scale. Showing the dorsal and sagittal views.

**Rate of bone formation:** Figure 3.15 captures the pattern of suture morphology and timing of suture closure up to 36 months across the various rates considered here. Only the time point of 36 months was observed, as this was the target timing for metopic and anterior fontanelle fusion. Figure 3.16 shows the cross-sectional observations for all approaches. Table 3.8 highlights the cephalic measurements at 76 months. The craniotomy was seen to have fully ‘fused’ (here, deemed as no remaining initial material property elements remaining) by 36 months of age across all predictions. Complete bone formation across all sutures was lacking under the baseline approach, while the two alternative methods achieved this by 36 months of age. For most of the growth, the lambdoid and squamosal sutures were seen to remain open, showing partial regions of closure by 36 months. However, this had reduced in both approaches 1 and 2.

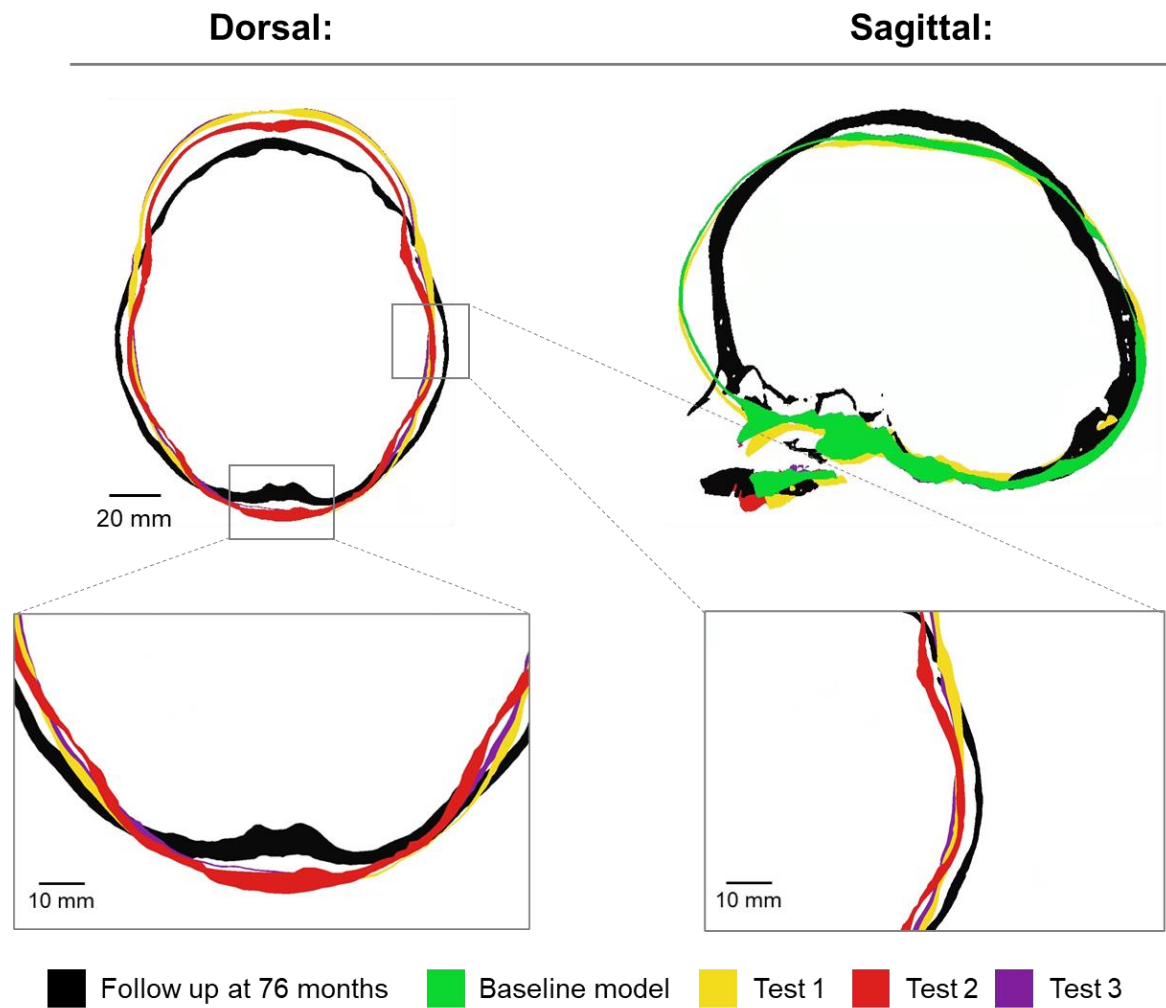


**Figure 3.14:** Material property sensitivity of predictive morphological against follow up CT data at 76 months. Boxes display enhanced regions of interest.

**Table 3.8:** Cephalic measurements of all material properties sensitivities at 76 months of age.

|                             | <b>Length<br/>(mm):</b> | <b>Width<br/>(mm):</b> | <b>Height<br/>(mm):</b> | <b>Cephalic<br/>Index:</b> |
|-----------------------------|-------------------------|------------------------|-------------------------|----------------------------|
| Baseline model              | 166.58                  | 131.87                 | 132.93                  | 79.16                      |
| Test 1                      | 166.9                   | 132.97                 | 132.43                  | 79.67                      |
| Test 2                      | 165.92                  | 129.91                 | 128                     | 78.29                      |
| Test 3                      | 166.52                  | 131.62                 | 132.87                  | 79.04                      |
| <i>In vivo</i> at 76 months | 166.17                  | 143.94                 | 137.23                  | 86.62                      |

**Table 3.9:** Cephalic measurements of all bone formation rate approaches validated against the follow up data at 76 months.

| Bone formation method:      | Length (mm): | Width (mm): | Height (mm): | Cephalic Index: |
|-----------------------------|--------------|-------------|--------------|-----------------|
| Baseline model              | 166.58       | 131.87      | 132.93       | 79.16           |
| Approach 1                  | 168.07       | 130.52      | 131.8        | 77.65           |
| Approach 2                  | 169.56       | 131.3       | 131.57       | 77.43           |
| <i>In vivo</i> at 76 months | 166.17       | 143.94      | 137.23       | 86.62           |

Both the baseline model and approach 1 failed to achieve complete closure of the anterior fontanelle, while approach 2 demonstrated near closure and successful closure by 12 months and 36 months, respectively. Only the baseline model failed to fuse the metopic suture, while both alternative approaches achieved fusion by 36 months. Little change was seen across all cephalometric measurements, with all predicting the follow up CT data length outcomes accurately, while underprediction was seen across the width and height. This was further seen in the cephalic index values.

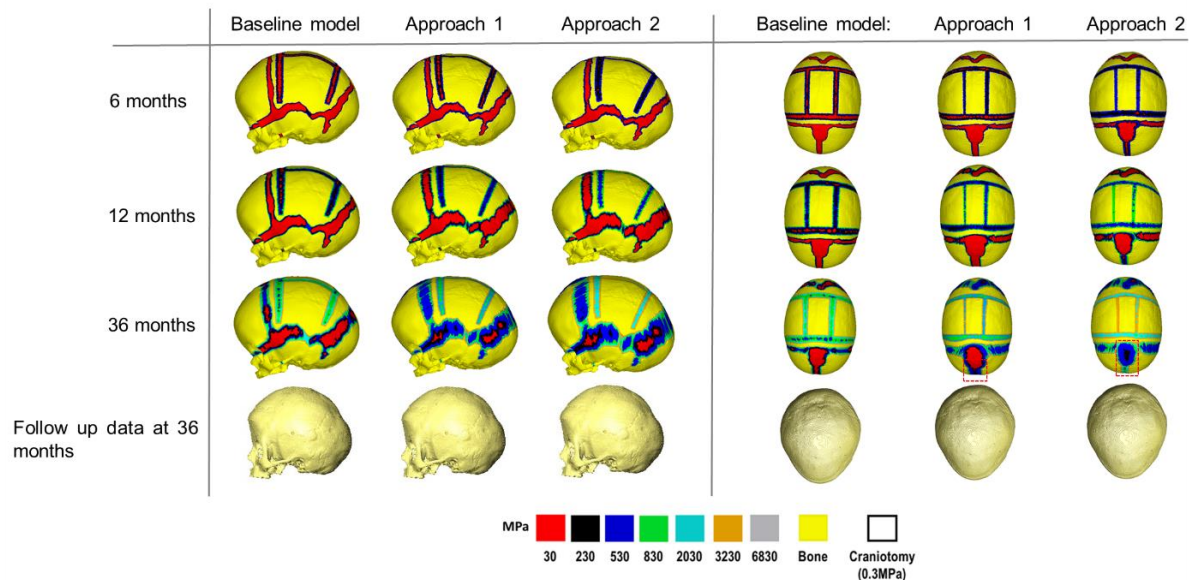


**Figure 3.15:** The gradual bone formation predictions across all various rate approaches. Showing the sagittal (Left) and dorsal (Right) viewpoints. Red boxes highlight regions where full closure has been achieved.

Little to no difference was seen in the cross-sectional morphological outcomes. Both alternative approaches suggest a minor reduction across the anteroposterior vs. the baseline method.

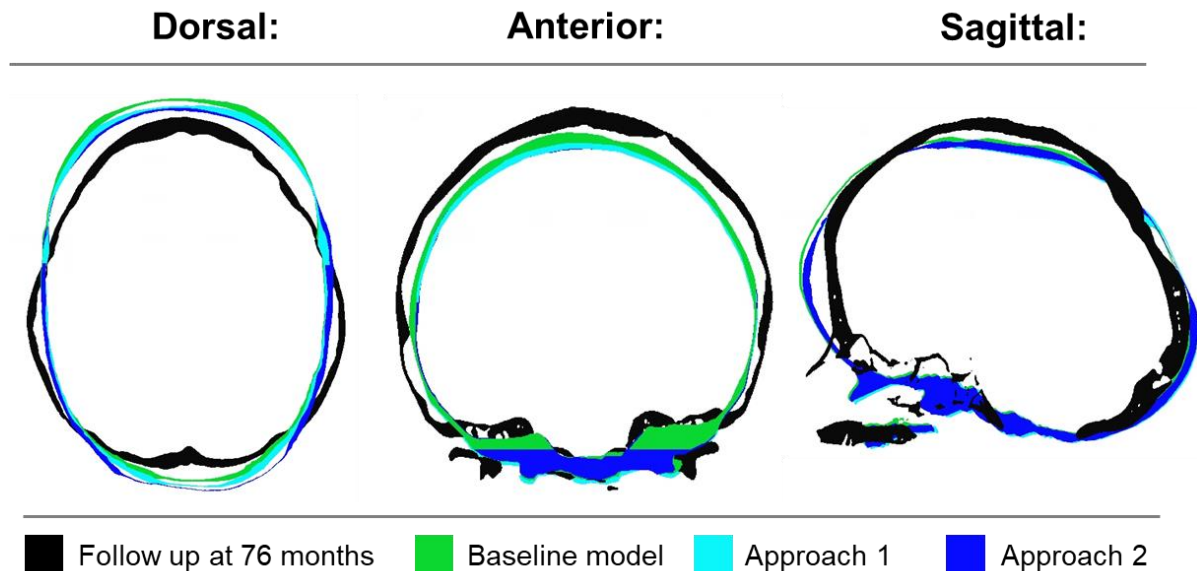


**Figure 3.16:** Cross-sectional outcomes of all bone formation rate approaches against follow up data at 76 months.

### 3.4 Discussion

In this chapter, a detailed analysis was undertaken to validate the generic pre-operative FE model to be used throughout the later studies of this thesis. To accommodate this, sensitivity studies regarding the method of bone formation, the rate of bone formation, the elastic moduli of components, and the impacts of modelling the CSF were all investigated. Where appropriate, morphological validation of the predictive growth was performed against the patient's CT data at the maximum follow up age of 76 months.

**Intracranial content:** Here, the properties of the modelled CSF were of isotropic behaviour. In reality, the CSF would act as a frictionless, incompressible fluid within the subarachnoid space (Sakka *et al.*, 2011). Although the FE method can simulate these effects, many computational based studies do not consider or do not require the

surface-based contact behaviour used here (Lapeer & Prager, 2001). Further to this, as the ability to accurately differentiate the brain and CSF could not be achieved, the alternative approach shown here was adopted. As a result, it is understandable that little impact was seen across both the morphological (Figure 3.11 and Table 3.6) and contact pressure observations when compared with the absence of CSF (Figure 3.12 and Table 3.7). This could be attributed to the characteristics of the CSF, where the elastic stiffness of this component (40 MPa) was far less than that of the ICV (100 MPa) and initial bone material (3000 MPa). Nevertheless, it was of interest to the project to assess the impacts of modelling the CSF could have on predicted outcomes. As such, implementing CSF is not a consideration for further simulations.

**Modelling bone formation:** Previously used in mouse and human models, the two methods of bone formation were replicated across the model shown here (Marghoub *et al.*, 2019; Malde *et al.*, 2020). Conversely to the above observations, the two methods of bone formation were seen to have large implications on contact pressure levels and little impact on the predictive shape. Predictions highlighted patency across the sutures using the baseline formation algorithm (Figure 3.13). This alleviation in restricting the growth may have led to a reduction of the pressure seen by 76 months (Figure 3.12) while the bulk formation method restricts this growth more aggressively. Although the impact on shape is minute, both methods did achieve a close match to CT data measurements (Table 3.6). As such, the gradual bone formation will be used throughout the remainder of this thesis.

**Material properties:** As many components are considered in the developed model, with larger ranges of biological tissues' elastic moduli properties in the literature, an analysis of the sensitivity of such properties was conducted. Here, predicted observations to changes in morphology were captured. Upon review, the reduction in elastic properties for the craniotomies (30 MPa to 0.3 MPa) resulted in the largest alteration in calvarial shape (Figure 3.14), intending to resemble the natural and unrestrictive 'gaps' seen postoperatively. The presence of sudden bitemporal widening is clinically seen *in situ* (due to alleviation of the constricted parietal bones), achieving the surgical goal of anteroposterior shortening while increasing the bitemporal widening (Rocco *et al.*, 2012). Although this function could not be replicated

here, manipulation (i.e., bulging) of the temporal bones is seen by 76 months of age, matching closely to the *in vivo* CT scan. While the other analysed scenarios could impact the morphology, the elastic modulus of the craniotomy is a crucial component in these predictions. Although the impact of the type of surgery is absent here, along with combining these material properties into a single modelling scenario, such considerations are addressed in the following chapters.

**Rate of bone formation:** To maintain the clinical timings of sutural closure across the developed model, various formation rates were assessed. Here, it was found that doubling the rate of suture formation (0.1mm/month to 0.2mm/month) in combination with accelerating both the metopic suture and anterior fontanelle (i.e., approach 2) maintained the closest visual match to CT data by 36 months (Figure 3.15). Conversely, all approaches to bone formation rates yielded near identical morphological appearances (Figure 3.16 and Table 3.9), suggesting that the current method of bone formation may require optimisation. A limitation of the current method lies in the extensive need for parameterisation. For example, the sutures and craniotomy rate of bone formation are currently dictated by the users' inputs, providing little in the way of computationally predicting the outcomes. Biologically, bone formation is governed by a combination of natural strain and chemical processes, neither of which are present (Beederman *et al.*, 2014). Nevertheless, a good match of the timing of both suture and anterior fontanelle closure was seen with the current method (Teager *et al.*, 2018; Pindrik, 2014).

### 3.5 Summary

This chapter presented a series of sensitivity tests which investigated the impacts of various input parameters of the proposed modelling approach on the calvarial growth morphology and the level of contact pressure at the interface of ICV and calvarial bones, while the predictive morphology was validated against patient-specific data at 76 months of age. Lessons from this chapter highlight how sensitive the model is to the choice of such parameters and its subsequent impact on predictions. The largest impact on predicted growth was seen on the choice of material properties for the craniotomies. It was also seen that the choice of bone formation had little impact on



### Chapter 3: Patient-specific model

the growth, but had significant impacts on the contact pressure. Although the rate of calvarial healing was not analysed here, along with only a single technique being replicated, the next chapter will expand on these areas.

## **Chapter 4: Predicting the postoperative outcomes of three surgical techniques**

## 4.1 Introduction

For the overall purposes of this thesis, the patient-specific model that developed in Chapter 3 was used in this chapter as a generic model to investigate the biomechanics of three alternative treatment methods for sagittal craniosynostosis. These include using 2 and 3 springs for a technique called spring-assisted cranioplasty (SAC) and strip craniotomy. Here, a description of the techniques performed is highlighted, that differ in overall dimensions and invasiveness. Secondly, as two of the three procedures adopted the use of distractor devices, a new set of sensitivity analysis were performed and is described. Thirdly, an investigation into alternative bone formation rates (exclusively for calvarial healing) is performed. Where possible, technique-specific CT data sets were used for predictive morphological comparison. Where this was not possible, reported cephalometric measurements from the literature were used.

## 4.2 Materials and methods

This section summarises the parameters and modelling approaches used throughout the chapter. The first sub-section discusses the CT and literature data used for morphological comparison, accompanied by a brief description of each replicated technique. Secondly, an overview of the parameters and constraints across the patient-specific model will be explained. Finally, a summary of all sensitivity studies performed is highlighted, concluding with the qualitative and quantitative data being recorded for each technique.

### 4.2.1 *In vivo* CT and literature data

**CT data:** For validation of two of the replicated techniques, CT data of patients undergoing the spring-assisted cranioplasty (SAC) techniques, totalling 18 individual cases, were provided by the Department of Plastic Surgery at the Sahlgrenska University Hospital (Gothenburg, Sweden). Patients had undergone the standard Gothenburg technique, in which patients had either two ( $n=10$ ) or three ( $n=8$ ) springs inserted during surgery. These patient cases were grouped accordingly as having been treated with two springs (2 SAC) or three springs (3 SAC).

## Chapter 4: Predicting three techniques

Patient CT data was recorded at pre-operative (4 months), post-operative (10 months), and follow up (37 months) time points. Table 4.1 summarises the average cephalometric and intracranial volume measurements across both groups at their respective time points.

**Table 4.1:** CT data across both spring-assisted cranioplasty groups at each captured age. Data shows overall average measurements with standard deviations.

|                       | 2 SAC          | 3 SAC          |
|-----------------------|----------------|----------------|
| n:                    | 10             | 8              |
| Male (%):             | 80             | 50             |
| <b>Preoperative:</b>  |                |                |
| Age (months):         | 4.9 ± 1.3      | 4.1 ± 0.7      |
| Length (mm):          | 148.5 ± 6.1    | 150.5 ± 9.9    |
| Width (mm):           | 114.3 ± 5.7    | 111.5 ± 5.6    |
| Circumference (mm):   | 455.3 ± 68.0   | 457.2 ± 27.0   |
| ICV (ml):             | 800.9 ± 102.1  | 800.8 ± 88.6   |
| Cephalic index:       | 76.9 ± 2.7     | 74.0 ± 3.4     |
| <b>Postoperative:</b> |                |                |
| Age (months):         | 10.9 ± 1.3     | 10.6 ± 0.3     |
| Length (mm):          | 162.5 ± 8.0    | 165.2 ± 6.1    |
| Width (mm):           | 129.8 ± 5.0    | 129.1 ± 6.6    |
| Circumference (mm):   | 486.5 ± 59.4   | 429.0 ± 107.0  |
| ICV (ml):             | 1089.2 ± 144.9 | 1131.2 ± 130.5 |
| Cephalic index:       | 79.9 ± 2.9     | 78.2 ± 4.5     |
| <b>Follow up:</b>     |                |                |
| Age (months):         | 37.1 ± 2.0     | 37.6 ± 1.3     |
| Length (mm):          | 176.9 ± 9.3    | 178.8 ± 8.8    |
| Width (mm):           | 135.1 ± 5.4    | 132.7 ± 6.4    |
| Circumference (mm):   | 512.4 ± 35.4   | 523.2 ± 37.0   |
| ICV (ml):             | 1245.0 ± 166.8 | 1239.0 ± 133.8 |
| Cephalic index:       | 76.4 ± 2.5     | 74.3 ± 3.8     |

**SAC:** spring-assisted cranioplasty; **ICV:** intracranial volume.

**Literature data:** For the third replicated technique, a modified strip craniectomy (MSC) technique was adopted from the detailed report of Thomas *et al.*, (2015), undertaken at the craniofacial centre of Oxford University Hospital (Oxford, UK). Such literature data was used in the absence of patient CT data, as this technique was previously used for several years in the unit. Cephalic data within the literature were reported across 34 individuals at pre-operative ( $6.0 \pm 3.1$ –9.5 months), postoperative (12 months) and follow up (60 months). The cephalic index was reported at these time points, measuring  $65.7 \pm 4.7$ ,  $73.3 \pm 5.2$  and  $71.5 \pm 4.3$ , respectively. Using this data, a comparison of the reported literature CI and predicted cephalic index measurements was carried out.

**Surgical intervention:** Figure 4.1 shows the techniques replicated in this chapter. The methods of corrections were as follows:

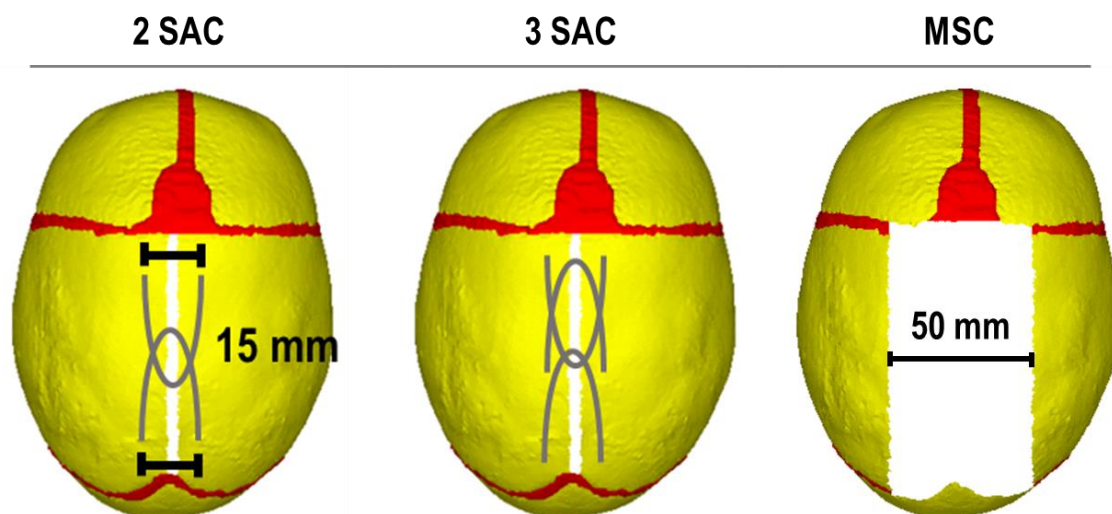


**Figure 4.1:** Illustrations of all three replicated surgical techniques performed on the patient specific model at 4 months of age. Dorsal view.

*Spring-assisted cranioplasty (2 SAC and 3 SAC):* Guidance from the relevant surgical teams, in addition to references to the reports from Lauritzen *et al.*, (1998) and more recently Satanin *et al.*, (2019), were used to replicate the surgical techniques discussed here. In short, a 1-5 mm suturectomy, extending from the anterior to posterior fontanelles, was made across the fused sagittal suture. Clinically, burr holes

were made for spring insertion across the parietal bones (5 mm from the craniotomy site). It should be noted that clinically, upon the springs being placed in the burr holes, an initial displacement of 5 mm is seen across the spring (measured from one spring leg to the other). This effect was considered and simulated here prior to calvarial growth.

Here, the anterior, middle, and posterior springs were simply attached to adjoining elements across the segmented parietal bones, with an initial leg-to-leg distance of 15 mm across the created craniotomy. The springs were then placed 40 mm (most anterior spring), 55 mm (middle spring – 3 SAC) and 75 mm (most posterior spring) posteriorly from the coronal suture. After 5 months post insertion, the springs were removed in a second procedure, allowing the skull to continue growing unaided. To model this, the elements representing the springs were simply deleted at the 5 month post-operative time point.

*Modified strip craniectomy (MSC):* As a comparative technique, the MSC technique was adopted from the descriptive report by Thomas *et al.*, (2015). In this technique a 50 mm wide craniotomy, extending from the coronal to lambdoid sutures, was performed across the vertex of the parietal bones. As a simple corrective process, no other incisions were performed, nor are any devices inserted. This technique was intentionally used here as a direct comparison with the SAC as, biomechanically, it only differed in terms of the width of the craniotomy and the absence of the spring.

### 4.2.2 Finite element method

The modelled boundary conditions and parameters used here were discussed previously in section 3.2.2. Further, the ‘baseline’ formation algorithm, in conjunction with the accelerated formation of the metopic and fontanelle sutures, was used here. Finally, the modelling approach denoted previously as ‘Model II’ along with the contact behaviours were also adopted.

**Material properties:** An initial elastic modulus of 421 MPa, 10 MPa, 30 MPa, and 0.3 MPa were established for the calvarial bones, ICV, sutures and craniotomy, respectively. The Poisons ratio values remain unchanged from section 3.2.3.

**Spring mechanics:** Mechanically, springs abide under Hookean's law, where the spring's tensile forces are directly proportional to the level of compression made (Borghetti *et al.*, 2017). To replicate this behaviour, linear spring elements (COMBIN14) were used, in which the initial forces and spring stiffnesses were parameterised. Relative to the Gothenburg technique, *ex vivo* measurements of these springs' mechanical responses under compression were recorded by the clinicians and recorded in the appendix (See: Appendix II). The springs' leg-to-leg distance while under no relative compression was 100 mm. Once compressed by 85 mm (i.e., a leg-to-leg distance of 15 mm, replicating the SAC procedure), a unilateral force of 8 Newtons was generated. Using these values, the FE method calculated the spring stiffness ( $k$ ) via equation (1):

$$(1) k = f/dx$$

Where ( $f$ ) represents the spring force and  $dx$  the leg-to-leg distance of each spring under the stated compression. Using this, a constant spring stiffness of 0.0094 N/mm was calculated. To update the tensile forces across the bone during simulated growth, equation (2) was used:

$$(2) f = k \times dx$$

Here, the forces ( $f$ ) were automatically updated based on the changes in  $dx$ . The spring stiffness remained unchanged.

### 4.2.3 Sensitivity studies

**Simulated spring release:** To understand the sensitivity of replicating the springs naturally expanding upon insertion, as well as achieving a target leg-to-leg displacement of 5 mm (denoted here as 'release', see section 4.2.1) before simulated growth, ten variations were investigated using the 2 SAC model. Table 4.2 highlights each scenario considered during this simulated spring 'release'. A brief description of each variation is as follows:

**Baseline:** All geometric, material and contact properties remain unchanged from the reported model in section 4.2.2. As the complete geometry of the model was present, in the confines of this sensitivity analysis, this was denoted as ‘whole skull’.

**Scenario 1:** Adopted from the reported modelling approach of Borghi *et al.*, (2018), the calvaria was divided across the vertex using the left and right euryons as anatomical landmarks, removing the lower half of the model completely. This method was denoted as ‘half skull’. The ICV component was removed, leaving the calvarial bone, sutures, craniotomy, and springs. All remaining material properties were unchanged from the baseline model. Justification for such a scenario was to understand the impact incorporating the facial region and lower calvarial portion (i.e., temporal, occipital and frontal bones) could have on resistance of the spring expansion.

**Scenario 2:** The complete geometry of the skull is restored to the baseline structure (i.e., whole skull). The ICV component remains absent and material properties unchanged.

**Scenario 3:** The craniotomies elastic modulus was reduced by an order of magnitude from the baseline value of 0.3 MPa to 0.03 MPa. All other properties remain unchanged. The ICV component remained absent from the model.

**Scenario 4:** The calvarial bones' elastic modulus was reduced by an order of magnitude from the baseline value of 421 MPa to 41 MPa. All other parameters remain unchanged. The ICV component remained absent from the model.

**Scenario 5:** The sutures' elastic modulus was reduced from the initial 30 MPa to 3 MPa. All other material properties remain unchanged. The ICV component remained absent from the model.

**Scenario 6:** To analyse the overall impact the present the ICV has on predictions, the ICV component is re-introduced. The elastic modulus was reduced to the value of 1 MPa. Further, the contact interfaces between the ICV-internal bone are removed, maintaining a fixed, rigid behaviour.



**Scenario 7:** Conditions from the previous scenarios are combined into a single approach. Here, the material properties from scenarios 4 (Calvarial bone – 41 MPa) and 5 (Suture – 3 MPa) are introduced. This also includes the absence of the ICV.

**Scenario 8:** The conditions of scenarios 4 (Calvarial bone – 41 MPa) and 6 (ICV – 1 MPa) are combined and assessed here. The ICV maintains a fixed contact behaviour with the internal bone interface.

**Scenario 9:** Only the contact interface was assessed here. Where all material properties are restored to the baseline values and the interface between the ICV-calvarial bone is fixed.

**Scenario 10:** As a comparative assessment to scenario 6, the ICV contact parameters are restored to a frictionless penalty-based behaviour whilst retaining the elastic moduli changes to the bone (41 MPa) and ICV (1 MPa).

## Chapter 4: Predicting three techniques

**Table 4.2:** Conditions of each sensitivity scenario. N/a indicates no change from baseline values or conditions. E represents the elastic modulus. Areas marked in grey highlight the changes made from the baseline model.

| Scenario:      | Skull geometry: | Bone E (MPa): | Sutures E (MPa): | Craniotomy E (MPa): | ICV E (MPa): | ICV present: | Bone-ICV contact behaviour: |
|----------------|-----------------|---------------|------------------|---------------------|--------------|--------------|-----------------------------|
| Baseline model | Whole skull     | 421           | 30               | 0.3                 | 10           | Yes          | contact                     |
| 1              | Half skull      | n/a           | n/a              | n/a                 | n/a          | No           | none                        |
| 2              | Whole skull     | n/a           | n/a              | n/a                 | n/a          | No           | none                        |
| 3              | Whole skull     | n/a           | n/a              | 0.03                | n/a          | No           | none                        |
| 4              | Whole skull     | 41            | n/a              | n/a                 | n/a          | No           | none                        |
| 5              | Whole skull     | n/a           | 3                | n/a                 | n/a          | No           | none                        |
| 6              | Whole skull     | n/a           | n/a              | n/a                 | 1            | Yes          | fixed                       |
| 7              | Whole skull     | 41            | 3                | n/a                 | n/a          | No           | none                        |
| 8              | Whole skull     | 41            | n/a              | n/a                 | 1            | Yes          | fixed                       |
| 9              | Whole skull     | n/a           | n/a              | n/a                 | n/a          | Yes          | fixed                       |
| 10             | Whole skull     | 41            | n/a              | n/a                 | 1            | Yes          | contact                     |

**Spring forces sensitivity:** To assess the impact various spring forces during ‘release’ could have on the simulated growth, the spring stiffnesses were altered across two additional models. Figure 4.2 illustrates each respective model’s parameters. Here, the baseline approach was used as a comparison. These spring stiffnesses were valued at 0.094 N/mm (baseline), 0.105 N/mm (Test 1) and 0.117 N/mm (Test 2), which generated an initial force of 8, 9, and 10 Newtons, respectively. All approaches underwent growth from the pre-operative age of 4 months up to 9 months of age. The residual forces across the springs under each approach were calculated and compared during simulated growth.

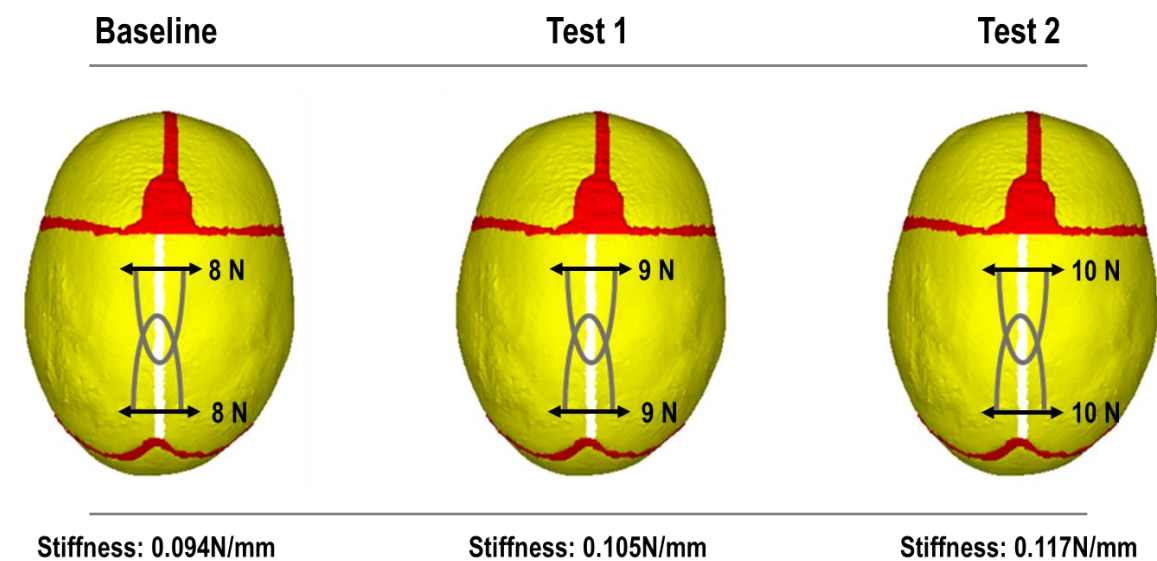


**Figure 4.2:** Illustration of each spring force sensitivity analysis under the 2 SAC technique with the spring stiffnesses used. Dorsal view.

**Craniotomy bone formation rate:** Extending on the sensitivities discussed in chapter 3, an analysis of the alterations to the rate of bone formation exclusively across the craniotomy was performed. Table 4.3 highlights the parameters under each model used for the sensitivity analyses. Building on the ‘baseline’ formation rate of 0.8 mm for every month of calvarial growth (here, models 1 and 2), the radius of formation from the bone lining was increased to 10.8 mm for every month of growth (models 3 and 4). To understand the impact across the diverse surgical techniques, both the 2 SAC and MSC replicated techniques were introduced. All techniques underwent growth from 4 months up to 36 months of age, where the impacts on morphology and contact pressure levels were assessed.

## Chapter 4: Predicting three techniques

**Table 4.3:** Conditions of each scenario of analysing the formation rate across the craniotomy. Sutures, metopic and anterior fontanelle formation rate remain unchanged from baseline model.

| Model: | Craniotomy formation rate (mm/month): | Craniotomy width (mm): | Surgical technique: |
|--------|---------------------------------------|------------------------|---------------------|
| 1      | 0.8                                   | 5                      | SAC                 |
| 2      | 0.8                                   | 50                     | MSC                 |
| 3      | 10.8                                  | 5                      | SAC                 |
| 4      | 10.8                                  | 50                     | MSC                 |

**Simulations and measurements:** All three replicated techniques underwent calvarial growth and bone formation up to 36 months of age. For both the 2 and 3 SAC techniques, the simulated ‘release’ phase of spring expansion was performed prior to skull growth. As literature data for MSC was presented at a follow up age of 60 months, the follow up predicted data underwent further growth up to 60 months of age. Cephalometric measurements of the length, width, cephalic index, circumference, and intracranial volume measurement were undertaken for all predicted models. An attempt to validate the morphological predictions of both SAC techniques was performed using 3D distance mapping. For this, a single CT image at each respective time point matching closest to the overall average cephalic measurement reported in Table 4.1, was selected. Bone formation and contact pressure patterns were captured during simulated growth for all predicted techniques. In addition to morphological validation, the predicted spring opening distance by spring removal (9 months of age) was validated against the measurements recorded across all SAC CT data sets. For all sensitivity studies, morphological measurements and spring opening distances were recorded.

## 4.3 Results

**Simulated spring release:** Figure 4.3 highlights the leg-to-leg distances under each considered scenario. The target expansion upon release (noted from surgical

## Chapter 4: Predicting three techniques

guidance) was 5 mm for all scenarios. The baseline scenario resulted in the greatest resistance across the springs, achieving only 0.1 mm of expansion in both springs upon release. Removal of the lower half of the skull (i.e., 'Half skull') improved this prediction, achieving a leg-to-leg distance of 1.4 mm.

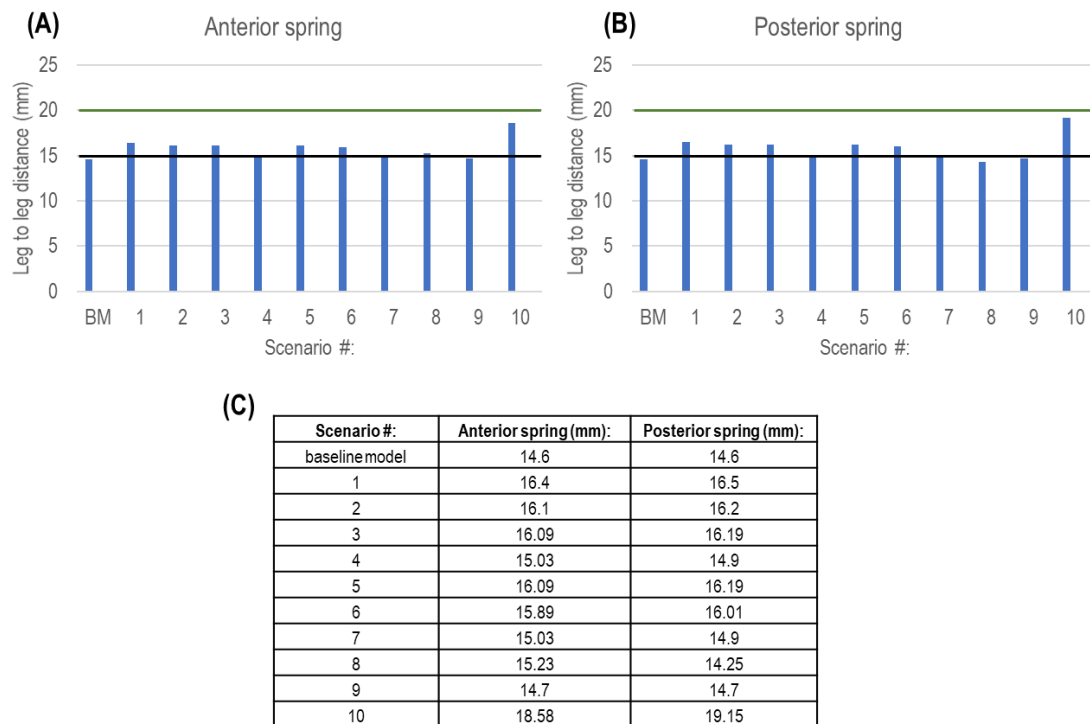


**Figure 4.3:** Material property, contact behaviour and skull geometry impacts on spring displacement at release. The level of expansion was measured by capturing the leg-to-leg distance of both anterior (A) and posterior (B) springs and their distances from the initial distance (Black line) to see which condition best predicted with the target displacement of 5 mm (Green line). All numerical values are also present (C). Note that BM is the abbreviation of the baseline model.

All remaining scenarios had a moderate restriction on spring displacement, compared to the baseline model. The conditions of scenario 10 were seen to have the least impact on spring displacement, achieving 3.5 to 4 mm upon release. Though the target displacement of 5 mm was not achieved, scenario 10's parameters predicted the most suitable conditions to replicate this, and thus, were used for the release phase of both the 2 SAC and 3 SAC for the remaining simulations.

**Spring force sensitivity:** Figure 4.4 captures the spring displacement and residual forces under the various spring forces. Figure 4.5 further examines the morphological outcomes across the various spring forces.

## Chapter 4: Predicting three techniques

By 9 months of age, minor difference was seen in the level of spring displacement between each spring force evaluation in which springs with a value of 8, 9, and 10 Newtons achieved a final leg-to-leg distance of 36, 37 mm, and 40 mm respectively. A residual force level of approximately 80 % was still present across all springs by the time of removal.

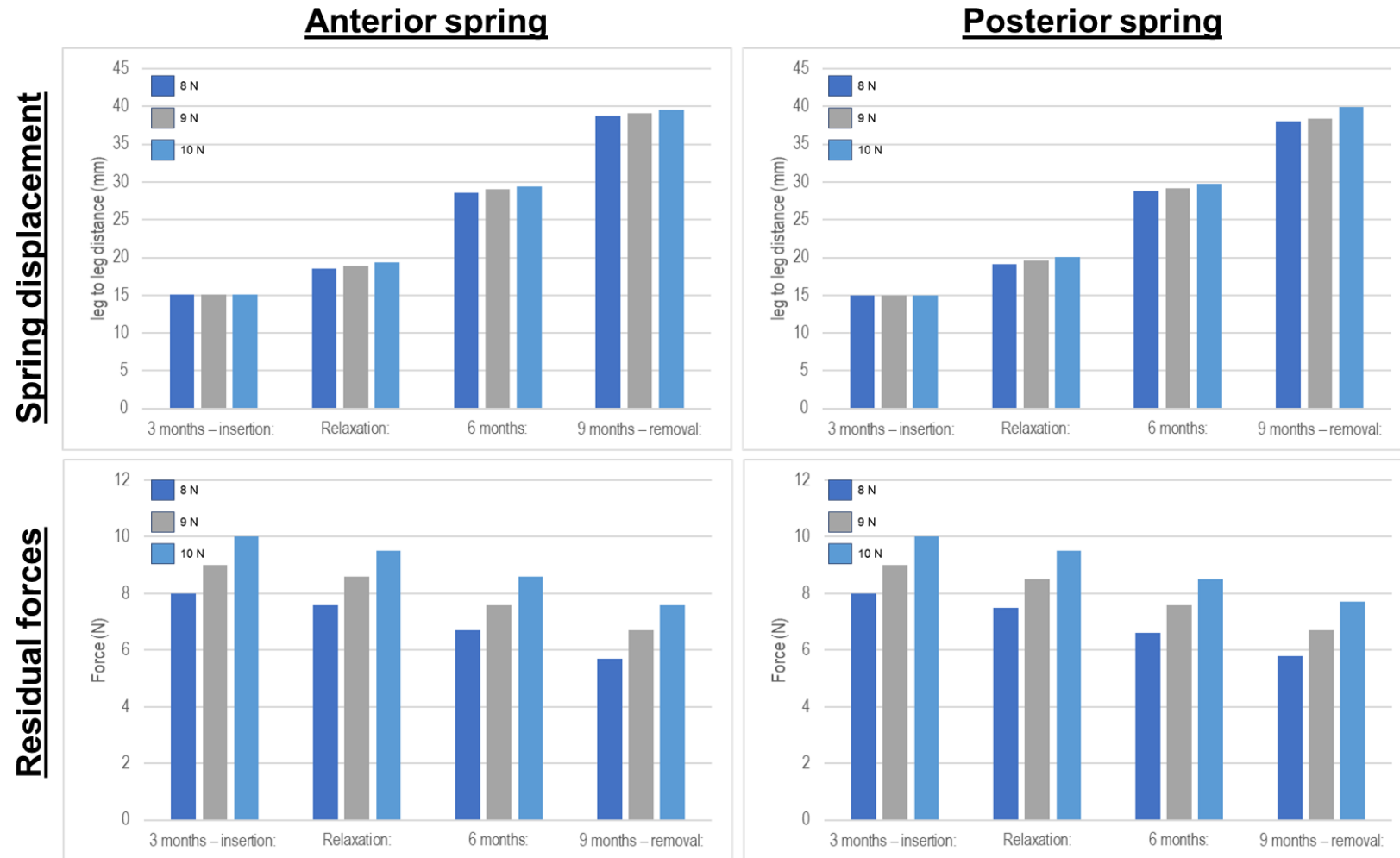


**Figure 4.4:** Predicted spring displacement (top row) and residual forces (bottom row) captured across the anterior (left column) and posterior springs (right column) under each spring force sensitivity from 4 months to 9 months of age.

## Chapter 4: Predicting three techniques

When considering the impacts on the skull morphology, a close match in length by 9 months was seen across all spring force sensitivities, reaching within the range of 139 to 139.5 mm. A reduction in width was seen in the 10 N of force predictions (110.5 mm) when compared with both 8 N and 9 N conditions (114 mm – 115 mm) at the same age. This was further captured in the cephalic index outcomes, where a lack of improvement was seen in the 10 N scenario (79.2) and an increase in the cephalic index was seen in both lower force values (81.7 for 8 N and 82.5 for 9 N).

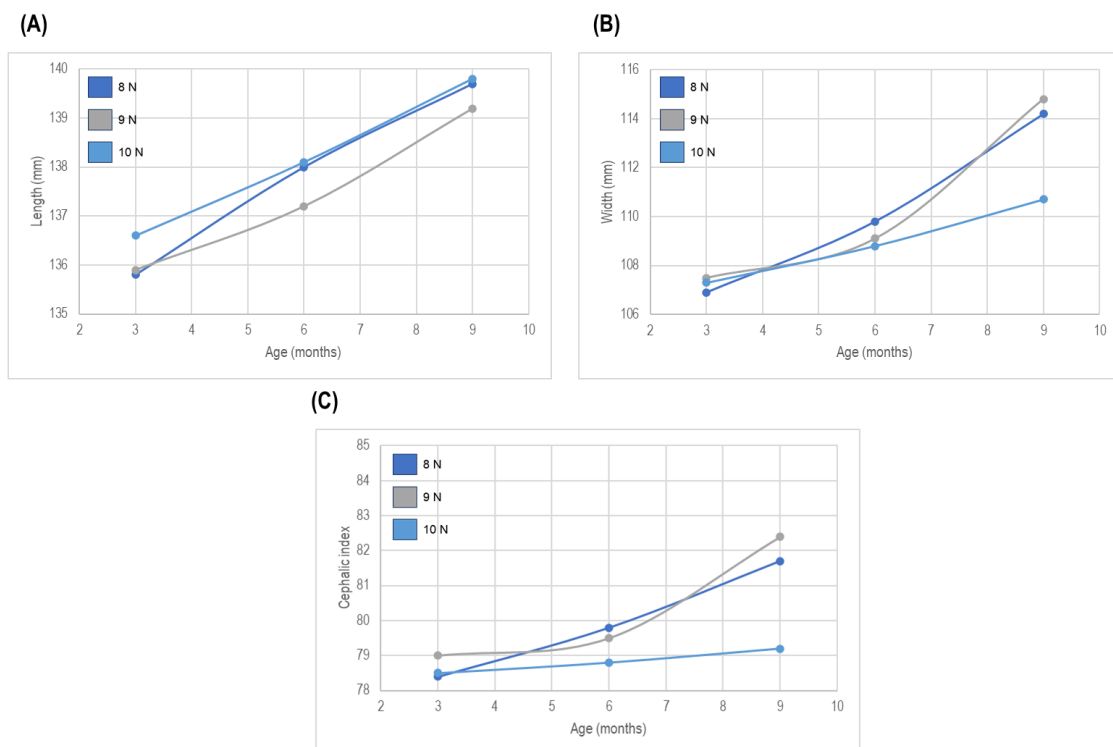


**Figure 4.5:** Predicting outcomes across each spring force sensitivity. Cephalometric predictions of the length (A), width (B), and cephalic index (C).

**Craniotomy bone formation rate:** Figure 4.6 displays the predicted pattern of bone formation across each model. Models 1 predicted complete craniotomy closure by 9 months of age. Conversely, when applying a faster bone formation rate (i.e., model 3), closure was achieved by the first load-step of growth (i.e., 6 months of age). This also accelerated the fusion of the anterior fontanelle. By 36 months of age, the minor delay in closure of the craniotomy in model 1 led to minor flattening across the occipital, a characteristic that was absent in model 3.



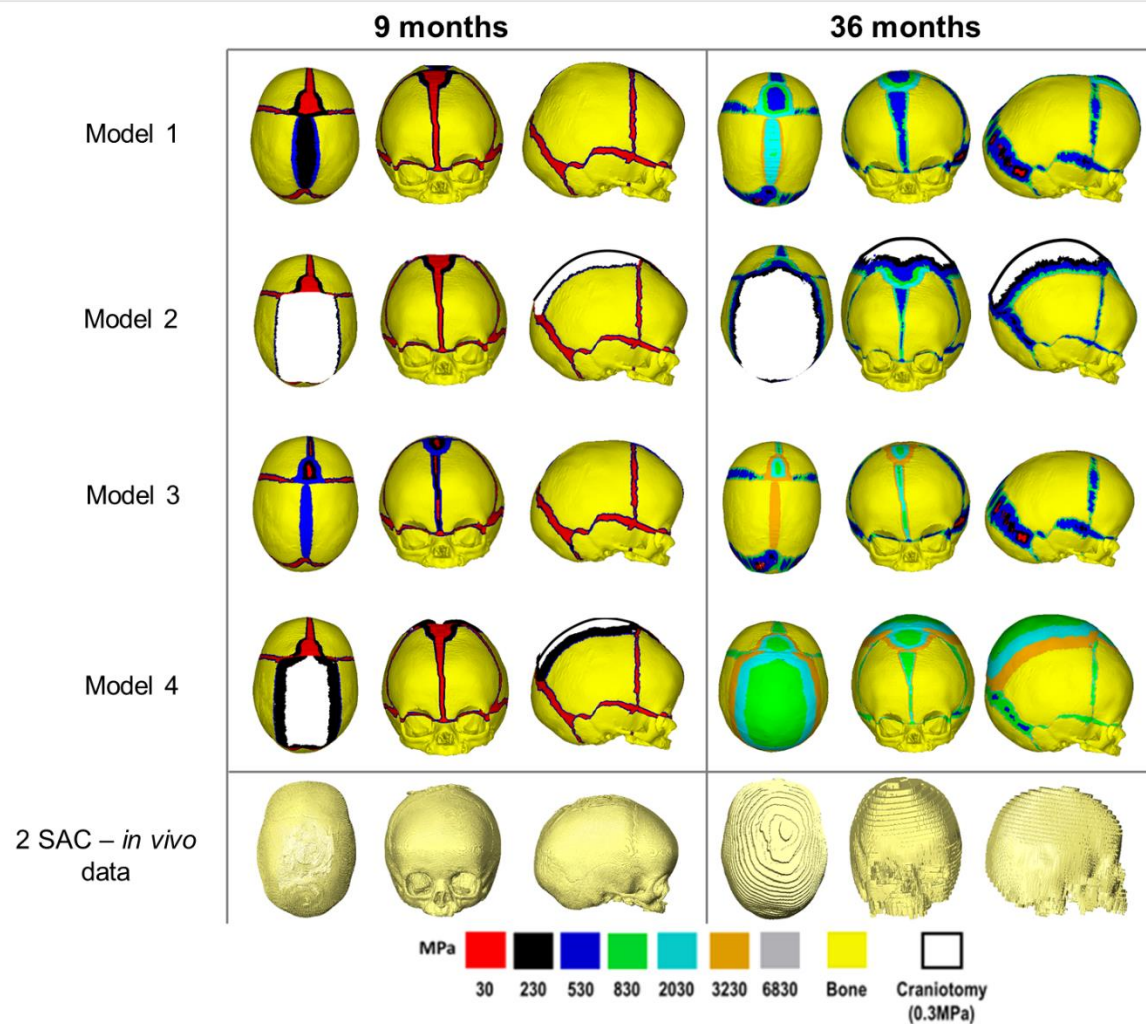


**Figure 4.6:** Predictive closures at 9 and 36 months of age for all scenarios. *In vivo* data from a patient case during SAC correction was used for comparison. Note that the follow up CT data quality differs between time points, resulting in decreased image quality.

Regarding the additional technique (models 2 and 4), at 9 months of age, increased bone formation was evident in model 4 vs. model 2, with a bitemporal patency of 20 mm still present. Model 2 achieved little bone formation under the baseline bone formation rate of 0.8 mm. At 36 months of age, model 2 predicted an uncharacteristic dorsal 'bulge' caused by the continuous lack of bone formation. This impacted the bone formation across all sutures when compared to the successful closure of sutures and craniotomies in model 4 by 36 months of age. The earlier closure of model 4 appeared to minimise this dorsal 'bulge'.

## Chapter 4: Predicting three techniques

Figure 4.7 highlights the pattern of ICV contact pressure across each model at 9 and 36 months of age. At 9 months, the large patency of the craniotomy across the MSC techniques led to both models 2 and 4, exhibiting little uniform pressure.

For the SAC techniques, greater concentrated pressure levels were seen in model 3, while also maintaining similar predictive pressures across model 1. At 36 months, minor change in pressure was observed in model 2, due to the continuous lack of bone formation being present. Conversely, model 4 presented greater level of contact pressure across the temporal and occipital regions vs. the 9 month predictions. Both models 1 and 3 demonstrated similar findings, although more concentrated and higher dorsal pressure levels were predicted in model 3.

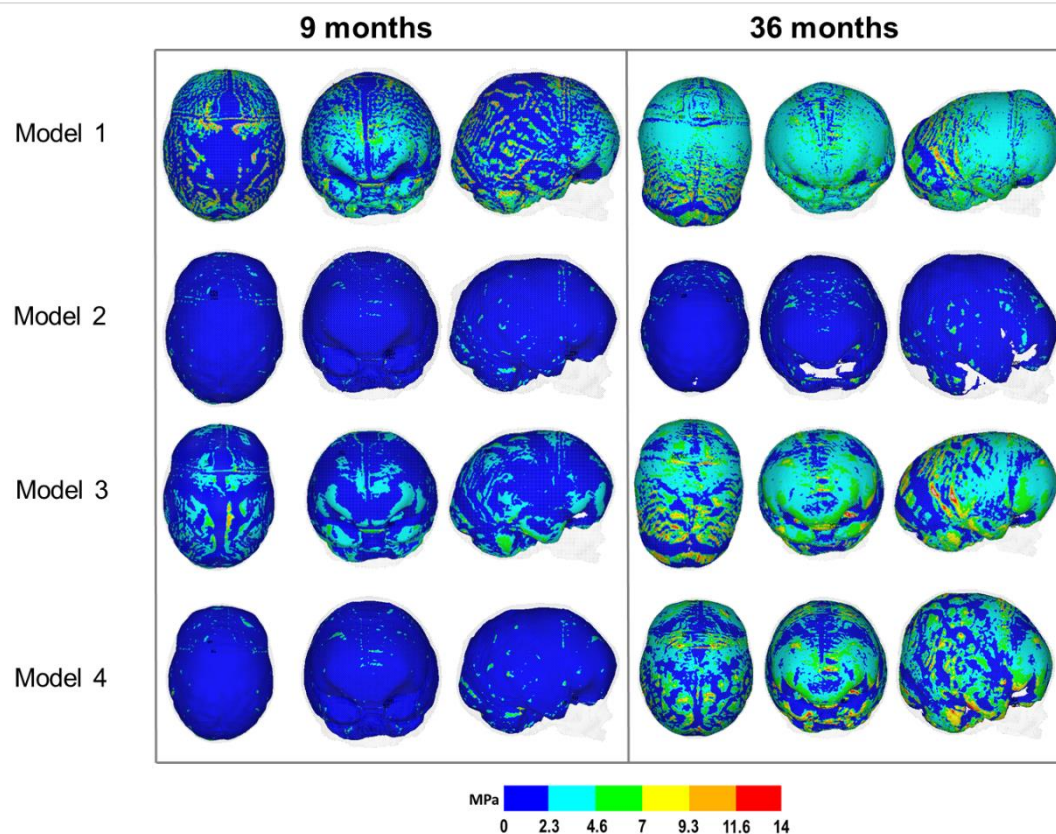
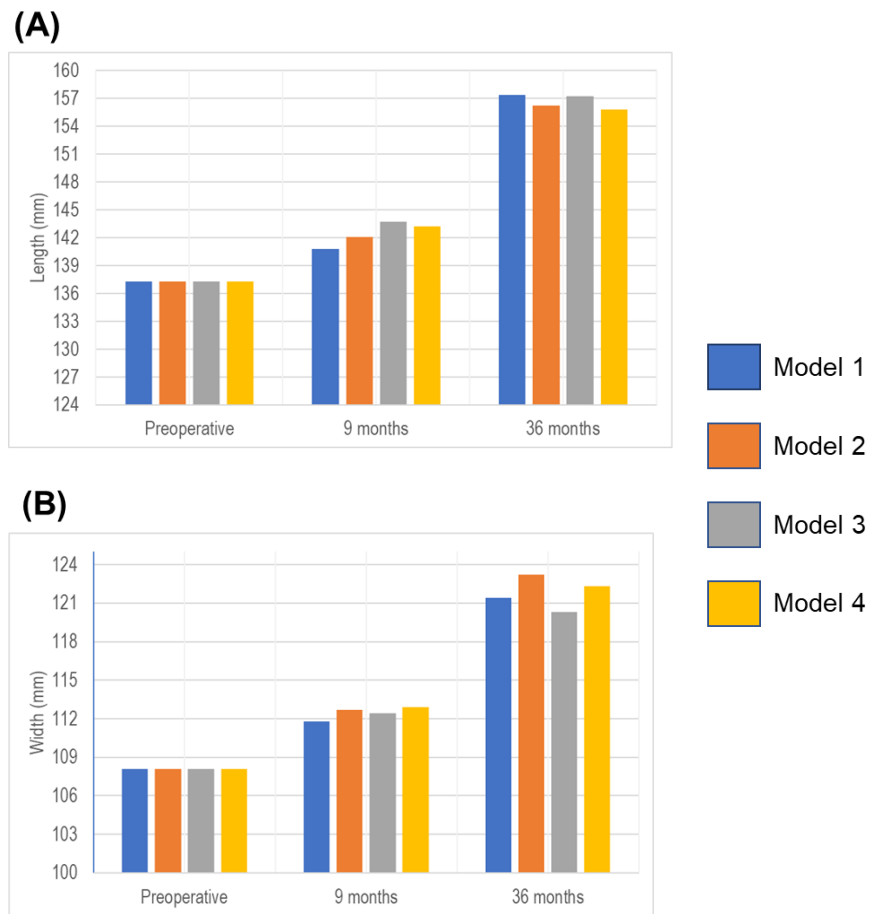


**Figure 4.7:** Predicted level of contact pressure across the ICV for each predicted craniotomy bone formation model. Highlighting results at 9 and 36 months of age.

Figure 4.8 quantifies the length, width, and cephalic index across all models. Both the rate of bone formation and chosen technique were seen to have minor impact on predictions. Ranging between 155.8-157.4 mm, 120.3-123.2 mm, and 76.5-77.1 for

## Chapter 4: Predicting three techniques

the length, width, and cephalic index at 36 months of age, respectively, across all models.



### 9 months

| Model number: | Length (mm): | Width (mm): | CI:  |
|---------------|--------------|-------------|------|
| 1             | 140.8        | 111.8       | 79.4 |
| 2             | 143.7        | 112.4       | 78.2 |
| 3             | 142.1        | 112.7       | 79.3 |
| 4             | 143.2        | 112.9       | 78.8 |

### 36 months

| Model number: | Length (mm): | Width (mm): | CI:  |
|---------------|--------------|-------------|------|
| 1             | 157.4        | 121.4       | 77.1 |
| 2             | 157.2        | 120.3       | 76.5 |
| 3             | 156.2        | 123.2       | 78.8 |
| 4             | 155.8        | 122.3       | 78.4 |

**Figure 4.8:** Cephalometric measurements across each craniotomy formation rate model. Highlighting the predicted length **(A)** and width **(B)**. Measurements were further quantified at 9 (above table) and 36 months of age (below table). CI represents the calculated cephalic index.

**Comparison of techniques:** Table 4.4 and Figure 4.9 (A-C) display the cephalometric measurements for the CT data, literature data and predictive data at preoperative, postoperative and at follow up time points. Note that all three replicated techniques share the same initial morphology at 4 months.

Initially, the pre-operative data highlighted lower overall cephalic measurements vs. both CT and literature data. At the post-operative stages, although length and width outcomes had been underpredicted, the cephalic index across both the 2 SAC (78.5) and 3 SAC (79.7) techniques matched well against the applicable CT data groups ( $79.9 \pm 2.9$  and  $78.2 \pm 4.5$ , respectively). A difference in the measured ICV was seen between the model (829.5 ml) and the CT data ( $1089.2 \pm 144.9$  for 2 SAC and  $1131.2 \pm 130.5$  for 3 SAC). In addition to observations at 9 months, the MSC technique predictive data was further examined at 12 months to match the age seen in the literature data. A large overprediction was captured between the predictive outcomes (81.1) vs. the literature ( $73.3 \pm 5.2$ ).

At 36 months follow up, the predictive outcomes for both SAC techniques estimated the same level of relapse in the cephalic index as seen across the CT data sets. The CT data's cephalic index decreased by 3.5 (2 SAC) and 3.9 (3 SAC), while the predictive data's cephalic index decreased by 5.6 and 3.9 for the 2 SAC and 3 SAC techniques, respectively. At 60 months of age, the MSC predictions failed to estimate the cephalic index seen in the literature (80.3 vs.  $71.5 \pm 4.3$ ). Estimations of cephalic relapse, while under predicted, were observed in both predicted and literature data from 12 months to the follow up age of 60 months.

## Chapter 4: Predicting three techniques

**Table 4.4:** Predicted cephalometric and ICV measurements across all three replicated techniques. Dashes indicate a lack of available data. All *in vivo* and literature data is the overall average with standard deviations.

|                     | 2 SAC          |                | 3 SAC          |                | MSC [Thomas <i>et al.</i> , 2015] |                |        |
|---------------------|----------------|----------------|----------------|----------------|-----------------------------------|----------------|--------|
|                     | CT data        | Predicted data | CT data        | Predicted data | MSC data                          | Predicted data |        |
| n:                  | 10             | 1              | 8              | 1              | 34                                | 1              |        |
| (%) male:           | 80             | 1              | 50             | 1              | N/A                               | 1              |        |
| Preoperative:       |                |                |                |                |                                   |                |        |
| Age (months):       | 4.9 ± 1.3      | 4.0            | 4.1 ± 0.7      | 4.0            | 6.0 ± 3.1-9.5                     | 4.0            |        |
| Length (mm):        | 148.5 ± 6.1    | 137.2          | 150.5 ± 9.9    | 137.2          | -                                 | 137.2          |        |
| Width (mm):         | 114.3 ± 5.7    | 108.1          | 111.5 ± 5.6    | 108.1          | -                                 | 108.1          |        |
| Circumference (mm): | 455.3 ± 68.0   | 430.6          | 457.2 ± 27     | 430.6          | -                                 | 430.6          |        |
| ICV (ml):           | 800.9 ±102.1   | 659.9          | 800.8 ± 88.6   | 659.9          | -                                 | 659.9          |        |
| Cephalic index:     | 76.9 ± 2.7     | 78.7           | 74.3 ± 4       | 78.7           | 65.7± 4.7                         | 78.7           |        |
| Postoperative:      |                |                |                |                |                                   |                |        |
| Age (months):       | 10.9 ± 1.3     | 9.0            | 10.6 ± 0.3     | 9.0            | 12                                | 9.0            | 12.0   |
| Length (mm):        | 162.5 ± 8.0    | 143.3          | 165.2 ± 6.1    | 142.4          | -                                 | 143.2          | 143.4  |
| Width (mm):         | 129.8 ± 5.0    | 112.5          | 129.1 ± 6.6    | 113.6          | -                                 | 112.9          | 116.2  |
| Circumference (mm): | 486.5 ± 59.4   | 397.3          | 429.0 ± 107.0  | 397.2          | -                                 | 395.5          | 416.8  |
| ICV (ml):           | 1089.2 ± 144.9 | 829.5          | 1131.2 ± 130.5 | 829.5          | -                                 | 817.4          | 1007.0 |
| Cephalic index:     | 79.9 ± 2.9     | 78.5           | 78.2 ± 4.5     | 79.7           | 73.3 ± 5.2                        | 78.8           | 81.1   |
| Follow up:          |                |                |                |                |                                   |                |        |
| Age (months):       | 37.15 ± 2.0    | 36.0           | 37.6 ± 1.3     | 36.0           | 60                                | 60             |        |
| Length (mm):        | 176.9 ± 9.3    | 163.8          | 178.8 ± 8.8    | 163.4          | -                                 | 155.1          |        |
| Width (mm):         | 135.1 ± 5.4    | 122.3          | 132.7 ± 6.4    | 121.2          | -                                 | 124.7          |        |
| Circumference (mm): | 512.4 ± 35.4   | 454.4          | 523.2 ± 37.0   | 453.3          | -                                 | 437.0          |        |
| ICV (ml):           | 1245.0 ± 166.8 | 1261.0         | 1239.0 ± 133.8 | 1261.0         | -                                 | 1376.9         |        |
| Cephalic index:     | 76.4 ± 2.5     | 74.6           | 74.3 ± 3.8     | 74.1           | 71.5 ± 4.3                        | 80.3           |        |

## Chapter 4: Predicting three techniques

The level of spring displacement by 9 months of age was further compared against the CT data, highlighted in Figure 4.9 (D-F). Although an additional 10 mm was achieved across all modelled springs from the point of 'release' to the removal, the predicted leg-to-leg distance was underestimate across all springs by the time of removal at 9 months of age.

## Chapter 4: Predicting three techniques

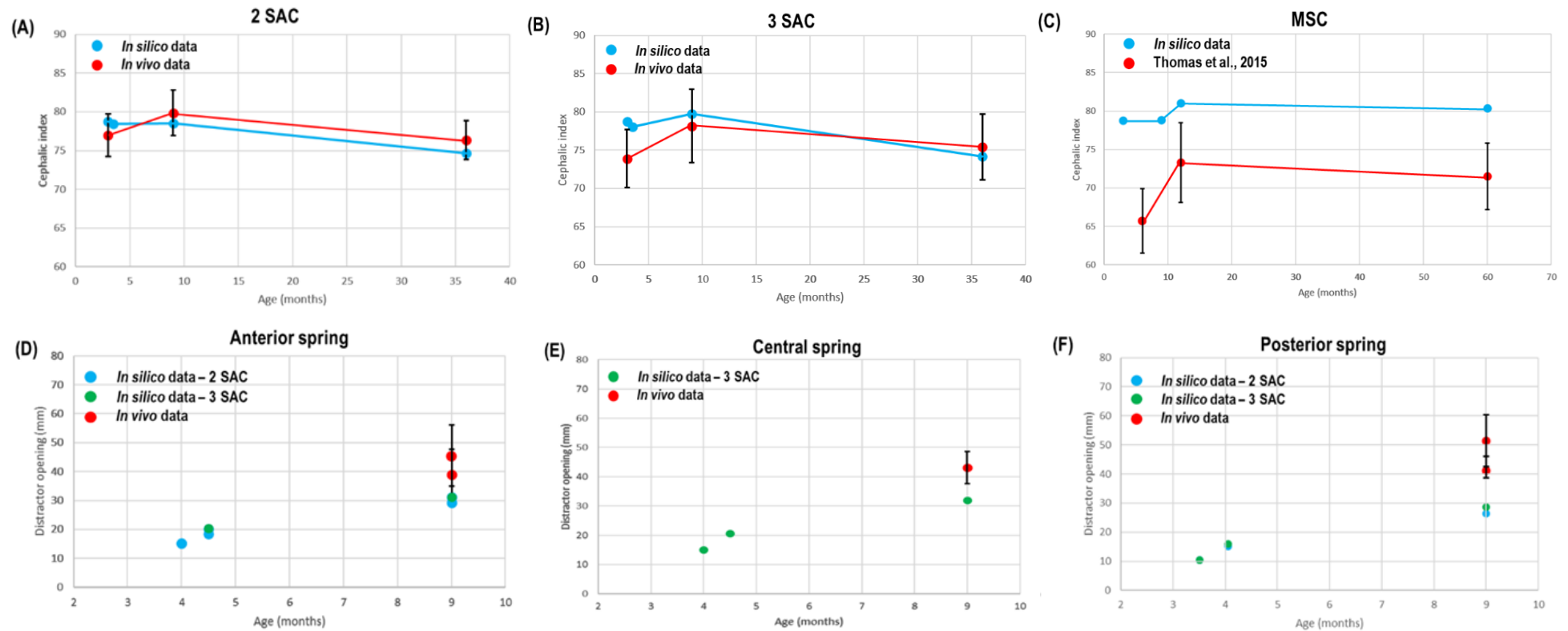


**Figure 4.9:** Comparison of predictive vs. CT & literature outcomes across all three techniques. Both 2 SAC (A), 3 SAC (B) cephalic index were validated against CT data, while the MSC (C) was compared with the literature data. In addition to cephalometric outcomes, both SAC techniques anterior (D), central (E), and posterior (F) spring dimensions were compared with *in vivo* CT data up to 9 months of age. All acquired data is presented with SD.

Figure 4.10 highlights the pattern of bone formation and contact pressure levels across all three replicated techniques. By 9 months of age, both SAC techniques demonstrated complete healing of the craniotomy, while the MSC failed to achieve complete fusion. All sutures remained marginally open, with the largest seen across the anterior fontanelle for all techniques.

By 36 months, all techniques predicted complete healing of the craniotomies as well as the complete fusion of the sutures. An exception was predicted across the lambdoid sutures for both SAC predictions, where a minor lack of fusion was seen. Interestingly, earlier formation and narrowing of the sutures were captured across the MSC technique. The metopic and anterior fontanelle was seen to close by 24 months across all techniques. Morphologically, a larger anteroposterior growth was seen in both SAC predictions, while a larger dorsal ‘budge’ was captured in the MSC outcomes.

With regards to the levels of contact pressure, the simulated ‘release’ of all springs across both techniques did not affect the change in pressure. By 9 months of age, at which springs were removed, a greater level of pressure was captured across both SAC predictions vs. the MSC. At 36 months, a uniform level of pressure, ranging by approximately 7 MPa, was predicted in both SAC techniques. Only a slight increase in pressure levels was captured across the bitemporal regions. Although certain areas of pressure were seen to be close to zero in the MSC predictions, greater regions of concentrated pressure, ranging close to 14 MPa, were seen across the anterior, posterior and mediolateral regions.

To validate the morphological shape for both predicted SAC techniques, Figure 4.11 presents a 3D distance maps, comparing the FE predictions versus the CT data at different time points. The chosen geometry for comparison against the predictions was selected by obtaining the overall mean CT skull which matched the data seen in Table 4.4. Note that at 4 months pre-operative, for both techniques, the ‘release’ predicted data were validated against CT pre-operative data. Observations revealed that large underpredictions were seen across the anterior region for both techniques. Alternatively, a reasonable agreement between the predictions and CT data was obtained across the bitemporal and occipital morphology. At 9 months post-operative,



## Chapter 4: Predicting three techniques

at which the springs were removed, the trend of frontal underprediction became more progressive in both techniques. In addition to this, minor bitemporal underprediction was also captured, while dorsal growth was agreeable across both techniques. By 36 months, a well-matched prediction was achieved across the whole morphology.

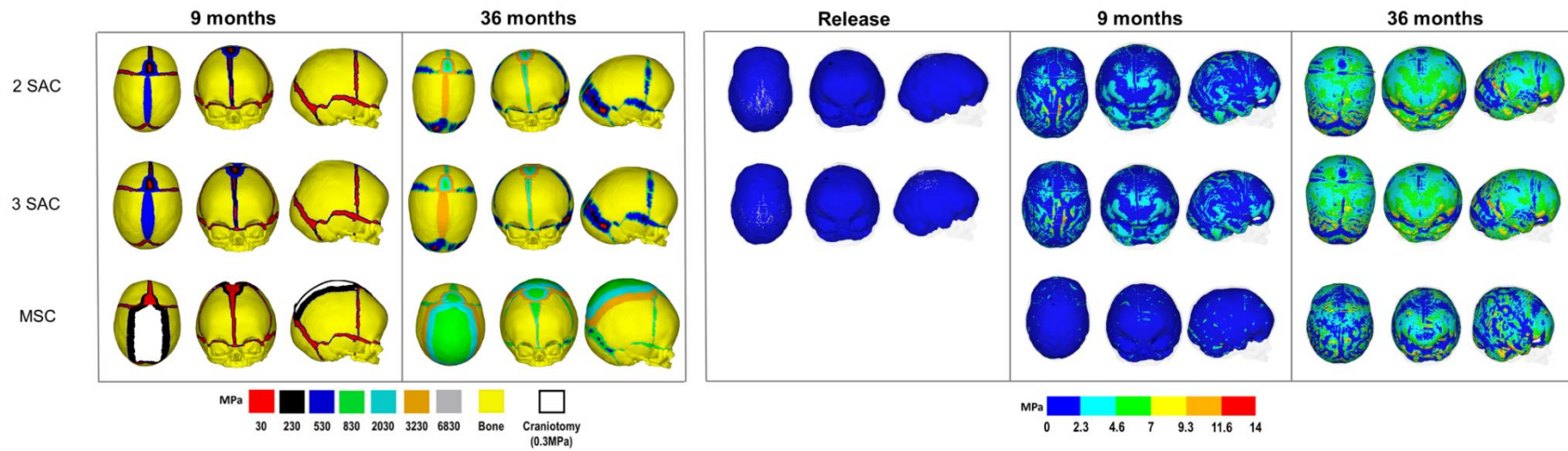


**Figure 4.10:** Predicted bone formation (Left) at both postoperative 9 months and follow up 36 months of age. Predicted ICV contact pressure (Right) was captured further at 'release' in addition to the previously specified age stages.

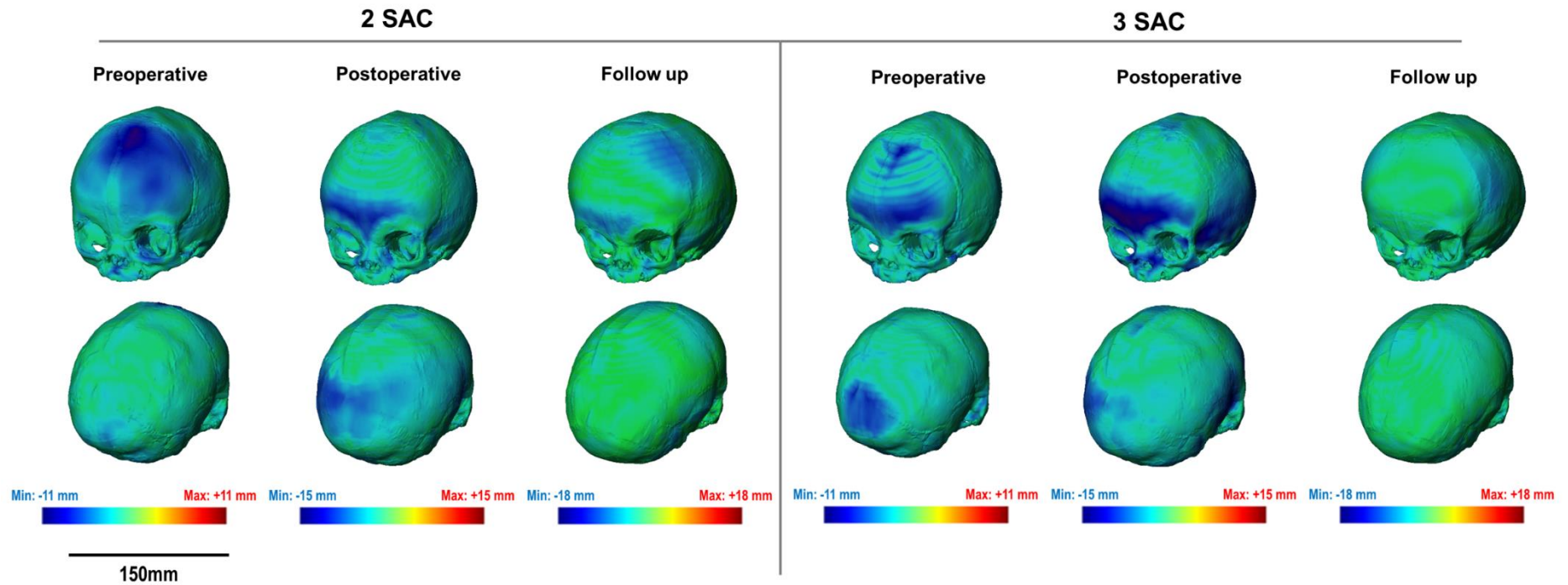


**Figure 4.11:** 3D distance maps of predicted morphological skull vs. the 'average' CT data patient skull at respective ages across both spring techniques. Note, that the predicted morphology following 'release' of *in silico* springs was compared against the pre-operative *in vivo* skull for both techniques. Alignment position was marked at the foramen magnum for comparison.

## 4.4 Discussion

Within this chapter, the previously validated generic pre-operative model was used to replicate, predict, and compare the biomechanics of three additional surgical techniques for the correction of sagittal craniosynostosis. In addition, sensitivity studies into the choice of material properties, skull geometry, contact parameters, and forces acting across the spring and their respective outcomes on the skull morphology were investigated. The final investigative area here examined the sensitivity of alternating the rate of bone formation exclusively across the created craniotomies.

**Simulated spring release:** Several modelling approaches were tested to model and mimic the effect of springs clinically used in the modelling approach presented in Chapter 3. Several key factors and parameters lead to higher or lower resistance to spring displacement, as it is modelled here. While the goal was to achieve a displacement of 5 mm across the spring upon release, this was only seen in scenario 10. Based on this, it is understandable that the properties of bone may lead to such a resistance being present. By reducing the elastic modulus by a magnitude of 10 (i.e., 421 MPa to 41 MPa) followed by a reduction in the ICV properties (i.e., 10 MPa to 1 MPa), less resistance was enforced at the position of the springs and reducing the level of compression required across the ICV upon release. Further, applying a fixed boundary condition between the interior skull and ICV surfaces applies too much rigidity to spring displacement. Applying a frictional yet separable interface here achieved an outcome better representing clinical observations.

**Craniotomy bone formation rate:** While only two rates of bone formation across the craniotomies were compared here (0.8 mm vs. 10.8 mm per month of growth), these values provided a broad analysis for both SAC and MSC techniques, which themselves, possess the two extreme levels of craniotomy dimensions (i.e., 5 mm – SAC and 50 mm – MSC).

Here, the SAC was seen to heal completely by 9 months across both rates. This is understandable, as the radius distance from the bone lining envelopes the craniotomy faster than that seen in MSC. As a comparative observation, *in vivo* data from the CT

cohort was used, in which the patients craniotomy had fully healed (no visible gaps remaining). What is unclear of course, is the tensile strength (mechanical properties) of such bone within the clinical settings once healing is achieved. For example, model 1 presents the craniotomy with an elastic property of 230 MPa, while model 3, also fully healed, presents an elastic value of 530 MPa. It is unclear as to which presents the most realistic outcome. Nonetheless, the model does predict complete healing by 9 months of age.

In contrast to this, the MSC techniques of models 2 and 4 present vastly different predictions in healing. While a rate of 0.8 mm (model 2) never achieves craniotomy closure, a rate of 10.8 mm (model 4) accomplishes this by 36 months of age. Although the same argument in estimating the accurate value of elastic properties can be made for model 4, such an analysis would require a larger investigation. Further, the rate of 10.8 mm could be interpreted as a biased method of 'forcing' the model to heal by 36 months, whereas, clinically, numerous biological and biomechanical strains dictate the closure of the craniotomy using the dura mater as its foundation. Nevertheless, based on these observations, a larger rate of 10.8 mm can provide accurate timing of 'closure', and thus, will be further used.

**Cephalometric outcomes:** While validating the morphological predictions with that of the CT data (Table 4.4 and Figure 4.9), it is evident that length and width measurements were underpredicted. One key consideration here is the 20 % discrepancy between the predicted intracranial volume and average CT data volume at 9 months ( $1131.2 \text{ ml} \pm 130.5 \text{ ml}$  vs.  $829.5 \text{ ml}$ ), leading to an overall underprediction of the computational data. One observation that supports this is the fact that the size of ICV matched well at 36 months, leading to predictive morphology agreeing well with the CT data.

Despite this limitation, it was interesting that the computer simulations could capture the anteroposterior growth vector, between the ages of 9 to 36 months, which was also observed within the CT data (Figure 4.9 – A and B), demonstrating that relapses in correction can be predicted as much as improvements.

In addition to the SAC predictions, the MSC technique was used for comparison. Difficulties in producing a truly comparative analysis between the predictive data and literature data were evident here, resulting in only a comparative analysis of cephalic index outcomes. As such data is limited, this may be the reason for predictive outcomes disagreeing with the literature throughout the time points (Table 4.4 and Figure 4.9 – C). There was a clear difference in the initial value of the cephalic index between the generic pre-operative model (78.7) and literature data ( $65.7 \pm 4.7$ ), which may have led to the larger overall differences during growth. Further, as apparent in the SAC outcomes, discrepancies in the ICV measurements may explain the over predictive outcomes seen here. Nonetheless, it is interesting that a small relapse was captured in predictive outcomes which are also evident in the literature data. This could be due to the larger dorsal-ventral growth seen within the model. Such a prediction may promote a varied level of confidence in accurately replicating this form of correction and its outcomes, however, further data is required for a true valid analysis.

**Spring opening:** For the validation of *in silico* spring displacement during growth, a comparison was made against CT data during spring removal at 9 months of age (Figure 4.9 – D-F). Although unfortunately, such validation was restricted to a single time point, predictive outcomes underestimate the level of spring displacement, reaching a final mean length of 30 mm (length gain: ~ 11 mm). This was despite an accurate measurement across the springs at release for both techniques. According to both the CT and predictive data, the incorporation of a third spring (3 SAC) showed negligible effect on spring displacement or morphological outcomes. Key considerations for surgeons undertaking a technique of this nature are: (1) Reduce the risks of spring dislodgment while in position and (2) limit the impact and damage made to the sagittal sinus, located directly across the craniotomy performed here. By examining the lack of gain in correction between 2 vs. 3 SAC, it could be argued that the same corrective outcomes could be achieved without the inclusion of a third spring, a hypothesis supported by the predictive methods here.

**Bone formation:** It is evident that the generic model used is sensitive to the choice of techniques replicated here (Figure 4.6), leading to various morphological characteristics. For instance, the rapid fusion of both SAC techniques and increase

lambdoid suture patency resulted in occipital-posterior displacement and angular narrowing, an observation seen within the CT cohort (Figure 4.4). Further to this, a vertex budge is evident under the MSC predictions by 9 and 36 months of age. Patients undergoing this technique which results in a similar aesthetic appearance due to a lack of ossification (i.e., 'copper beaten') have previously been reported (Marucci *et al.*, 2008). As evident at 9 months, predictive outcomes show a slower rate of closure across the craniotomy.

**Contact pressure:** Further to morphological outcomes, predictive ICV contact pressure appears to be sensitive to the method of replicated correction (Figure 4.8). Overall, higher concentrated pressure regions were captured in the MSC vs. both SAC techniques by 36 months. Although the MSC technique here suggests improvements in the cephalic outcomes, this appears to not directly collate with improved ICV pressure. This, in turn, could play a key role in determining neurofunctional defects by this age. Unfortunately, such a method to validate this notion is beyond the scope of this work, in which highly specific clinical data and analysis would be required. While acknowledging this limitation, it is clear the method performed here can lead to a greater understanding of the interactions between skull growth and functional outcomes.

Similar to that of the spring opening outcomes, minor difference was observed against 2 vs. 3 SAC predictive contact pressures by 36 months. This prediction could suggest, once again, that minor impact may be seen when using an alternative number of springs greater than the standard two. In the similar nature of the MSC predictions, the validity of these outcomes cannot be commented on. However, it further highlights the possible impacts such modelling approaches can have on the understanding of the biomechanics of skull growth.

**Spring forces:** Although the technique approach here centralises on the parameters of the Gothenburg technique, a further sensitivity was undertaken regarding the spring stiffnesses and thus, the bilateral forces generated in a range between 8 and 10 Newtons. Negligible impact was seen in the cephalometric outcomes (Figure 4.5), despite a large level of residual force remaining by 9 months of removal. One probability of this is the majority of the spring displacement occurs in the transverse

plane, leading to minimal differences in the changes to bitemporal widening. Such an observation is further supported in the reported literature from the surgical teams (Satanin *et al.*, 2019). However, such an analysis was felt to be important, as greater levels of spring stiffness have been used in additional craniofacial centres (Borghi *et al.*, 2017).

### 4.5 Summary

This chapter presented the first initial comparative analysis of three corrective outcomes for sagittal synostosis. All techniques presented here were compared with CT data or, where absent, literature data. Based on the predicted techniques here, it could be suggested that the SAC technique provides the most positive outcome. While the method of bone formation has been improved upon, the model must consider the influence that the level of mechanical strain could have on the level of bone formation. As this item was not taken into account in this chapter, the next chapter will prioritise the refinement of the current bone formation algorithms used thus far in this thesis with the goal of considering the strain produced across the calvaria to regulate the predicted patterns of ossification and bone healing.



## **Chapter 5: A new approach for modelling the bone formation during calvarial growth**

## 5.1 Introduction

Chapters 3 and 4 of this thesis implemented 2 different approaches to model the bone formation across the sutures and craniotomies during the calvarial growth. The implemented approaches did not consider the level of mechanical strain experienced by the tissues in these regions. This was a major limitation that was identified in Chapter 4, where the gradual bone formation approach imposing a radius of bone formation (independent of the level of strain) was not able to consistently model the bone formation across both small and wide craniotomies. Hence, the focus of this chapter is to consider the level of mechanical strain experienced by the soft tissues across the sutures/craniotomies in the bone formation in these regions. A novel approach is proposed here, and various sensitivity tests are reported to investigate their impact on the output of this new modelling approach that was then implemented across a much wider range of reconstruction techniques in Chapter 6.

## 5.2 Materials and methods

The finite element model described in section 4.2 was used in this chapter. All input parameters remained the same except the bone formation method across the sutures and craniotomies that were altered and are described in the following section. It must be highlighted that the replicated surgical technique used was the approach described in section 3.2.2 of this thesis, under the title: Renier's 'H' technique. This approach was used to enable comparison of the results obtained here with those described in Chapter 3. To reiterate, based on the findings of Chapter 3, the initial elastic modulus of the bone, sutures, and craniotomy used here was 421 MPa, 30 MPa, and 10 MPa, respectively.

### 5.2.1 Bone formation methods

Two new methods for bone formation were introduced here. The previously used methods (discussed in Chapters 3 and 4) were used as a 'control' scenario. Figure 5.1 illustrates the key factor across all bone formation methods.

**Model A (control):** The approach here remained unchanged from the approach used and discussed in section 3.2.3.

**Model B (Strain dependent):** As a direct comparison to the control approach, bone formation across the model was only undertaken if individual elements meet a specified hydrostatic strain threshold (various threshold are tested see section 5.2.2). These elements, as previously described in section 3.2.4, will then had their elastic modulus updated to reflect newly formed bone (i.e., 100 MPa per month for the sutures and 125 MPa per month of the bone). The restrictive ‘radius dependent’ behaviour previously used was absent here, allowing bone to freely form across both the sutures and craniotomy.

**Model C (Strain and radius dependent):** The third approach combined the concepts of both models A and B, in which both the strain seen across the elements and radius from the bone linings regulated the patterns of bone formation. Only elements that met both conditions had their elastic moduli updated. Calvarial growth was simulated to model the skull growth from the pre-operative age of 4 months to the follow up age of 76 months.

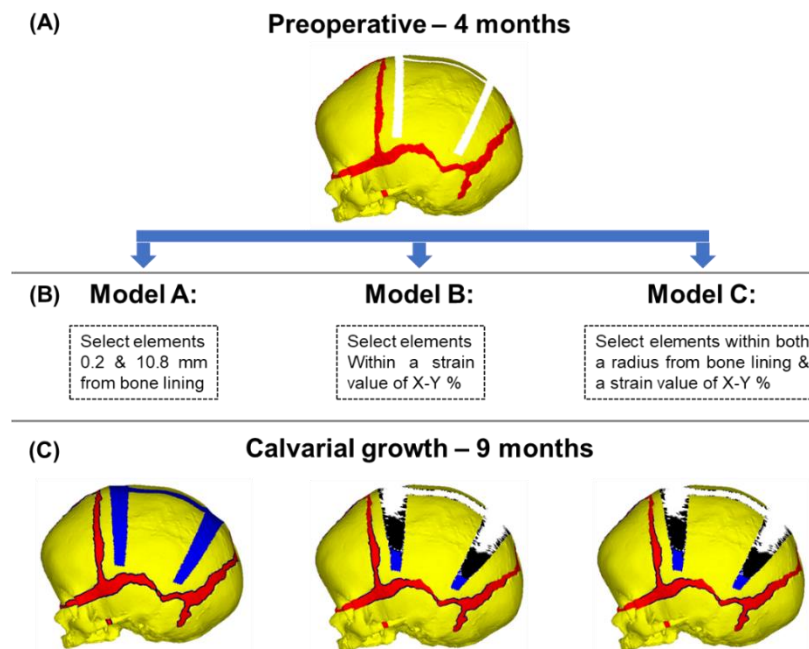


**Figure 5.1:** Illustrations of all three formation methods. The same pre-operative model used within Chapter 3 is used here (A). Three conditions for determining formation across the calvarial are introduced in three separate simulations (B). The location and level of bone formation is recorded at each load step, here being at 9 months of age (C).

The patient-specific CT data, provided at 36 and 76 months of age, were used for morphological validation and as a qualitative comparison to the predicted patterns of bone formation at a macroscopic level.

### 5.2.2 Sensitivity study

Across various computational studies, the process of natural bone formation has been replicated by calculating the level of hydrostatic strain generated across the respective bone formation sites (e.g., Claes & Heigele, 1999; Marghoub *et al.*, 2019). The method of calculating the hydrostatic strain was performed by obtaining all three principal strains and dividing the sum by three. However, as such an aspect has not been simulated or investigated in the context of human skull growth during corrective surgery, a sensitivity study to the level/threshold of hydrostatic strain initiating or prohibiting bone formation was performed here. In addition, to understand the interaction between highlight and lower levels of strain across the skull, the sensitivity study was divided into two parts.

A total of five variations that alternated the minimum and maximum level of hydrostatic strain required to generate the bone formation were compared and their impacts on the calvarial morphological predictions were accessed at 76 months of age. Figure 5.2 details each variation. Note that only the 'Model B', denoted at the *strain dependent* method (see section 5.2.3), was used here.

The first three scenarios increase the lower threshold from 0 to 2%:

**Scenario 1:** A threshold between the values of 0 and 15% of hydrostatic strain was introduced across the model. This was to observe elements which may lay within the negative values of strain. Elements which were seen to be within the negative values were not selected.

**Scenario 2:** The minimum threshold was increased from 0 to 1%. The maximum threshold remains unchanged from scenario 1.

**Scenario 3:** The minimum threshold was increased from 1 to 2%. Again, the maximum threshold remains unchanged.

As a comparison, the most applicable maximum threshold value was investigated under two scenarios from 15% to 35%:

**Scenario 4:** The maximum threshold was increased from the initial 15% to 25%.

**Scenario 5:** Further to the above, the maximum threshold was again increased from 25% to 35%.

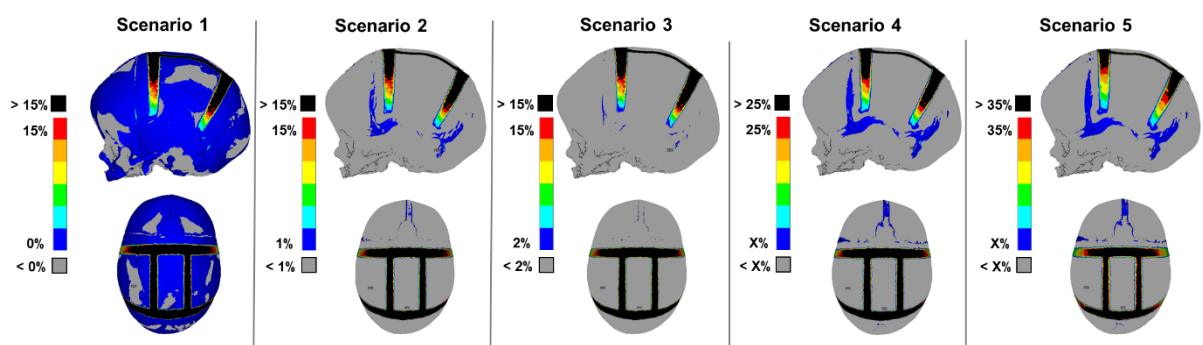


**Figure 5.2:** Parameters of each sensitivity scenarios. 3D model highlights the overall hydrostatic strain across the skull under each range level after a single growth load-step. Once scenarios 1 to 3 are complete, the most applicable minimum threshold value (marked with 'X') is brought forward for scenarios 4 and 5, where the maximum threshold value is altered. Note that regions shown in grey and black represent regions below or above the specified thresholds, respectively.

**Simulations and measurements:** All scenarios were investigated up to 76 months of age, in which the morphological changes and bone formation patterns were compared against the patient-specific CT data at both 36 and 76 months. A cross-sectional analysis and a 3D displacement map approach were used for morphological validation for all bone formation methods being simulated. Further, the length, width, and cephalic index were compared against the CT data up to 76 months of age.

## 5.3 Results

### 5.3.1 Sensitivity study

**Minimum threshold sensitivity:** Figure 5.3 highlights the patterns of bone formation across all minimum threshold scenarios (here, scenarios 1 to 3). Scenario 1 demonstrated complete closure of all sutures by the first growth load step, equivalent to 2 months post-operative or 6 months of age, while the craniotomy showed large patency at the same time point. By 76 months of age, dorsal bulging was captured

across the model as a result of the craniotomies' lack of closure. Scenario 2 demonstrated an overall improvement with regards to the calvarial healing vs. scenario 1, in which full closure was achieved by 24 months of age. Interestingly, small regions across the sutures remained open by 76 months of age. However, the majority of sutures and craniotomies demonstrated closure by 36 months of age. Scenario 3 highlighted similar predictions to scenario 2, with the pattern and timing of calvarial healing showing little difference. Regions of patency were visible across the squamosal and coronal regions by 76 months of age (Figure 5.3 – black box).

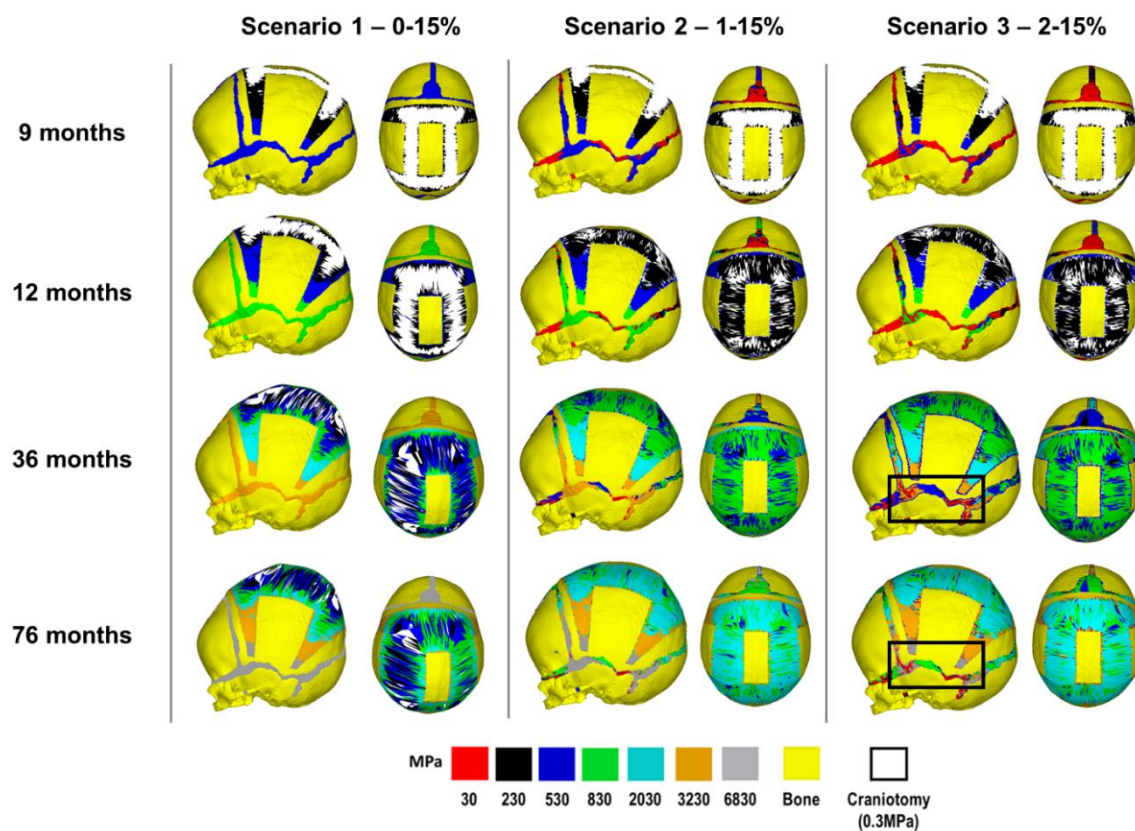


**Figure 5.3:** Predictive bone formation outcomes across all minimum threshold sensitivity scenarios. Black box indicates a region of interest.

Figure 5.4 compares the morphological predictions against the CT patient-specific data using a cross-sectional analysis. Both the 36 and 76 months of age predictions for scenario 1 highlight large dorsal overprediction. The bilateral predictions agreed well with the patient CT data at both time points. A flattening of the forehead resulted in anterior underprediction but agreeable posterior predictions by 76 months. Scenarios 2 and 3 were seen to correct the dorsal disfigurements seen in scenario 1,

with only minor overprediction seen across the posterior fontanelle region in both scenarios. By 76 months, this overprediction decreased in both scenarios, with both shape outcomes being near identical. Due to the greater level of bone formation achieved and the overall adequate morphological predictions seen, scenario 2's minimum threshold (i.e., 2%) was chosen as the most suitable to be brought forward for the remaining sensitivity scenarios (scenarios 4 and 5).

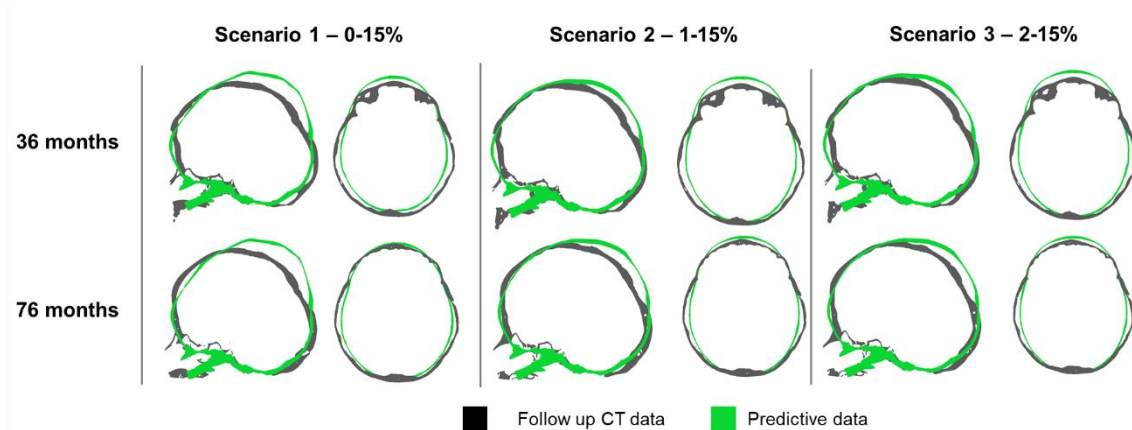


**Figure 5.4:** Cross sectional morphological predictions across all minimum threshold sensitivity outcomes validated against patient-specific CT data at 36 and 76 months of age.

**Maximum threshold sensitivity:** Figure 5.5 shows the pattern of bone formation and the cross-section comparison (vs. CT data) analysis across the two further scenarios. Scenario 4 demonstrated complete calvarial healing by 36 months of age, while scenario 5 showed a small level of distortion across the left region of the craniotomy (Figure 5.5 – black box). This distortion was seen to continue up to 76 months of age. Disregarding this abnormality, both scenarios showed little change in their patterns of bone formation. Where the majority of selected bone reached a final elastic modulus value of 3230 MPa, little difference was seen across the sutures for both scenarios throughout the simulated growth. Cross-sectional analysis suggested little difference in the overall skull morphology between the two predictive scenarios. At 76 months, a small overprediction was seen across the posterior fontanelle when validated against the CT patient data. However, a consistently good match across the anteroposterior and bilateral regions was achieved.



Based on the observations and the applicable timings of bone formation for both the sutures and craniotomy, scenario 4's threshold values (1 – 25 %) of hydrostatic strain were used for further analysis.

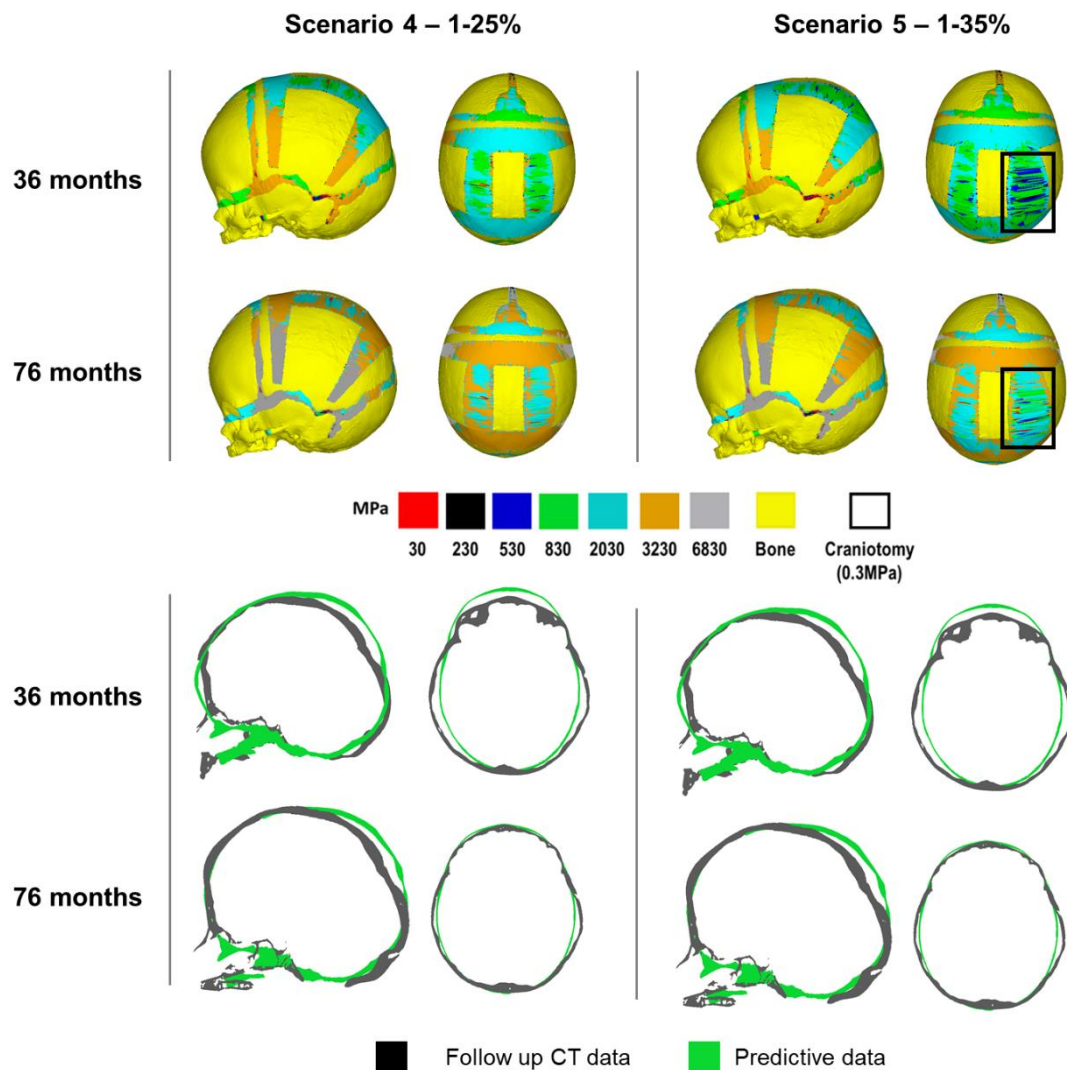


**Figure 5.5:** Predictive bone formation (Above) and cross-sectional morphology (below) for both scenarios 4 and 5. Black box indicates a region of interest.

### 5.3.2 Bone formation methods

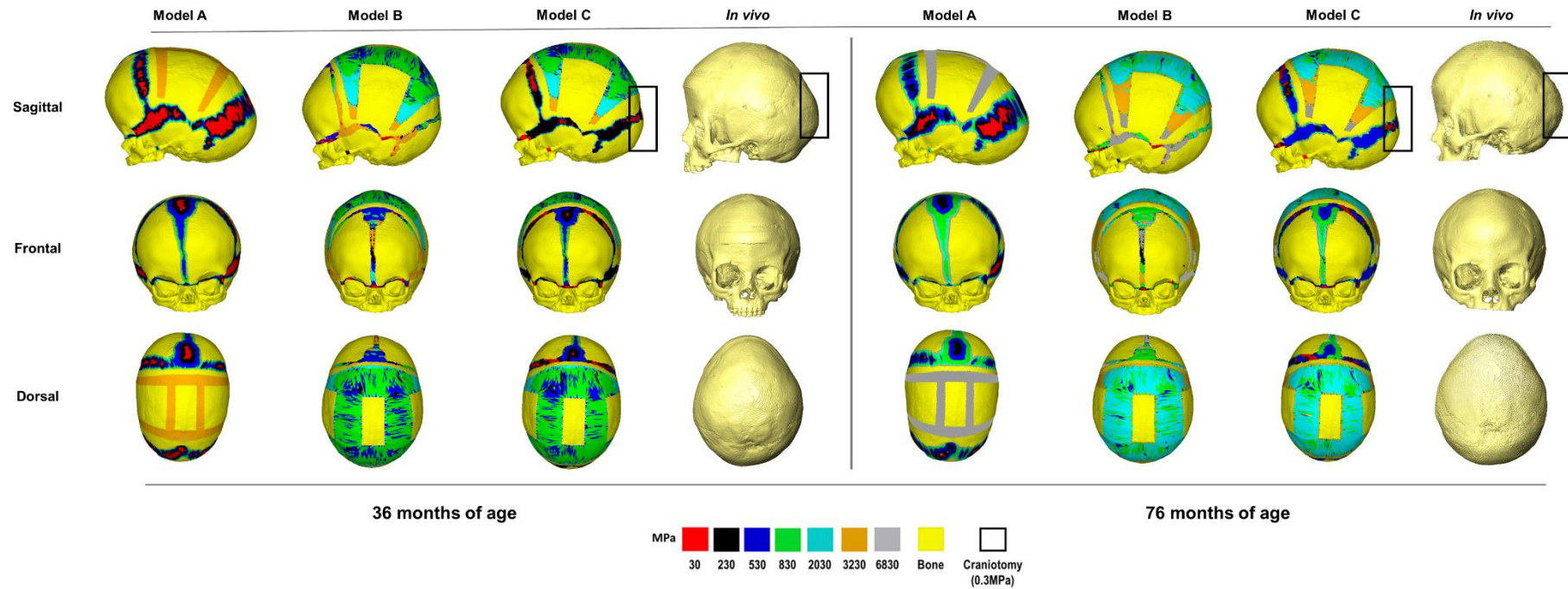
Figure 5.6 highlights the patterns of bone formation and calvarial healing between the three considered algorithms in this chapter. The abrupt closure of the craniotomy was captured in model A by 2 months postoperative. Large patency was evident across the squamosal and lambdoid sutures by 76 months of age. Conversely, the metopic, anterior fontanelle and coronal sutures were fully fused by 76 months of age. Model B



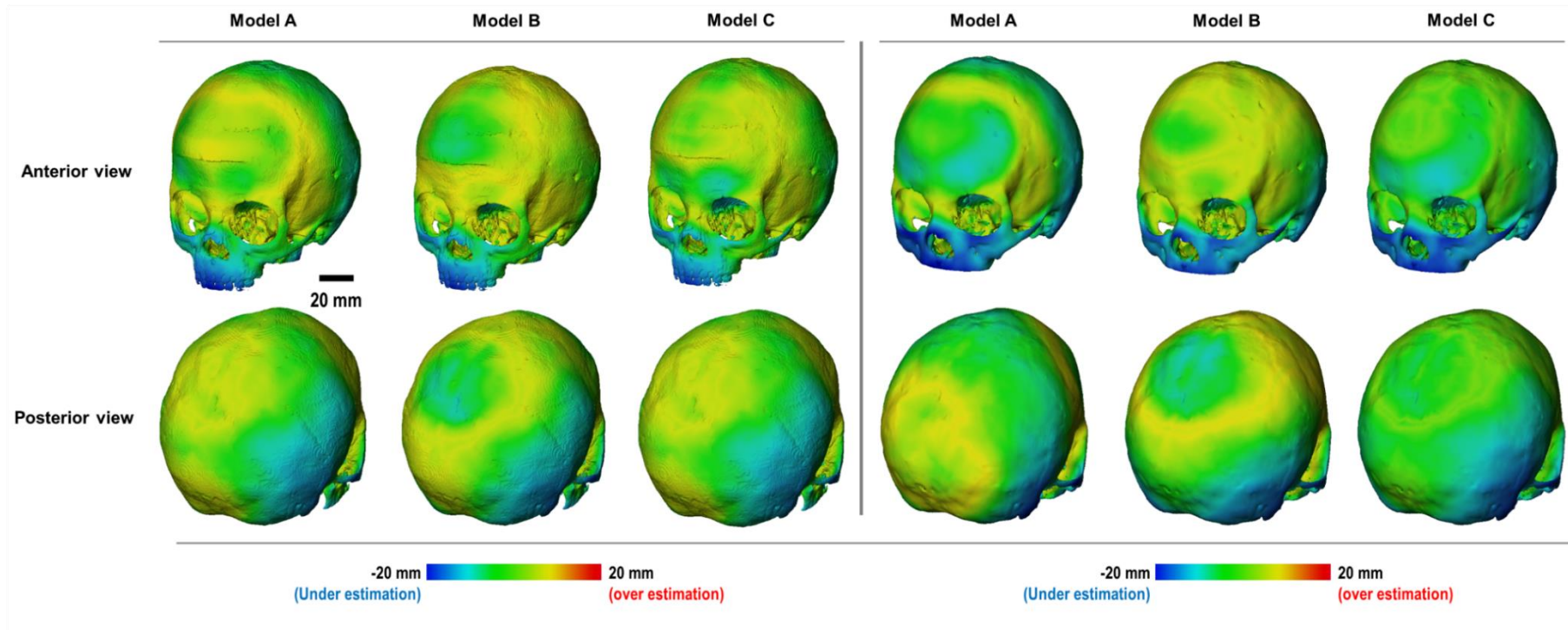
predicted minor squamosal suture patency at 36 months, while the craniotomy had achieved complete closure. The metopic and anterior fontanelle achieved fusion by 36 months. However, there was evidence of bone formation away from the bone borders due to the *radius dependent* parameter not being present in this method. Little difference in the patency or the pattern of bone formation was seen between the 36 and 76 month outcomes. Model C's pattern of calvarial healing represented the same outcomes as seen in model B, fusing completely by 24 months of age. Little patency was seen across the coronal and lambdoid sutures at 36 months of age, which formed completely by 76 months. Metopic and anterior fontanelle suture fusion were captured at 36 months of age.

Figure 5.7 compares the overall skull shape predictions of each method using a 3D distance mapping approach against the patient-specific CT data. Global alignment of the models was performed at the foramen magnum. At 36 months, all models overpredicted the anteroposterior growth and underpredicted the bilateral widening. Minor dorsal overprediction was captured only in model B's outcomes, while both models A and C agreed well with the CT data. At 76 months, the trend of anteroposterior overprediction continued across models A and B. Model C predicted an agreeable match with the CT data concerning the aforementioned regions. Model B continued to overpredict the dorsal growth, while model C continued to agree with the CT data. Interestingly, a small level of dorsal underprediction was captured in model A at this age.

Figure 5.8 quantifies the cephalometric measurements for each method. By 76 months, model C's predicted length (163.3 mm) matched closest with the CT data (166.1 mm), while models A and B were seen to overpredict (170.4 mm) and underpredict (161.9 mm) the length, respectively. All models' width predictions (Range: 124.1 mm – 127.6 mm) greatly underestimated the CT data's value (143.9 mm). Model B's cephalic index predictions (80.2) were seen to match closest to the CT data's cephalic index (86.6), while both models A (74.9) and C (76.0) underpredict this value. However, a relapse in the cephalic index between the ages of 36 and 76 months of age was seen only in both the CT data (87.7 regressing to 86.6) and model C (76.2 regressing to 76.0).



**Figure 5.6:** Predicted bone formation outcomes across all methods at 36 and 76 months of age.



**Figure 5.7:** 3D distance mapping of predictive morphology vs. *in vivo* CT data at 36 (Left) and 76 (Right) months of age. Note that alignment was achieved using the foramen magnum as the reference point.

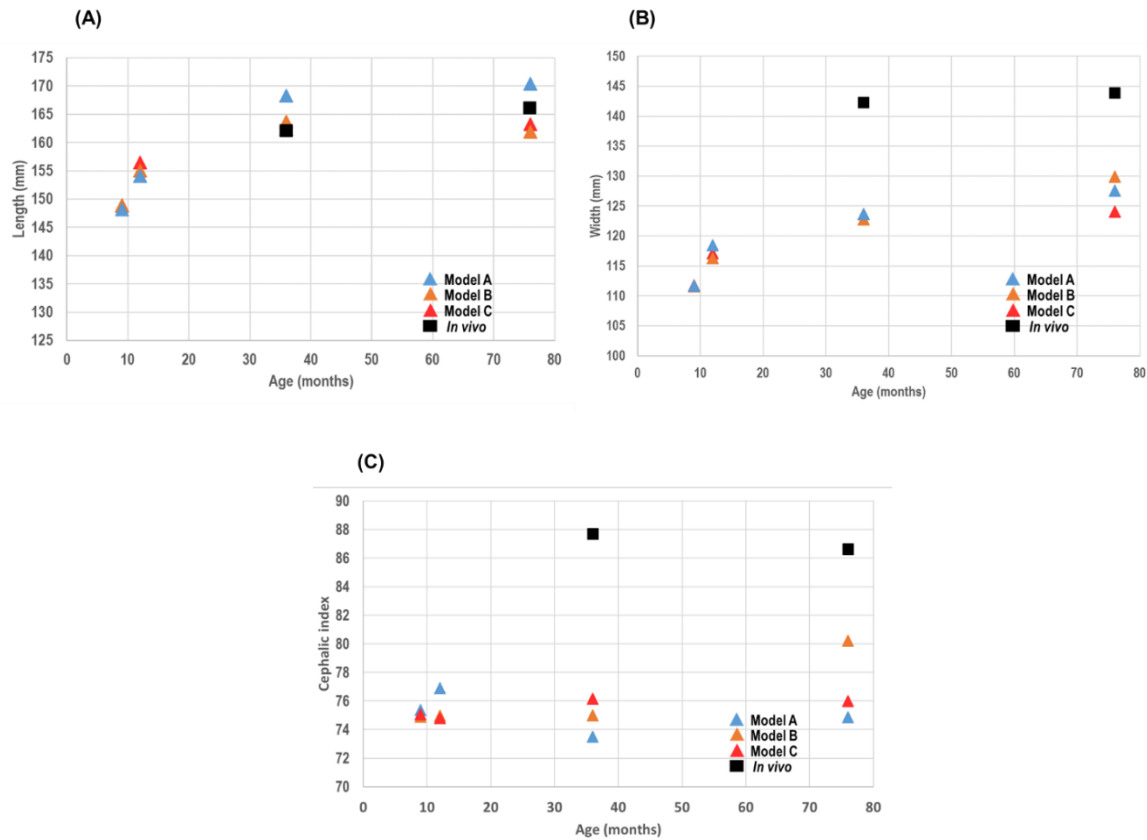


**Figure 5.8:** Cephalometric measurement predictions against *in vivo* CT data. Showing the length (A), width (B) and cephalic index (C).

## 5.4 Discussion

This chapter aimed to implement, investigate, and optimise the pre-existing method of bone formation across the cranial sutures and craniotomies following the skull reconstruction in sagittal craniosynostosis (discussed in Chapter 3). The results were compared against the existing patient-specific CT data, allowing for the validation of the predicted morphologies and for a comparative analysis of the timing of suture and craniotomy closure to be undertaken.

**Sensitivity study:** Firstly, a sensitivity study was performed which varied the minimum and maximum threshold values with relevance to the hydrostatic strain to dictate the patterns of bone formation across the model. The goal of these observations was to understand the mechanobiological behaviour of the model and introduce a level of strain-dependent formation into the pre-existing method. In our first analysis (i.e., a minimum threshold value of 0%) the sutures were seen to fuse (see: Figure 5.3) upon

the first load step (4 to 6 months of growth). This justified the decision to subsection the ongoing study, where the former three scenarios increase the minimum threshold value, and the latter increase the maximum threshold value. These were seen to alter the patterns and timings of bone formation at the sutures and craniotomies.

Due to the rate and timing of suture closure, exclusively the metopic and anterior fontanelle, it could be argued that the current level/threshold utilised here (scenario two – 1 %) may be close to resembling the real world conditions (Teager *et al.*, 2018; Pindrik, 2014). Further, under scenario 3 (i.e., 2 %), greater levels of patency were still visible across the squamosal suture (Figure 5.3 – black box), indicating the optimal range to be between 0 and 1 % given the current models' geometries and parameters. Although the patterns of bone formation differed between each scenario, the morphological outcomes remained largely similar vs. the CT data (Figure 5.4), indicating that the differences in suture formation had little impact on morphological outcomes.

The patterns of bone healing were seen to be impacted by the fourth (i.e., 25 %) and fifth (i.e., 35 %) scenarios. As such, a more realistic timing of closure for scenario four was captured. Interestingly, the higher value resulted in the distortion of the bone healing, most notably on the right lateral segment (See: Figure 5.5 – black box), leading to a regional delay in bone formation. One hypothesis for this cause is the result of larger and more concentrated strain being experienced by these regions owed to the progressively rapid formation at later load steps, which may have exceeded the specified 35 % threshold value in these small regions of craniotomy patency. Despite this, little difference was seen across the morphological predictions (Figure 5.5), with both agreeing well with the CT data. Owing to the observations here and considering the changes in craniotomy dimensions for later analysis to minimise possible difficulties, scenario four's values were chosen for models B and C.

**Bone formation method:** Initially, a *radius dependent* (Model A) and *strain-dependent* (Model B) method was parameterised, to compare the former and latter outcomes against the CT data. Model A's craniotomy was seen to close by the first load-step (Figure 5.6), produced by the over-extensive range of the specified

craniotomy radius (i.e. 10.8 mm/month). Hence, using the former as a comparative baseline, only the alternating levels of strain across model B dictated the bone formation.

It could be argued why hydrostatic strain was chosen above other principal strains. The selection of hydrostatic strain was based on a previous study from Marghoub *et al.*, (2019), who performs a direct comparison between each principal strains vs. hydrostatic strain to model and predict the bone formation across the FE model of a mouse. The use of hydrostatic strain was found to be the most accurate to resemble the real-world conditions, highlighting accurate times of suture closure. Due to the method and parameters in this thesis based off this study, the parameter of hydrostatic strain was chosen.

The observations here showed promise in capturing the accurate timing of suture and craniotomy closure. However, deviation of ossification from the bone lining was seen most notably across the anterior fontanelle. As established, it is known that the process of ossification is retained along with the bony linings of the sutures and fontanelles (Katsianou *et al.*, 2016). These characteristics result in spontaneous growth appearing in regions not clinically expected. Conversely, this spontaneous growth was seen across the craniotomies in model B's predictions. Clinically, during postoperative recoveries, it is not unusual to capture these 'islands' of bone growth, as it is reportedly due to the biological changes in the dura mater (Aalami *et al.*, 2004; Lee *et al.*, 2016). Although the modelling approach here does not consider these, it is interesting such patterns were captured by the proposed modelling approach. As such, justification felt sufficient to explore an alternative approach to replicate the bone formation (here, model C).

As the radius exceeds the overall craniotomy dimensions (As previously mentioned), little difference was seen between the pattern of bone formation of models B and C. By its nature, allowing the bone formation at the craniotomies to be dictated by *strain-levels* alone is applicable in achieving clinical accuracy here (Thenier-Villa *et al.*, 2018; Delye *et al.*, 2018). As such a rule does not apply to the sutures (i.e., 0.8 mm/month), this aspect was 'controlled' by both the radius and strain values, which achieved a

more promising result. As a more accurate representation of suture closure is overall achieved here, it could be argued that model C's approach provided the most suitable outcomes for further computational analysis.

Although all approaches varied in anteroposterior overprediction by 36 months, model C matched the closest by 76 months to the CT data. Further to this, only model C estimated (within generous proximity) the relapse in the cephalic index from these two age points, showing a good resemblance to the CT data. This could be caused by the minor 'budge' appearing across the occipital region in both model C and the CT data at both time-points (See: Figure 5.6 – black boxes), producing greater lengthening while minimising the bilateral growth. However, it cannot be overlooked that all models were unable to predict the cephalic index or skull width with complete accuracy.

Several previously stated limitations could be responsible for this: 1) the linear growth of the ICV here is a far more simplistic approach to that of the anisotropic structure and growth behaviour of the brain 2) the effect of various other soft tissues present within the craniofacial system were not considered here. For example, it is very likely that different muscle groups contribute to the skull morphology from about 2 years of age as children start to eat harder food.

### **5.5 Summary**

In this chapter, a promising method of simulating bone formation was established for the computational framework developed here. The next chapter will use Model C and compare the biomechanics of different techniques used for the management of the sagittal synostosis based on the patient-specific model described in Chapter 3 (i.e., acting as generic model).





## **Chapter 6: Comparative analysis of ten corrective techniques for sagittal craniosynostosis**

## 6.1 Introduction

The aim of this chapter was to expand on the comparative analysis of the three corrective techniques discussed in Chapter 4 and apply the new methodologies of bone formation developed in Chapter 5 across different techniques. Here, a total of ten surgical options were replicated, with three methods' timing of intervention differing from the original pre-operative age of 4 months. Several sensitivity studies were carried out, to understand the impact of: (a) a 'non-correction' scenario could have on the contact pressure of the intracranial volume; (b) the modelled fixators could have on the prediction under a specific method of correction (total calvarial remodelling); (c) a modelled postoperative helmet on predictions when alternating the duration in which it is applied.

## 6.2 Materials and methods

As the methods and modelling approaches here closely follow previous chapters (i.e., 3, 4, and 5), the first subsection here will provide a summary of the parameters used (See: Figure 6.1). The second portion will highlight the techniques replicated while discussing the method of alternating the pre-operative age of the model. A summary of the sensitivity studies undertaken will then be highlighted.

### 6.2.1 Model development

The pre-operative modelling geometry used here was described in Chapters 3, 4 and 5. No alteration to the meshing or geometry was performed.

### 6.2.2 Bone formation algorithm

The parameters for bone formation used across all techniques are described in Chapter 5 under section 5.2.3 under the abbreviation 'Model C (*Strain-radius dependent*)'. Figure 6.1. shows the bone formation algorithm workflow.

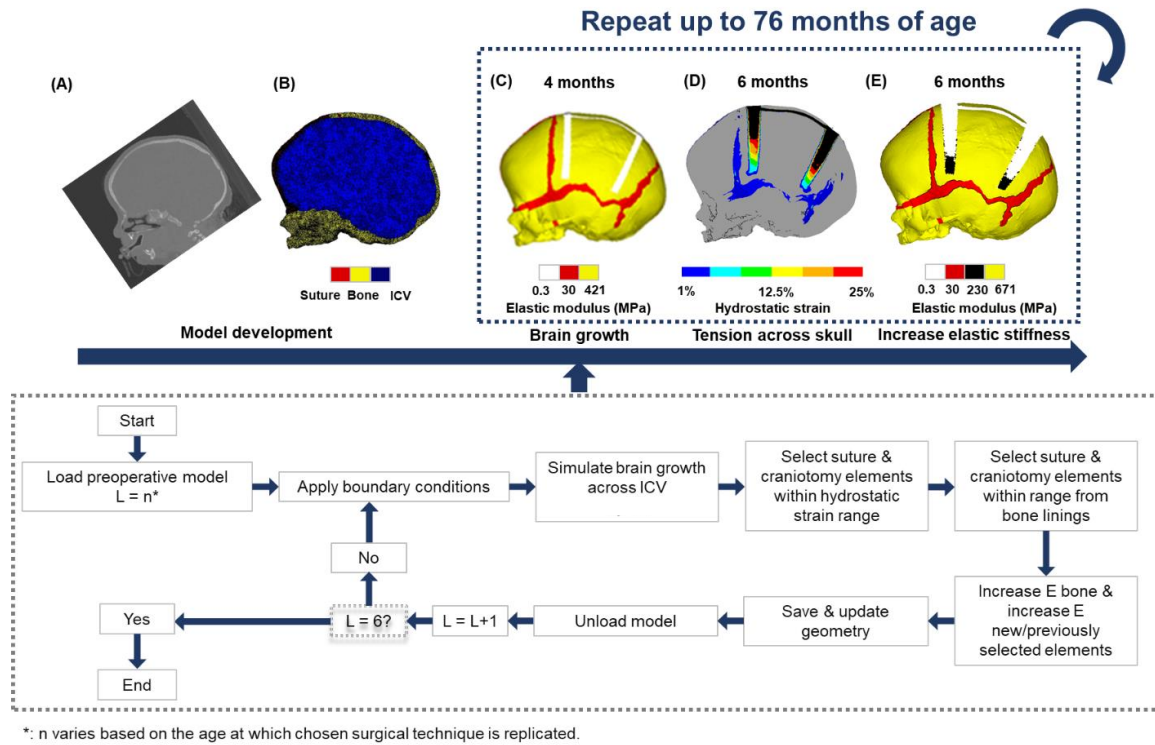


**Figure 6.1:** Workflow of the finalised methodology for predicting bone formation patterns across the patient-specific model (A, B). The technique replicated across the flat bones (C) then undergoes growth from the timing of intervention to 76 months. Hydrostatic strain and radius parameters (D) are defined to dictate the bone formation (See flowchart) until the target age was reached. As previously mentioned, the selected elements have their elastic moduli updated (E) to represent the changes in bone differentiation.

### 6.2.3 Replicated techniques

Figure 6.2 shows all considered techniques in this chapter. These techniques were chosen based on the collaboration with four craniofacial units (in Oxford, Paris, Gothenberg, Nijmegen and Olszyl) who advised on the details of the craniotomies based on their current clinical practice. Table 6.1 displays the CT data used to compare the predicted outcomes across each reconstructed technique. The details of each technique are as follows:

**Table 6.1:** Comparative CT data used for all replicated techniques.

|                        | # of scans: | Age (months):      | Mean length (mm):    | Mean width (mm):    | Mean cephalic index: |
|------------------------|-------------|--------------------|----------------------|---------------------|----------------------|
| Renier's H (4 months): |             |                    |                      |                     |                      |
|                        | 2           | 79 ( $\pm 0.1$ )   | 176.6 ( $\pm 10.5$ ) | 138.1 ( $\pm 5.8$ ) | 78.6 ( $\pm 7.9$ )   |
| Renier's H Modified:   |             |                    |                      |                     |                      |
|                        | 3           | 64 ( $\pm 3.0$ )   | 182.8 ( $\pm 5.2$ )  | 133.5 ( $\pm 5.6$ ) | 73.1 ( $\pm 4.6$ )   |
| Endoscopic:            |             |                    |                      |                     |                      |
|                        | 1           | 27                 | 193.1                | 142.7               | 73.9                 |
| 2 SAC:                 |             |                    |                      |                     |                      |
|                        | 10          | 38 ( $\pm 2.0$ )   | 171.6 ( $\pm 20.5$ ) | 134.9 ( $\pm 5.1$ ) | 75.8 ( $\pm 2.7$ )   |
| 3 SAC:                 |             |                    |                      |                     |                      |
|                        | 8           | 38 ( $\pm 2.0$ )   | 177.9 ( $\pm 7.9$ )  | 130.9 ( $\pm 3.2$ ) | 73.7 ( $\pm 4.4$ )   |
| Renier's H (6 months): |             |                    |                      |                     |                      |
|                        | 2           | 53.5 ( $\pm 3.5$ ) | 178.0 ( $\pm 1.4$ )  | 128.9 ( $\pm 0.7$ ) | 72.4 ( $\pm 0.9$ )   |
| TCR 1:                 |             |                    |                      |                     |                      |
|                        | 2           | 54.5 ( $\pm 3.5$ ) | 193.9 ( $\pm 3.2$ )  | 136.3 ( $\pm 1.6$ ) | 70.3 ( $\pm 0.3$ )   |
| TCR 2:                 |             |                    |                      |                     |                      |
|                        | 1           | 63                 | 183                  | 144.1               | 78.7                 |

**Renier's 'H' technique (4 months):** The technique used here was adopted from the Hôpital—Necker Enfants—Malades Cranio-facial Surgery Unit (Paris, France). This technique was discussed in section 3.2.2 and remained unaltered here. It was also included in this chapter for the sake of comparison with other considered techniques in this chapter.

**Renier's 'H' modified (4 months intervention):** Expanding on the concepts of the original Renier's H, also performed at the Hôpital—Necker Enfants—Malades Cranio-facial Surgery Unit (Paris, France), the level of invasiveness was increased here. The coronal suture was removed across the entire bilateral width and replaced with a 10-15 mm rectangular craniotomy. Across the mid-dorsal plane, two parallel incisions extending from the posterior of the anterior fontanelle to the anterior of the lambdoid sutures were created. This resulted in a segmented piece of free-floating bone in place of the fused sagittal suture.

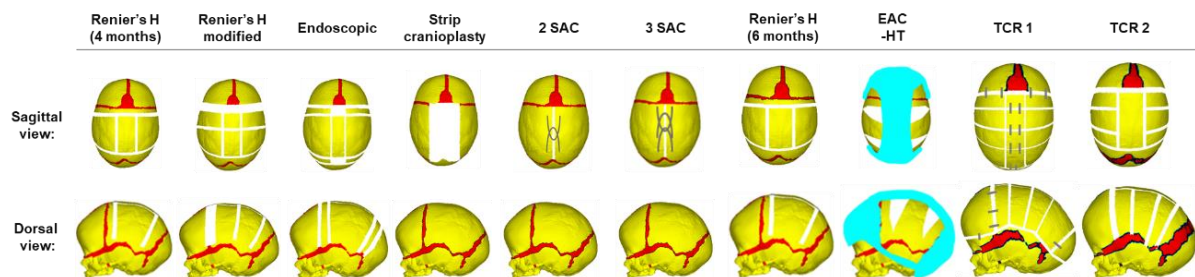


**Figure 6.2:** All technique illustrations across the patient-specific model at times of intervention. Images are 1:1 scale.

Two bilateral craniotomies were then made; the first was created across the mid-dorsal of the parietal bone, dividing the floating bony segments into two dissimilar size segments. The second connected the anteroposterior craniotomies by running adjacent to the lambdoid sutures.

**Endoscopic (4 months intervention):** This technique was adapted from the Department of Head and Neck Surgery for Children and Adolescents located at the University of Warmia and Mazury (Olsztyn, Poland). Four bilateral incisions, two each across the coronal and lambdoid sutures, were made, resulting in the suture formations being obliterated (i.e., complete removal). Two additional incisions, running perpendicular to the coronal suture, extend from the anterior to the posterior fontanelles, releasing a rectangular portion of bone across the centre, measuring approximately 50 mm in length. The cubic strips of remaining bone at either end of the bone portion are removed.

**Strip Cranioplasty (4 months intervention):** The strip cranioplasty highlighted here was adopted from the craniofacial centre of Oxford University Hospital (Oxford, UK). A full description of this technique is provided in section 4.2.1.

**2 spring-assisted craniectomy – 2SAC (4 months intervention):** A full description of this technique is provided in section 4.2.1 and remains unaltered here. Taken from the Sahlgrenska University Hospital (Gothenburg, Sweden).

**3 spring-assisted craniectomy – 3SAC (4 months intervention):** A full description of this technique is provided in section 4.2.1 and remains unaltered here. Taken from the Sahlgrenska University Hospital (Gothenburg, Sweden).

**Renier's 'H' technique (6 months intervention):** As a comparative analysis of the timing of intervention, the previously detailed Renier's H technique was replicated here across the generic model at 6 months of age. No further alternations were made.

**Endoscopic-assisted strip craniectomy with helmet therapy – EAC-HT (4 months intervention):** The technique here has been used by the team located in the

Department of Oral and Maxillofacial Surgery at Radboud University Medical Centre (Nijmegen, The Netherlands). It incorporates a period of post-operative morphological manipulation using a helmet to constrain the head post-intervention. A large rectangular wedge of bone was removed across the mid-dorsal of the parietal bone, ending just below and above the coronal and lambdoid sutures, respectively. At its corners, triangular-shaped wedges are made bilaterally and extend towards the squamosal. The helmet was then placed immediately postoperatively, constraining the skull across the anterior and posterior, encouraging freedom of growth across the bitemporal and dorsal regions. Here, the helmet was modelled to incorporate a 2 cm wide gap between the skull and helmet upon placement at 4 months. A full description of the algorithm and parameters used to model the effects of the helmet are discussed in the Appendix III. The helmet was then removed 8 months after correction, although this duration varied under the sensitivity study to be discussed.

**Total calvarial remodelling 1 – TCR1 (12 months):** Presented at the later age of 12 months, the technique was replicated as performed at the Department of Maxillofacial Surgery and Plastic Surgery at Necker – Enfants Malades University Hospital (Paris, France). The invasive procedure performs extensive craniotomies across the suture, leaving only the squamosal and anterior fontanelle unaltered. A bilateral incision above the orbitals and extending the complete width of the frontal bones are made, segmenting the metopic suture into two portions. The same method was performed across the occipital bone. Three craniotomies, reaching from the left to right squamosal are performed. Two additional anteroposterior incisions are made from the anterior fontanelle to the posterior fontanelle, creating four cubic regions of separated bone. Bioabsorbable fixators are then positioned and secured, which will be discussed in the next section.

**Total calvarial remodelling 2 – TCR2 (12 months):** Also performed by the same team as the endoscopic treatment (the Department of Head and Neck Surgery for Children and Adolescents, the University of Warmia and Mazury, Olsztyn, Poland), the second comparative TCR technique does not require any positional fixators. The technique is similar to that of the Renier's H option, with the addition of two bitemporal

craniotomies on either side of the two anteroposterior incisions, extending to the squamosal suture.

### 6.2.3 'non-operation' scenario

To understand the impacts on the contact pressure across the ICV, a scenario, in which no craniotomies were replicated, was carried out. Calvarial growth was simulated from 4 months to 12 months of age. In addition, three techniques (i.e., Renier's H at 6 months and both TCR 1 and 2 at 12 months) intended to be replicated across the model required a later age of intervention than the actual age that the patient-specific model in this study had. The bone formation was predicted across the sutures during simulated growth (Figure 6.3). Further to the contact pressure, the cephalic measurements were also recorded for comparison.

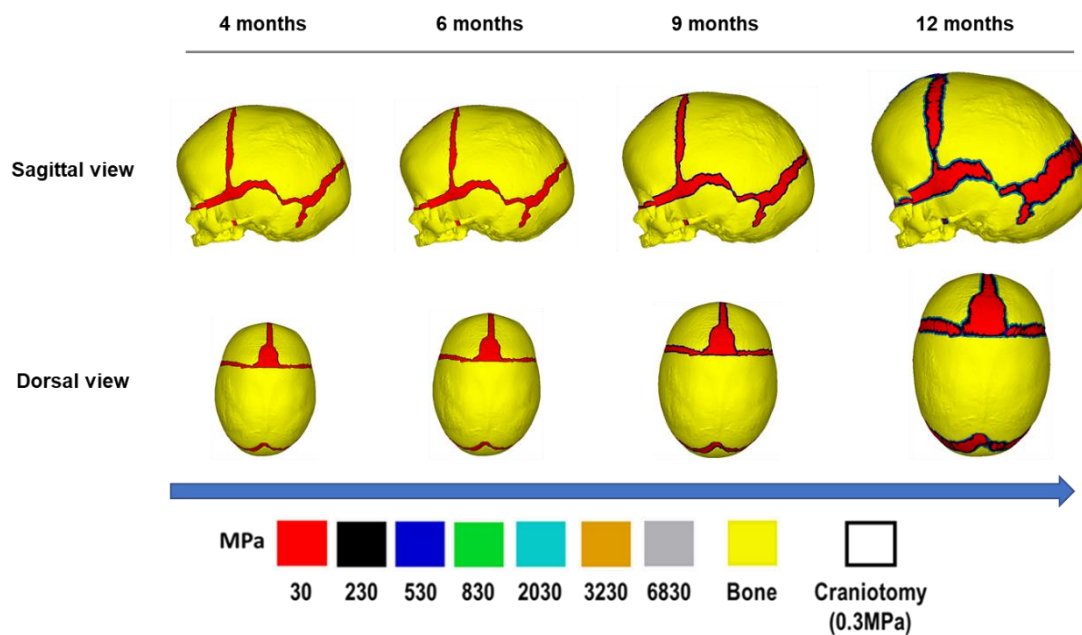


**Figure 6.3:** Simulating the natural changes in growth and bone formation under a 'non-operation' condition. Geometries at 6 months and 12 months were used to replicate three techniques performed at the later pre-operative age of 4 months for this chapter.

## 6.2.4 Sensitivity studies

**Fixators sensitivity:** To ascertain the impacts simulating fixators has on the overall skull shape and ICV pressure of the model, a comparative analysis was undertaken using the TCR 1 model under two methods (Figure 6.3).

The first (denoted: with fixators) positions 16 fixators, which connected the calvarial bones and regions of the craniotomies, using 3D-spar elements (i.e., LINK180). The chosen placement of these elements relied on observations from the CT data provided by the clinical institution. An initial elastic modulus of 2000 MPa and a Poisson's ratio of 0.1 were selected for all fixators (Landes *et al.*, 2006). 'Absorption' of the fixators was simulated by linearly reducing the elastic modulus values to simulate the degradation fully achieved at 3 months post-insertion (Ashammakhi *et al.*, 2004). As such, the replicated fixators were presented across the model from 12 months and were deleted (representing full absorption) by 24 months.

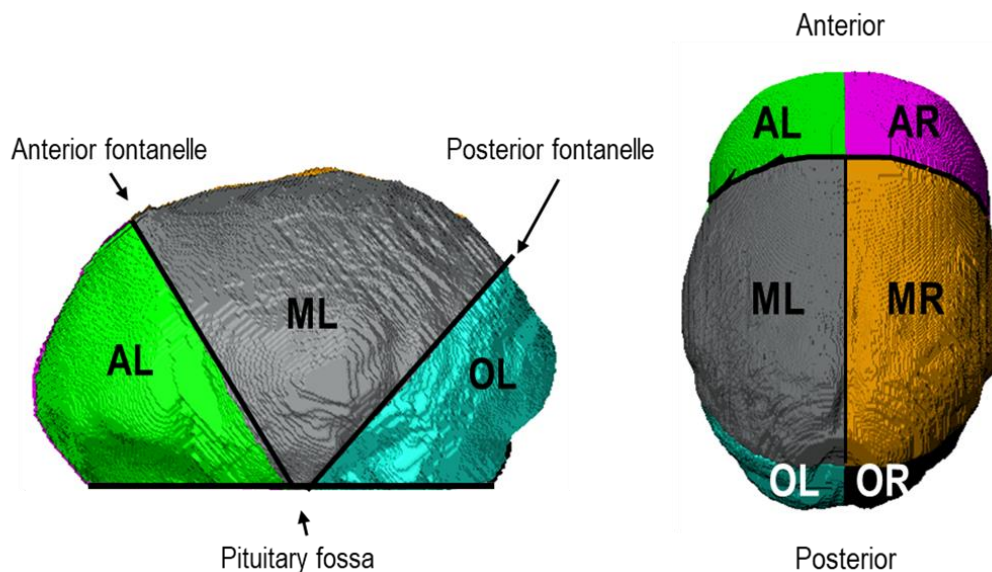


**Figure 6.4:** Regions of ICV distribution and ICV pressure level measurements. Sagittal (left) and dorsal views (right). Method adopted from Liaw *et al.*, (2019).

The second method (i.e., no fixators) replicated TCR 1 procedure with no fixators being present, allowing for a direct comparison. Both approaches were simulated from the 12 months intervention age to the follow up age of 76 months. Morphological and ICV contact pressure changes were compared.



**Duration of helmet therapy:** To capture the impacts of applying the modelled helmet could have on predictions, four additional helmeting scenarios (including the baseline 8 months of helmet duration) were investigated. The first negates the use of the helmet for the complete duration of the growth, with only the endoscopic assisted strip craniotomy being replicated across the skull. The second and third scenarios have the modelled helmet applied for the duration of 2 (removal at 6 months of age) and 5 months (removal at 9 months of age) after surgery, respectively, after which the modelled helmet was removed (i.e., all constraints representing the helmet were deleted). All four scenarios underwent growth up to the follow up age of 36 months of age, which were then analysed.

### 6.2.6 Measurements and comparisons

A method of analysing the changes in volume distributions and assessing the regions of contact pressure across the predicted ICV was introduced here. Figure 6.4 illustrates these specified regions. For consistency across all replicated techniques, the pituitary fossa landmark was used to create three large areas (Liaw *et al.*, 2019). The anterior and posterior fontanelles were further used to split these regions into two, indicating any asymmetric outcomes, which totalled six regions of interest. These were, respectively, the anterior left and right (AL, AR), middle left and right (ML, MR) and occipital left and right (OL, OR). An attempt to compare the predictive shapes across all techniques versus clinical data was performed using the obtained CT data where possible.

## 6.3 Results

**‘Non-operation’ scenario:** Figure 6.5 highlights the changes in length, width, and cephalic index under a ‘non-operated’ scenario, allowing the later three techniques (i.e., Renier’s H – 6 months, TCR 1, and TCR 2) to be replicated at the correct intervention age. The greatest level of growth was seen in the length from 4 months (137.2 mm) to 12 months (157.3 mm), while the lowest was seen across the width (108.1 mm to 115.0 mm). This difference led to a lower cephalic index by 12 months (73.1) when compared to 4 months of age (78.8).

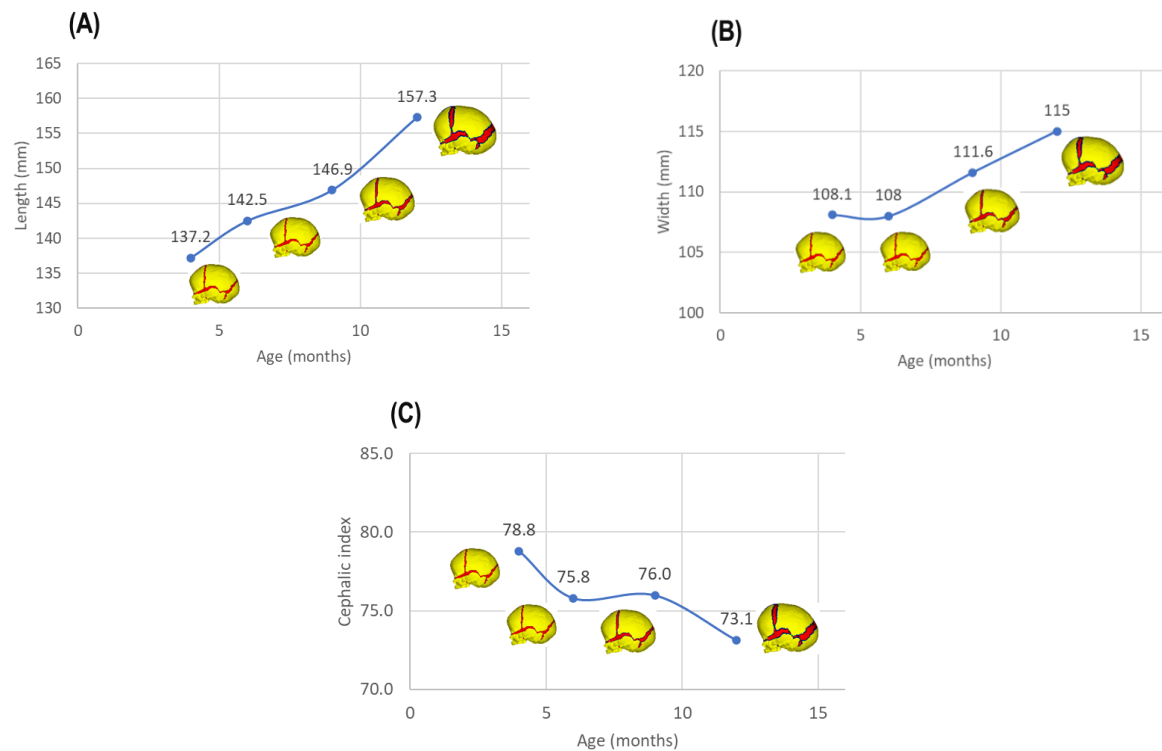


**Figure 6.5:** Cephalometric measurements of the predictive model under a 'non-operative' scenario. Highlight the outcomes in length (A), width (B), and cephalic index (C).

Figure 6.6 quantifies the changes in regional displacement of the ICV under the same scenario. An overall symmetry was seen between all left and right regions of interest during growth. The largest volume was consistently seen across the middle region by 12 months of age (ML: 280 ml – MR: 287.3 ml). A low increase in volume was seen across the anterior (AL: 107.3 ml – AR: 119.2 ml) while a plateau was seen across the occipital region for the entirety of the growth (OL: 68.8 ml – OR: 71.4 ml).

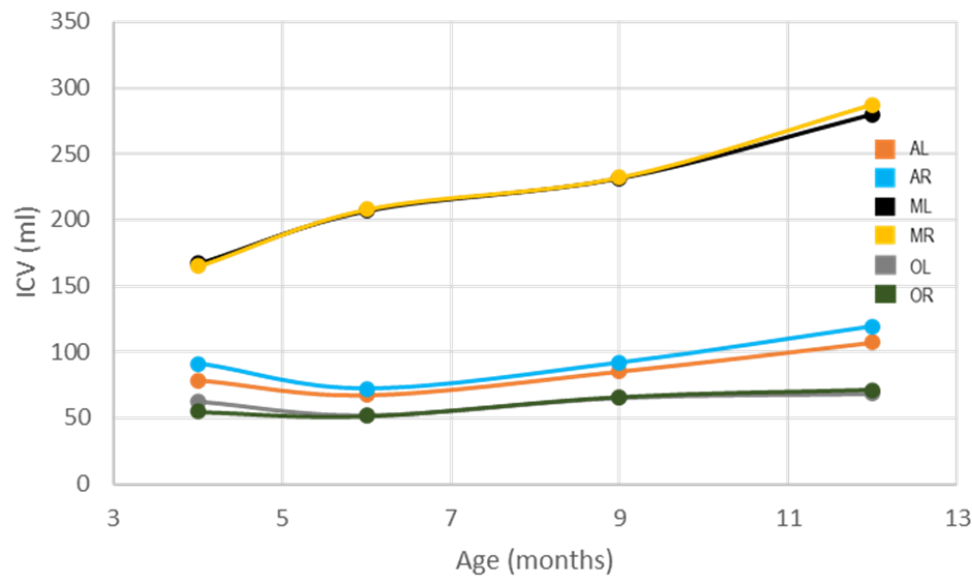


**Figure 6.6:** Changes in the regional distributions of the ICV from 4 months of 12 months of age under the 'non-operated' scenario.

Figure 6.7 compares the average contact pressure readings among the ICV regions of interest (Figure 6.4) from 6 months to 12 months of age. A comparison of the pressure seen at 4 months was unobtainable, due to the initial geometry being presented at this age.

A continuous rise in pressure was seen across the left anterior region from 9 months ( $1.18 \pm 1.0$  MPa) to 12 months ( $1.6 \pm 0.76$  MPa). This trend was not seen in the right region showing a reduction in pressure across the same time points ( $1.28 \pm 0.98$  MPa to  $1.14 \pm 0.78$  MPa, respectively). By 12 months of age, all other regions displayed elevated pressure with age, most notably the occipital region at a value of  $1.92 \pm 1.0$  MPa and  $2.01 \pm 1.0$  MPa for the left and right hemispheres, respectively. Both middle regions predicted highly similar pressure readings by 12 months of age. A value across the left region measured  $1.39 \pm 1.2$  MPa and  $1.4 \pm 1.0$  MPa for the right region.

## Chapter 6: Biomechanical comparison of ten techniques

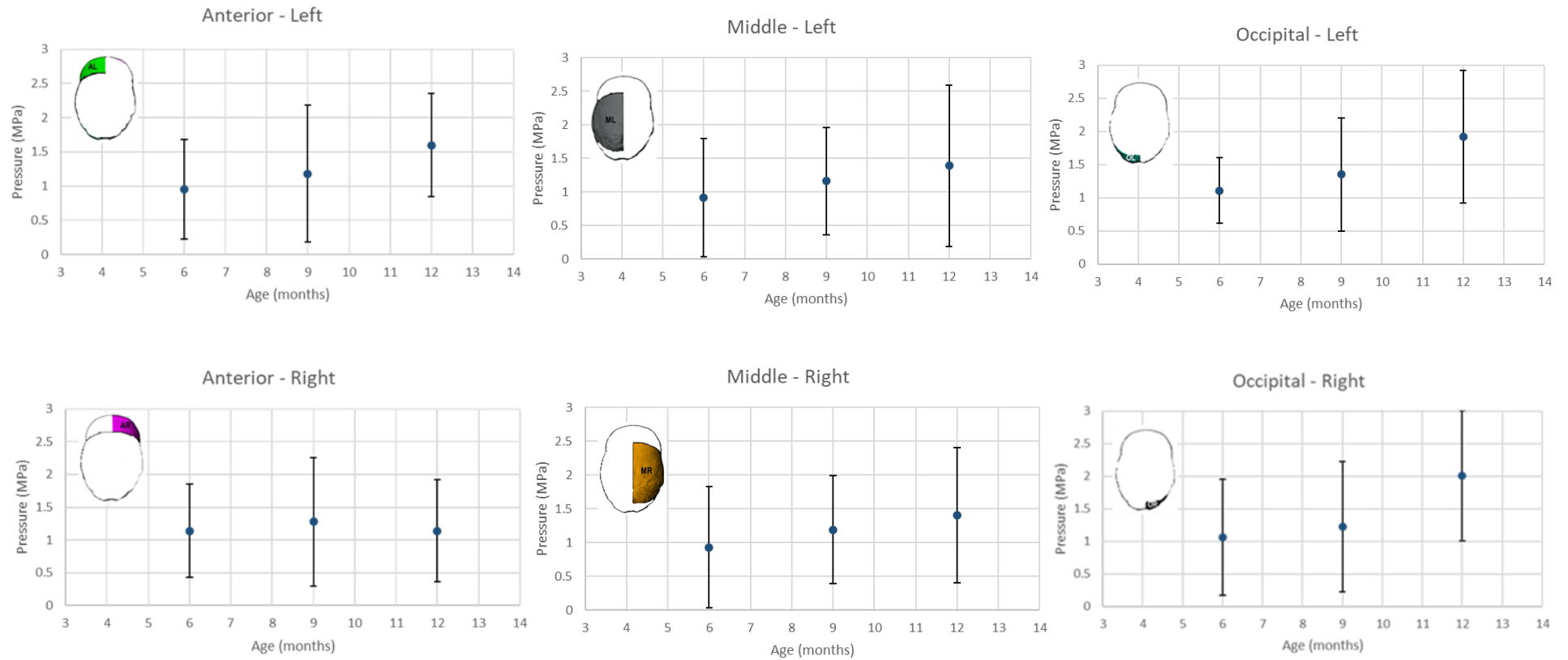


**Figure 6.7:** Changes in the regional contact pressure of the ICV from 4 months to 12 months of age under the 'non-operated' scenario.

**Absorbable fixators:** Table 6.2 summarises the skull length, width, and cephalic index across both approaches at different time points. Both approaches showed an improvement in the cephalic index from the pre-operative stage to the postoperative stages at 24, 36 and 72 months of age. This was more evident without the use of fixators (73.1 to 76.8) vs. with (73.1 to 74.6), as bitemporal widening and a lack of anteroposterior growth was more evident in the former. Despite this, both approaches demonstrated a remarkably similar cephalic index by 76 months (77.4 vs. 77.5).

Figure 6.8 shows the predicted pattern of both bone formation and ICV contact pressure. During the absence of fixators (i.e., no fixators), progressive morphological distortion and failure for craniotomy fusion were evident by 76 months of age. Affected regions appeared across the anterior, posterior, and left dorsal craniotomies, explaining the changes in both length and width across the later time points of Table 6.2. Further, a low level of bone formation was seen across the remaining sutures, most notably the squamosal and anterior fontanelle, where full fusion was not achieved. The inclusion of fixators was seen to address the former issues, where full craniotomy healing and anterior fontanelle closure were achieved by 76 months of age.

**Table 6.2:** Cephalometric measurement between both fixator modelling approaches.



|                                  | No fixators | With fixators |
|----------------------------------|-------------|---------------|
| <b>Preoperative (12 months):</b> |             |               |
| Length (mm):                     | 157.3       | 157.3         |
| Width (mm):                      | 115.0       | 115.0         |
| Cephalic index:                  | 73.1        | 73.1          |
| <b>24 months:</b>                |             |               |
| Length (mm):                     | 163.6       | 164.3         |
| Width (mm):                      | 123.8       | 122.6         |
| Cephalic index:                  | 75.7        | 74.6          |
| <b>36 months:</b>                |             |               |
| Length (mm):                     | 166.6       | 168.0         |
| Width (mm):                      | 128.0       | 125.4         |
| Cephalic index:                  | 76.8        | 74.6          |
| <b>76 months:</b>                |             |               |
| Length (mm):                     | 169.7       | 169.9         |
| Width (mm):                      | 131.3       | 131.7         |
| Cephalic index:                  | 77.4        | 77.5          |

Contact analysis showed the lack of bone formation at the craniotomies for the control approach gave rise to little contact pressure across the intracranial volume by 76 months of age vs. the 'With fixators' scenario. The highest levels of contact pressure were captured across the lower temporal regions for both approaches (Figure 6.8 – black box).

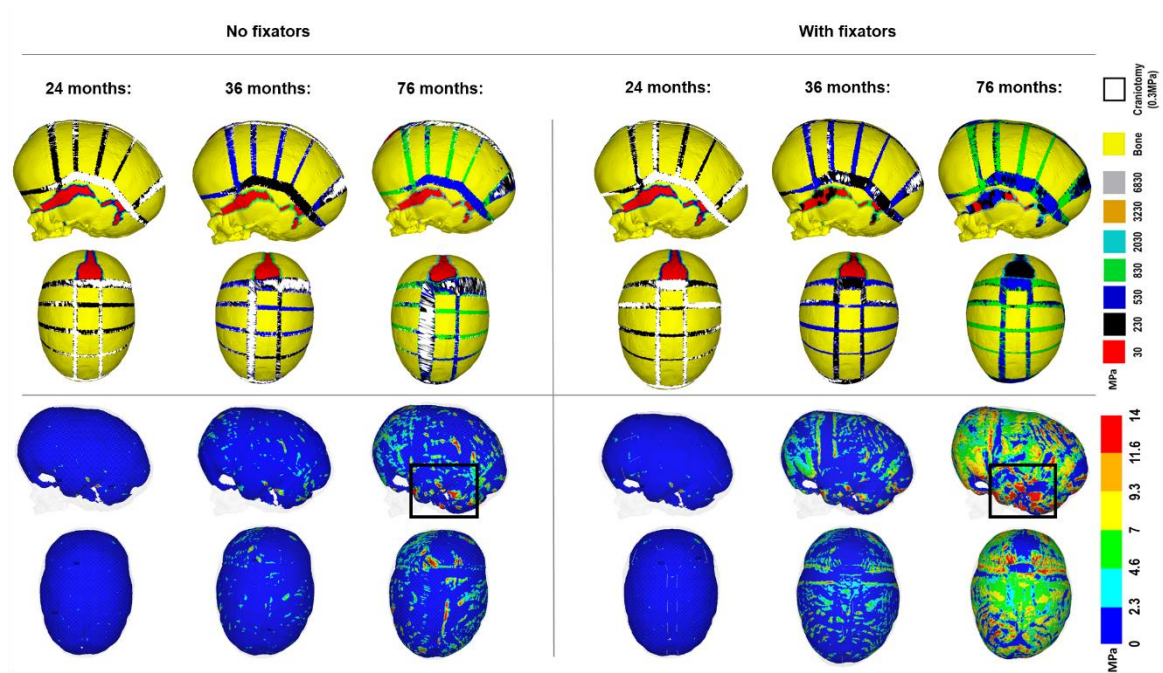


**Figure 6.8:** Predictive pattern of bone formation (above) and ICV contact pressure (below) across both approaches.

Figure 6.9 summarises the changes in regional distribution of the ICV during simulated growth across both approaches. Little difference in volume was seen across both approaches in the AL (No fixator – 157.2 ml vs. With fixators– 154.5 ml) and MR regions (No fixator – 371.8 ml vs. With fixators – 368.4 ml). A notable difference was seen in the ‘no fixators’ approach (AR: 178.4 ml, ML: 383.1 ml, OL: 102.2 ml, OR: 98.0 ml) vs. the ‘with fixator’ scenario (AR: 154.5 ml, ML: 365.9 ml, OL: 88.6 ml, OR: 91.1 ml) for the remaining regions.

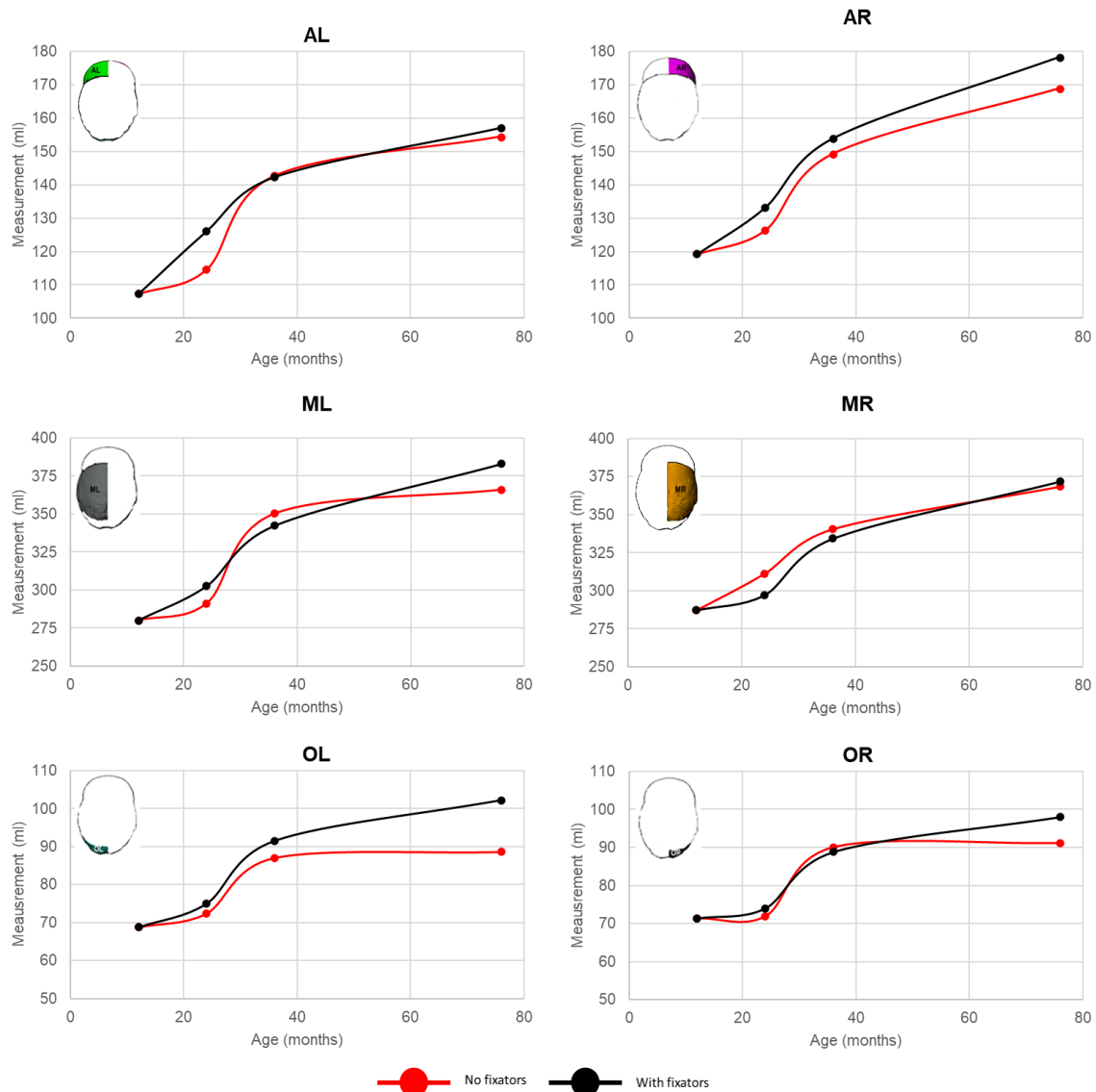


**Figure 6.9:** Predictive pattern of ICV growth across each regional measurement from 12 to 76 months of age.

**Duration of helmet therapy:** Figure 6.10 presents the predicted patterns of bone formation captured across each duration of simulated helmet therapy. All scenarios, including the lack of a helmet, presented complete calvarial healing by 20 months after surgery (24 months of age). Although bone was formed across all sutures by 36 months of age, the anterior fontanelle was an exception where there were areas that were still open (see Figure 6.7 for 36 months column for the red regions). Regarding the calvarial morphology at 36 months, a characteristic budge was predicted under a lack of helmet therapy. This abnormality was seen to have been corrected upon the



introduction of the simulated helmet, regardless of the duration it was placed across the model. The model further predicted a more uniform spherical shaped skull the longer that the helmet was applied, a result of restricting the level of anteroposterior growth.

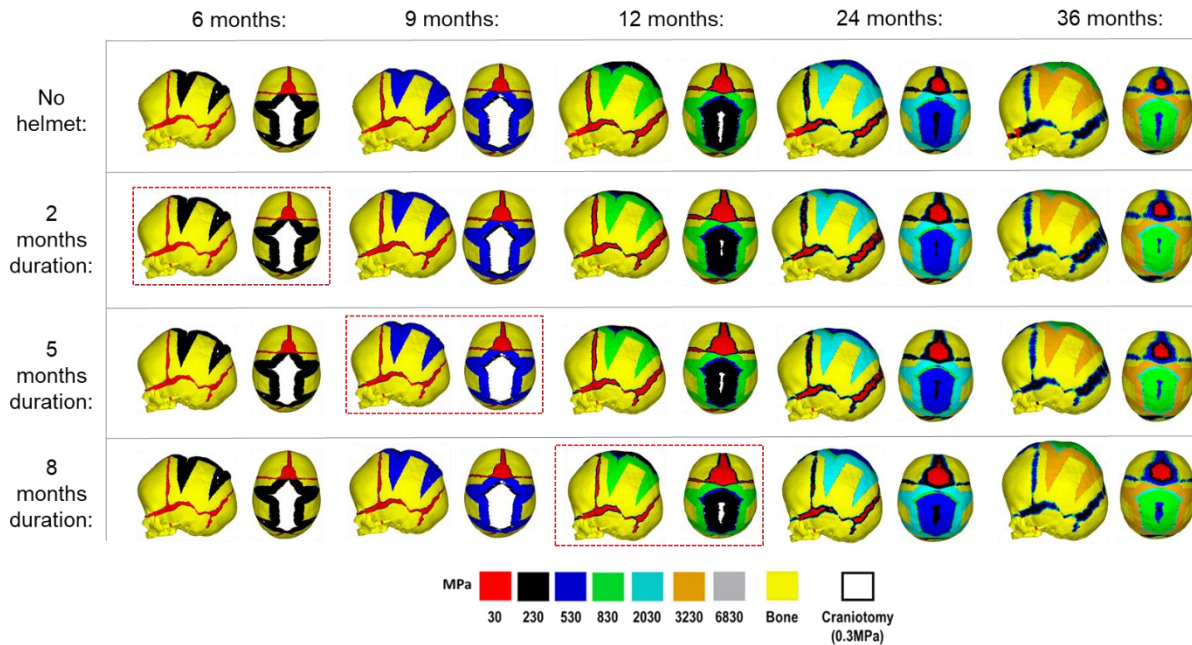


**Figure 6.10:** Predicted patterns of bone formation across various durations of simulated helmet therapy during growth. From 4 months to 36 months of age. Red boxes represent the respective timings of helmet removal.

Figure 6.11 quantifies the cephalometric measurements across all helmet duration scenarios. Predictive data presented a linear behaviour in which the longer the helmet remains across the model, the greater the cephalic improvements. By 36 months, the lack of a helmet presented the greatest overall length (162.9 mm). Prolonging the removal of the helmet to 8 months resulted in the shortest overall predicted length (146.6 mm). The predicted width of all scenarios varied only by 4 mm, with the highest seen in the 8 month helmet duration (126.4 mm) and the lowest in the scenario which lacks the use of the helmet (122.2 mm). The highest cephalic index prediction was seen in the 8 month helmet scenario (86.2) while the lowest was seen in the lack of helmet scenario (75.0).

## Chapter 6: Biomechanical comparison of ten techniques

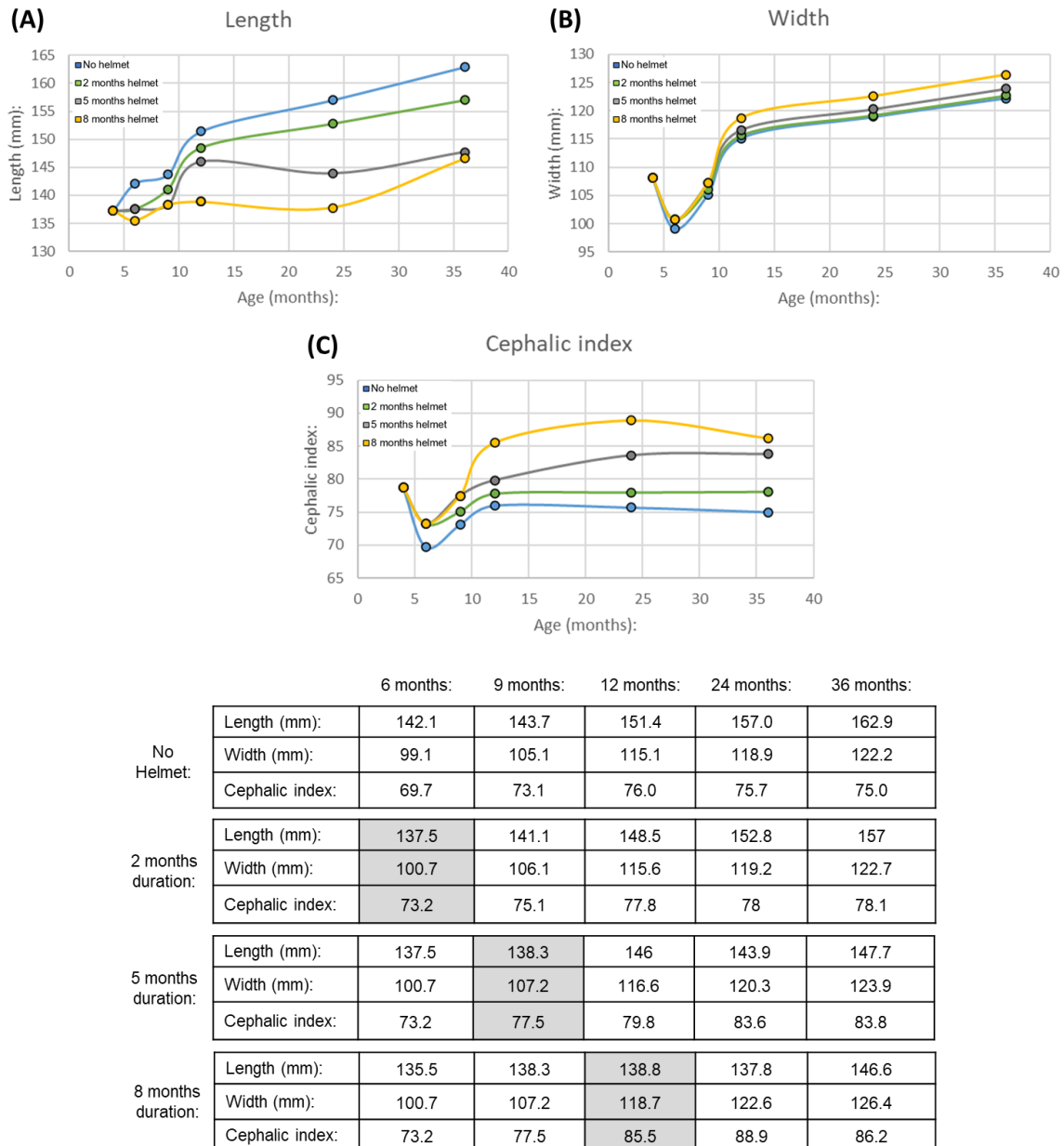


**Figure 6.11:** Cephalometric predictions across various durations of simulated helmet therapy during growth. Showing the length (A), width (B), and cephalic index (C) in scatter plots, while also presenting the numerical values at from 4 months to 36 months (below table). Grey boxes represent the respective timings of helmet removal across each scenario.

Figure 6.12 compares the predicted patterns of contact pressure across the ICV interface for all helmet scenarios. By 36 months of age, similar pressure levels were captured across all helmet duration scenarios. Regions of concentrated high pressure were seen when applying the helmet vs. not, where a more even and consistent distribution of pressure was seen. The helmet was further seen to raise the level of

pressure across the frontal and temporal regions by the time of respective removals, which persisted by 36 months of age.

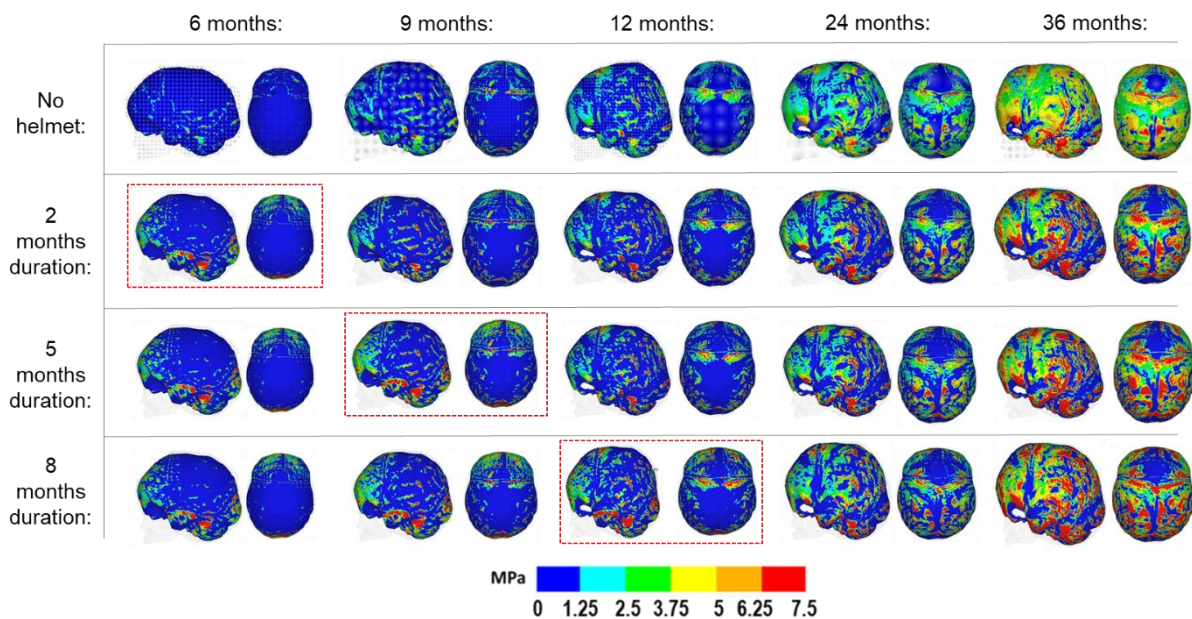


**Figure 6.12:** Predicted pattern of contact pressure across the ICV interface across various durations of simulated helmet therapy during growth from 4 months to 36 months of age. Red boxes represent the respective timings of helmet removal.

**Morphological comparison between the predictions and CT data:** It should be noted that due to the absence of relevant data, both the strip cranioplasty and helmet technique are not present here. Table 6.3 compares the cephalometric length, width and cephalic index across all technique-specific CT data and predictive data. All simulations showed underprediction across the length and width across all replicated techniques. There was a good match in the cephalic index across the predictive Renier's 'H' (4 months), 2SAC, 3SAC, and TCR 2 when compared with the CT data. All other methods indicate an overprediction in this value.

Figure 6.13 highlights the dorsal and sagittal cross sectional comparison between the predicted and CT data for each technique. Seven out of the eight techniques compared achieved a reasonable match against their CT data comparative data. The endoscopic technique was able to predict the dorsal and bitemporal growth but underpredicted the anteroposterior growth. It was also clear that all techniques underpredict around the facial region due to the lack of growth.

**Table 6.3:** Cephalometric validations of predictive data against technique-specific CT data sets.

|                               | # of scans: | Age (months): | Mean length (mm): | Mean width (mm): | Mean cephalic index: |
|-------------------------------|-------------|---------------|-------------------|------------------|----------------------|
| <b>Renier's H (4 months):</b> |             |               |                   |                  |                      |
| <i>In vivo</i> CT data        | 2           | 79 ± 0.1      | 176.6 ± 10.5      | 138.1 ± 5.8      | 78.6 ± 7.9           |
| Predictive data               | 1           | 76            | 163.3             | 124.1            | 76                   |
| <b>Renier's H Modified:</b>   |             |               |                   |                  |                      |
| <i>In vivo</i> CT data        | 3           | 64 ± 3.0      | 182.8 ± 5.2       | 133.5 ± 5.6      | 73.1 ± 4.6           |
| Predictive data               | 1           | 76            | 170.7             | 128.1            | 75                   |
| <b>Endoscopic:</b>            |             |               |                   |                  |                      |
| <i>In vivo</i> CT data        | 1           | 27            | 193.1             | 142.7            | 73.9                 |
| Predictive data               | 1           | 36            | 169               | 130.7            | 77.2                 |
| <b>2 SAC:</b>                 |             |               |                   |                  |                      |
| <i>In vivo</i> CT data        | 10          | 38 ± 2.0      | 171.6 ± 20.5      | 134.9 ± 5.1      | 75.8 ± 2.7           |
| Predictive data               | 1           | 36            | 167.1             | 122.5            | 74.6                 |
| <b>3 SAC:</b>                 |             |               |                   |                  |                      |
| <i>In vivo</i> CT data        | 8           | 38 ± 2.0      | 177.9 ± 7.9       | 130.9 ± 3.2      | 73.7 ± 4.4           |
| Predictive data               | 1           | 36            | 167.3             | 125.9            | 75.3                 |
| <b>Renier's H (6 months):</b> |             |               |                   |                  |                      |
| <i>In vivo</i> CT data        | 2           | 53.5 ± 3.5    | 178.0 ± 1.4       | 128.9 ± 0.7      | 72.4 ± 0.9           |
| Predictive data               | 1           | 76            | 169.7             | 127.6            | 75.2                 |
| <b>TCR 1:</b>                 |             |               |                   |                  |                      |
| <i>In vivo</i> CT data        | 2           | 54.5 ± 3.5    | 193.9 ± 3.2       | 136.3 ± 1.6      | 70.3 ± 0.3           |
| Predictive data               | 1           | 76            | 169.9             | 131.7            | 77.5                 |
| <b>TCR 2:</b>                 |             |               |                   |                  |                      |
| <i>In vivo</i> CT data        | 1           | 63            | 183               | 144.1            | 78.7                 |
| Predictive data               | 1           | 76            | 168.9             | 130.7            | 77.4                 |

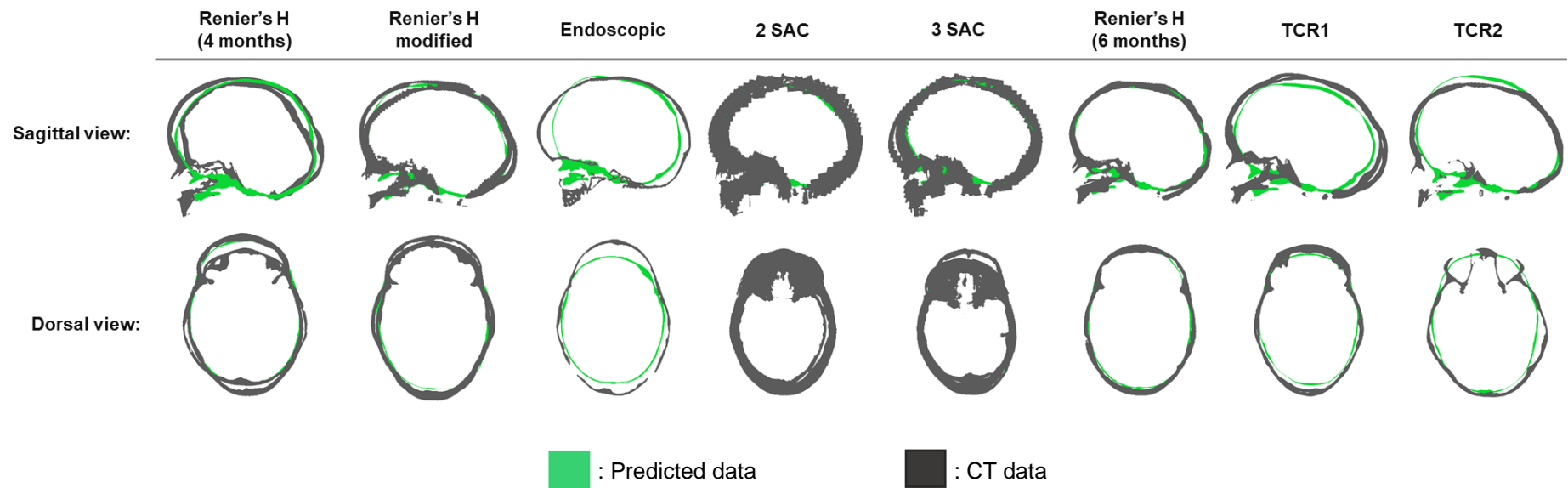


**Figure 6.13:** Morphological validation of predictive data against technique-specific CT data under a cross section analysis. Note that both the helmet therapy and strip techniques are absent due to a lack of comparative CT data.

**Surgical comparison:** Figures 6.14 and 6.15 highlight the patterns of predictive bone formation across all techniques in the sagittal and dorsal views, respectively. Within the context of this work, 'fusion' of both the sutures and craniotomies will be denoted as a lack of initial elements (30 MPa and 0.3 MPa, respectively) remaining across the models. Regarding both SAC options, both were seen to predict complete craniotomy fusion by 6 months postoperative, at the time of spring removal. Both the Renier's modified and endoscopic techniques resembled a similar pattern of craniotomy bone formation, first forming at the front and back before beginning to form across the sides. Both techniques achieved complete craniotomy fusion by 12 months of age, and 8 months postoperative. Conversely, the Renier's H (4 months) technique was seen to form from the bilateral osteotomies. By 9 months of age, the bone begins to form around the 'island' placed across the centre, before achieving complete fusion by 24 months of age (21 months postoperatively). The strip cranioplasty showed the same timing of fusion as that of the Renier's H (4 months), as bone forms across all bony borders towards to centre.

For the later performed techniques, the Renier's H (6 months) indicated a faster bone formation than its earlier intervention counterpart, reaching craniotomy fusion by 18 months postoperatively. Both TCR techniques followed a similar pattern when compared, achieving fusion by 76 months of age, or 64 months postoperatively. However, a greater level of overall fusion was seen by 36 months in the TCR 1 approach, which consisted of absorbable fixators (See above).

The Renier's modified, Strip cranioplasty, and both SAC replicated options achieved complete fusion of all sutures by 76 months of age, whereas both Renier's H (4 months) and endoscopic procedures highlighted patency across the coronal and squamosal sutures, respectively, by the same age. Such an observation was not seen in the later performed Renier's H procedure, reaching complete fusion of all sutures by 76 months. Regarding both TCR approaches, delayed formation was evident across the squamosal sutures for the first method (TCR 1), while complete fusion was seen in the second (TCR 2).

## Chapter 6: Biomechanical comparison of ten techniques

Figures 6.16 and 6.17 highlight the predictive contact pressure maps across the ICV for all techniques. During the first stages of growth (4 to 12 months), a low level of pressure was seen across the Renier's H (4 months) and Strip cranioplasty across the ICV. These levels were seen to elevate after this time, marginally across the bitemporal and occipital regions. A high level of pressure was captured across the Renier's modified and Renier's H (6 months) procedures, most noticeably across the dorsal, bitemporal and anterior regions.



## Chapter 6: Biomechanical comparison of ten techniques

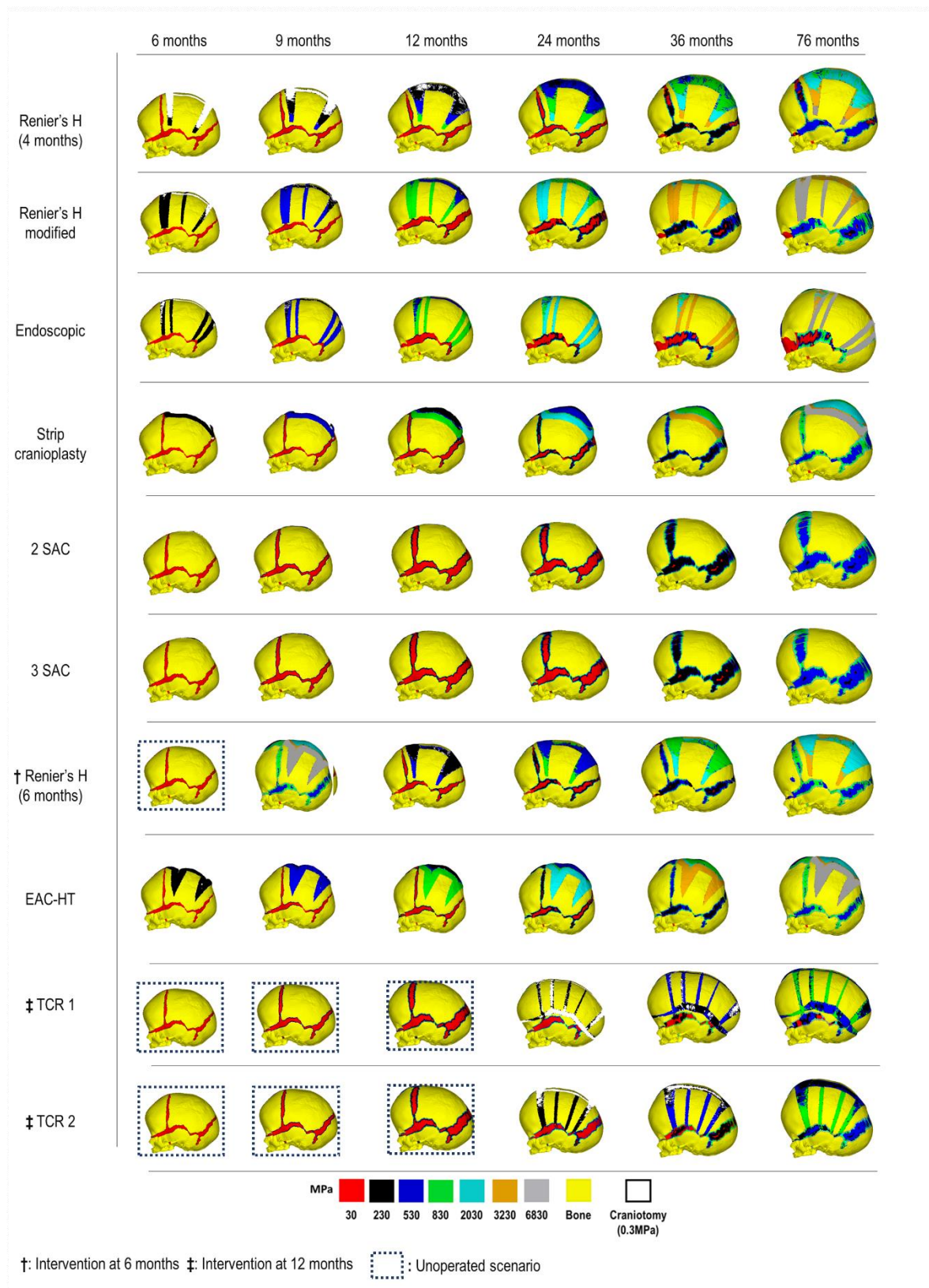


**Figure 6.14:** Predictive pattern of bone formation across all replicated techniques – sagittal view. Note that blue dotted boxes indicate a lack of correction to reach the required age of intervention.



## Chapter 6: Biomechanical comparison of ten techniques

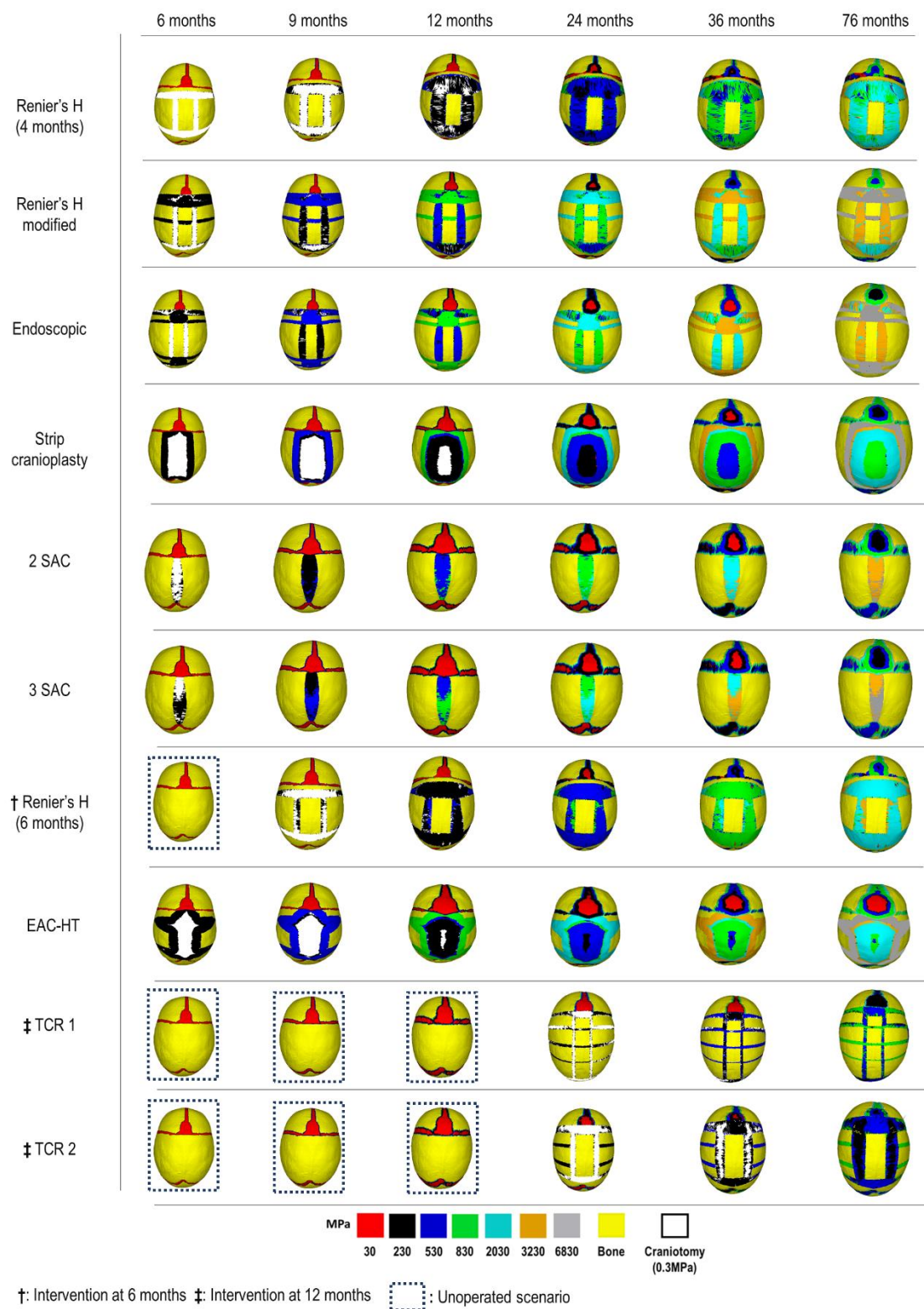
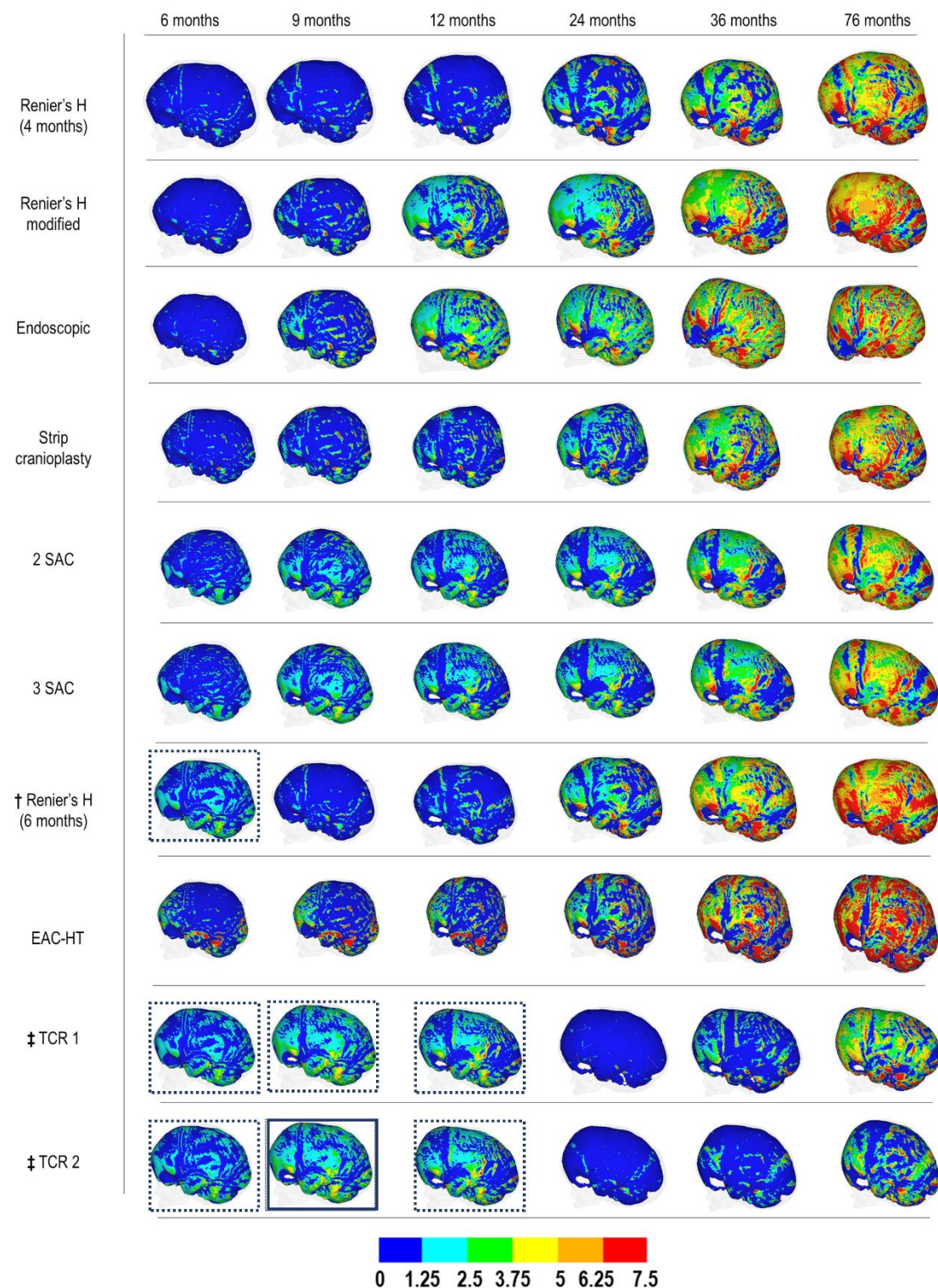


**Figure 6.15:** Predictive pattern of bone formation across all replicated techniques – dorsal view. Note that blue dotted boxes indicate a lack of correction to reach the required age of intervention

## Chapter 6: Biomechanical comparison of ten techniques



†: Intervention at 6 months ‡: Intervention at 12 months : Unoperated scenario

**Figure 6.16:** Predictive pattern of contact pressure across all replicated techniques – sagittal view. Note that blue dotted boxes indicate a lack of correction to reach the required age of intervention.



## Chapter 6: Biomechanical comparison of ten techniques

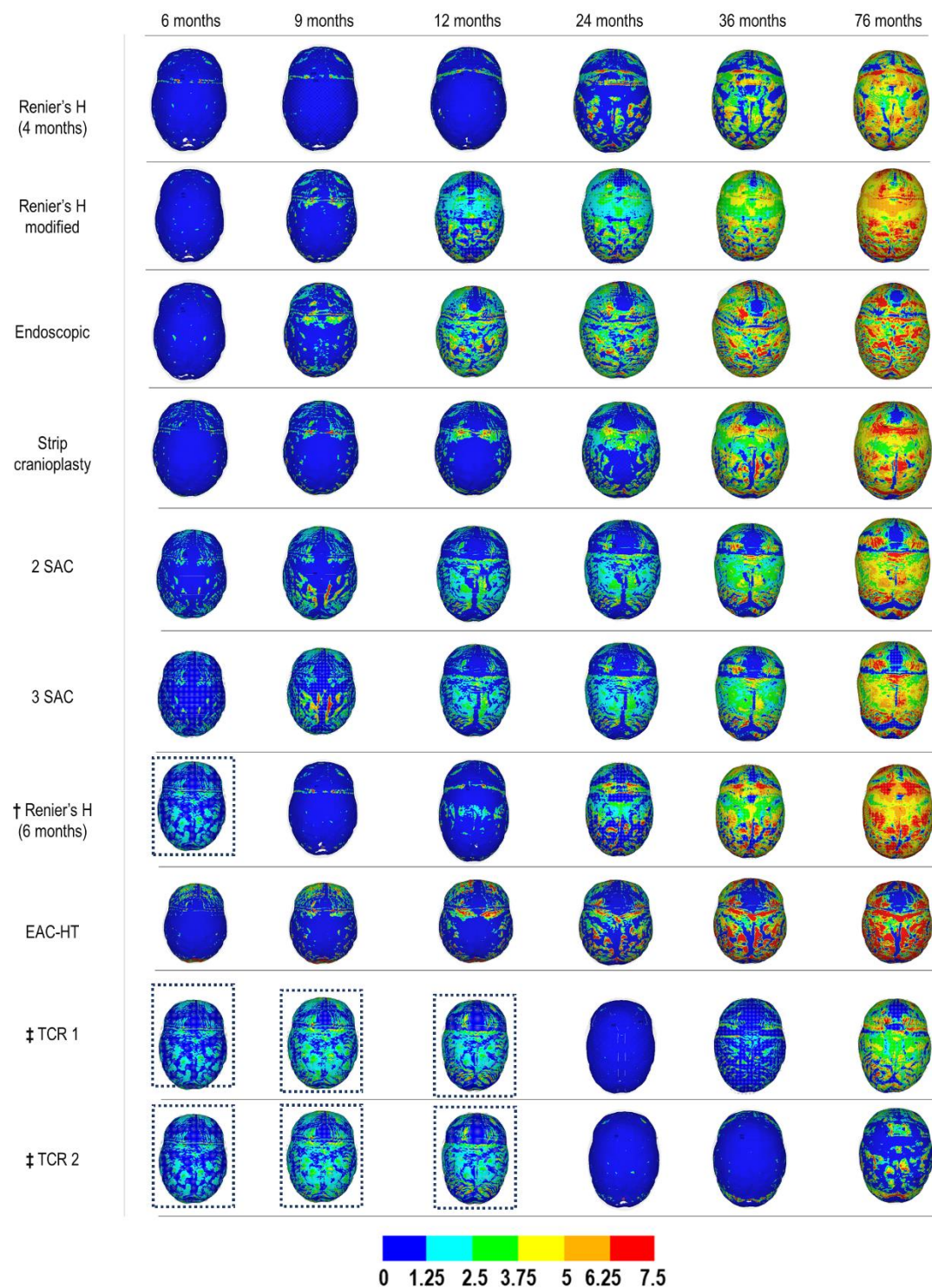


**Figure 6.17:** Predictive pattern of contact pressure across all replicated techniques – dorsal view. Note that blue dotted boxes indicate a lack of correction to reach the required age of intervention.

Both the Renier's modified and endoscopic procedures highlighted an increase in pressure from 12 months to 76 months of age, reaching a high magnitude across the anterior and occipital regions. Both SAC procedures achieved a similar display of overall pressure throughout the entire growth cycle. When comparing earlier and later intervention, the Renier's H (6 months) was seen to alleviate the pressure after intervention. This however rapidly increased from 24 months onwards, predicting large levels of bitemporal, anterior and occipital pressure when compared to earlier intervention (4 months). A similar trend was seen in both TCR approaches, where intervention (here at 12 months) was seen to alleviate the pressure build up (seen at 12 months). However, it was noted that a higher pressure was seen in the TCR 1 approach vs. TCR 2, most obvious across the anterior and bitemporal regions at 76 months.

Figure 6.18 quantify the findings of regional contact pressure levels across all analysed techniques at 76 months of age. Regarding the anterior lobes, the Renier's modified displayed the most elevated pressure levels (AL:  $5.0 \pm 1.7$  MPa – AR:  $4.2 \pm 2.7$  MPa). This was closely followed by the Renier's H technique when intervention was performed at 6 months of age (AL:  $4.8 \pm 2.1$  MPa – AR:  $3.9 \pm 2.6$  MPa). As seen in the qualitative outcomes, when performed at 4 months of intervention, the Renier's H procedure predicted a far lower pressure level in this region (AL:  $3.9 \pm 2.4$  MPa – AR:  $2.9 \pm 2.5$  MPa).

Both SAC and TCR 1 approaches highlighted a similar finding to that of Renier's H at 4 months across the left (2 SAC:  $3.2 \pm 2.4$  MPa – 3 SAC:  $3.1 \pm 2.4$  MPa – TCR 1:  $3.1 \pm 2.3$  MPa) and right regions (2 SAC:  $3.6 \pm 2.3$  MPa – 3 SAC:  $2.9 \pm 2.4$  MPa – TCR 1:  $2.2 \pm 2.2$  MPa). Both endoscopic across the left ( $4.7 \pm 3.6$  MPa) and right ( $3.6 \pm 3.1$  MPa) regions maintained a similar level when compared to the strip cranioplasty (AL:  $4.3 \pm 2.4$  MPa – AR:  $3.7 \pm 2.7$  MPa). The overall lowest reading was from the TCR 2 procedure across both the left ( $1.2 \pm 1.0$  MPa) and right region ( $1.3 \pm 1.2$  MPa) when compared with all options.

A similar or larger pressure difference was seen across the middle region for all techniques when compared to the anterior. The lowest was seen in the TCR 2 (ML:

## Chapter 6: Biomechanical comparison of ten techniques

1.3 ± 1.2 MPa – MR: 1.4 ± 1.2 MPa) and TCR 1 techniques (ML: 2.5 ± 2.1 MPa – MR: 3.0 ± 2.0 MPa). Both 2 SAC (ML: 3.6 ± 2.3 MPa – MR: 3.7 ± 2.2 MPa) and 3 SAC (ML: 3.8 ± 2.3 MPa – MR: 4.1 ± 2.3 MPa) displayed similar pressure readings. The same was also seen between the endoscopic (ML: 4.2 ± 2.9 MPa – MR: 4.6 ± 2.8 MPa) and strip cranioplasty predictions (ML: 4.5 ± 2.4 MPa – MR: 4.6 ± 2.4 MPa).

## Chapter 6: Biomechanical comparison of ten techniques

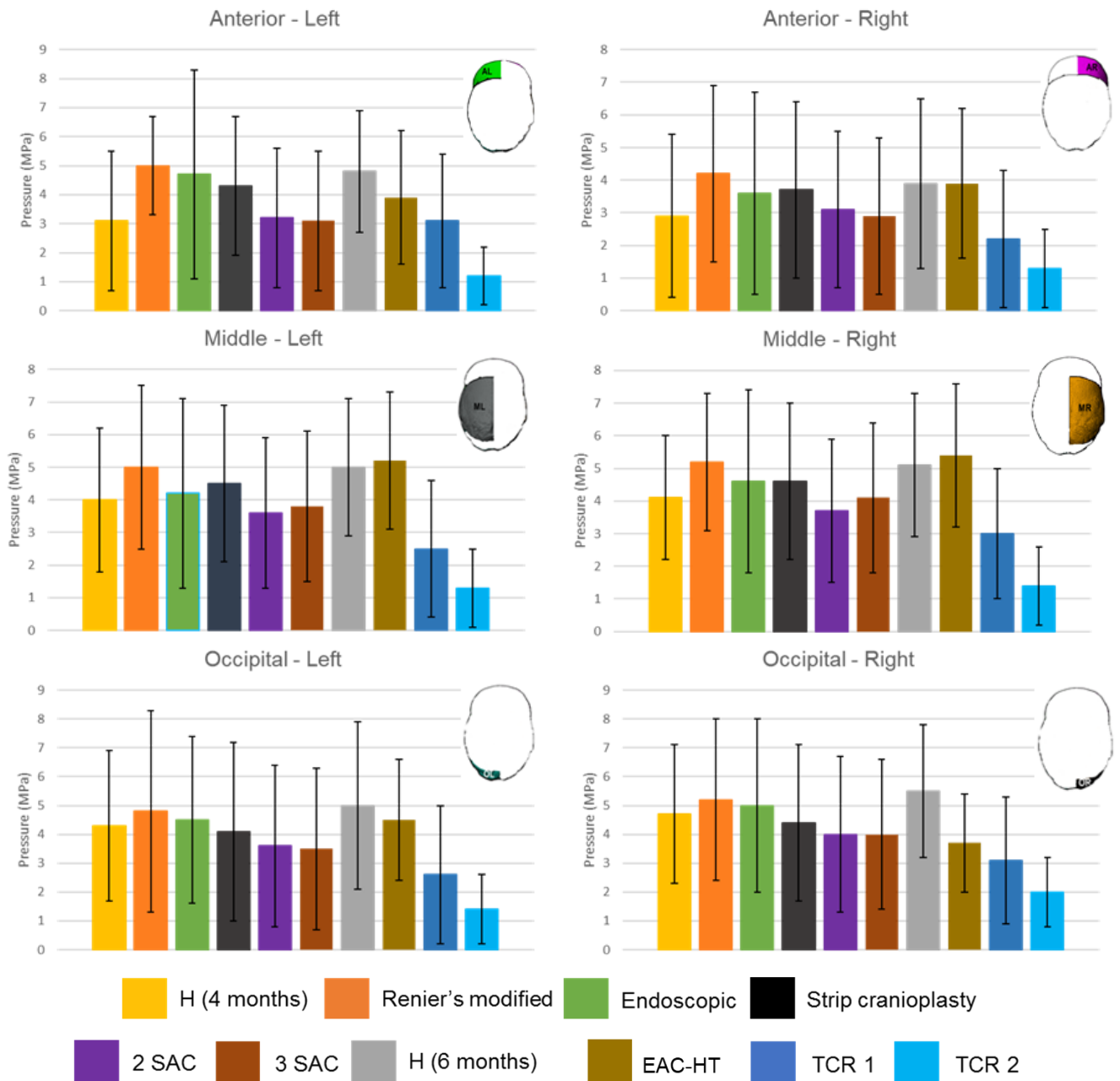


**Figure 6.18:** Numerical average of regional ICV contact pressure across all replicated techniques at 76 months of age.

## Chapter 6: Biomechanical comparison of ten techniques

Both Renier's H at 6 months intervention (ML:  $5.0 \pm 2.1$  MPa – MR:  $5.1 \pm 2.2$  MPa) and Renier's modified techniques (ML:  $5.0 \pm 2.5$  MPa – MR:  $5.2 \pm 2.1$  MPa) predicted some of the highest overall pressure levels. However, the highest was seen in the EAC with helmet therapy (ML:  $5.2 \pm 2.2$  MPa - MR:  $5.3 \pm 2.5$  MPa). Once again, the earlier intervention of the Renier's H (ML:  $4.0 \pm 2.2$  MPa – MR:  $4.1 \pm 1.9$  MPa) provided lower readings when compared to the later intervention counterpart.

Occipital lobe values closely matched with the readings seen across the middle regions for all techniques. Both the TCR 1 (OL:  $2.6 \pm 2.4$  MPa – OR:  $3.1 \pm 2.2$  MPa) and TCR 2 (OL:  $1.4 \pm 1.2$  MPa – OR:  $2.0 \pm 1.2$  MPa) predicted the lowest average value, while the largest were seen in both Renier's H at 6 months (OL:  $5.0 \pm 2.9$  MPa – OR:  $5.5 \pm 2.3$  MPa) and Renier's modified options (OL:  $4.8 \pm 3.5$  MPa – OR:  $5.2 \pm 2.8$  MPa). Both 2 SAC (OL:  $3.6 \pm 2.8$  MPa – OR:  $4.0 \pm 2.7$  MPa) and 3 SAC (OL:  $3.5 \pm 2.8$  MPa – OR:  $3.7 \pm 2.6$  MPa) produced similar values, whereas in contrast to the previous findings, the endoscopic (OL:  $4.5 \pm 2.9$  MPa – OR:  $5.0 \pm 3.0$  MPa) was seen to generate a higher pressure level than the strip cranioplasty technique (OL:  $4.1 \pm 3.1$  MPa – OR:  $4.4 \pm 2.7$  MPa). Comparing the later to the earlier intervention of the Reiner's H yielded a lower reading in the former approach (OL:  $4.3 \pm 2.6$  MPa – OR:  $4.7 \pm 2.4$  MPa) vs. the latter.

## Chapter 6: Biomechanical comparison of ten techniques

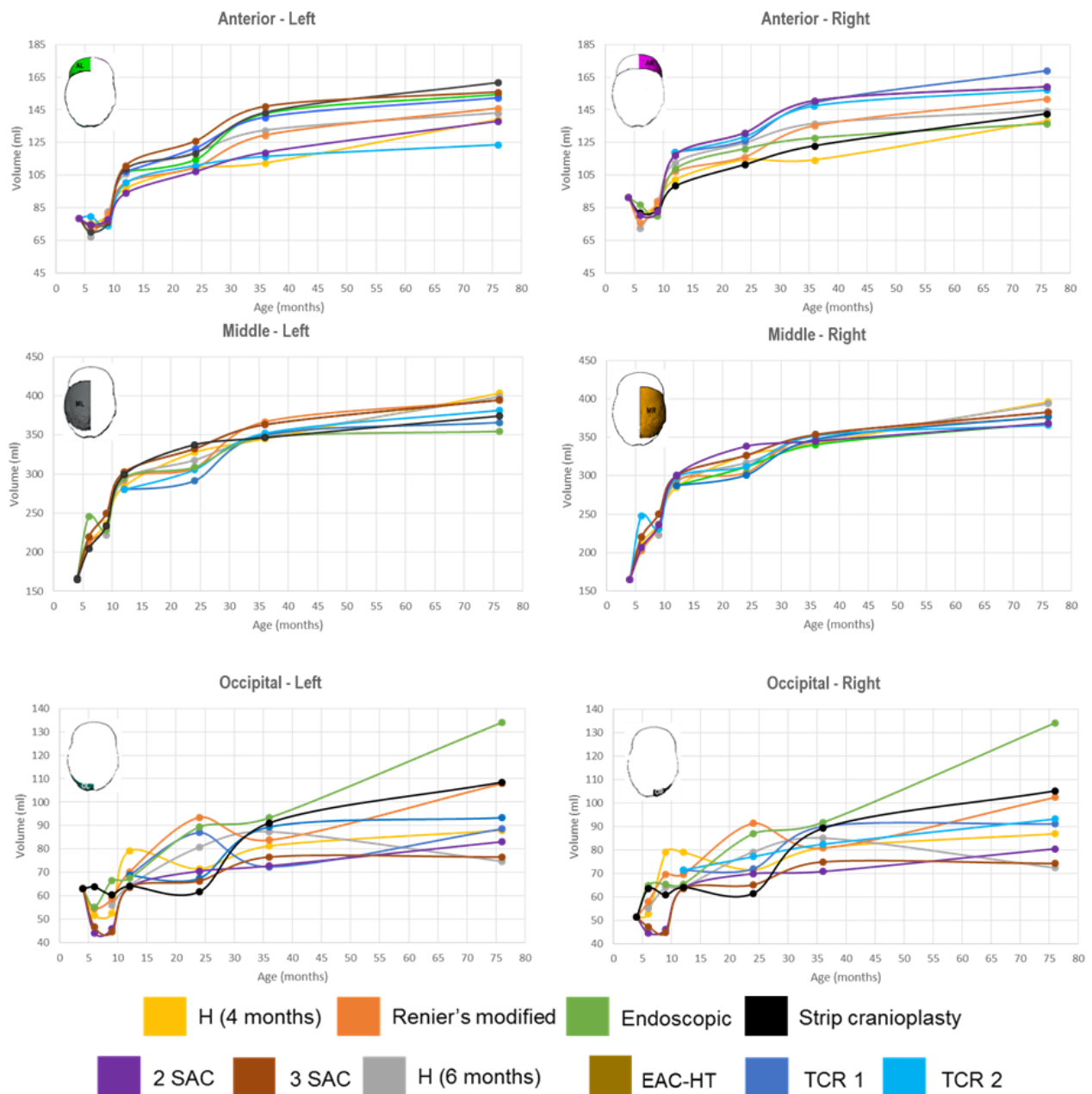


**Figure 6.19:** quantitative predictions of regions ICV distributions for all replicated techniques from their respective timings of intervention. to 76 months of age.

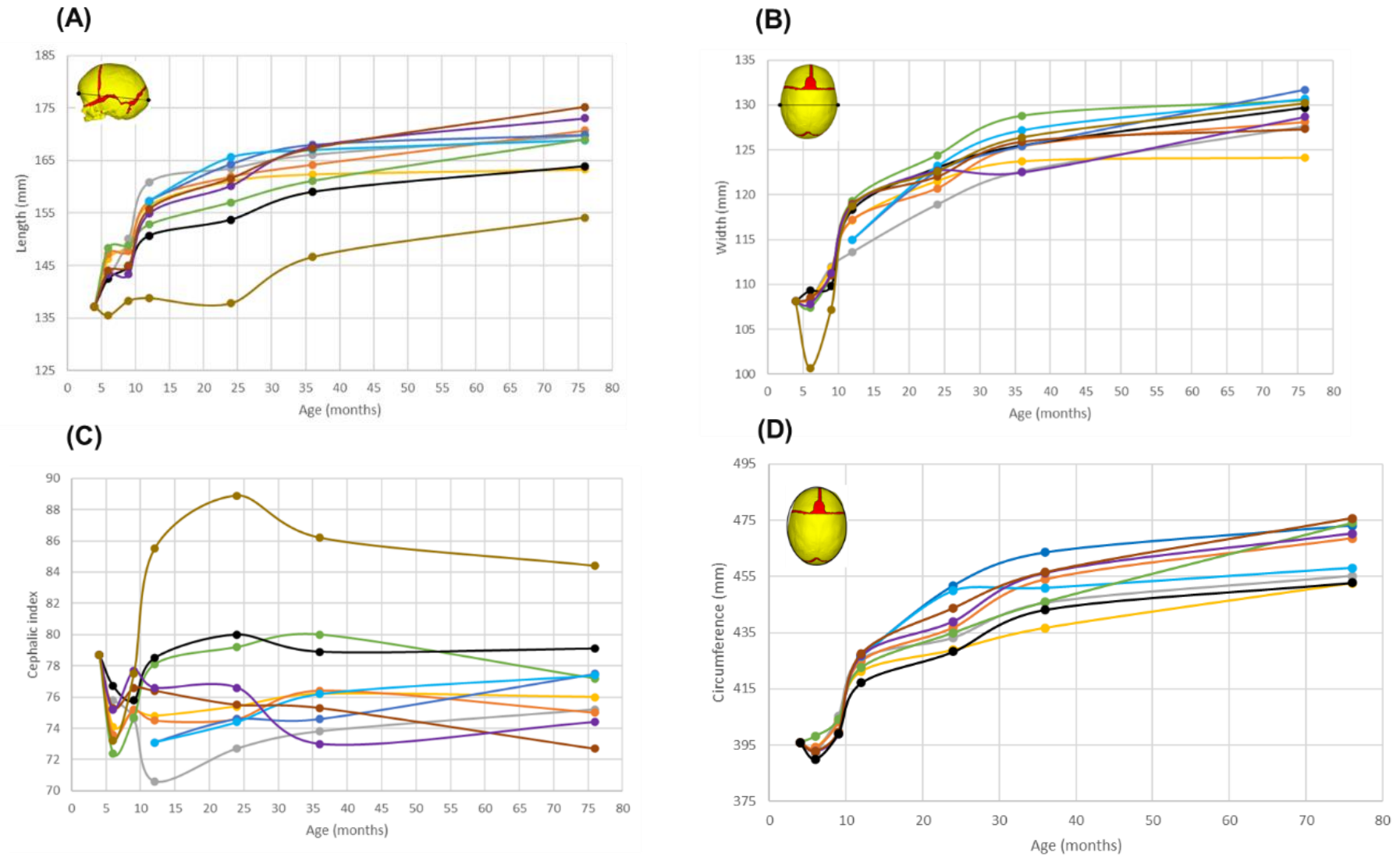


Figure 6.19 analyses the changes in volume distribution for the ICV for all techniques replicated here. A relapse in the anterior left and right regional volumes was captured for all techniques after growth was simulated post-intervention. However, all techniques showed various levels of increased volume by 76 months of age. The largest of which was seen in the 2 SAC approach for the left region (161.8 ml) while the TCR 1 techniques achieved the largest volume in the right (169.0 ml). The middle regions predicted the largest overall volume for all techniques investigated. The largest measurement was seen in the Renier's H performed at 4 months (ML: 403.3 ml – MR: 396.1 ml) while the endoscopic predicted the lowest volumes (ML: 354.6 ml – MR: 365.8 ml). Relapse was also seen across the occipital volumes across each approach, although these did not occur at the timings of intervention, as discussed above. The largest volume for both left and right occipital regions was seen in the endoscopic technique (OL: 134.0 ml – OR: 134.2 ml), seen to be three times larger than the lowest volume predictions across the Renier's H performed at 6 months (OL: 74.8 ml – OR: 72.4 ml).

Figure 6.20 analyses all cephalometric measurements for all approaches. All techniques experienced a larger growth in length vs. width by the time growth had reached 76 months of age. For example, the greatest anteroposterior measurement was seen in the 3 SAC approach (175.2 mm), while the lowest was captured in the Renier's H performed at 4 months (163.3 mm), closely followed by the strip cranioplasty option (163.9 mm).

Although the changes were lower than that of the length, all techniques displayed an accelerated and greater measurement of the width when compared with the 'non-operative' scenario (Figure 6.8-B). The greatest was achieved in the TCR 1 technique (131.7 mm), which matched close to the alternative TCR 2 approach (130.7 mm). Although the difference was less than 10 mm, the lowest reading was seen in the Renier's H performed at 4 months (124.1 mm).

## Chapter 6: Biomechanical comparison of ten techniques



**Figure 6.20:** Predictive cephalometric changes across all replicated approaches up to 76 months of age. Highlighting the changes in length (A), width (B), cephalic index (C) and circumference (D).

These changes in length and width subsequently affected the predictive relapse of the cephalic index. Predictive techniques performed at 12 months of intervention (here, TCR 1 and TCR 2) were seen to result in little to no relapse during the growth up to 76 months. However, all techniques performed at both 4 and 6 months intervention resulted in an initial relapse (from 4 to 6 months or 6 or 6 to 9 months) before producing a value higher or lower than that of the 4 month cephalic index (78.7). The lowest was seen in the 3 SAC approach (72.7) while the highest was captured in the strip cranioplasty (79.1). Although all techniques predicted a cephalic index between these margins, none were able to normalise the skull shape ( $> 80.0$ ).

The circumference was taken by using the width landmark points and measuring across the anteroposterior of the skull. All techniques presented an increase from the originally presented value at 4 months (396.0 mm). The 3 SAC predictions were seen to be the greatest (475.7 mm) while the lowest was captured in the Renier's H at 4 months of intervention (452.6 mm). This prediction closely matched the values seen in the strip cranioplasty (452.8 mm).

## 6.4 Discussion

In this chapter, a total of ten corrective techniques were replicated across the generic FE model used throughout this thesis, including the three techniques described in Chapters 3 and 4. All techniques underwent simulated growth in addition to the bone formation algorithm adopted from Chapter 5. Two sensitivity studies were conducted, that analysed the predictive growth under a 'non-operated' state and the potential impacts of bioabsorbable fixators on the total calvarial remodelling approach predictions. All techniques underwent growth from their respective ages of intervention to 76 months of age. The overall pattern of skull morphology, bone formation, contact pressure, and volume distribution were compared across all considered techniques.

**Absorbable fixators:** Clinically, the technique denoted as TCR 1 combines the use of absorbable fixators to assist with correcting the calvarial shape *in situ*. It was unknown when the fixators were no longer present (i.e., full absorption had been achieved) in this patient-specific case. Therefore, an average timeline of 3 months

postinsertion was chosen (Ashammakhi *et al.*, 2004). Interestingly, little change was seen in the cephalic index between the 'With fixators' vs. 'No fixators' by 76 months of age, where both had achieved a greater outcome when compared to the pre-operative age of 12 months (Table 6.2). It should be considered that immediate alterations in the calvarial shape seen after surgery, due to the alleviation of stress across the bone or the placement of fixators, were not considered in this study and may well have an impact on the biomechanics of skull growth but perhaps more in the short term than in the long term.

Differences were captured between the pattern of bone formation and contact pressure during simulated growth (Figure 6.5). Large patency across the vertex and anterior craniotomy was seen when fixators were absent. The introduction of these fixators was seen to aid with such defects across the model. This, in turn, appears to have led to elevated contact pressure in the latter model, showing a similar consistency between regional ICV levels and contact pressure levels when compared (Figure 6.8 and 6.9). When using computational models, a link between elevated strain levels across the bone have been seen when using such fixators (Li *et al.*, 2017). This strain may further lead to such contact pressures found in these predictions.

**Duration of helmet therapy:** Although the advancements in optimising the correction of sagittal craniosynostosis have stemmed from the use of postoperative helmeting devices (Delye *et al.*, 2016; Delye *et al.*, 2018), our fundamental understanding of the mechanics of this technique is still limited. Here, three variations of the duration of helmet therapy (altered from the clinical average of 8 months) were simulated. Based on the simplistic approach to mimicking the constraints of the helmet shown here, there is a clear distinction between the use and non-use of the helmet, regardless of its duration (Figure 6.10). Most notable is the impact on the skull length, although the morphological outcomes were overestimated when compared to the literature (Sholnick *et al.*, 2021; Delye *et al.*, 2018). An understandable outcome given the greater changes in the length vs. the width (Figure 6.11). The level of contact pressure was seen to have increased by the respective timings of helmet removal, across the frontal and temporal regions of the ICV (Figure 6.12), again, such predictions were associated with the method of replicating the helmet here. In response to this, the

dorsal regions represent minimal pressure readings. As the calvarial healing has yet to be completed and allows for minimally restricted dorsal growth.

**'non-operation' scenario:** To achieve the later intervention age of greater than 4 months for applicable techniques, the generic model underwent an untreated state of growth from this time up to 12 months of age. The computer simulation results predicted an anterior-posterior growth of the skull in line with clinical findings in unoperated children with sagittal synostosis (Cunningham & Heike, 2007). In the instance of scaphocephaly, restricted growth is seen across the vertex and bitemporal, while compensatory is seen across the anteroposterior. The predictive length vs. width was consistent with such behaviour, with a large reduction in the cephalic index seen by 12 months when compared with the initial value. While it was interesting to capture such quantitative outcomes, there appeared to be no correlation between the volume distributions of the ICV and the cephalometric outcomes, as the largest increase in volume was seen across the middle regions (Figure 6.5 and 6.6).

However, there appears to be a link between a reduction in the volume with the possibility of increased contact pressure (Figure 6.7). Mechanically, the ICV here maintained the path of least resistance to grow into. For this unoperated state, both the coronal and lambdoid suture (while maintaining large patency by 12 months) provided this path during the simulated growth. This led to elevated level of contact pressure across the anteroposterior regions of the ICV. This could advise surgeons, that while more invasive techniques performed at a later age could yield improved cephalic outcomes (Thomas *et al.*, 2015; Al-shaqsi *et al.*, 2021), this delay could postpone relieving such pressure on the brain.

**Comparison against CT data:** As a direct patient-specific method was unobtainable, a framework of 'technique-specific' and 'age-specific' validation was performed (Table 6.2 and Figure 6.10). While the number of acquired CTs was limited for validation, a suitable age match was achieved between the CT and the predictive data sets. Differences in the overall measurements recorded (length and width) may be due to the differences in the ICV between predictive and CT data, as a similar observation was captured in the SAC techniques in Chapter 4 (See section: 4.4). Despite this,

realistic cephalic index values were seen, with a difference of only two in certain techniques. Although such validation was not the main premise of this chapter, the work continues to provide a level of confidence in the modelling approaches adopted here.

**Surgical comparison:** Considered here were a total of ten replicated techniques for sagittal craniosynostosis treatment utilised by various craniofacial institutions (Figure 6.3). The results attempted to predict the patterns of bone formation, level of contact pressure on the ICV, regional volume distribution, and cephalometric changes during simulating growth (Figure 6.14 – 6.20).

There was an impact on the morphological shape and timing of suture and craniotomy fusion when considering various technique options and the level of invasiveness of such techniques. Notably, less invasive techniques with smaller craniotomy dimensions (i.e. 2 SAC and 3 SAC) were seen to fuse rapidly. In turn, wider displacements of the sutures were seen. The opposite characteristic was captured in wider and more complex geometric craniotomies (i.e., strip cranioplasty and Renier's H). This is an understandable outcome, as the 'un-operated' scenario suggested a large displacement and patency across the sutures by 12 months of age (Figure 6.2). Such findings are consistent with observations in the literature when measuring the impacts of healing rates between techniques (Thienier-Villa *et al.*, 2018). Further, there is a clear delay in the fusion of the craniotomy in techniques performed at 12 months of age (i.e., TCR 1 and 2). Clinically, the changes in biological factors with age contribute to the deficiency in calvarial healing (Alleyne *et al.*, 2016). Although such factors are not present here, the characteristics in later fusion with delayed intervention remain in the predictive outcomes.

Here, restrictions of the predictive calvarial growth continue to be monitored using contact pressure qualification (Figure 6.16 and 6.17) and regional quantification (Figure 6.18). These observations aim to assist with the disputes in literature over the most optimum outcomes between techniques when considering neurophysiological attainment (Hashim *et al.*, 2014; Care *et al.*, 2019). There is a clear distinction between techniques performed earlier (Renier's H at 4 months) and later (Renier's H at 6

months) when considering the predictive pressure levels. This level of pressure when compared with postoperative defects agrees with the study from Bellew *et al.*, (2019), who reports on a variation of this technique, while more invasive techniques were performed by 12 months (TCR 1 and 2) maintained the lowest pressure readings. Such findings are consistent with the advocacy of more invasive techniques to lower postoperative defects (Hashim *et al.*, 2014). This is however, if such pressure readings correlate to functional attainment, which may not be the case. It is clear that the levels of pressure predicted here are highly exaggerated (i.e., extremely large levels of pressure) when compared to real-world scenarios. Nonetheless, the method here could prove to be a possible method to measure such defects after the intervention.

The volume distribution was further considered across all replicated techniques (Figure 6.19). As seen in the previous sensitivity study, there is a correlation between the pressure levels and volume levels seen across the predictive data. Such a method is a new consideration for maintaining postoperative observation after sagittal craniosynostosis correction and was adopted here (Liaw *et al.*, 2019). Although the literature evaluates head volumes, this was modified to measure the ICV distribution. The method aims to correlate the changes in pressure with the volume changes, a characteristic which was achieved. Such predictions could aid surgeons in relieving the need for postoperative invasive ICP monitoring (Thomas *et al.*, 2015).

The standard approach to measuring the cephalic shape was also undertaken here (Figure 6.20). While also producing the lowest pressure values, both TCR techniques predicted the lowest level of relapse in the cephalic index. Further, the techniques also estimated a higher cephalic index vs. the pre-operative values. While all other alternative techniques maintain a lower cephalic index, there does not appear to be a large statistical difference between such values, maintaining a clear connection with literature data (Le *et al.*, 2014; Gerety *et al.*, 2015). However, the difference between the number of springs used was not drastic across the predictive data, contradicting the findings of Fischer *et al.*, (2021). It should be considered that various biomechanical factors during spring insertion and their interactions with the growth may be missing from this work (See Chapter 4).

## **6.5 Summary**

This chapter adopted all developed methodologies throughout this thesis and replicated a total of ten different treatment options for sagittal craniosynostosis correction. This was the first attempt, within the literature, to compare the biomechanics of different treatment options for this condition and to predict a cohort of different surgical techniques outcomes years after surgery in a generic model. The findings here suggest that the TCR could provide the most positive impact on the overall long term predicted outcomes. The next chapter will highlight the key findings throughout this thesis and the limitations observed throughout.



## **Chapter 7: Discussion**

## 7.1 Introduction

Calvarial development during the early stages of life is influenced by a series of biological, chemical and mechanical signals, functioning in unison across both hard and soft tissues, most notably, the cranial bones, growing brain, cranial sutures, and the dura mater (Morriss-Kay & Wilkie, 2005; Hegazy, A. & Hegazy, M., 2018; Falland-Cheung *et al.*, 2018). The premature fusion of the cranial sutures, known medically as craniosynostosis. This condition has an occurrence rate of 1 in every 2,000 live births (Kimonis *et al.*, 2007) with its prevalence having increased by 2-3 times in recent years for unknown reasons (Cornelissen *et al.*, 2016; Tonne *et al.*, 2020). The most affected suture is the sagittal (known as sagittal craniosynostosis), with an appearance rate of 3 in every 10,000 live births. Although the exact cause of sagittal craniosynostosis is still uncertain, its prevalence has increased in line with all other forms of this condition (Johnson & Wilkie, 2011).

As a repercussion of the calvarial deformation, normal functional characteristics, along with the delicate homeostatic nature of the ICP, are at risk of being disrupted if the condition is left untreated. Craniofacial surgeons have developed a series of surgical techniques to alleviate the symptoms seen in sagittal craniosynostosis, with each centre adopting their respective approaches to optimise the postoperative outcomes (Guimarães-Ferreira *et al.*, 2001; Rocco *et al.*, 2012; Thomas *et al.*, 2015; Micovic *et al.*, 2016; Delye *et al.*, 2018). As the number of techniques and their complexities progress, discussions of the most optimal approach and timing of intervention have remained an area of ongoing debate and comparison in the literature (Panchal *et al.*, 1999; Thomas *et al.*, 2015; Gerety *et al.*, 2015; Skolnick *et al.*, 2021).

This project aimed to first develop a generic pre-operative 3D model using a single patient CT data set at 4 months of age suffering from sagittal craniosynostosis. The finite element method was then used to simulate the calvarial growth, replicate the pattern of bone formation and calvarial healing, and estimate the level of contact pressure across the intracranial volume. Here, morphological predictions were validated against the same patient's CT data at 76 months of age, confirming the parameters of our approach (Chapter 3). Building on this, three additional replicated

surgical techniques were replicated (Chapter 4). The techniques considered in Chapter 4 were two minimally invasive techniques with small and large craniotomies. The results of this chapter effectively highlighted that our modelling approach to consider the effect of bone formation at the sutures and craniotomies requires further investigations. This then formed the foundation for Chapter 5 where a new approach taking into account the level of mechanical strain induced due to the ICV growth at the sutures and craniotomies was developed. Once this approach was established the patient-specific model developed in Chapter 3 was used and functioned as a generic model to compare calvarial growth following ten different treatment options (Chapter 6). Observations and quantifications of the predicted morphological shape, cephalometric measurements, bone formation and the level of ICV contact pressure were all undertaken where possible throughout the project. In this chapter, an overview of the key findings are highlighted and discussed.

## **7.2 Morphological validation and sensitivity of the finite element model**

In Chapter 3, a patient-specific model was developed and used to assess the sensitivity and validity of the calvarial growth approach used in this thesis. Pre-operative CT data were used to predict the calvarial growth and results were compared vs. the follow up CT data at the age of 76 months. The estimated morphological shape and contact pressure predictions at the same age showed that the model was sensitive to the choice of material properties of the craniotomy and the method of bone formation, respectively.

Although other parameters considered here had little impact on the sensitivities, the majority did nonetheless accurately predict the calvarial shape by follow up. A close match was found to the measured *in vivo* skull length, and height based on the follow up CT data. Achieving the overall width seen in the CT data may be limited by the lack of spontaneous bilateral bone displacement upon relieving the fused suture, in addition to other surgical parameters (i.e., bone manipulation) that were not considered here (Rocco *et al.*, 2012). As little change was seen morphologically across the additional

material property scenarios, it remained a factor that the properties of the craniotomy were of importance, as seen in section 3.3.

Assessments into the impact of modelling the subarachnoid space, consisting of a modelled variation of the cerebrospinal fluid (CSF), was also performed to monitor its impacts on the predicted calvarial growth. The CSF flow around the brain and provides nutrients for the brain and perhaps functions as a shock absorber during head impact injuries (Couper & Albermani, 2009). The major limitation of the way that CSF was modelled in Chapter 3 was that it was modelled with solid elements as opposed to modelling the fluid-solid interaction at the brain-bone interface (which was beyond the scope of this project). Although the impacts of modelling the CSF proved to be limiting, it provided a greater level of understanding of certain factors affecting the interactions between the growing brain and the calvarial shape.

### **7.3 Predicting the pattern of contact pressure**

Although several recent computational studies have explored the biomechanics of craniosynostosis (See Chapter 2 – Table 2.9), such studies have several major shortcomings. For example, they have not modelled the growth of the brain, nor established the contact behaviours between the hard/soft tissues during the brain growth, both of which were considering in this thesis. (You *et al.*, 2010; Wolański *et al.*, 2013; Li *et al.*, 2017; Borghi *et al.*, 2018; Bozkurt *et al.*, 2020). Here a penalty-based approach was used to assess the level of contact pressure across the modelled ICV and all connective tissues.

One major limitation of the predicted contact pressures in this study, is its validation. It is known that the level of pressure within the calvarial is maintained across the subarachnoid space (Couper & Albermani, 2009), separating the surface of the brain from the dura of the skull (Ellis & Mahadevan, 2014). An elevation of this pressure is known to cause substantial functional defects if left untreated. The most notable cause for this elevation is attributed to severe cases of craniosynostosis (Thompson *et al.*, 1995; Thomas *et al.*, 2015).

Such findings here could, in theory, resemble the elevation of ICP pre and postoperative after sagittal craniosynostosis correction and in turn, compared functional characteristics between techniques (Gewalli *et al.*, 2001; Hashim *et al.*, 2014; Care *et al.*, 2019). Although such a statement cannot be directly supported with evidence, it is nonetheless, the first a step toward understanding the potential impact of different treatment options on the growing brain. Nonetheless, if validated, it could provide critical insights into the biomechanics of craniosynostosis.

### 7.4 Material properties of biological tissues

The mechanical structures of the biological tissues across the human calvaria are highly anisotropic, resulting in many different readings across the specimens that have been assessed in the literature. The aim of this research was to predict the calvarial growth appreciating that mechanical properties of various constraints of the model changes during the growth (that was considering using adaptive remodelling). Nonetheless, on one side there were uncertainties as per exact values used in this study, on the other side it appeared that isotropic linear elastic material properties that were adapted/alterd age by age led to a reasonable prediction of the overall calvarial morphology.

It was beyond the scope of this thesis to investigate the effect of different material models on the outcomes of the predictions, nonetheless various sensitivity tests were performed throughout the thesis to the choice of elastic modules. For example, two extreme values for the elastic modulus of the modelled calvarial bones were investigated, ranging between the values of 3000 MPa and 421 MPa (McPherson & Kriewall, 1980; Coats & Margulies, 2006). Such values are seen to represent the stiffness of bone at approximately 4 months of age. It is noteworthy that, Margulies & Thibault (2000) captured an elastic modulus of 2111 MPa at the age of 6 months. In addition to this, Wang *et al.*, (2014) measured an elastic modulus of 1103 MPa in 1.5-year-old specimen samples. Defining an absolute value for the calvarial bones, based on these studies, is challenging. However, this study at the very least highlights the importance and impacts of two extreme values, a finding which proved invaluable to understanding the mechanics of the model.

In addition to the calvarial bone, the properties of the brain (Here, the ICV) were also varied. My studies here, similar to that of the calvarial bone, compared two extreme values, ranging between 100 MPa (Libby *et al.*, 2017) and 0.003 MPa (Gefen *et al.*, 2003). A limitation with these values is the method by which they were obtained. Neither study reflects the properties of human brain tissue specimens (*Ex vivo* modelling study for the former value and rat specimens were used for the latter value). In addition, further literature studies continue to rebut such values used here (Budday *et al.*, 2015). Despite this, it is informative to understand the impacts on the predictive growth using the highlighted values. It could be argued that the modelling approach that was used here uses the ICV as a surrogate to drive and model the growth of the skull hence the exact properties of the ICV were perhaps of limited interest and importance on the key outcomes that were focus of this study.

### 7.5 Replicating the calvarial growth

Replicating skull growth was accomplished here using a radial thermal analogy across the ICV under six load steps. Here, the level of growth was linear between each load step and the estimated age of the model was assessed and compared to literature data (Sgouros *et al.*, 1999). Naturally, the level of human brain growth fluctuates between individuals. It is further known that, when considering the complex structure of the brain, various layers and regions of the brain can alternate in accelerated growth (Matsuzawa *et al.*, 2001). This anisotropic growth of the brain was not considered in this study and can be considered in future studies. Nonetheless, the adopted approach here can lead to a good estimation of the calvarial growth up to about 76 months of age.

### 7.6 Modelling of the bone formation

Several variations of the algorithm for predicting bone formation were assessed in this project. Initially, a radial element selective approach from the bone borders across the sutures and craniotomy was developed. Although the timing of the suture closure (in particular, the metopic and anterior fontanelles) on a qualitative level matched that of the CT follow up data, this approach lacked the computational (i.e., unguided)

independence desired for the model. Naturally, maintaining and considering the complexities of the intramembranous ossification processes and the behaviours of the mesenchymal cells seen clinically (Opperman, 2000; Beederman *et al.*, 2014) is still beyond computational capabilities. Nevertheless, novel attempts have been undertaken (Khonsari *et al.*, 2013; Lee *et al.*, 2015; Marghoub *et al.*, 2019).

This led to the consideration of a second alternative method, in which the increasing or decreasing levels of hydrostatic strain would regulate the pattern of bone formation across the model during the growth. This allows a greater computational predictability in calvarial healing and suture bone formation across the various surgical techniques (Chapter 5). Such an approach was seen to have an impact on the overall morphological shape and cephalic measurement vs. the former approach. Although constraints (i.e., applying a *radial boundary* for the suture formation) were still required along with the lack of validity in the strain values used, I believe the method shown here could prove an invaluable tool for detecting a range of postoperative comparisons, as surgeons and clinicians monitor the possibility of calvarial defects and a lack of ossification after surgery (Thenier-Villa *et al.*, 2018; Skolnick *et al.*, 2019).

## 7.7 Comparison of surgical techniques

The overall goal of this project was to develop a framework for comparing and predicting the surgical outcomes of various techniques for the treatment of sagittal craniosynostosis. Previous computational studies focused on the biomechanics of a single treatment option for this condition (You *et al.*, 2010; Li *et al.*, 2017; Borghi *et al.*, 2018; Malde *et al.*, 2020). Here, I wished to expand my proposed computational framework for comparing multiple techniques that was the focus of Chapter 6 of this thesis.

The validity of predictions of calvarial growth for different techniques summarised in Chapter 6 was performed by cross referencing the cephalic measurements (Table 6.2) using the technique-specific CT data obtained from the clinical collaborators involved in this project. Although the estimated length was overpredicted in many techniques, an overall good match was obtained in the width estimations. It should be noted

however that some clinical features were absent in the replicated approaches in Chapter 6. For example, Renier's 'H' technique often adopts the process of bone flaring, which can have drastic implications on the follow up skull shape (Rocco *et al.*, 2012). A similar characteristic is also present in the spring-assisted methods, where spontaneous skull widening is seen at the time of extracting the fused suture, due to the built-up tensile stress across the parietal (Lauritzen *et al.*, 1998). As the modelling approach here did not consider these mechanical functional *in situ* features, this may explain the underprediction of the cephalic measurements in Chapter 6. At the same time, it must be acknowledged the modelling approach proposed here does not consider the effect of muscle forces that perhaps play a role from about 2 years of age in deforming the craniofacial system as children start to bite harder and harder objects (Kiliaridis, 1995).

In addition to the chosen surgical techniques, a comparison of the age at which interventions were conducted was assessed. A comparison of the Renier's 'H' technique performed at 4 and 6 months of age had an alternating impact on the calvarial shape, measurements, and the overall level of contact pressure predictions. Although an improved shape was seen in the 6 months of intervention, by 76 months, a higher level of contact pressure was also estimated. When compared with relevant literature data, infants undergoing less invasive surgical approaches at a younger age, demonstrated improved functional characteristic (Hashim *et al.*, 2014). If the higher levels of pressure seen in the models' predictions could be correlated to worst functional outcomes, then these predictions agree with the findings in the literature.

However, the same was not seen in the total calvarial remodelling predictions (performed at 12 months of age), which estimated the lowest overall level of pressure by 76 months. One justification for these differences could lie in the delayed bone formation seen in both TCR techniques from 12 to 76 months of age. With little constraint caused to the overall growth, a lower pressure may have been predicted. This lack of formation, however, is characteristic of clinical observations. In which the regenerative capabilities of the bone begin to lessen during maturity (Alleyne *et al.*, 2016). Given the predictions captured throughout this thesis, suggests that not only do the TCR techniques provide a good long-term morphology, but further predict low



levels of pressure across the ICS. As such, it is the opinion of this thesis author that such a technique proves to be the most beneficial to long term patient improvements.

By assessing a combination of different surgical approaches, it is hoped that critical biomechanical questions could be answered here. What is clear in the literature is that various techniques could impact the functional characteristics of patient's years after surgery (Gewalli *et al.*, 2001; Hashim *et al.*, 2014; Care *et al.*, 2019; Bellew *et al.*, 2019). Although the contact pressure predictions shown here cannot be directly related to functional outcomes, this study clearly highlights that different techniques constrain the growth of the brain to a different extent, leading to a different level of mechanical pressure on the growing intracranial volume. The main question that remains to be answered and to be further investigated is where brain can tolerate and adjust itself in response to these levels of pressures or even such small differences in the contact pressures found in this study can have functional impacts whether it being in terms of increased in intracranial pressure or neurodevelopmental impacts. It should be unequivocally noted that, due to the lack of validation in these outcomes, such results should be assessed with caution.

## **Chapter 8: Conclusions and future work**

## 8.1 Conclusions

Our understanding of the biomechanical behaviour of craniosynostosis and the overall impacts various surgical techniques for treating sagittal craniosynostosis can have on the growing brain and skull morphology is still limited. By utilising a computational approach, surgeons have the potential to better understand both the positive and negative impacts various surgical techniques could have on long term postoperative outcomes.

The main aim of this thesis was to firstly develop and validate a generic pre-operative finite element model capable of undergoing a total of ten replicated surgical techniques for the correction of sagittal craniosynostosis. Morphological validation, improvements to the overall method of bone formation, and comparing the key cephalic measurements and contact pressure predictions across the modelling ICV were all subsequently investigated in the different chapters of this thesis. The main conclusions of this study are as follows:

- Under the current method of a linear thermal analogy across the modelled ICV, the FE model was capable of accurately predicting the follow up morphology, as demonstrated in Chapter 3 and 4. Although, if possible, the anisotropic behaviour of the brain growth may need to be considered for future studies.
- Access to a greater cohort of postoperative CT data to compare these predictive outcomes could strengthen the overall work across this thesis.
- The material properties of the craniotomy had the most significant effect on the overall calvarial morphology predictions. However, further *ex vivo* research on the change in material properties, regarding the formation of the bone across the sutures, is required to further improve the modelling approach shown here.
- The method of bone formation demonstrated here may reflect the characteristics seen *in vivo*. However, only the mechanobiological effects while abstaining from the possible biological impacts were considered here.

- The work here demonstrated the impacts various techniques could have on the ICP contact pressure interface during growth. Although this could not be validated on a qualitative or quantitative level, such predictions hope to inform surgeons about the potential postoperative ICP or neurocognitive impacts.
- With regards to the aim of this thesis, the modelling approach here has demonstrated the strength of this finite element method in replicating multiple corrective techniques for sagittal craniosynostosis. The model is sensitive to the particular technique replicated across the calvarial bones, which hopes to inform surgeons on which technique may provide the most optimal outcome.
- Clinically, the findings of this study show that an earlier intervention (before 6 month of age) releases the pressure on the growing brain earlier, which can potentially lead to a higher level of pressure on the brain at a later age. Based on the predictions shown, later interventions naturally release the pressure on the brain and lead to a lower level of pressure on the brain later in life (Figure 6.16 and 6.17). Whether this has any functional impact on the brain or not requires further investigation.

### 8.2 Future work

The modelling approach demonstrated across this thesis can be both improved upon and used for additional forms of craniofacial growth and defects. This section will detail both of these areas of interest.

The limitations of the model are described throughout the respective chapters of this thesis. The first of two key areas is the absence of growth across the facial region. The lack of facial growth throughout all simulations could have had an impact on the predictive outcomes across all techniques, particularly when validated with respective CT data sets using a cross-sectional or 3D distance map approach. This has led to the recruitment of an additional PhD student (Mr Ce Liang) in investigating this approach by adopting the methodologies discussed throughout this thesis to a self-

developed normocephalic infant skull model. The addition of this parameter in the modelling approach could see even more accurate predictive data generated.

The second area is relative to the method of helmet therapy. As such, only simple nodal constraints are used to represent the restrictions across the anteroposterior growth and semi-restrictive growth across the dorsal region of the model (explained in Appendix III). Given more time devoted to replicating the helmet's effects, a complete *in silico* 3D rendered model, designed specifically for the generic model shown here, may more accurately represent this corrective process. Further, the use of an *in vitro* 3D printing calvarial model could assist with the further validation of these predicted outcomes, as the nature of obtaining CT data relative to this technique has proved challenging. At the time of this thesis, there are ongoing discussions and funding attempts devoted to an additional PhD project in exploring this area of interest. This, in conjunction with the aforementioned facial growth consideration, could prove to be a vitally important step in enhancing the methodologies shown in this thesis.

In conclusion, the current modelling approach here provides a suitable foundation for predicting the outcomes of sagittal craniosynostosis correction. While there are improvements to be made, it is hoped that, while relevant areas of improvement are being addressed, the findings shown here can aid in optimising the outcomes of this condition and enhance the mechanical understanding of the effects of corrective surgery.

## References:

Adeyemo, A.A. & Omotade, O.O. (1999), "Variation in fontanelle size with gestation age". *Early Human Development*. Vol. 54, No. 3, pp. 207-214.

Adolph, K. & Eppler, M. (1998), "Development of visually guided locomotion". *Ecological Psychology*. Vol. 10, No. 3-4, pp. 303–321.

Ahmad, N. Lyles, J. Panchal, J. Deschamps-Braly, J. (2008), "Outcomes and complications based on experience with resorbable plates in pediatric craniosynostosis patients". *The Journal of Craniofacial Surgery*. Vol. 19, No. 3, pp. 855-860.

Ajami, S. Rodriguez-Florez, N. Ong, J. Jeelani, N.U.O. Dunaway, D. James, G. Angullia, F. Budden, C. Bozkurt, S. Ibrahim, A. Ferretti, P. Schievano, S. Borghi, A. (2022), "Mechanical and morphological properties of parietal bone in patients with sagittal craniosynostosis". *Journal of the Mechanical Behaviour of Biomedical Materials*. Vol. 125, pp. 104929.

Alamer, O.B. Jimenez, A.E. Azad, T.D. (2021), "Single-suture craniosynostosis and the epigenome: current evidence and a review of epigenetic principles". *Neurosurgical Focus*. Vol. 50, No. 4, pp. E10.

Alleyne, B. Varghai, D. Askeroglu, U. Zwiebel, S. Tobin, K. Gosain, A.K. (2016), "The impact of age upon healing: absolute quantification of osteogenic genes in calvarial critical-sized defects". *Journal of Craniofacial Surgery*. Vol. 27, No. 1, pp. 258-263.

Al-Shaqsi, S.Z. Lam, N.W. Forrest, C.R. Phillips, J.H. (2021), "Endoscopic versus open total vault reconstruction of sagittal craniosynostosis". *Journal of Craniofacial Surgery*. Vol. 32, No. 3, pp. 915-919.

Alvarez, J.A. & Emory, E. (2006), "Executive function and the frontal lobes: a meta-analytic review". *Neuropsychology Review*. Vol. 16, No. 1, pp. 17–42.

Anatole, S. & Dekaban, M. (1977), "Tables of cranial and orbital measurements, cranial volume, and derived indexes in males and females from 7 days to 20 years of age". *Annals of Neurology*. Vol. 2, No.6, pp. 485-491.

Ashammakhi, N. Renier, D. Arnaud, E. Marchac, D. Ninkovic, M. Donaway, D. Jones, B. Serlo, W. Laurikainen, K. Törmälä, P. Waris, T (2004), "Successful use of biosorb osteofixation devices in 165 cranial and maxillofacial cases: a multicenter report". *The Journal of Craniofacial Surgery*. Vol. 15, No. 4, pp. 692-701.

Barbeito-Andrés, J. Bonfili, N. Nogué, J.M. Bernal, V. Gonzalez, P.N. (2020), "Modeling the effect of brain growth on cranial bones using finite-element analysis and geometric morphometrics". *Surgical and Radiological Anatomy: SRA*. Vol. 42, No. 7, pp. 741-748.

Bastir, M. & Rosas, A. (2013), "Cranial airways and the integration between the inner and outer facial skeleton in humans". *American Journal of Physical Anthropology*. Vol. 152, No. 2, pp. 287-293.

Becker, D.B. Peterson, J.D. Kane, A.A. Cradock, M.M. Pilgram, T. K. Marsh, J.L. (2005), "Speech, cognitive, and behavioural outcomes in nonsyndromic craniosynostosis". *Plastic and Reconstructive Surgery*. Vol. 116, No. 2, pp. 400-407.

Beederman, M. Farina, E.M. Reid, R.R. (2014), "Molecular basis of cranial suture biology and disease: Osteoblastic and osteoclastic perspectives". *Genes and Diseases*. Vol. 1, No. 1, pp. 120–125.

Bellew, M. & Chumas, P. (2015), "Long term developmental follow up children with nonsyndromic craniosynostosis". *Journal of Neurosurgical Paediatrics*. Vol. 16, No. 4, pp. 445-451.

Bellew, M. Chumas, P. Mueller, R. Liddington, M. Russell, J. (2005), "Pre- and postoperative developmental attainment in sagittal synostosis". *Archives of Disease in Childhood*. Vol. 90, No. 4, pp. 346-350.

Bellew, M. Liddington, M. Chumas, P. Russell, J. (2011), "Preoperative and postoperative developmental attainment in patients with sagittal synostosis: 5-year follow up". *Journal of Neurosurgical Pediatrics*. Vol. 7, No. 2, pp. 121-126.

Bellew, M. Mandela, R.J. Chumas, P.D. (2019), "Impact of age at surgery on neurodevelopmental outcomes in sagittal synostosis". *Journal of Neurosurgery Paediatrics*. Vol. 23, No. 4, pp. 434–441.

Blaser, S.I (2008), "Abnormal skull shape". *Pediatric Radiology*. Vol. 38, No. S3, pp. 488-496.

Borghi, A. Rodriguez-Florez, N. Rodgers, W. James, G. Hayward, R. Dunaway, D. Jeelani, O. Schievano, S. (2018), "Spring assisted cranioplasty: a patient specific computational model". *Medical Engineering & Physics*. Vol. 53, pp. 58-65.

Borghi, A. Rodriguez-Florez, N. Ruggiero, F. James, G. O'Hara, J. Ong, J. Jeelani, O. Dunaway, D. Schievano, S. (2019), "A population-specific material model for sagittal craniosynostosis to predict surgical shape outcomes". *Biomechanics and Modelling in Mechanobiology*, Vol. 19, No. 4, pp. 1319-1329.

Borghi, A. Schievano, S. Florez, N.R. McNicholas, R. Rodgers, W. Ponniah, A. James, G. Hayward, R. Dunaway, D. Jeelani, N.U.O. (2017), "Assessment of spring cranioplasty biomechanics in sagittal craniosynostosis patients". *Journal of Neurosurgical Paediatrics*. Vol. 20, No. 5, pp. 400-409.

Bozkurt, S. Borghi, A. Van de Lande, L.S. Owase Jeelani, N.U. Dunaway, D.J. Schievano, S. (2020), "Computational modelling of patient specific spring assisted lambdoid craniosynostosis correction". *Scientific Reports*. Vol. 10, No. 1, pp. 18693.



Brownsett, S.L.E. & Wise, R.J.S. (2010), "The contribution of the parietal lobes to speaking and writing". *Cerebral Cortex*. Vol. 20, No. 3, pp. 517–523.

Buckner, R.L. & DiNicola, L.M. (2019), "The brain's default network: updated anatomy, physiology and evolving insights". *Nature Reviews Neuroscience*. Vol. 20 No. 10, pp. 593–608.

Budday, S. Nay, R. Rooji, R. Steinmann, P. Wyrobek, T. Ovaert, T.C. Kuhl, E. (2015), "Mechanical properties of gray and white matter brain tissue by indentation". *Journal of the Mechanical Behaviour of Biomedical Materials*. Vol. 46, pp. 318-330.

Burgos-Flórez, F.J. Gavilán-Alfonso, M.E. Garzón-Alvarado, D.A. (2016), "Flat bones and sutures formation in the human cranial vault during prenatal development and infancy: a computational model". *Journal of Theoretical Biology*. Vol. 393, pp. 127-144.

Calandrelli, R. D'Apolito, G. Gaudino, S. Stefanetti, M. Massimi, L. Di Rocco, C. Colosimo, C. (2014), "Radiological assessment of skull base changes in children with syndromic craniosynostosis: role of "minor" sutures". *Neuroradiology*. Vol. 56, No. 10, pp. 865–875.

Cappelletti, M. Lee, H.L. Freeman, E. Price, C.J. (2010), "The role of right and left parietal lobes in the conceptual processing of numbers". *Journal of Cognitive Neuroscience*. Vol. 22, No. 2, pp. 331–346.

Care, H. Kennedy-Williams, P. Cunliffe, A. Denly, S. Horton, J. Kearney, A. Knapp, M. O'Leary, G. Piggott, K. Pinckston, M. Rooney, N. Thomas, S. Dalton, L. (2019), "Preliminary analysis from the craniofacial collaboration United Kingdom developmental outcomes in children with sagittal synostosis". *Journal of Craniofacial Surgery*. Vol. 30, No. 6, pp. 1740-1744.

Carter, D.R. Beaupré, G.S. Giori, N.J. Helms, J.A. (1998), "Mechanobiology of skeletal regeneration". *Clinical Orthopaedics and Related Research*. pp. S41-55.

Chan, J.W.H. Stewart, C.L. Stalder, M.W. St Hilaire, H. McBride, L. Moses, M.H. (2013), "Endoscope-assisted versus open repair of craniosynostosis: A comparison of perioperative cost and risk". *The Journal of Craniofacial Surgery*. Vol. 24, No. 1, pp. 170-174.

Chen, J. & Cohen-Adad, J. (2018), "Functional magnetic resonance imaging". *Encyclopaedia of Biomedical Engineering*. Vol. 1, No. 3, pp. 533–544.

Chen, L. & Yang, B. (2019), "Three-dimensional finite element biomechanical analysis of unilateral coronal synostosis and reconstructive operation". *Chinese Journal of Plastic and Reconstructive Surgery*. Vol. 1, No. 1, pp. 24-30.

Chieffo, D. Tamburrini, G. Massimi, L. Giovanni, S.D. Giansanti, C. Caldarelli, M. Rocco, C.D. (2010), "Long term neuropsychological development in single-suture craniosynostosis treated early". *Journal of Neurosurgical Paediatrics*. Vol. 5, No. 3, pp. 232-237.

Claes, L.E. & Heigele, C.A. (1999), "Magnitudes of local stress and strain along bony surfaces predict the course and type of fracture healing". *Journal of Biomechanics*. Vol. 32, No. 3, pp. 255-266.

Clouchoux, C. Guizard, N. Evans, A.C. Plessis, A.J. Limperopoulos, C. (2012), "Normative fetal brain growth by quantitative in vivo magnetic resonance imaging". *American Journal of Obstetrics and Gynecology*. Vol. 206, No. 2, pp. 173.e1-8.

Coats, B. & Margulies, S.S (2006), "Material properties of human infant skull and suture at high rates". *Journal of Neurotrauma*. Vol. 23, No. 8, pp. 1222-1232.

Cocker, K.D. Moseley, M.J. Stirling, H.F. Fielder, A.R. (1998), "Delayed visual maturation: pupillary responses implicate subcortical and cortical visual systems". *Developmental Medicine and Child Neurology*. Vol. 40, No. 3, pp. 160-162.

Cornelissen, M. Otterlander, B. Rizopoulos, D. Hulst, R.A. Molen, A.M. Horst, C. Delye, H. Veelen, M. Bonsel, G. Mathijssen, I. (2016), "Increase of prevalence of

craniosynostosis". *Journal of Cranio-maxillo-facial Surgery*. Vol. 44, No. 9, pp. 1273-1279.

Couper, Z. & Albermani, F. (2009), "Mechanical response of infant brain to manually inflicted shaking". *Journal of Engineering in Medicine*. Vol. 224, No. 1, pp. 1-15.

Courchesne, E. Chisum, H.J. Townsend, J. Cowles, A. Covington, J. Egaas, B. Harwood, M. Hinds, S. (2000), "Normal brain development and aging: quantitative analysis at *in vivo* MR imaging in healthy volunteers". *Radiology*. Vol. 216, No. 3, pp. 672-682.

Cunningham, M.L. & Heike, C.L. (2007), "Evaluation of the infant with an abnormal skull shape". *Current Opinion in Paediatrics*. Vol. 19, No. 6, pp. 645-651.

Davis, M.T. Loyd, A.M. Shen, H.H. Murloy, M.H. Nightingale, R.W. Myers, B.S. Bass, C.D. (2012), "The mechanical and morphological properties of 6-year-old cranial bone". *Journal of Biomechanics*. Vol. 45, No. 15, pp. 2493-2498.

Delye, H.H.K. Arts, S. Borstlap, W.A. Blok, L.M. Driessen, J.J. Meulstee, J.W. Maal, T.J.J. Van Limbert, E.J. (2016), "Endoscopically assisted craniosynostosis surgery (EACS): the craniofacial team Nijmegen experience". *Journal of Cranio-maxillo-facial Surgery*. Vol. 44, No. 8, pp. 1029-1036.

Delye, H.H.K. Borstlap, W.A. Van Lindert, E.J. (2018), "Endoscopy-assisted craniosynostosis surgery followed by helmet therapy". *Surgical Neurology International*. Vol. 9, No. 59.

Ellis, H. & Mahadevan, V. (2014), "The surgical anatomy of the scalp". *Surgery (Oxford)*. Vol. 32, No. 1, pp. e1-e5.

Faber, H.K. & Lannelongue-Lane (1962). "Operation and scaphocephaly". *Journal of Pediatrics*. Vol. 60, No. 470.

Fagan, M.J. (1992), "Finite element analysis: theory and practice". *Longman Scientific & Technical*.

Falland-Cheung, L. Scholze, M. Lozano, P.F. Ondruschka, B. Tong, D.C. Brunton, P.A. Waddell, J.A. Hammer, N. (2018), "Mechanical properties of the human scalp in tension". *Journal of the Mechanical Behaviour Materials*. Vol. 84, pp. 188-197.

Fearon, J.A. Singh, D.J. Beals, S.P. Yu, J.C. (2007), "The diagnosis and treatment of single-sutural synostoses: are computed tomographic scans necessary?". *Plastic and Reconstructive Surgery*. Vol. 120, No. 5, pp. 1327-1331.

Fischer, S. Maltese, G. Tarnow, P. Wikberg, E. Søfteland, M.B. Kölby, L. (2021), "Comparisons of intracranial volume and cephalic index after correction of sagittal craniosynostosis with either two or three springs". *Journal of Craniofacial Surgery*. Vol. 32, No. 8, pp. 2636-2640.

Frost, H.M. (1982), "Mechanical determinants of bone modelling". *Metabolic Bone Disease & Related Research*. Vol. 4, No. 4, pp. 217-229.

Funamura, J.L. & Tollefson, T.T. (2016), "Congenital anomalies of the nose". *Facial Plastic Surgery*. Vol. 32, No. 2, pp. 133-141.

Gaffan, D. (1994), "Interaction of temporal lobe and frontal lobe in memory". *Research and Perspectives in Neuroscience*. Springer.

García-Lázaro, H.G. Ramirez-Carmona, R. Lara-Romero, R. Roldan-Valadez, E. (2012), "Neuroanatomy of episodic and semantic memory in humans: a brief review of neuroimaging studies". *Neurology India*. Vol. 60, No. 6, pp. 613–617.

Garzón-Alvarado, D.A. (2013), "A hypothesis on the formation of the primary ossification centers in the membranous neurocranium: a mathematical and computational model". *Journal of Theoretical Biology*. Vol. 317, pp. 366-376.

Gefen, A. Gefen, N. Zhu, Q. Raghupathi, R. Margulies, S. (2003), "Age-dependent changes in material properties of the brain and braincase of the rat". *Journal of Neurotrauma*. Vol. 20, No. 11, pp. 1163-1177.

Gerety, P.A. Basta, M.N. Fischer, J.P. Taylor, J.A. (2015), "Operative management of nonsynodromic sagittal synostosis". *Journal of Craniofacial Surgery*. Vol. 26, No. 4, pp. 1251–1257.

Gewalli, F. Silva Guimarães-Ferreira, J.P. Sahlin, P. Emanuelsson, I. Horneman, G. Stephensen, H. Lauritzen, C. (2001), "Mental development after modified  $\pi$  procedure: Dynamic cranioplasty for sagittal synostosis". *Annals of Plastic Surgery*. Vol. 46, No. 4, pp. 415-420.

Godde, B. & Voelcker-Rehage, C. (2010), "More automation and less cognitive control of imagined walking movements in high- versus low-fit older adults". *Frontiers in Aging Neuroscience*. Vol. 2, No. 139, pp. 1–13.

Greensmith, A.L. Holmes, A.D. Lo, P. Maxiner, W. Heggie, A.A. Meara, J.G. (2008), "Complete correction of severe scaphocephaly: the Melbourne method of total vault remodelling". *Plastic and Reconstructive Surgery*. Vol. 121, No. 4, pp. 1300-1310.

Greenwood, J. Flodman, P. Osann, K. Boyadijiev, S.A. Kimonis, V. (2014), "Familial incidence and associated symptoms in a population of individuals with non-syndromic craniosynostosis". *Genetics in Medicine: Official Journal of American College of Medical Genetics*. Vol. 16, No. 4, pp. 302-310.

Grisoni, L. Miller, T.M.C. Pulvermüller, F. (2017), "Neural correlates of semantic prediction and resolution in sentence processing". *Journal of Neuroscience*. Vol. 37, No. 18, pp. 4848–4858.

Guimarães-Ferreira, J. Gewalli, F. David, L. Olsson, R. Friede, H. Lauritzen C.G. (2001), "Clinical outcome of the modified  $\pi$ -plasty procedure for sagittal synostosis". *The Journal of Craniofacial Surgery*. Vol. 12, No. 3, pp. 218-224.

Hardy, C.H. & Marcal, P.V. (1971), "Elastic analysis of a skull". *Journal of Applied Mechanics: Transactions ASME*. Vol. 40, No. 4, pp. 838–842.

Hashim, P.W. Patel, A. Yang, J.F. Travieso, R. Turner, J. Losee, J.E. Pollack, I. Jane, J. Jane, J. Kanev, P. Mayes, L. Duncan, C. Bridgett, D.J. Persing, J.A. (2014), "The effects of whole-vault cranioplasty versus strip craniectomy on long term neuropsychological outcomes in sagittal craniosynostosis". *Plastic and Reconstructive Surgery*. Vol. 134, No. 2, pp. 491-501.

Hegazy, A.A. & Hegazy, H.A. (2018), "Newborns' cranial vault: clinical anatomy and authors' perspective". *International Journal of Human Anatomy*. Vol. 1, No. 2, pp. 21-25.

Henderson, J.H. Longaker, M.T. Carter, D.R. (2004), "Sutural bone deposition rate and strain magnitude during cranial development". *Bone*. Vol. 34, No. 2, pp. 271-280.

Herring, S.W. (2008), "Mechanical influences on suture development and patency". *Frontal Orbital Biology*. Vol. 12, pp. 41-56.

Heuzé, Y. Kawasaki, K. Schwarz, T. Schoenebeck, J.J. Richtsmeier, J.T. (2016), "Developmental and evolutionary significance of the zygomatic bone". *Anatomical Record*. Vol. 299, No. 12, pp. 1616-1630.

Ichim, I. Swain, M. Kieser, J.A. (2006), "Mandibular biomechanics and development of the human chin". *Journal of Dental Research*. Vol. 85, No. 7, pp. 638-642.

Idriz, S. Patel, J.H. Renani, S.A. Allan, R. Vlahos, L. (2015), "CT of normal brain developmental and variant anatomy of the paediatric skull: distinguishing trauma from normality". *Radiographics*. Vol. 35, No. 5, pp. 1585-1601.

Isaac, K.V. Meara, J.G. Proctor, M.R. (2018), "Analysis of clinical outcomes for treatment of sagittal craniosynostosis: a comparison of endoscopic suturectomy and cranial vault remodeling". *Journal of Neurosurgery*. Vol. 22, No. 5, pp. 467-474.

Jasinoski, S.C. Reddy, B.D. Louw, K.K. Chinsamy, A. (2010), "Mechanics of cranial sutures using the finite element method". *Journal of Biomechanics*. Vol. 43, No. 16, pp. 3104-3111.

Jimenez, D.F. & Barone, C.M. (1998), "Endoscopic craniectomy for early surgical correction of sagittal craniosynostosis". *Journal of Neurosurgery*. Vol. 88, No. 1, pp. 77-81.

Jivraj, B.A. Ahmed, N. Karia, K. Menon, R. Robertson, E. Sodha, A. Wormald, J.C.R. O'hara, J. Dunaway, D. James, G. Ong, J. (2019), "A 24-month cost and outcome analysis comparing traditional fronto-orbital advancement and remodeling with endoscopic strip craniectomy and molding helmet in the management of unicoronal craniosynostosis: A retrospective bi-institutional review". *JPRAS Open*. Vol. 20, pp. 35-42.

Johnson, D. Wilkie, A.O. (2011), "Craniosynostosis". *European Journal of Human Genetics*. Vol. 19, No. 4, pp. 369-376.

Kamdar, M. Gomez, R.A. Ascherman, J.A. (2009), "Intracranial volumes in a large series of healthy children". *Journal of the American Society of Plastic Surgeons*. Vol. 124, No. 6, pp. 2072-2075.

Khonsari, R.H. Oliver, J. Vigneaux, P. Sanchez, S. Tafforeau, P. Ahlberg, P.E. Di Rocco, F. Bresch, D. Corre, P. Ohazama, A. Sharpe, P.T. Calvez, V. (2013), "A mathematical model for mechanotransduction at the early steps of suture formation". *Proceedings. Biological Sciences*. Vol. 280, No. 1759, pp. 20122670.

Kiernan, J.A. (2012), "Anatomy of the temporal lobe". *Epilepsy Research and Treatment*. Vol. 2012, pp. 1–12.

Kiliaridis, S. (1995), "Masticatory muscle influence on craniofacial growth". *Acta Odontologica Scandinavica*. Vol. 53, No. 3, pp. 196-202.

Kim, S.Y. Choi, J.W. Shin, H.J. Lim, S.Y. (2019), "Reliable manifestations of increased intracranial pressure in patients with syndromic craniosynostosis". *Journal of Cranio-Maxillofacial Surgery*. Vol. 47, No. 1, pp. 158-164.

Kimonis, V. Gold, J.A. Hoffman, T.L. Panchal, J. Boyadijiev, S.A. (2007), "Genetics of craniosynostosis". *Seminars in Paediatric Neurology*. Vol. 14, No. 3, pp. 150-161.

Koser, D.E. Moeendrabary, E. Kuerten, S. Franze, K. (2018), "Predicting local tissue mechanics using immunohistochemistry". *BioRxiv*.

Kriewall, T.J. McPherson, G.K. Tsai, A.C. (1981), "Bending properties and ash content of fetal cranial bone". *Journal of Biomechanics*, Vol. 14, No. 2, pp. 73-79.

Lam, W.W. Ai, V.H. Wong, V. Leong, L.L. (2001), "Ultrasonographic measurement of subarachnoid space in normal infants and children". *Pediatric Neurology*. Vol. 25, No. 5, pp. 380-384.

Landes, C.A. Ballon, A. Roth, C. (2006), "In-patient versus in vitro degradation of P(L/DL)LA and PLGA". *Journal of Biomedical Material's Research, Part B, Applied Biomaterials*. Vol. 76, No. 2, pp. 403-411.

Lapeer, R.J. & Prager, R.W. (2001), "Fetal head moulding: finite element analysis of a fetal skull subject to uterine pressures during the first stages of labour". *Journal of Biomechanics*. Vol. 34, No. 9, pp. 1125-1133.

Lauritzen, C. Sugawara, Y. Kocabalkan, O. Olsson, R. (1998), "Spring mediated dynamic craniofacial reshaping: Case report". *Scandinavian Journal of Plastic and Reconstructive Surgery and Hand Surgery*. Vol. 32, No. 3, pp. 331-338.

Law, J. Lee, M. Hu"lse, M. Tomassetti, A. (2011), "The infant development timeline and its application to robot shaping". *Adaptive behaviour*. Vol. 19, No. 5, pp. 335-358.

Le, M.B. Patel, K. Skolnick, G. Naidoo, S. Smyth, M. Kane, A. Woo, A.S. (2014), "Assessing long term outcomes of open and endoscopic sagittal synostosis



reconstruction using three-dimensional photography". *Journal of Craniofacial Surgery*. Vol. 25, No. 2, pp. 573-576.

Lee, C. Richtsmeier, J.T. Kraft, R.H. (2015), "A computational analysis of bone formation in the cranial vault in the mouse". *Frontiers in Bioengineering and Biotechnology*. Vol. 3, No. 24.

Li, X. Zhu, W. He, J. Di, F. Wang, L. Li, X. Liu, W. Li, C. Gong, J. (2017), "Application of computer assisted three-dimensional simulation operation and biomechanics analysis in the treatment of sagittal craniosynostosis". *Journal of Clinical Neuroscience*. Vol. 44, pp. 323–329.

Liaw, W.X.Z. Parr, W.C.H. Peltz, T.S. Varey, A. Hunt, J. Ginaoutsos, M. Marucci, D.D. Walsh, W. (2019), "Quantification of head shape and cranioplasty outcomes: six-compartment volume method applied to sagittal synostosis". *Plastic and Reconstructive Surgery*. Vol. 7, No. 4, pp. e2171.

Libby, J. Marghoub, A. Johnson, D. Khonsari, R.H. Fagan, M.J. Moazen, M. (2017), "Modelling human skull growth: a validated computational model". *Journal of the Royal Society Interface*. Vol. 14, No. 130, pp. 20170202.

Likus, W. Bajor, G. Gruszczyńska, K. Baron, J. Markowski, J. Machnikowska-Sokołowska, M. Milka, D. Lepich, T. (2014), "Cephalic index in the first three years of life: study of children with normal brain development based on computed tomography". *The Scientific World Journal*. Vol. 502836, pp. 6.

Lipski, M. Tomaszewska, I.M. Lipska, W. Lis, G.J. Tomaszewski, K.A. (2013), "The mandible and its foramen: anatomy, anthropology, embryology and resulting clinical implications". *Folia Morphologica*. Vol. 72, No. 4, pp. 285-292.

Magge, S.N. Bartolozzi, A.R. Almeida, N.D. Tsering, D. Myseros, J.S. Oluigbo, C.O. Rogers, G.F. Keating, R.F. (2019), "A comparison of endoscopic strip craniectomy and pi craniectomy for treatment of sagittal craniosynostosis". *Journal of Neurosurgery Pediatrics*. Vol. 23, No. 6, pp. 708-714.

Mahinda, H.A.M. & Murty, O.P. (2009), "Variability in thickness of human skull bones and sternum – an autopsy experience". *Journal of Forensic Medicine and Toxicology*. Vol. 26, No. 6, pp. 26-31.

Main, R. Lynch, M. Meulen, M. (2014), "Load-induced changes in bone stiffness and cancellous and cortical bone mass following tibial compression diminish with age in female mice". *The Journal of Experimental Biology*. Vol. 217, No. 10, pp. 1775-1783.

Malde, O. Libby, J. Moazen, M. (2019), "An overview of modelling craniosynostosis using the finite element method". *Molecular Syndromology*. Vol. 10, No. 1-2, pp. 74-82.

Malde, O. Cross, C. Lim, C.L. Marghoub, A. Cunningham, M.L. Hopper, R.A. Moazen, M. (2020), "Predicting calvarial morphology in sagittal craniosynostosis". *Scientific Reports*. Vol. 10, No. 3.

Marghoub, A. Libby, J. Babbs, C. Pauws, E. Fagan, M.J. Moazen, M. (2018), "Predicting calvarial growth in normal and craniosynostosis mice using a computational approach". *Journal of Anatomy*. Vol. 232, No. 3, pp. 440-448.

Marghoub, A. Libby, J. Babbs, C. Ventikos, Y. Fagan, M.J. Moazen, M. (2019), "Characterizing and modeling bone formation during mouse calvarial development". *Physical Review Letters*. Vol. 122, No. 4, pp. 048103.

Margulies, S.S. & Thibault, K.L. (2000), "Infant skull and suture properties: Measurements and implications for mechanisms of pediatric brain". *Journal of Biomechanics*. Vol. 122, No. 4, pp. 364-371.

Marucci, D. D. Johnson, C. P. Anslow, P. Jayamohan, J. Richards, P.G. Wilkie, A.O.M. Wall, S.A. (2008), "Implications of a vertex bulge following modified strip craniectomy for sagittal synostosis". *Plastic and Reconstructive Surgery*. Vol. 122, No. 1, pp. 217-224.

Mathijssen, I.M.J. (2015), "Guideline for care of patients with the diagnoses of craniosynostosis: working group on craniosynostosis". *Journal of Craniofacial Surgery*. Vol. 26, pp. 1735–1807.

Matsuzawa, J. Matsui, M. Konishi, T. Noguchi, K. Gru, R.C. Bilker, W. Miyawaki, T. (2001), "Age-related volumetric changes of brain gray and white matter in healthy infants and children". *Cerebral Cortex*. Vol. 11, No. 4, pp. 335-342.

McPherson, G.K. & Kriewall, T.J. (1980), "The elastic modulus of fetal cranial bone: a first step towards an understanding of the biomechanics of fetal head moulding". *Journal of Biomechanics*. Vol. 13, No. 1, pp. 9-16.

Melo, J.R.T. Portella Jr, C.S.A. Lelis, L.C. Lima, E.P. (2013) "Scaphocephaly and cranial vault reconstruction: Renier's 'H' technique". *Pediatric Neurosurgery*. Vol. 49, No. 4, pp. 223-228.

Melott, M.J. (1999), "Apert syndrome: A case report and discussion". *Clinical Eye and Vision Care*. Vol. 11, No. 4, pp. 215–220.

Micovic, M. Zivkovic, B. Bascarevic, V. Mijalčić, R. Rasulic, L. (2016) "Triple square extended osteotomies for treatment of scaphocephaly (Renier's "H" technique modification)". *Neurosurgical Review*. Vol. 39, No. 1, pp. 115-122.

Mitchell, L.A. Kitley, C.A. Armitage, T.L. Krasnokutsky, M.V. Rooks, V.J. (2011), "Normal sagittal and coronal suture widths by using CT imaging". *American Journal of Neuroradiology*. Vol. 32, No. 10, pp. 1801-1805.

Moazen, M. Peskett, E. Babbs, C. Pauws, E. Fagan, M.J. (2015), "Mechanical properties of calvarial bones in a mouse model for craniosynostosis". *PLoS One*. Vol. 10, No. 5, pp. e0125757.

Moazen, M. Curtis, N. O'Higgins, P. Jones, M.E.H. Evans, S.E. Fagan, M.J. (2009), "Assessment of the role of sutures in a lizard skull: a computer modelling study". *Proceedings: Biological Sciences*. Vol. 276, No. 1654, pp. 39-46.

Morriss-Kay, G.M. & Wilkie A.O.M. (2005), "Growth of the normal skull vault and its alteration in craniosynostosis: Insights from human genetics and experimental studies". *Journal of Anatomy*. Vol. 207 No. 5, pp. 637-653.

Nelson, C. & Collins, P. (1991), "Event-related potential and looking-time analysis of infants' responses to familiar and novel events: implications for visual recognition memory". *Developmental Psychological*. Vol. 27, No. 1, pp. 50-58.

Nyman, J.S. Ling, H. Dong, X. Wang, X. (2009), "Differences in the mechanical behavior of cortical bone between compression and tension when subjected to progressive loading"

Obenaus, A. (2016), "Traumatic brain injury". *Encyclopedia of Mental Health (Second Edition)*, Elsevier. pp. 329-340.

O'Higgins, P. Cobb, S.N. Fitton, L.C. Gröning, F. Phillips, R. Liu, J. Fagan, M.J. (2011), "Combining geometric morphometrics and functional simulation: an emerging toolkit for virtual functional analyses". *Journal of Anatomy*. Vol. 218, No. 1, pp. 3-15.

Opperman, L.A. (2000), "Cranial sutures as intramembranous bone growth sites". *Developmental Dynamics*. Vol. 219, No. 4, pp. 472-485.

Otto, A.W. (1830), "Lehrbuch der pathologischen Anatomie des Meuschen und der Thiere". *Rücker*.

Panchal, J. Marsh, J.L. Park, T.S. Kaufman, B. Pilgram, T. Haung, S.H. (1999), "Sagittal craniosynostosis outcome assessment for two methods and timing of intervention". *Plastic and Reconstructive Surgery*. Vol. 103, No. 6, pp. 1574-84.

Pindrik, J. Ye, X. Ji, B. Pendelton, C. Ahn, E.S. (2014) "Anterior fontanelle closure and size in full-term children based on head computed tomography". *Clinical Pediatrics*. Vol. 53, No. 12, pp. 1149–1157.

Pivonka, P. Park, A. Forwood, M.R. (2018), "Functional adaptation of bone: The mechanostat and beyond", in Pivonka, P. (Ed.), *Multiscale Mechanobiology of Bone Remodeling and Adaptation*, Springer International Publishing. pp. 1–60.

Proctor, M.R. (2014), "Endoscopic craniosynostosis repair". *Translational Pediatrics*. Vol. 3, No. 3, pp. 247-258.

Radlanski, R.J. Renz, H. Klarkowski, M.C. (2003), "Prenatal development of the human mandible - 3D reconstruction, morphometry and bone remodelling pattern, sizes 12-17 mm CRL". *Anatomy and Embryology*. Vol. 207, No. 3, pp. 221-232.

Rafferty, K.L. Baldwin, M.C. Soh, S.H. Herring, S.W. (2019), "Mechanobiology of bone and suture – results from a pig model". *Orthodontics and Craniofacial Research*. Vol. 22, No. S1, pp. 82-89.

Rasmussen, S.A. Yazdy, M.M. Frias, J.L. Honein, M.A. (2008), "Priorities for public health research on craniosynostosis - summary and recommendations from a centers for disease control and prevention-sponsored meeting". *American Journal of Medical Genetics. Part A*. Vol. 146A, No. 2, pp. 149-158.

Rayfield, E.J. (2007), "Finite element analysis and understanding the biomechanics and evolution of living and fossil organisms". *Annual Review of Earth and Planetary Sciences*. Vol. 35, pp. 541-576

Riahinezhad, M. Hajizadeh, M. Farghadani, M. (2019), "Normal cranial sutures' width in an Iranian infant population". *Journal of Medical and Surgical Research*. Vol. 5, No. 3, pp. 564-569.

Richtsmeier, J.T. & Flaherty, K. (2013), "Hand in glove: brain and skull in development and dysmorphogenesis". *Acta Neuropathologica*. Vol. 125, No. 4, pp. 469-489.

Rocco, F.D. Arnaud, E. Renier, D. (2009), "Evolution in the frequency of nonsynodromic craniosynostosis". *Journal of Neurosurgical Pediatrics*. Vol. 4, No. 1, pp. 21-25.

Rocco, F.D. Knoll, B.I. Arnaud, E. Blanot, S. Meyer, P. Cuttarree, H. Sainte-Rose, C. Masrchac, D. (2012), "Scaphocephaly correction with retrocoronal and prelamdboid craniotomies (Renier's "H" technique)". *Childs Nervous Systems*. Vol. 28, No. 9, pp. 1327-1332.

Roth, S. Raul, J.S. Ludes, B. Willinger, R. (2007), "Finite element analysis of impact and shaking inflicted to a child". *International Journal of Legal Medicine*. Vol. 121, No. 3, pp. 223-228.

Rovee-Collier, C.K. Sullivan, M.W. Enright, M. Fagen, D.L. (1980), "Reactivation of infant memory". *Science (New York, N.Y.)*. Vol. 208, No. 4448, pp. 1159-1161.

Sakka, L. Coll, G. Chazel, J. (2011), "Aantomy and physiology of cerebrospinal fluid". *European Annals of Otorhinolaryngology, Head and Neck Disease*. Vol, 128, No. 6, pp. 309-316.

Samadian, M. Nazparvar, B. Haddadian, K. Rezaei, O. Khormae, F. (2011), "The anatomical relation between the superior sagittal sinus and the sagittal suture with surgical considerations". *Clinical Neurology and Neurosurgery*. Vol. 113, No. 2, pp. 89-91.

Satanin, L. Teterin, I. Evteev, A. Sakharov, A. Kölby, L. Lemeneva, N. Roginsky, V. (2019), "Introduction of spring-assisted cranioplasty for scaphocephaly in Russia: first cases evaluated using detailed craniometry and principal component analysis". *Journal of Plastic Surgery and Hand Surgery*. Vol. 53, No. 3, pp. 173-179.

Scheuer, L. & Black, S. (2004), "The juvenile skeleton". *London: Elsevier Academic Press*.

Scheuer, L. & Maclaughlin-Black, S. (1994), "Age estimation from the pars Basiliaris of the fetal and juvenile occipital bone". *International Journal of Osteoarchaeology*. Vol. 4, No. 4, pp. 377-380.

Schneider, L. W. Lehman, R.J. Pflug, M.A. Owings, C.L. (1986) "Size and shape of the head and neck from birth to four years". *Final Report to The Consumer Product Safety Commission*.

Schotten, M.T. Urbanski, M. Valabregue, R. Bayle, D.J. Volle, E. (2014), "Subdivision of the occipital lobes: An anatomical and functional MRI connectivity study". *Cortex*. Vol. 56, pp. 121–137.

Sgouros, S. Goldin, J.H. Hockley, A.D. Wake, M.J. Natarajan, K. (1999), "Intracranial volume changes in children". *Journal of Neurosurgery*. Vol. 91, No. 4, pp. 610-616.

Sheridan, M. D. (1973), "From birth to five years". *Windsor, USA: NFER Publishing*.

Shim, K. Park, E. Kim, J. Kim, Y. Kim, D. (2016), "Neurodevelopmental problems in non-syndromic craniosynostosis". *Journal of Korean Neurosurgical Society*. Vol. 59, No. 3, pp. 242-246.

Simpson. A, Wong. A.L. Bezuhyly, M. (2017), "Surgical comparison of nonsyndromic sagittal craniosynostosis. concepts and controversies". *Annals of Plastic Surgery*. Vol. 78, No. 1, pp. 103-110.

Skolnick, G.B. Murthy, S. Patel, K.B. Huang, Z. Naidoo, S.D. Ju, T. Smyth, M.D. Woo, A.S. (2019), "Long term characterization of cranial defects after surgical correction for single-suture craniosynostosis". *Annals of Plastic Surgery*. Vol. 82, No. 6, pp. 679-685.

Slater, B.J. Kwan, M.D. Gupta, D.M. Lee, J.K. Longaker, M.T. (2009), "The role of regional posterior frontal dura mater in the overlying suture morphology". *Plastic and Reconstructive Surgery*. Vol. 123, No. 2, pp. 463-469.

Soboleski, D. McCloskey, D. Mussari, B. Sauerbrei, E. Clarke, M. Fletcher, A. (1997), "Sonography of normal cranial sutures". *AJR. American Journal of Roentgenology*. Vol. 168, No. 3, pp. 819-821.

Speltz, M.L. Kapp-Simon, K. Collett, B. Keich, Y. Gaither, R. Craddock, M.M. Buono, L. Cunningham, M.L. (2007), "Neurodevelopment of infants with single-suture craniosynostosis: presurgery comparisons with case-matched controls". *Plastic and Reconstructive Surgery*. Vol. 119, No. 6, pp. 1874-1881.

Sperber, G.H. (1989), "Craniofacial embryology. 4th edition". *London: Wright, Butterworths*. p. 102.

Sridharan, A. Rajan, S.D. Muthuswamy, J. (2013), "Long term changes in the material properties of brain tissue at the implant–tissue interface". *Journal of Neural Engineering*. Vol. 10, No. 6, pp. 066001.

Takemura, H. Rokem, A. Winawer, J. Yeatman, J.D. Wandell, B.A. Pestilli, F. (2016), "A major human white matter pathway between dorsal and ventral visual cortex". *Cerebral Cortex*. Vol. 26, No. 5, pp. 2205-2214.

Taylor, J.A. & Maugans, T.A. (2011), "Comparison of spring-mediated cranioplasty to minimally invasive strip craniectomy and barrel staving for early treatment of sagittal craniosynostosis". *Journal of Craniofacial Surgery*. Vol. 22, No. 4, pp. 1225-1229.

Teager, S.J. Constantine, S. Lottering, N. Anderson, P.J. (2018), "Physiologic closure time of the metopic suture in South Australian infants from 3D CT scans". *Child's Nervous System: ChNS: Official Journal of the International Society for Paediatric Neurosurgery*. Vol. 35, No. 2, pp. 329-335.

Thenier-Villa, J.L. Sanromán-Álvarez, P. Miranda-Lloret, P. Ramirez, M.E.P. (2018), "Incomplete reossification after craniosynostosis surgery-incidence and analysis of risk factors: a clinical-radiological assessment study". *Journal of Neurosurgical Pediatrics*. Vol. 22, No. 2, pp. 120-127.

Thomas, G.P.L. Johnson, D. Bryen, J.C. Jayaratnam, J. Magdum, S.A. Richards, P.G. Wall, S.A. (2014), "Long term morphological outcomes in nonsyndromic sagittal craniosynostosis: a comparison of 2 techniques". *Journal of Craniofacial Surgery*. Vol. 26, No. 1, pp. 19-25.



Thomas, G.P.L. Johnson, D. Bryen, J.C. Judge, A.D. Jayamohan, J. Magdum, S.A. Richards, P.G. Wall, A.S. (2015), "The incidence of raised intracranial pressure in nonsyndromic sagittal craniosynostosis following primary surgery". *Journal of Neurosurgical Pediatrics*. Vol. 15, No. 4, pp. 350-360.

Thompson, D.N. Malcolm, G.P. Jones, B.M. Harkness, W.J. Hayward, R.D. (1995), "Intracranial pressure in single-suture craniosynostosis". *Pediatric Neurosurgery*. Vol. 22, No. 5, pp. 235-240.

Tonne, E. Due-Tonnessen, B.J. Wiig, U. Stadheim, B.F. Meling, T.R. Helseth, E. Heimdal, K.R. (2020), "Epidemiology of craniosynostosis in Norway". *Journal of Neurosurgery Pediatric* Vol. 26, pp 68-75.

Van De Beeten, S.D.C. Mathijssen, I.M.J. Kamst, N.W. Veelen, M.C. (2019), "Headache in postoperative isolated sagittal synostosis". *Plastic and Reconstructive Surgery*. Vol. 143, No. 4, pp. 798-805.

Vu, H.L. Panchal, J. Parker, E.E. Levine, N.S. Francel, P. (2001), "The timing of physiologic closure of the metopic suture: a review of 159 patients using reconstructed 3D CT scans of the craniofacial region". *The Journal of Craniofacial Surgery*. Vol. 12, No. 6, pp. 527-532.

Wagemans, P.A. Van de Velde, J.P. Kuijpers-Jagtman, A.M. (1988), "Sutures and forces: a review". *American Journal of Orthodontics and dentofacial orthopedics*. Vol. 94, No. 2, pp. 129-141.

Wang, J. Zou, D. Li, Z. Huang, P. Li, D. Shao, Y. Wang, H. Chen, Y. (2014), "Mechanical properties of cranial bones and sutures in 1–2-year-old infants". *Medical Science Monitor*. Vol. 20, pp. 1808-1813.

Weickenmeier, J. Fischer, C. Carter, D. Kuhl, E. Goriely, A. (2017), "Dimensional, geometrical, and physical constraints in skull growth". *Physical Review Letters*. Vol. 118, No. 24, pp. 248101.

White, T.D. Black, M.T. Folkens, P.A. (2011), "Human osteology: third edition". London: Elsevier Academic Press.

Wilkie, A.O. Tang, Z. Elanko, N. Walsh, S. Twigg, S.R. Hurst, J.A. Wall, S.A. Chrzanowska, K.H. Maxson Jr, R.E. (2000), "Functional haploinsufficiency of the human homeobox gene MSX2 causes defects in skull ossification". *Nature Genetics*. Vol. 24, No. 4, pp. 387-390.

Wilkie, A.O.M. Patey, S.J. Kan, S. Van de Ouweland, A.M.W. Hamel, B.C.J. (2002), "FGFs, their receptors, and human limb malformations: clinical and molecular correlations". *American Journal of Medical Genetics*. Vol. 122, No. 3, pp. 266-278.

Wolański, W. Larysz, D. Gzik, M. Kawlewska, E. (2013), "Modelling and biomechanical analysis of craniosynostosis correction with the use of finite element method". *International Journal for Numerical Methods in Biomedical Engineering*. Vol. 29 No. 9, pp. 916–925.

You, J. Jiang, X. Hu, M. Wang, N. Shen, Z. Li, J. Peng, W. (2010), "The bone slot effect study of PI procedure for craniosynostosis correction plan based on finite element method". *Proceedings - 2010 3rd International Conference on Biomedical Engineering and Informatics*. Vol. 2, pp. 605-608.

Yu, M. & Wang, S. (2021), "Anatomy, head and neck, zygomatic". *Statpearls*.

Zapata, U. & Wang, Q. (2020) "Material properties of the skull layers of the primate parietal bone: a single-subject study". *PLoS ONE*. Vol. 15, No. 3, pp. e0229244.

Zhang, L. Yang, K. King, A. (2001), "Comparison of brain response between frontal and lateral impacts by finite element modelling". *Journal of Neurotrauma*. Vol. 18, No. 1, pp. 21-30.

Zhang, Z.Q. & Yang, J.L. (2015), "Biomechanical dynamics of cranial sutures during simulated impulsive loading". *Applied Bionics and Biomechanics*. pp. 596843.

Zollikofer, C.P.E. & Weissmann, J.D. (2011), "A bidirectional interface growth model for cranial interosseous suture morphogenesis". *Journal of Anatomy*. Vol. 219, No. 2, pp. 100-114.

## Appendix I: Contact interface

When two or more surfaces are touching one another in such a way they become mutually tangent, they are defined to be in 'contact'. Contacts defined during computational simulations become highly sensitive to the level of interpenetration and the compressive and tangential forces applied between surfaces. For ANSYS (18.0) APDL, there are four main contact types:

- **Bonded:** Allowing for no relative sliding or separation between interfaces.
- **No separation:** Upon contact, the normal direction is fixed while still allowing for tangential movement.
- **Frictionless:** Allowing for complete separation between interfaces, tangential directional sliding is still granted.
- **Frictional:** Application of shear stress applied to the tangential direction while still allowing for normal directional separation.

For the avoidance of interpenetration of interfaces, a stiffness applied to the two or more interfaces must be established, allowing for contact compatibility. In the absence of such behaviour, surfaces are free to pass through one another (Figure A.1).

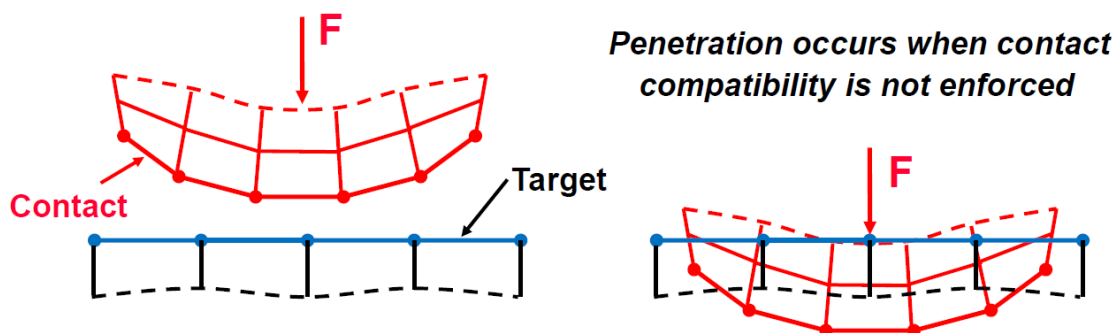


**Figure A.1:** Illustration of two surfaces interacting when no contact compatibility is enforced (Adopted from ANSYS®, 2010)

Achieving a suitable contact capability between interfaces relies on the application of various parameters across the contact (the surface moving into the various surfaces) and target (typically a rigid body to resist the pressure applied from the contact surfaces) interfaces. As such, using one of two algorithms defined by the FEA

software, the contact pressure across the contact interface can be calculated by ANSYS. For nonlinear solid body simulation as the one shown across this work, two common types of algorithms were available, the pure penalty (1) and Augmented Lagrange (2).

(1) **Pure penalty:**  $F_{normal} = K_{normal} x_{penetration}$

(2) **Augmented Lagrange:**  $F_{normal} = K_{normal} x_{penetration} + \lambda$

The *pure penalty method* allows for the manual inputting of the necessary contact parameters to minimise this interpenetration of surfaces. These include the normal penalty stiffness: **K<sub>normal</sub>** (the level of force applied across a unit of area, typically represented as N/mm), friction coefficient (applies only to the frictional contact type), and the allowable penetration tolerance. While the *augmented Lagrange method* negates the use of these parameters resulting in a less sensitive model. As the level of penetration had to be controlled between the surfaces during simulated growth (Here, the ICV and the inner calvarial interfaces), the latter method was applied to all modelling scenarios. Such as the correct values of contact stiffness could be identified through sensitivity tests.

As interfaces more into one another across the normal direction, a method of detection is applied, specified as integration point detection (IPD). Although not used across the two algorithmic approaches, a secondary detection approach is available, known as nodal detection (ND). Figure A.2 highlights the differences between the two detection approaches.

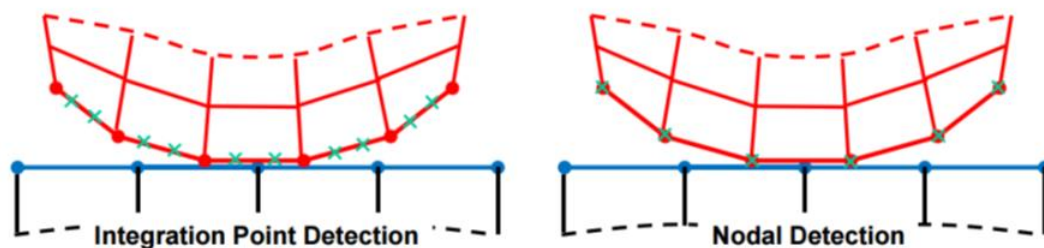


**Figure A.2:** Illustration of the two contact detection methods used during FEA simulations (Adopted from ANSYS®, 2010).

IDPs used the volume of elements across an area to define the number of points to be used for calculations, giving greater accuracy over the overall predictive outcomes. ND utilises only the nodes across a volume, resulting in only the corners of the element's integrals being calculated. Although the corners of elements defined with IDP contain fewer detection points, this can be resolved with the refinement of the mesh. Providing a greater number of detection points across the interface.

When considering the *in vivo* environment of the intracranial volume, with the associational friction between the brain and the calvarial bones, an appropriate frictional coefficient needs to be defined. For tangential forces acting during simulated growth, this can only be calculated under the penalty method. Therefore, if the frictional constraints seen across the ICV (sticking) are seen, the FE software uses equation (3) to calculate the tangential forces.

$$(3) F_{tangential} = K_{tangential} x_{sliding}$$

When considering the overall parameters of the penalty-based contact method, the penalty stiffness is perhaps the primary input in achieving convergence of the model. While higher values achieve more accurate solutions, the computational costs are increased. Therefore, achieving a suitable balance between accuracy and computational cost is a factor to be considered under any nonlinear analysis. On the other hand, if the stiffness is excessive, the oscillation between interfaces can begin to manifest (Figure A.3).

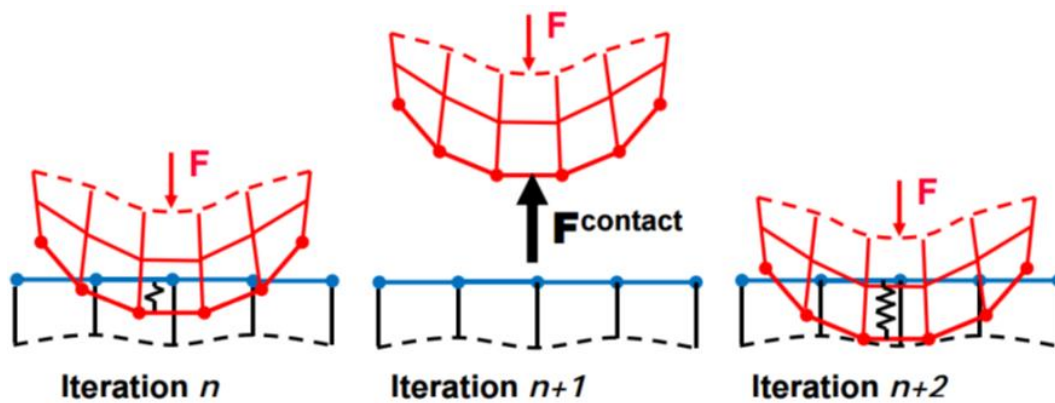


**Figure A.3:** Illustration of oscillation occurring between the target (blue) and contact (red) interfaces across several iterations of loading (Adopted from ANSYS®, 2010).

## Appendix II: Measurement of clinically used spring devices

Mechanically, materials such as steel, when subjected to compression and/or tension, a level of plasticity is enforced once the modulus of resilience and yield strength has been exceeded. During the clinical surgical procedure of spring assisted cranioplasty, linear spring devices are subjected to a large level of compression to apply tensile forces across the calvarial to correct the anteroposterior overdevelopment.

To parameterise the level of compression across the spring *in silico*, the surgical team within The Department of Plastic Surgery, located at The Sahlgrenska University Hospital (The University of Gothenburg, Gothenburg, Sweden) kindly performed a series of *in vitro* measurements to assess the resulting tensile forces under the following conditions:

- (1) : The initial resulting forces created while the springs are subjected to a level of compression
- (2) : The level of subjected plasticity the springs have suffered after the initial compressive forces have been applied
- (3) : Finally, comment on the level of tensile force available after the subjected plasticity

The analysis was performed across nine individual springs and their outcomes are detailed in table A.1. These outcomes provided a greater understanding of the mechanics of the springs used during this procedure. Further, the initial spring length under zero loading (i.e., 100 mm) and the forces generated (i.e., 8 N) under compression of 85 mm was used to model the technique discussed in chapter 4 and 6.

**Table A.1:** Outcomes of sensitivity data performed across nine individual springs. Highlighting the spring length and tensile forces generated.

| <b>Spring No:</b> | <b>Primary Spring length<br/>under zero load (mm):</b> | <b>Primary tensile forces under<br/>85 mm compression (N):</b> | <b>Secondary Spring length<br/>under zero load (mm):</b> | <b>Secondary tensile<br/>forces under 85 mm<br/>compression (N):</b> |
|-------------------|--|--|--|--|
| 1                 | 101  | 8.0  | 91   | 8.0  |
| 2                 | 96   | 8.4  | 90   | 8.3  |
| 3                 | 103  | 8.4  | 96   | 8.4  |
| 4                 | 98   | 8.7  | 91   | 8.7  |
| 5                 | 102  | 8.3  | 96   | 8.3  |
| 6                 | 100  | 8.5  | 95   | 8.5  |
| 7                 | 104  | 8.3  | 97   | 8.3  |
| 8                 | 98   | 8.8  | 92   | 8.8  |
| 9                 | 101  | 8.1  | 93   | 7.8  |



## Appendix III: Parameters for modelling the *in silico* helmet device

The modelling approach used for the creation of the postoperative helmet device used within this work is a far more simplistic variation than the ones used clinically after surgery has been performed. Here, an APDL macro code was generated to constrain the nodes located across the anterior and posterior of the modelled calvarial bones. The position of these nodes ranged above and across the orbital region for the anterior and extended down towards the foramen magnum across the occipital. Further, a thin region was also constrained across the temporal region where the preauricular pit would reside (i.e., just about the ear hole). Figure A.4 illustrates the approximate location of these constrained nodes.

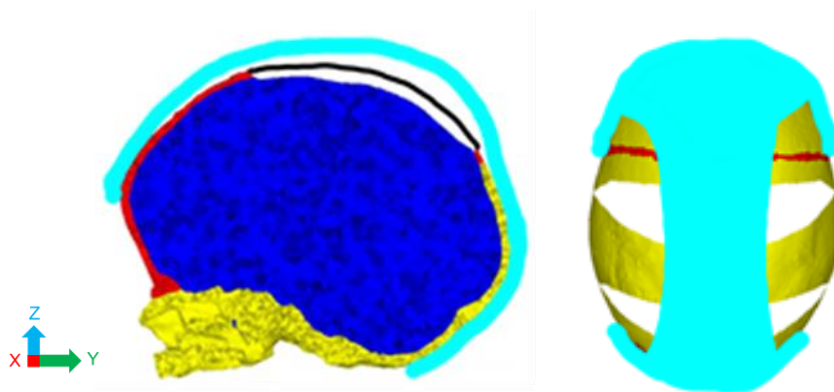


**Figure A.4:** *In silico* modelling of the helmeting device used in chapter 6. Internal sagittal view (left) and dorsal view (right). Constraints placed across the nodes are marked in light blue.

To represent the constraints that would be seen in reality, the anterior and occipital regional nodes are constrained in the Y-axis, while the temporal regional nodes are constrained in the X-axis throughout the application to the model.

Under the surgical team's advice, it was known that a level of allowable growth was granted across the dorsal region of the helmet. Provided by a small area between the helmet and the skull. To simulate this gap, several sensitivities were carried out using a generated APDL code. Figure A.5 provides a flowchart of the created code used in this technique.

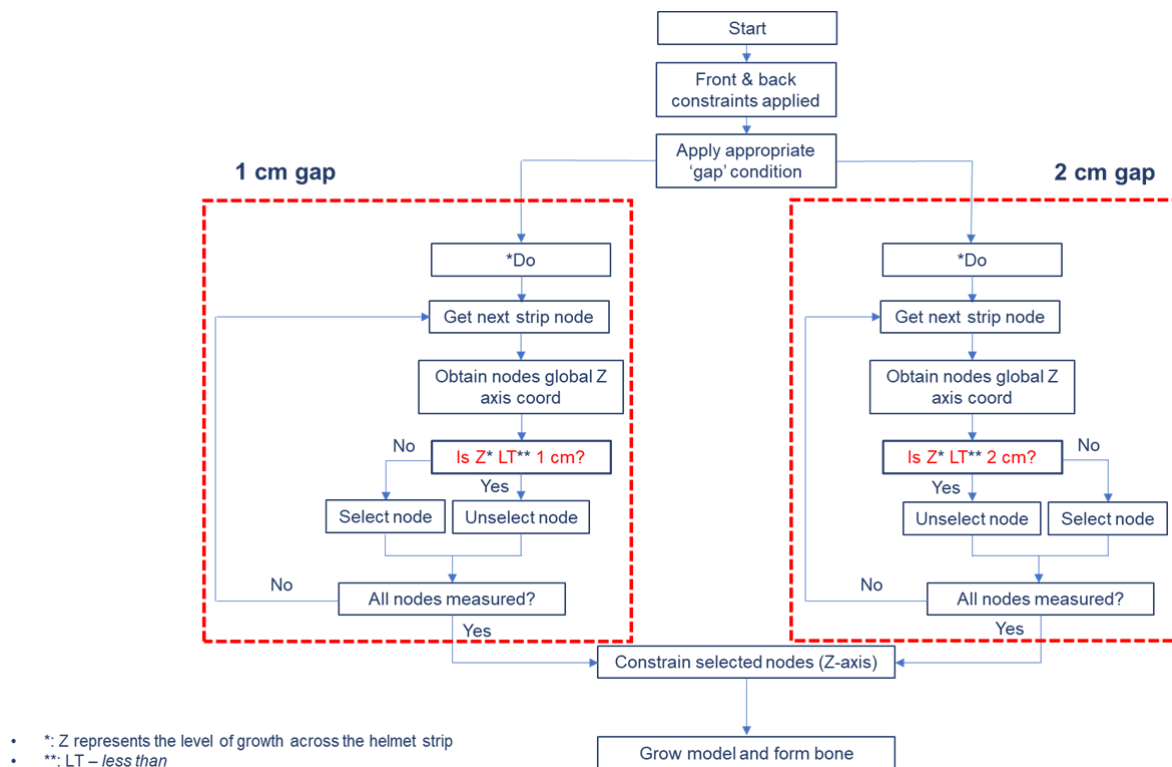


**Figure A.5:** Flow chart to illustrate the do loop used in assessing the level of dorsal growth between the skull and helmet. Individual nodes are measured across the global coordinates after each load step. A sensitivity study was carried out to understand the impacts between a defined 1 cm and 2 cm ‘gap’ (i.e., the distance between the skull and ‘helmet’). Nodes seen to exceed this gap were constrained in the Z-axis until helmet ‘removal’ was performed.

An assessment of the impact on the morphology and patterns of bone formation was investigated for both sensitivity codes. As a control scenario, the third helmet with no restrictions on the dorsal growth was introduced (denoted as ‘open gap’). All three scenarios underwent growth up to 12 months of age (helmet applied for 8 months), where the overall morphology and patterns of bone formation were assessed. Figure V.6 highlights these findings.

Displaying a similar finding to the outcomes seen in chapter 7 of this work, an uncharacteristic dorsal budge is seen when an unlimited level of dorsal growth was granted (Red box). When restricting this growth to only 1 cm, the opposite effect was captured (Black box) leading to a flattening across the dorsal region of the skull. When introducing a 2 cm limit, this was seen to overall represent the most realistic outcome (Blue box) and as such, was used throughout the main body of this work.

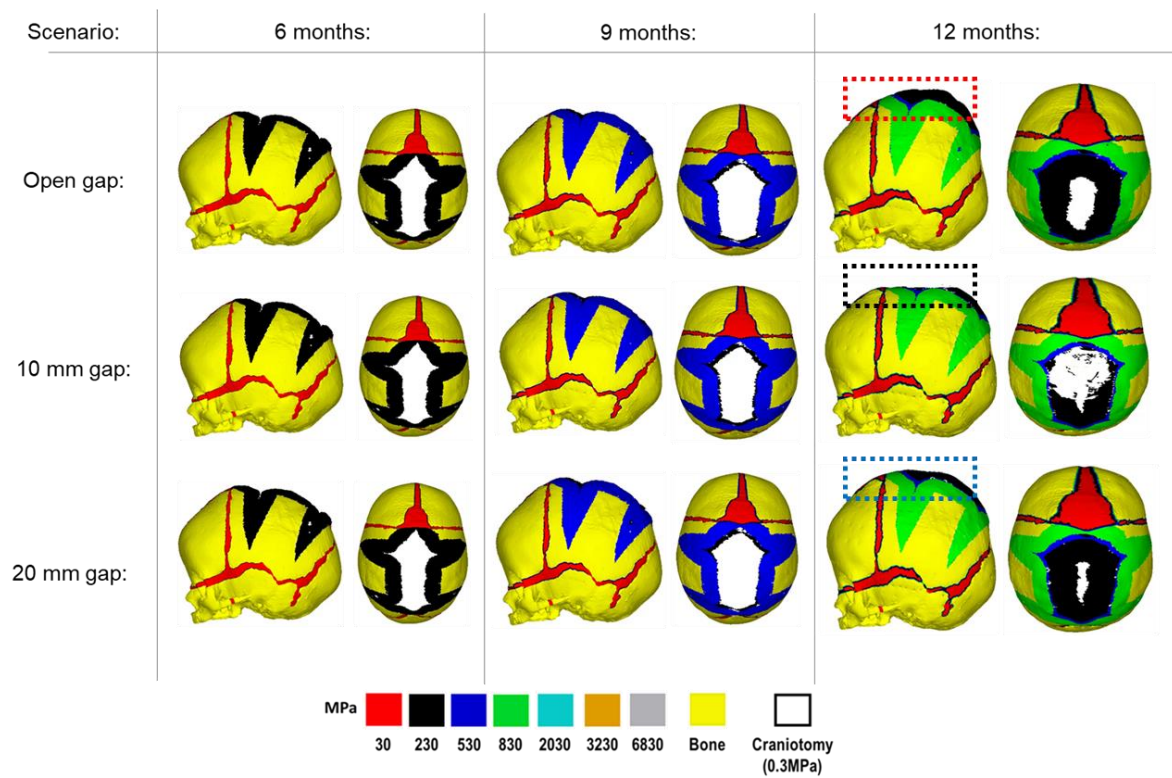


**Figure A.6:** The predicted pattern of bone formation captured across all sensitivity scenarios.

## Appendix IV: List of publications

### Journal papers:

- Malde, O., **Cross, C.**, Lim, L., Marghoub, A., Cunningham, L., Hopper, R.A., Moazen, M. (2020), “**Predicting calvarial morphology in sagittal craniosynostosis**”. *Scientific Reports*. 10:3.
- **Cross, C.**, Khonsari, R.H., Gailay, L., Paternoster, G., Johnson, D., Ventikos, Y., Moazen, M. (2021), “**Using a sensitivity analysis to develop a validated computational model of post-operative calvarial growth in sagittal craniosynostosis**”. *Frontiers in Cell and Developmental Biology*. 9. pp: 621249.
- Gailay, L., Hennocq, Q., **Cross, C.**, Arnaud, E., Larysz, D., Kölby, L., Paternoster, G., Khonsari, R.H., Moazen, M. (2021), “**Management of sagittal craniosynostosis: morphological comparison of 8 surgical techniques**”. *The British Journal of Oral & Maxillofacial Surgery*. S0266-4356:21. pp: 00350-8.
- **Cross, C.**, Khonsari, R.H., Larysz, D., Johnson, D., Kölby, L., Moazen, M. (2021), “**Predicting and comparing three corrective techniques for sagittal craniosynostosis**”. *Scientific Reports*. 11:1. pp: 21216.
- Gailay, L., Cornette, R., Laliève, L., Hennocq, Q., **Cross, C.**, Alazmani, A., Moazen, M., Khonsari, R.H. (2022), “**International craniofacial remodelling in Europe in the XIXth century: Quantitative evidence of soft tissue modifications from Toulouse, France**”. *Journal of Stomatology, Oral and Maxillofacial Surgery*. S2468-7855:22. pp: 00133-1.
- **Cross, C.**, Khonsari, R.H., Paternoster, G., Arnaud, E., Larysz, D., Kölby, L., Johnson, D., Ventikos, Y., Moazen, M. (2022), “**A computational framework to predict calvarial growth: optimising management of sagittal craniosynostosis**”. *Frontiers in Bioengineering and Biotechnology*. 10. pp: 913190.

- **Cross, C.**, Deyle, H., Khonsari, R.H., Ventikos, Y., Moazen, M., (Under review), “**A preliminary analysis of replicating the biomechanics of helmet therapy for sagittal craniosynostosis**”. *Journal of Plastic, Reconstructive & Aesthetic Surgery*.

#### Conferences:

- **Cross, C.**, Gailay, L., Khonsari, R.H., Paternoster, G., Johnson, D., Ventikos, Y., Moazen, M., “**Predicting calvarial growth in sagittal craniosynostosis – a sensitivity study**”. *Anatomical Society Virtual Winter Meeting*, (online) 6<sup>th</sup>-8<sup>th</sup> January (2021).
- **Cross, C.**, Khonsari, R.H., Paternoster, G., Larysz, D., Johnson, D., Kölby, L., Moazen, M., “**Predicting outcomes in sagittal craniosynostosis corrective techniques**”. *26<sup>th</sup> Congress of the European Society of Biomechanics*, (online) 11<sup>th</sup>-14<sup>th</sup> July, (2021)
- **Cross, C.**, Khonsari, R.H., Paternoster, G., Larysz, D., Johnson, D., Kölby, L., Moazen, M., “**Predicting and optimising surgical outcomes in sagittal craniosynostosis**” *BioMedEng21*, Sheffield, UK, 6<sup>th</sup>-7<sup>th</sup> September (2021)
- **Cross, C.**, Khonsari, R.H., Paternoster, G., Larysz, D., Johnson, D., Kölby, L., Moazen, M., “**Predicting outcomes in sagittal craniosynostosis corrective techniques**”. *XVI International Conference on Computational Plasticity. Fundamentals and Applications*, (online) 7<sup>th</sup>-9<sup>th</sup> September (2021).
- **Cross, C.**, Khonsari, R.H., Paternoster, G., Larysz, D., Johnson, D., Kölby, L., Moazen, M., “**Comparing the biomechanics of four reconstructive techniques for the management of sagittal synostosis**”. *Congress of International Society of Craniofacial Surgery*, (online) 15<sup>th</sup>-16<sup>th</sup> October (2021).
- **Cross, C.**, Khonsari, R.H., Paternoster, G., Arnaud, E.J., Larysz, D., Kölby, L., Johnson, D., Ventikos, Y., Moazen, M., “**Predicting surgical outcomes across**

**nine corrective techniques for sagittal craniosynostosis".** *27<sup>th</sup> Congress of the European Society of Biomechanics*, Porto, Portugal, 26<sup>th</sup>-29<sup>th</sup> June (2022).

- **Cross, C.**, Delye, H., Ventikos, Y., Moazen, M., "**Modelling the effects of helmet therapy during sagittal craniosynostosis correction**". *BioMedEng22*, London, UK, 8<sup>th</sup>-9<sup>th</sup> September (2022).
- **Cross, C.**, Khonsari, R.H., Paternoster, G., Arnaud, E.J., Larysz, D., Kölby, L., Johnson, D., Ventikos, Y., Moazen, M., "**A computational framework to optimise the management of sagittal craniosynostosis**". *European Society of Craniofacial Surgery*. Oxford, UK, 23<sup>rd</sup>- 24<sup>th</sup> September (2022).
- **Cross, C.**, Delye, H., Ventikos, Y., Moazen, M., "**Modelling the effects of helmet therapy during sagittal craniosynostosis correction**". *European Society of Craniofacial Surgery*. Oxford, UK, 23<sup>rd</sup>- 24<sup>th</sup> September (2022).

## **Appendix V: Published papers**

**Using sensitivity analysis to develop a validated computational model of postoperative calvarial growth in sagittal craniosynostosis**

**Connor Cross, M. Eng<sup>1</sup>, Roman H Khonsari, MD, Ph.D<sup>2</sup>, Leila Galiay, MD<sup>2</sup>, Giovanna Paternoster, MD<sup>3</sup>, David Johnson, Ph.D<sup>4</sup>, Yiannis Ventikos, Ph.D<sup>1</sup>, Mehran Moazen, Ph.D<sup>1</sup>**

<sup>1</sup>Department of Mechanical Engineering, University College London, London, UK

<sup>2</sup>Service de Chirurgie Maxillo-Faciale et plastique, Assistance Publique des Hôpitaux de Paris, France

<sup>3</sup>Department of Neurosurgery, Craniofacial 16 surgery unit, Necker – Enfants Malades University Hospital, Assistance Publique – Hôpitaux de 17 Paris; Université de Paris; Paris, France

<sup>4</sup>Oxford Craniofacial Unit, Oxford University Hospital, NHS foundation trust, Oxford, UK

**Correspondence:**

Mehran Moazen, Ph.D.

Email: [m.moazen@ucl.ac.uk](mailto:m.moazen@ucl.ac.uk)

**Keywords: craniosynostosis, cerebrospinal fluid, finite element, calvarial growth, sagittal synostosis, biomechanics**

**Word count: 4,145**

**Figure count: 6**

**Supplementary figure count: 1**

**Table count: 4**



## **Abstract**

Craniosynostosis is the premature fusion of one or more sutures across the calvaria, resulting in morphological and health complications that require invasive corrective surgery. Finite element (FE) method is a powerful tool that can aid with preoperative planning and postoperative predictions of craniosynostosis outcomes. However, input factors can influence the prediction of skull growth and the pressure on the growing brain using this approach. Therefore, the aim of this study was to carry out a series of sensitivity studies to understand the effect of various input parameters on predicting the skull morphology of a sagittal synostosis patient post-operatively. Preoperative CT images of a 4-month old patient were used to develop a 3D model of the skull, in which calvarial bones, sutures, cerebrospinal fluid (CSF), and brain were segmented. Calvarial reconstructive surgery was virtually modelled and two intracranial content scenarios labelled 'CSF present' and 'CSF absent', were then developed. FE method was used to predict the calvarial morphology up to 76 months of age with intracranial volume-bone contact parameters being established across the models. Sensitivity tests with regards to the choice of material properties, methods of simulating bone formation and the rate of bone formation across the sutures were undertaken. Results were compared to the in vivo data from the same patient. Sensitivity tests to the choice of various material properties highlighted that the defined elastic modulus for the craniotomies appears to have the greatest influence on the predicted overall skull morphology. The bone formation modelling approach across the sutures/craniotomies had a considerable impact on the level of contact pressure across the brain with minimum impact on the overall predicated morphology of the skull. Including the effect of CSF (based on the approach adopted here) displayed only a slight reduction in brain pressure outcomes. The sensitivity tests performed in this study set the foundation for future comparative studies using FE method to compare outcomes of different reconstruction techniques for the management of craniosynostosis.

## **1 Introduction**

The cranium consists of several bones that are connected via cranial joints or sutures. Sutures facilitate the birth and accommodate the radial expansion of the brain during infancy (Anatole and Dekaban, 1977; Morris-Kay and Wilkie, 2005; Lieberman, 2011; Richtsmeier and Flaherty, 2013; Jin et al., 2016; Adigun and Al-Dhahir, 2017; Hegazy and Hegazy, 2018). Early fusion of the sutures is a medical condition called

craniosynostosis with the most common form of this condition being the early fusion of the sagittal suture i.e. occurring in ca. 3 per 10000 live births (Morris-Kay and Wilkie, 2005; Cunningham and Heike, 2007; Johnson and Wilkie, 2011; Cornelissen et al., 2016; Kalantar-Hormozi et al., 2019). The condition results in limited expansion of the skull perpendicular to the fused suture, leading to compensatory anteroposterior growth. In addition, raised intracranial pressure may cause cognitive impairment and visual loss (Lo L & Chen Y, 1999; Gault et al., 1992). Various calvarial reconstructions to alleviate and correct these abnormalities have existed since the late 19th century (Lane, 1892; Lauritzen et al., 2006; Rocco et al., 2012; Simpson et al., 2015; Mathijssen, 2015; Microvic et al., 2016) with their various cognitive and morphological outcomes debated and compared to optimize the management of this condition (Hashim et al., 2014; Isaac et al., 2018; Magge et al., 2019).

Finite element (FE) method is a powerful computational tool that has been widely used in the field of biomechanics for the design and development of various structures and systems. The same technique has huge potentials to optimize the management of various form of craniosynostosis (e.g. You et al., 2010; Wolański et al., 2013; Malde et al., 2018; Dolack et al., 2020). Several recent studies have developed validated computational model of calvarial growth in rodent (Lee et al., 2017; Marghoub et al., 2018), and human infant models (Weickenmeier et al., 2017; Libby et al., 2017) as well as predicting follow up results in treated sagittal craniosynostosis patients (Malde et al., 2020). However, few studies have carried out detail investigations to understand the sensitivity of these models to the choice of their input parameters (Barbelto-Andres et al., 2020). Such sensitivity studies are crucial to advance our understanding of the limitations of FE models as well as achieving more accurate predictions of the skull growth using this method.

The aim of this study was to carry out a series of sensitivity studies to understand the effect of various input parameters on predicting the skull morphology of a sagittal synostosis patient post-operatively. Therefore, a preoperative patient-specific finite element model was developed. The post-operative skull morphology and the level of contact pressure at the intracranial volume (ICV)-bone interface were quantified and compared across a number of sensitivity tests.

## **2 Materials and methods**

### **2.1 Patient computed tomography data**

Computed tomography (CT) images of a sagittal craniosynostosis patient were retrieved from the Hôpital - Necker Enfants – Malades Cranio-facial Surgery Unit (Paris, France) at a resolution of 0.625 x 0.625 mm. Full ethical consent from the centre and the patients' guardians was granted for the purposes of this study. Preoperative and immediate postoperative images were taken at 4 months of age and 6 days after the operation respectively. Long term follow up CT images were taken at 76 months of age (i.e. 72 months after the operation). Anatomical 3D segmentation of the preoperative CT data was performed in Avizo image processing software (Thermo Fisher Scientific, Mass, USA). The follow up data at 76 months was used for morphological validation. 3D reconstructions of all CT data are highlighted in Figure 1A at each time point.

### **2.2 Model development**

Segmentation of the calvarial bone, sutures, and the ICV was undertaken. The segmentation consisted of four components: (1) Calvarial bone (frontal, parietal, occipital, temporal and craniofacial bones); (2) Sutures (metopic, squamosal, coronal, lambdoid, anterior fontanelle, frontozygomatic and zygomaticotemporal); (3) cerebrospinal fluid (CSF) and (4) the brain (frontal lobe, temporal lobe, parietal lobe, occipital lobe and cerebellum). Bone was segmented automatically based on greyscale values while other tissues were segmented manually. The mandible was removed from the segmentation as the primary focus was on calvarial growth.

The in vivo surgical craniotomies (i.e. Renier's 'H' technique) were also replicated across the calvaria (Rocco et al., 2012) and confirmed by the surgical team (i.e. Roman H Khonsari & Giovanna Paternoster). A 3 to 4-cm wide rectangular cut was performed across the parietal, posterior of the coronal and anterior of the lambdoid sutures. The fused suture was removed and divided into two square portions. These were then reinserted to aid with long term calvarial healing. Two wedges extending from craniotomy-squamosal were created on each side of the parietal bone to assist with postoperative skull widening and anteroposterior shortening.

The ICV was modelled under two conditions (Figure 1B-C):

Model I: CSF present consisted of a uniform 2-3 mm thick material layer defined as CSF between the cranial bones and the brain. Due to the resolution of the CT images, accurate *in vivo* representation of the CSF could not be achieved. Therefore, the aforementioned thickness was used based on previous studies (see e.g. Lam et al., 2001; Clouchoux et al., 2012).

Model II: CSF absent defined the total ICV as the brain for comparison. Model II was used as the baseline approach for our sensitivity studies. Following segmentation, the surface model of the skull was transformed into a meshed solid geometry in Avizo that was then imported into a finite element package.

### **2.3 Finite element analysis**

Both models were imported into ANSYS finite element software (Canonsburg, USA) as solid meshed models. A quadratic tetrahedral mesh consisting of 3,100,000 elements across the skull and 900,000 elements across the CSF-brain was chosen after a mesh convergence analysis (i.e. several models were imported from Avizo to ANSYS in this respect). Correction of element intersection and poor aspect ratios was performed prior to importation. All material properties were defined as linear isotropic. For both models, the cranial bones, sutures and craniotomies were initially assigned a baseline elastic modulus of 3000MPa, 30MPa and 30MPa respectively (McPherson and Kriewall, 1980; Moazen et al., 2015 – these were altered later - see sensitivity tests section). The brain (intracranial volume) elastic modulus was defined as 100MPa (Libby et al., 2017) and the CSF elastic modulus was defined as 40MPa. The Poisson's ratio of the cranial bones, sutures and craniotomies was assumed to be 0.3. The Poisson's ratio of CSF was assumed to be 0.48. Note, since the exact values/distribution of CSF pressure across the skull are not still clear, and modelling the CSF as fluid was beyond the scope of this study, we decided to model the impact of CSF on the prediction of calvarial growth and ICV surface pressures using solid elements.

### **2.4 Boundary conditions and modelling of the growth**

A surface-to-surface penalty-based contact was established between the ICV and inner-calvarial interface for both models. These interfaces were initially in contact, after which normal and tangential friction behavior during calvarial growth was granted. A

friction coefficient of 0.1, a penetration tolerance of 0.5, and a normal penalty stiffness of 600N/mm was used at all interfaces where contact was defined. These values were chosen based on our previous sensitivity tests (Malde et al., 2020). A 'bonded' interface behavior was enforced between bone, suture, craniotomies and CSF surfaces throughout all simulations i.e. allowing no relative motion at the aforementioned interfaces.

Nodal constraints in all degrees of freedom were placed around the foramen magnum and along the nasion to avoid rigid displacement during skull growth. The radial expansion of the brain/ICV was modelled using thermal analogy as described in detail elsewhere (see Libby et al., 2017; Marghoub et al., 2018, 2019; Malde et al., 2020). To summarize, a linear isotropic expansion was applied to the brain/ICV, where the preoperative ICV (measured at 659ml) was expanded to follow up ICV at 76 months of age (measured at 1245ml) in six intervals. The estimated age of each interval was calculated by measuring these new volumes (Sgouros et al., 1999). Two methods of bone formation were undertaken here:

Scenario I: applies a bone formation across the sutures/craniotomies as described in Marghoub et al., (2019) and here termed 'gradual bone formation' (Figure 1D). Here, the suture and craniotomy elements within a specified radius from the adjacent bone were selected, at a rate of 0.1 mm for the sutures and 0.8 mm for the craniotomies for every month of volume growth (Mitchell et al., 2011; Thenier-Villa et al., 2018; Riahi-nienzhad et al., 2019). To monitor for the level of strain in the selected elements, all elements with a hydrostatic strain (i.e. summation of all principal strains divided by three) within 0-50% were used. Scenario I was the baseline approach throughout the study.

Scenario II: here termed as 'bulk bone formation' increased the bulk elastic modulus of the sutures/craniotomy as oppose to simulating bone forming from the bone edge (Figure 1E). This method is computationally less expensive i.e. solves faster but perhaps not as physiologically representative as the 'gradual bone formation'. Further details are described by Malde et al., (2020).

## 2.5 Sensitivity tests

The baseline values as detailed above were changed using Model II under bone formation scenario I. Table 1 details respective sensitivity studies and their independent values i.e. to the choice of material properties and rate of bone formation.

**Material properties** Three sensitivity analyses were performed to the changes in material properties.

Test 1 - Bone sensitivity: the elastic modulus of the bone was reduced from 3000MPa to 421 MPa based on the previous study of Coats and Margulies (2006).

Test 2 - Craniotomy sensitivity: The elastic modulus of the craniotomies were reduced from 30MPa to 3kPa i.e. two extremes that can capture wide range of tissues that can be present in these defects (see e.g. Leong and Morgan 2008).

Test 3 - Brain sensitivity: the initial value of 100MPa was reduced to 3kPa based on nanoindentation studies performed on brain tissues (see e.g. Gefen et al., 2003).

**Bone formation rate** This test further expanded on scenario II's approach by altering the rate of bone formation across various sutures. This was carried out into two additional tests.

Test 4 – Increased formation rate: Here, we increased the original suture formation radius from 0.1 mm to 0.2 mm across all the sutures.

Test 5 – Metopic and anterior fontanelle closure: Here, the complexity of test 4 was increased further. The bone formation rate across the metopic and anterior fontanelle was increased (i.e. 0.6 mm for each month) to replicate the early closure of these sutures. The metopic and the anterior fontanelle progressively closing from 4 months of age until closure is evident by 24 months (Teager et al., 2018; Pindrik et al., 2014). The rate specified for the bone formation across the craniotomy remained unchanged for both scenarios as specified in section 2.4.

**Bone formation method and effects of CSF** A comparison of both bone formation scenarios under both models was also undertaken to understand the effects our established CSF and various formation scenarios have on calvarial morphology and contact pressure outcomes across the ICV.

## **2.6 Analysis**

All simulations were subject to morphological comparison against the 76 months of age follow up CT data (See: Section 2.1) through a cross-sectional comparison and dimensional measurement of the length (from glabella to opisthocranium), width (between the left and right euryons) and height (from basion to bregma). All measurement and landmark placements were performed manually. The cephalic index (CI) was also calculated by multiplying the width against the height and dividing by one hundred. Bone formation rates were compared at various time points to establish the predicted sutures time of closure. A cross-sectional comparison and the level of contact pressure across the ICV was analyzed for both bone formation scenarios (Scenario I vs. II) under both models (Model I vs. II). Overall regional pressure across the ICV was measured to quantify areas of higher pressure.

## **3 Results**

### **3.1 Material properties**

There was a close match between all considered FE simulations (Test 1, 2 and 3) and the follow up CT skull morphology at 76 months of age (Figure 2). Minimal differences were observed across all material property sensitivities considered here, in terms of skull length, width and height measurements (Figure 2 and Table 2). Skull width and height measurements were lower than the follow up data while there was a close match between skull length measurement. Cephalic indexes of all considered sensitivity tests with respect to the changes in the material properties were in the range of 79.04-79.67 vs. the follow up CI of 86.62 (Table 2).

### **3.2 Bone formation rate**

Figure 3 compares the various bone formation rates (Baseline vs. Test 4 vs. 5) as detailed in section 2.5. All outcomes predict the closure of the craniotomy by 12 months of age. The coronal suture displays complete closure between 36-76 months.

The metopic, lambdoid and squamosal regions remain marginally open, with various regions displaying closure. The anterior fontanelle remains open during the entirety of the growth cycle. Test 4 displays a near-complete closure of all sutures by 36 months of age, disregarding the anterior fontanelle which, similarly to the baseline comparison, remains open for the duration. All other sutures were found to have closed by the final 76 months of age interval. Test 5 displays an accelerated closure of the anterior fontanelle and metopic suture compared to the previous outcomes, which completely closes between 12-36 months of age. A close morphological match was seen against the follow up CT across all tests as seen in Figure 2.

### **3.3 Bone formation method and effects of CSF**

Figure 4 represents the state of the various bone formation approaches at various ages. Figure 5 highlights the cross-sectional comparison of these bone formation approaches and the effects of CSF against follow up data with numerical measurements summarized in Table 3. Biparietal under-prediction and anterior over-prediction was observed in all outcomes. Model I approach (ie: CSF present) does not appear to have any major implications to morphological outcomes when compared to Model II's approach (i.e. CSF absent). Interestingly, despite the changes in modelling and formation method, there was no greatly varying impact on morphological outcomes, with all scenarios matching close to follow up data. This is further supported in the numerical measurements, where the length, width and height show an average of 159.9 mm, 129.7 mm and 129.1 mm, respectively. Cephalic index measurements ranged between 79.16-83.28 vs. follow up CI of 86.62 (Table 3).

Contact pressure mapping across the ICV surface is displayed in Figure 6, with the minimum, maximum and average pressure across each lobe region shown in Table 4. Incorporating CSF appears to only slightly reduce the average pressure across all regions. This is further supported by numerical outcomes, where the mean values do not vary more than 1MPa between all scenarios. The chosen method of bone formation appears to have a greater role in contact pressure outcomes than the intracranial content chosen, where the average pressure across all lobes doubles, with the frontal and occipital lobe displaying the greatest difference (4.21MPa – 4.33MPa and 4.49MPa - 4.52MPa, respectively). A change that is also evident across the represented contact pressure maps.



## 4 Discussion

There is a growing body of computational studies based on finite element method that are using this approach to optimize the clinical management of craniosynostosis. To the best of our knowledge, a few studies have carried out detailed sensitivity analysis to the choice of input parameters on the outcome of these models. In this study we investigated the impact of several key parameters on the outcome of a FE model, predicting calvarial growth in a patient-specific sagittal synostosis case. The identified parameters were changes in limited scenarios, based on what is perceived to be a reasonable estimate of their in vivo values based on the data in the literature, rather than a wide range of values for each parameter. Our results highlighted that pending the output parameter of interest (i.e. overall skull morphology after surgery or impact of surgical technique on the ICP pressure) the choice of input parameters can have a limited to major impact on the outcomes.

Considering the material property sensitivity tests performed here, our measurements showed the choice of craniotomies elastic modulus has the largest reduction on length (165.9 mm), width (129.9 mm) and height (128 mm) out of all the analyzed parameters (Table 2). Clinically craniotomies are gaps with 'no material' present at these gaps post-operatively unless a medical device such as plates or springs are used. In the modelling approach implemented here, craniotomies were virtually assumed to be a 'material' with low elastic modulus (i.e. low resistance to the applied forces). This approach allows us to model bone formation across the craniotomies that occur post-operatively. While a relatively low baseline elastic modulus was used in the initial models (i.e. 30 MPa similar to the suture properties and 100 times lower than the bone), our cross-sectional results highlight that the predicted skull morphology can be highly sensitive to this choice (Figure 2; red outline). This can be explained by the fact that the large displacements occur during the brain/ICP radial expansion across the craniotomies. Clinically (i) considering the operation modelled in this study, this closely replicates the purpose of these bitemporal craniotomies, which aims to increase the displacement of the bone mediolaterally while reducing anterior-posterior length (Rocco et al., 2012); (ii) this highlights that perhaps the number, position and orientation of craniotomies all contribute to the overall long term morphological outcomes of the surgery and variations observed.

During the natural development and following the surgical operation on craniosynostotic skulls, radial expansion of the skull occur hand in hand with bone formation across the sutures and craniotomies (Richtsmeier and Flaherty, 2013). We recently described a validated finite element-based approach to model the aforementioned phenomena in mice (Marghoub et al., 2019cunning). In the present study for the first time, we applied the same methodologies to model the calvarial growth following calvarial reconstruction. A key unknown in translating our methodology from mouse to human was the rate of bone formation in the human, hence, the sensitivity tests to this choice were performed in this study. Our results highlighted that this parameter does not have a major impact on the overall predicted morphology of the skull (see Figure 2 for light and dark blue outlines). Gradually increasing the elastic modulus of the whole sutures/craniotomies sections under scenario II (i.e. 'bulk bone formation') also led to a close match between the overall predicted morphology of the skull and the in vivo data (see Figure 5 and also Malde et al., 2020). However, the rate of bone formation (Test 4 and 5) has an impact on the predicted pattern and timing (age) of sutures and craniotomies closure (see Figure 3 e.g. for highlighted dash lines across the anterior fontanel). Studies observing calvarial CT imaging and measurements observe that the majority of the sutures close between 30-40 months of age while small gaps might be present at most of the sutures except the metopic throughout life (Opperman 2000; Lottering et al., 2016). In fact, the metopic and anterior fontanelle are suggested to fuse as early as 9 months of age (Hugh et al., 2001; Boran et al., 2018). Due to the lack of regular CT data for the patient considered here (that clinically is unethical to perform), detail validation of our predictions is challenging while overall it appears that regardless of the rate of bone formation the overall pattern of suture closures is similar to the in vivo data. With regards to the craniotomies, all comparisons present a complete closure by 9 months post-operative (12 months of age). This appears to match well with reported in vivo literature (e.g. Thenier-Villa et al., 2018). An important consideration when varying surgical techniques in which calvarial healing may prolong, which has been found to vary between different age groups and surgical methods (Hassanein et al., 2011; Thenier-Villa et al., 2018).

An alternative approach to the gradual bone formation approach described above is the 'bulk bone formation'. The latter is computationally far less expensive and can

model the changes in the overall stiffness of the sutures and craniotomies during the development or after surgery. This approach was used in our recent patient-specific modelling of calvarial growth (Malde et al., 2020). Our results here show that both methodologies can reasonably predict the overall morphology of the skull, however, these approaches lead to different levels of contact pressure across the brain/ICV. The gradual bone formation approach (i.e. scenario I) led to a lower level of contact pressure across the brain/ICV in comparison to the 'bulk bone formation' (i.e. Scenario II) approach (see Figure 6 and Table 4). Another important parameter that can alter the predicted patterns of contact pressure across the brain is the CSF. CSF was modelled here using solid elements with low elastic modulus (see supplement data for sensitivity tests to the impact of CSF elastic modulus on the contact pressure on the ICV). In vivo, CSF is obviously a fluid that plays a crucial role in nutrient transfusion across the brain with varied pressure during the development (see e.g. Moazen et al., 2016). Modelling the fluid-solid interaction at this interface was beyond the scope of this work. Yet, the sensitivity analysis performed here, considering its limitations, highlighted that CSF perhaps plays a smaller role on the level of contact pressure across the brain compared to the methods of bone formation during the calvarial growth/healing. Obviously, in vivo obstruction of CSF can lead to raised intracranial pressure with potential impacts on the brain that given the approach that was implemented here can be predicted by investigating the level of strain across the modelled CSF elements. Nonetheless, it may prove highly informative to investigate the contact pressures across different surgical techniques for the management of craniosynostosis and to correlate such results to the cognitive data (e.g. Chieffo et al., 2010; Bellew and Chumas, 2015; Hashim et al., 2014) to optimize management of craniosynostosis.

Perhaps the key limitations of the FE models and sensitivity tests described here are that: (1) the pattern of contact pressures on the brain/ICV was not validated and despite the efforts put into this work on including the effect of CSF further studies are required to advance our understanding of the in vivo level of loading at this interface; (2) the pattern of tissue differentiation across the sutures/craniotomies were not validated as such studies in human can be challenging. Nonetheless, given our previous studies in mice (e.g. Moazen et al., 2015), these predictions could be within the range of in vivo data; (3) bone was modelled as linear elastic homogenous material despite wide literature highlighting its anisotropy, variation in density, elastic modulus

and mineral heterogeneity (e.g. Renders et al., 2008). Nonetheless given that at early stages of development and following calvarial reconstructions major deformations occur at the sutures and craniotomies perhaps this assumption could be acceptable or at least based on our results here it seems to have a minimal impact on predictions of calvarial growth in the age range and considering the treatment that was modelled here; (4) there are still differences between the predicted morphology at 76 month and the in vivo data (see differences between the outlines shown in Figure 2 & 5) that can be e.g. due to manual deformation of the bones during the surgery that were not modelled in this study or the fact that our current modelling approach does not model facial growth that occur hand in hand with calvarial growth. Nonetheless, given the large deformation that the model has predicted i.e. about 72 months of growth considering all its limitations we think this a valuable model and approach that can be used in optimising treatment of craniosynostosis while advancing the methodologies implemented here.

In summary, the present study highlights how variations in material property, intracranial content, bone formation methods and various bone formation rates may affect outcomes in predicting sagittal craniosynostosis correction. The discussed factors provided in this study lays the foundation to simulate various surgical reconstructions and observing their outcomes in correcting sagittal craniosynostosis.

## **Disclosures**

The authors declare that the research was conducted in the absence of any commercial or financial relationships that could be construed as a potential conflict of interest.

## **Acknowledgements**

This work was supported by the Rosetrees Trust (A1899). We also thank the reviewers for their insightful comments on the earlier version of this manuscript.

## **References**

- Adigun O, Al-Dhahir M (2017). Anatomy, head and neck, cerebrospinal fluid. Florida: StatPearls Publishing, Treasure Island.
- Anatole S, Dekaban M (1977). Tables of cranial and orbital measurements, cranial volume, and derived indexes in males and females from 7 days to 20 years of age.

Annals of Neurology. 2:6. 485-491. doi: <https://doi.org/10.1002/ana.410020607>

Barbelto-Andres J, Bonfill N, Marce Nogue J, Bernal V, Gonzalez PN. (2020). Modeling the effect of brain growth on cranial bones using finite-element analysis and geometric morphometrics. *Surgical and Radiologic Anatomy*. 42. 741-748.

Bellew M, Chumas P (2015). Long term development follow up in children with nonsynodromic craniosynostosis. *Journal of Neurosurgery Paediatrics*. 16:4. 445-451. doi: 10.3171/2015.3.PEDS14567

Boran P, Oğuz F, Furman A, Sakarya S (2018). Evaluation of fontanel size variation and closure time in children followed up from birth to 24 months. *Journal of Neurosurgery*. 22. 323-329. doi: <https://doi.org/10.3171/2018.3.PEDS17675>

Chieffo D, Tamburrini G, Massimi L, Giovanni SD, Gainsanti C, Caldarelli M et al (2010). Long term neuropsychological development in single-suture craniosynostosis treated early. *Journal of Neurosurgery Paediatrics*. 5:3. 232-237. doi: 10.3171/2009.10.PEDS09231

Clouchoux C, Guizard N, Evans C, Plessis A, Limperopoulos C (2012). Normative fetal brain growth by quantitative in vivo magnetic resonance imaging. *American Journal of Obstetrics and Gynecology*. 206. 173e1-173e8. doi: 10.1016/j.ajog.2011.10.002

Coats B, Margulies S (2006). Material properties of human infant skull and suture at high rates. *Journal of Neurotrauma*. 23:8. 1222-1232. doi: 10.1089/neu.2006.23.1222

Cornelissen M, Ottelander Bd, Rizopoulos D, van der Hulst R, Mink van der Molen A, et al (2016). Increase of prevalence of craniosynostosis. *Journal of Craniomaxillofacial Surgery* 44. 1273–1279.

Cunningham M, Heike C (2007). Evaluation of the infant with an abnormal skull shape. *Current Opinion in Pediatrics*. 19:6. 645–651. doi: 10.1097/MOP.0b013e3282f1581a

Dolack ME, Lee C, Ru Y, Marghoub A, Richtsmeier JT, Jabs EW, Moazen M, et al. Computational morphogenesis of embryonic bone development: past, present, and future. In Niebur GL. (Ed.), *Mechanobiology – From Molecular Sensing to Disease*. Elsevier. 2020.

Gault D, Renier D, Marchac D, Jones BMM (1992). Intracranial pressure and intracranial volume in children with craniosynostosis. *Plastic and Reconstructive Surgery*. 45:5. 394-7. doi: 10.1097/00006534-199209000-00003

Gefen A, Gefen N, Zhu Q, Raghupathi R, Margulies S. (2003). Age-dependent changes in material properties of the brain and braincase of the rat. *Journal of Neurotrauma*. 11. 1163-77. doi: 10.1089/089771503770802853

474 Hashim P, Patel A, Yang J, Travieso R, Turner J, Losee J (2014). The Effects of whole  
475 vault cranioplasty versus strip craniectomy on long term neuropsychological outcomes  
476 in sagittal craniosynostosis. *Plastic and Reconstructive Surgery*. 134:3. 491-501. doi:  
477 10.1097/PRS.0000000000000420

478 Hassanein A, Couto R, Nedder A, Zielins E, Greene A (2011). Critical-size defect  
479 ossification: Effect of leporid age in a cranioplasty model. *Journal of Craniofacial*  
480 *Surgery*. 22:6. 2341-2343. doi: 10.1097/SCS.0b013e318232a71d

481 Hegazy A, Hegazy M (2018). Newborns' cranial vault: Clinical anatomy and authors'  
482 perspective. *International Journal of Human Anatomy*. 1:2. 2577-2579. doi:  
483 10.14302/issn.2577-2279.ijha-18-2179

484 Hugh V, Jayesh P, Parker E, Levine N, Francel P (2001). The timing of physiologic  
485 closure of the metopic suture: A review of 159 patients using reconstructed 3D CT  
486 scans of the craniofacial region. *Journal of Craniofacial Surgery*. 12:6. 527-532. doi:  
487 10.1097/00001665-200111000-00005

488 Isaac K, Meara J, Proctor M (2018). Analysis of clinical outcomes for treatment of  
489 sagittal craniosynostosis: a comparison of endoscopic suturectomy and cranial vault  
490 remodelling. *Journal of Neurosurgery Paediatrics*. 22. 467-474. doi:  
491 10.3171/2018.5.PEDS1846

492 Jin S, Sim K, Kim S (2016). Development and growth of the normal cranial vault: an  
493 embryologic review. *Journal of Korean Neurosurgical Society*. 59:3. 192–196.  
494 doi:10.3340/jkns.2016.59.3.192

495 Johnson D, Wilkie AOM (2011). Craniosynostosis. *European Journal of Human*  
496 *Genetics* 19. 369–376.

497 Kalantar-Hormozi H, Abbaszadeh-Kasbi A, Sharifi G, Davai N, Kalantar-Hormozi A  
498 (2019). Incidence of familial craniosynostosis among patients with nonsyndromic  
499 craniosynostosis. *Journal of Craniofacial Surgery*. 30. 514–517. doi:  
500 10.1097/scs.00000000000005419

501 Lam W, Ai V, Wong V, Leong L (2001). Ultrasonographic measurement of  
502 subarachnoid space in normal infants and children. *Pediatric Neurology*. 25:5. 380-  
503 384. doi: 10.1016/s0887-8994(01)00349-6

504 Lane L (1892). Pioneer craniectomy for relief of mental imbecility due to premature  
505 sutural closure and microcephalus. *JAMA*. 18. 49–50. doi:  
506 10.1001/jama.1892.02411060019001f

507 Lauritzen C, Davis C, Ivarsson A, Sanger C, Hewitt T (2006). The evolving role of  
 508 springs in craniofacial surgery: The first 100 clinical cases. *Plastic and Reconstructive*  
 509 *Surgery*. 121:2. 545-554. doi: 10.1097/01.prs.0000297638.76602.de  
 510 Lee C, Richtsmeier JT, Kraft RH (2017). A computational analysis of bone formation  
 511 in the cranial vault using a coupled reaction-diffusion strain model. *Journal of*  
 512 *Mechanics in Medicine and Biology* 17: 1750073.  
 513 Leong PL, Morgan EF (2008). Measurement of fracture callus material properties via  
 514 nanoindentation. *Acta Biomaterialia* 4:1569-1575.  
 515 Libby J, Marghoub A, Johnson D, Khonsari R, Fagan M, Moazen M (2017). Modelling  
 516 human skull growth: A validated computational model. *Journal of the Royal Society*  
 517 *Interface*. 14:130. 20170202. doi: 10.1098/rsif.2017.0202  
 518 Lieberman D (2011). *Evolution of the human head*. London: Harvard University Press.  
 519 Lo LJ, Chen YR (1999). Airway obstruction in severe syndromic craniosynostosis.  
 520 *Annals of Plastic Surgery*. 43:3. 258-264. doi: 10.1097/00000637-199909000-00006  
 521 Lun-Jou, Lo M, Yu-Ray C (1999). Airway obstruction in severe syndromic  
 522 craniosynostosis. *Annals of Plastic Surgery*. 43. 258-64. doi: 10.1097/00000637-  
 523 199909000-00006  
 524 Lottering N, MacGregor D, Alston C, Watson D, Gregory L (2016). Introducing  
 525 computed tomography standards for age estimation of modern Australian subadults  
 526 using postnatal ossification timings of select cranial and cervical sites. *Journal of*  
 527 *Forensic Sciences*. 61:1. 39-52. doi: 10.1111/1556-4029.12956  
 528 Magge S, Bartolozzi IV A, Almeida N, Tsering D, Myseros J, Oluigbo C et al (2019). A  
 529 comparison of endoscopic strip craniectomy and pi craniectomy for treatment of  
 530 sagittal craniosynostosis. *Journal of Neurosurgery Paediatrics*. 23: 708-714. doi:  
 531 10.3171/2019.1.PEDS18203  
 532 Malde O, Cross C, Lim CL, Marghoub A, Cunningham ML, Hopper RA et al (2020).  
 533 Predicting calvarial morphology in sagittal craniosynostosis. *Scientific Reports*. 10:3.  
 534 doi: 10.1038/s41598-019-55224-5  
 535 Malde O, Libby J, Moazen M (2019). An overview of modelling craniosynostosis using  
 536 finite element method. *Molecular Syndromology*. 10:1-2. 74-82. doi:  
 537 10.1159/000490833  
 538 Marghoub A, Libby J, Babbs C, Pauws E, Fagan MJ, Moazen M (2018). Predicting  
 539 calvarial growth in normal and craniosynostotic mice using a computational approach.  
 540 *Journal of Anatomy*. 232:3. 440-448. doi: <https://doi.org/10.1111/joa.12764>

541 Marghoub A, Libby J, Babbs C, Ventikos Y, Fagan MJ, Moazen M (2019).  
 542 Characterizing and modelling bone formation during mouse calvarial development.  
 543 Physical Review Letters. 122:4. 048103. doi:  
 544 <https://doi.org/10.1103/PhysRevLett.122.048103>  
 545 Mathijssen IMJ (2015). Guideline for care of patients with the diagnoses of  
 546 craniosynostosis: working group on craniosynostosis. Journal of Craniofacial Surgery  
 547 26. 1735–1807.  
 548 McPherson G, Kriewall T (1980). The elastic modulus of fetal cranial bone: a first step  
 549 towards an understanding of the biomechanics of fetal head molding. Journal of  
 550 Biomechanics. 13:1. 9-16. doi: 10.1016/0021-9290(80)90003-2  
 551 Microvic M, Zivkovic B, Bascarevic V, Mijalčić R, Rasulic L (2016). Triple square  
 552 extended osteotomies for treatment of scaphocephaly (Renier's "H" technique  
 553 modification). Neurosurgery Review. 39. 115-122. doi: [https://doi.org/10.1007/s10143-](https://doi.org/10.1007/s10143-015-0661-z)  
 554 [015-0661-z](https://doi.org/10.1007/s10143-015-0661-z)  
 555 Mitchell L, Kitley C, Armitage T, Krasnokutsky M, Rooks V (2011). Normal sagittal and  
 556 coronal suture widths by using CT imaging. American Journal of Neuroradiology.  
 557 32:10. 1801-1805. doi: <https://doi.org/10.3174/ajnr.A2673>  
 558 Moazen M, Peskett E, Babbs C, Pauws E, Fagan M (2015). Mechanical properties of  
 559 calvarial bones in a mouse model for craniosynostosis. PloS One. 10:5. 1–13. doi:  
 560 <https://doi.org/10.1371/journal.pone.0125757>  
 561 Moazen M, Alazmani A, Rafferty K, Liu ZJ, Gustafson J, Cunningham ML, et al (2016).  
 562 Intracranial pressure changes during mouse development. Journal of Biomechanics.  
 563 49:123-126.  
 564 Morriss-Kay G, Wilkie A (2005). Growth of the normal skull vault and its alterations in  
 565 craniosynostosis: insight from human genetics and experimental studies. Journal of  
 566 Anatomy. 207:5. 637-653. doi: 10.1111/j.1469-7580.2005.00475.x  
 567 Opperman LA (2000). Cranial sutures as intramembranous bone growth sites.  
 568 Developmental Dynamics. 485. 472–485.  
 569 Pindrik J, Ye X, Ji B, Pendelton C, Ahn E (2014). Anterior fontanelle closure and size  
 570 in full-term children based on head computed tomography. Clinical Pediatrics. 53:12.  
 571 1149-1157. doi: 10.1177/0009922814538492  
 572 Renders GA, Mulder L, Langenbach GE, Van Ruijven LJ, Van Eijden TM (2008).  
 573 Biomechanical effect of mineral heterogeneity in trabecular bone. Journal of  
 574 Biomechanics. 41:13. 2793-2798. doi: 10.1016/j.jbiomech.2008.07.009



575 Riahiinezhad M, Hajizadeh M, Farghadani M (2019). Normal cranial sutures width in  
576 an Iranian infant population. *Journal of Research in Medical and Dental Science*. 5:3.  
577 564-569.

578 Richtsmeier JT, Flaherty K (2013) Hand in glove: brain and skull in development and  
579 dysmorphogenesis. *Acta Neuropathol* 125. 469–489.

580 Rocco F, Knoll B, Arnaud E, Balnot S, Meyer P, Cuttarree H et al. (2012).  
581 Scaphocephaly correction with retrocoronal and prelambdoid craniotomies (Renier's  
582 "H" technique). *Child's Nervous System*. 28. 1327-1332. doi: 10.1007/s00381-012-  
583 1811-z

584 Sgouros S, Goldin JH, Hockley AD, Wake MJC, Natarajan K (1999). Intracranial  
585 volume change in childhood. *Journal of Neurosurgery*. 91. 610-616. doi:  
586 10.3171/jns.1999.91.4.0610

587 Simpson A, Wong AL, Bezuhly M (2015). Surgical comparison of nonsyndromic  
588 sagittal craniosynostosis. Concepts and controversies. *Annals of Plastic Surgery*.  
589 78:1. 103-110. doi: 10.1097/sap.0000000000000713

590 Teager S, Constantine S, Lottering N, Anderson P (2018). Physiological closure time  
591 of the metopic suture in south Australian infants from 3D CT scans. *Child's Nervous*  
592 *System*. 35. 329-335. doi: <https://doi.org/10.1007/s00381-018-3957-9>

593 Thenier-Villa J, Sanromán-Álvarez P, Miranda-Lloret P, Ramirez M (2011). Incomplete  
594 reossification after craniosynostosis surgery—incidence and analysis of risk factors: a  
595 clinical-radiological assessment study. *Journal of Neurosurgery Pediatrics*. 22. 120-  
596 127. doi: 10.3171/2018.2.PEDS1771 <https://doi.org/10.3171/2018.2.peds17717>

597 Weickenmeier J, Fischer C, Carter D, Kuhl E, Goriely A (2017). Dimensional,  
598 geometrical, and physical constraints in skull growth. *Physical Review Letters*. 118.  
599 248101.

600 Wolański W, Larysz D, Gzik M, Kawlewska E (2013) Modeling and biomechanical  
601 analysis of craniosynostosis correction with the use of finite element method.  
602 *International Journal of Numerical Methods in Biomed Engineering*. 29:9. 916-925.  
603 doi:10.1002/cnm.2506

604 You J, Jiang X, Hu M, Wang N, Shen Z, Li J et al (2010). The bone slot effect study of  
605 pi procedure for craniosynostosis correction plan based on finite element method. 3rd  
606 International Conference on Biomedical Engineering and Informatics. 605-608, doi:  
607 10.1109/BMEI.2010.5640019

608 **Tables:**

609 **Table 1: Material property and bone formation rate sensitivity summary. Note, “E” refers to elastic modulus, “U” refers to**  
610 **Poisson’s ratio and “NA” indicates no change from the Baseline model values.**

611

|                       | <b>Bone E<br/>(MPa), U</b> | <b>Suture E<br/>(MPa), U</b> | <b>Brain E<br/>(MPa), U</b> | <b>Craniotomy E (MPa),<br/>U</b> | <b>Suture formation rate<br/>(mm/month)</b>  |
|-----------------------|----------------------------|------------------------------|-----------------------------|----------------------------------|--|
| <b>Baseline model</b> | 3000, 0.3                  | 30, 0.3                      | 100, 0.48                   | 30, 0.3                          | 0.1  |
| <b>Test 1</b>         | 421, 0.22                  | NA                           | NA                          | NA                               | NA   |
| <b>Test 2</b>         | NA                         | NA                           | NA                          | 0.003, 0.3                       | NA   |
| <b>Test 3</b>         | NA                         | NA                           | 0.003, 0.48                 | NA                               | NA   |
| <b>Test 4</b>         | NA                         | NA                           | NA                          | NA                               | 0.2  |
| <b>Test 5</b>         | NA                         | NA                           | NA                          | NA                               | 0.2 and 0.6 for suture<br>and metopic/anterior<br>fontanelle, respectively.<br>Closure by 24 months. |

612

613

614

615

616 **Table 2: Material property and bone formation rate sensitivity measurements.**

617

|                               | Length (mm) | Width (mm) | Height (mm) | Cephalic Index |
|-------------------------------|-------------|------------|-------------|----------------|
| <b>Baseline model</b>         | 166.58      | 131.87     | 132.93      | 79.16          |
| <b>Test 1</b>                 | 166.9       | 132.97     | 132.43      | 79.67          |
| <b>Test 2</b>                 | 165.92      | 129.91     | 128         | 78.29          |
| <b>Test 3</b>                 | 166.52      | 131.62     | 132.87      | 79.04          |
| <b>Test 4</b>                 | 168.07      | 130.52     | 131.8       | 77.65          |
| <b>Test 5</b>                 | 169.56      | 131.3      | 131.57      | 77.43          |
| <b>Follow up at 76 months</b> | 166.17      | 143.94     | 137.23      | 86.62          |

618

619

620

621

622

623

624

625

626

627

628

629

630 **Table 3: Summary of various Cerebrospinal fluid (CSF) model under each respective bone formation method.**

631

| Bone formation method:        | Model    | Length (mm) | Width (mm) | Height (mm) | Cephalic Index |
|-------------------------------|----------|-------------|------------|-------------|----------------|
| <b>Scenario I</b>             | Model I  | 160.97      | 129.46     | 122.18      | 80.42          |
|                               | Model II | 166.58      | 131.87     | 132.93      | 79.16          |
| <b>Scenario II</b>            | Model I  | 155.86      | 129.81     | 128.31      | 83.28          |
|                               | Model II | 160.95      | 132.52     | 132.96      | 82.52          |
| <b>follow up at 76 months</b> |          | 166.17      | 143.94     | 137.23      | 86.62          |

632

633

634

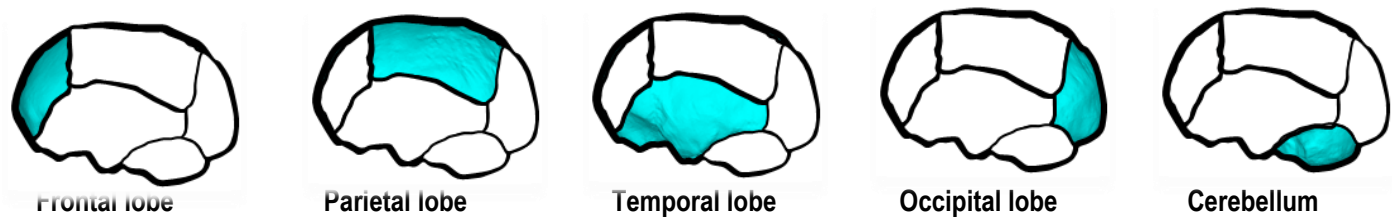
635

636

637

638

639    **Table 4: Summary of intracranial contact pressure outcomes across each region of interest. Values are in MPa.**

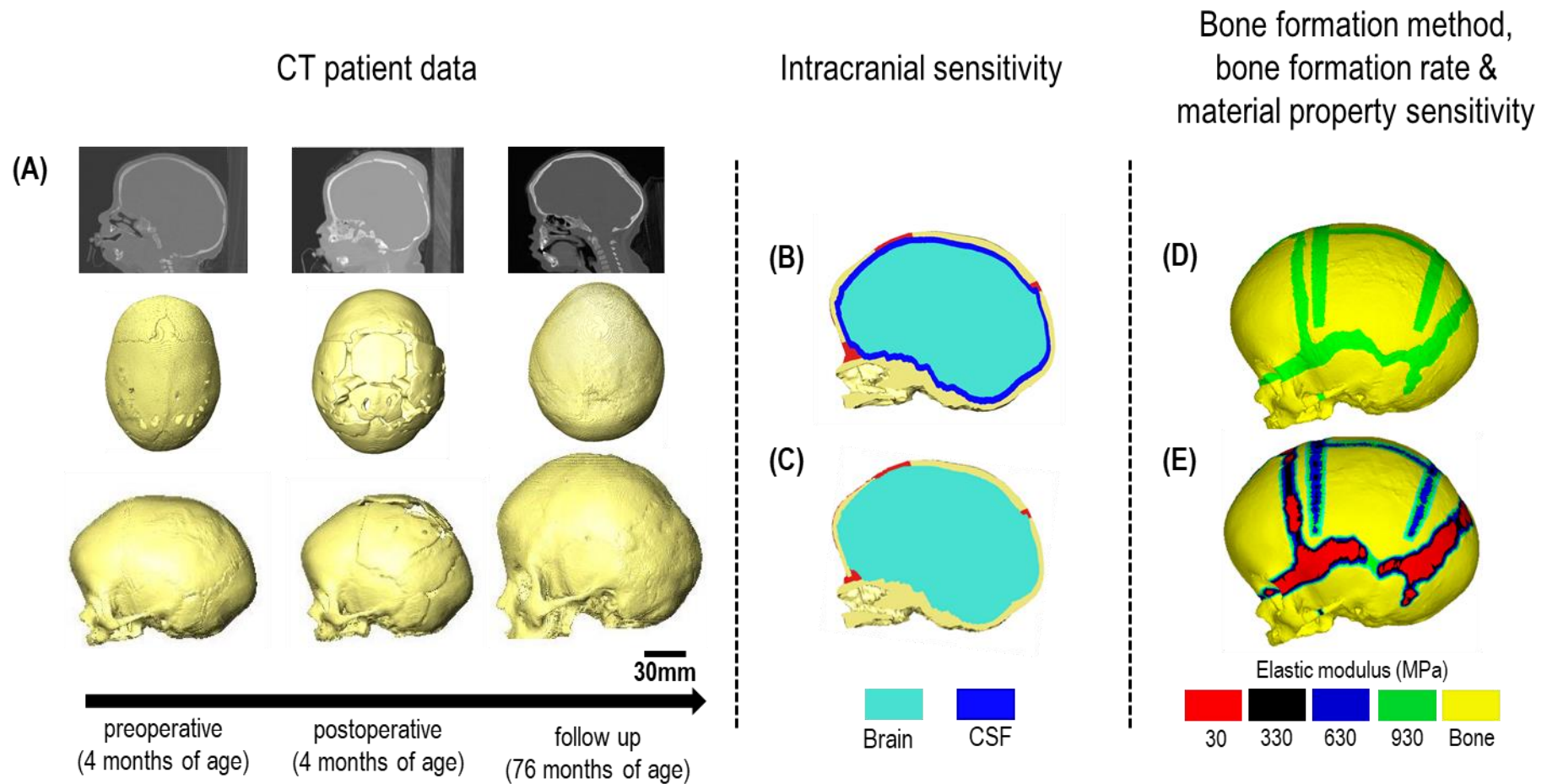


| Bone formation method: | Model    | Min | Max   | Mean | Min | Max   | Mean | Min | Max   | Mean | Min | Max   | Mean | Min | Max   | Mean |
|------------------------|----------|-----|-------|------|-----|-------|------|-----|-------|------|-----|-------|------|-----|-------|------|
| Scenario I             | Model I  | 0   | 17.36 | 1.65 | 0   | 20.82 | 2.19 | 0   | 20.61 | 1.83 | 0   | 22.94 | 1.45 | 0   | 17.49 | 2.17 |
|                        | Model II | 0   | 15.40 | 2.29 | 0   | 18.62 | 2.68 | 0   | 22.63 | 2.33 | 0   | 16.95 | 1.87 | 0   | 20.46 | 2.86 |
| Scenario II            | Model I  | 0   | 8.83  | 5.98 | 0   | 10.97 | 5.69 | 0   | 18.55 | 5.66 | 0   | 11.37 | 5.94 | 0   | 11.61 | 6.64 |
|                        | Model II | 0   | 18.58 | 6.41 | 0   | 23.28 | 6.08 | 0   | 20.82 | 6.06 | 0   | 31.57 | 6.39 | 0   | 31.98 | 6.88 |

640  
641  
642  
643

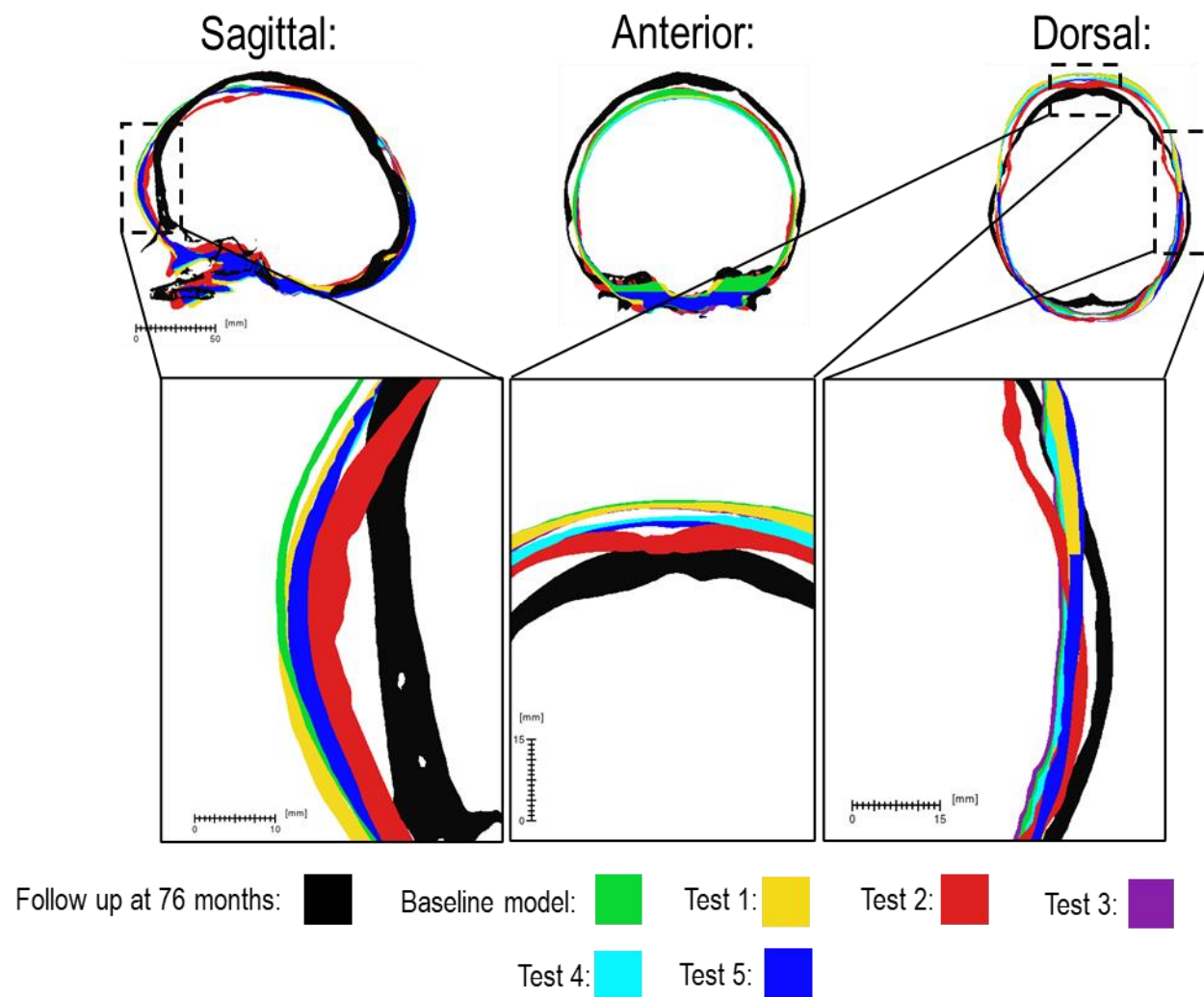
644 **Figures:**

645 **Figure 1: Workflow of the study. CT images of a patient are obtained at various treatment stages (A) The preoperative CT is**  
646 **used for image processing and 3D reconstruction. Two intracranial volume models (B-C) were then compared under**  
647 **differing bone formation methods (D-E).**



648

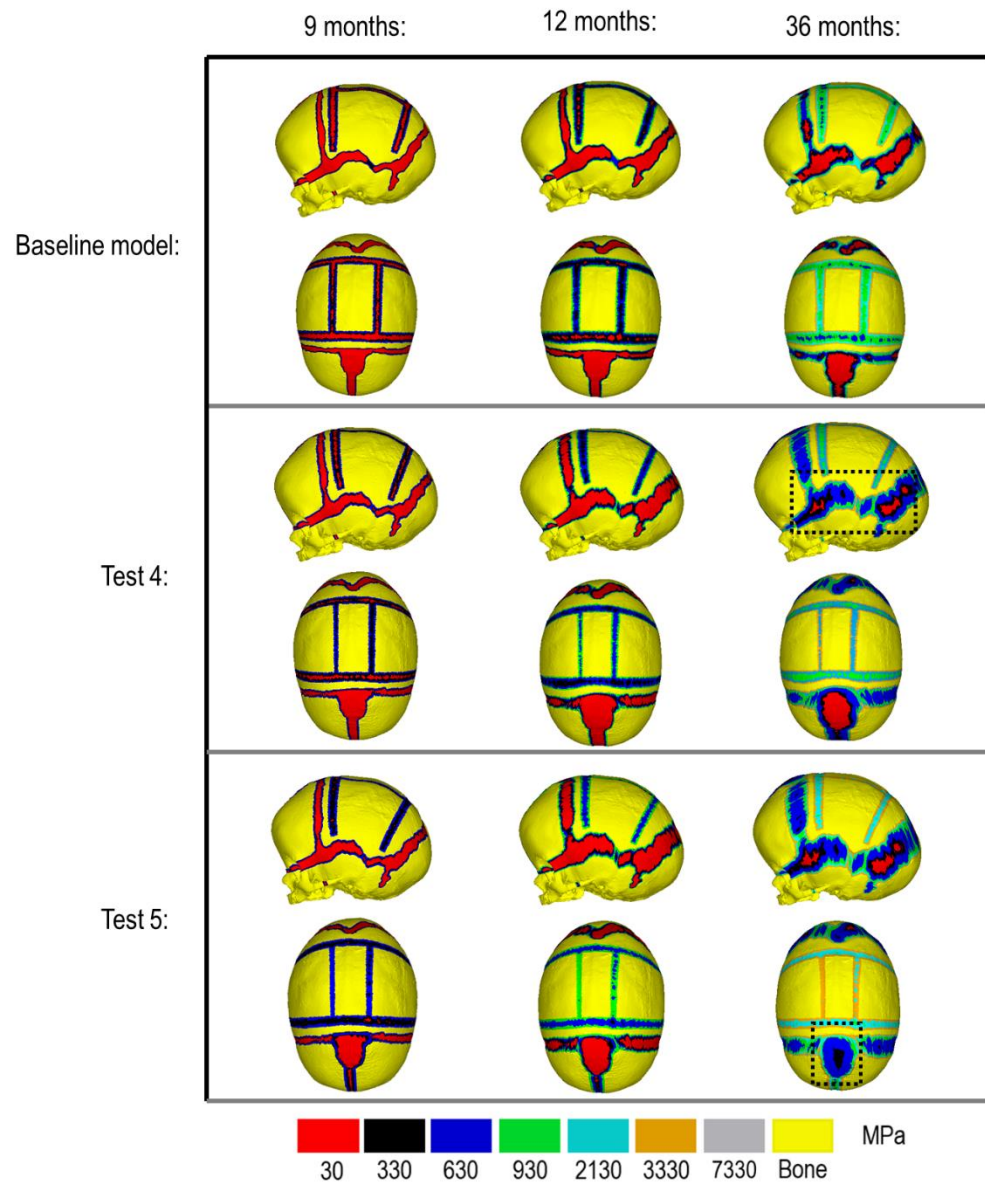
649 **Figure 2: Material property and bone formation rate sensitivity cross-sections vs. follow up at 76 months of age. Dashed**  
 650 **boxes indicate enhanced regions of interest.**



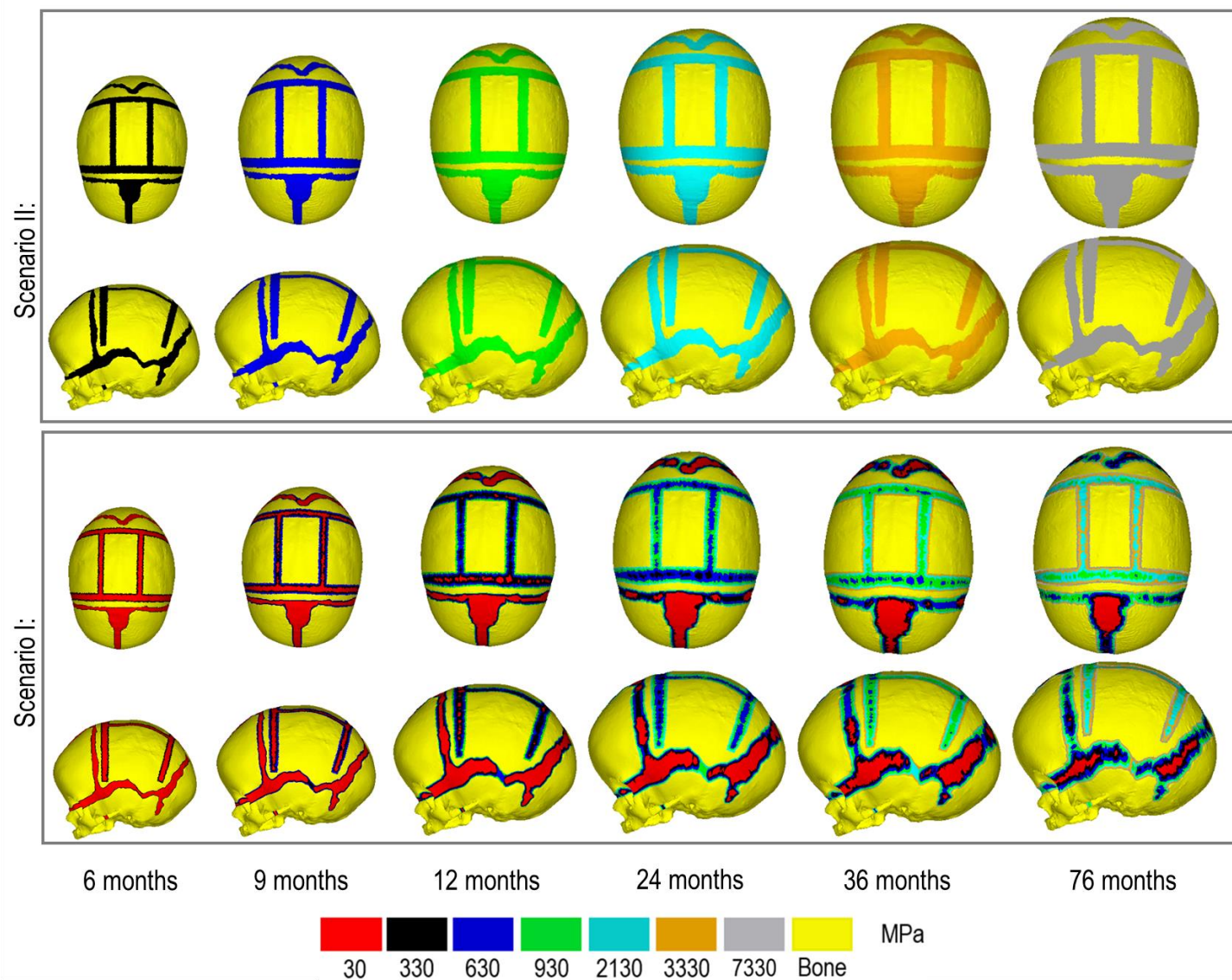
651

652 **Figure 3: Bone formation rate sensitivity at various stages, sagittal and dorsal views.**

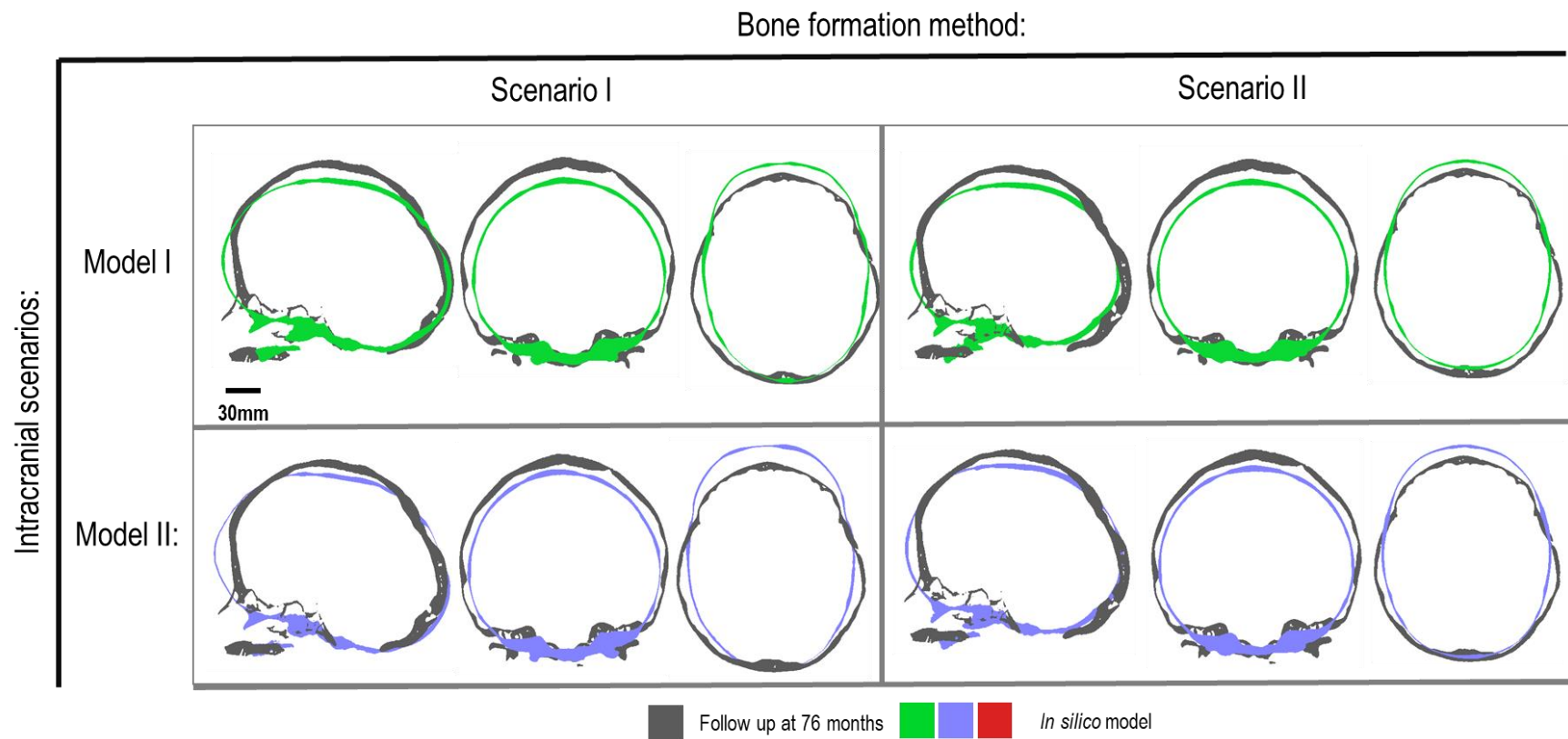




654 **Figure 4: Bone formation methods under scenario I (bottom) and scenario II (top) during calvarial growth, sagittal and dorsal**  
655 **views. (1:1 scale).**



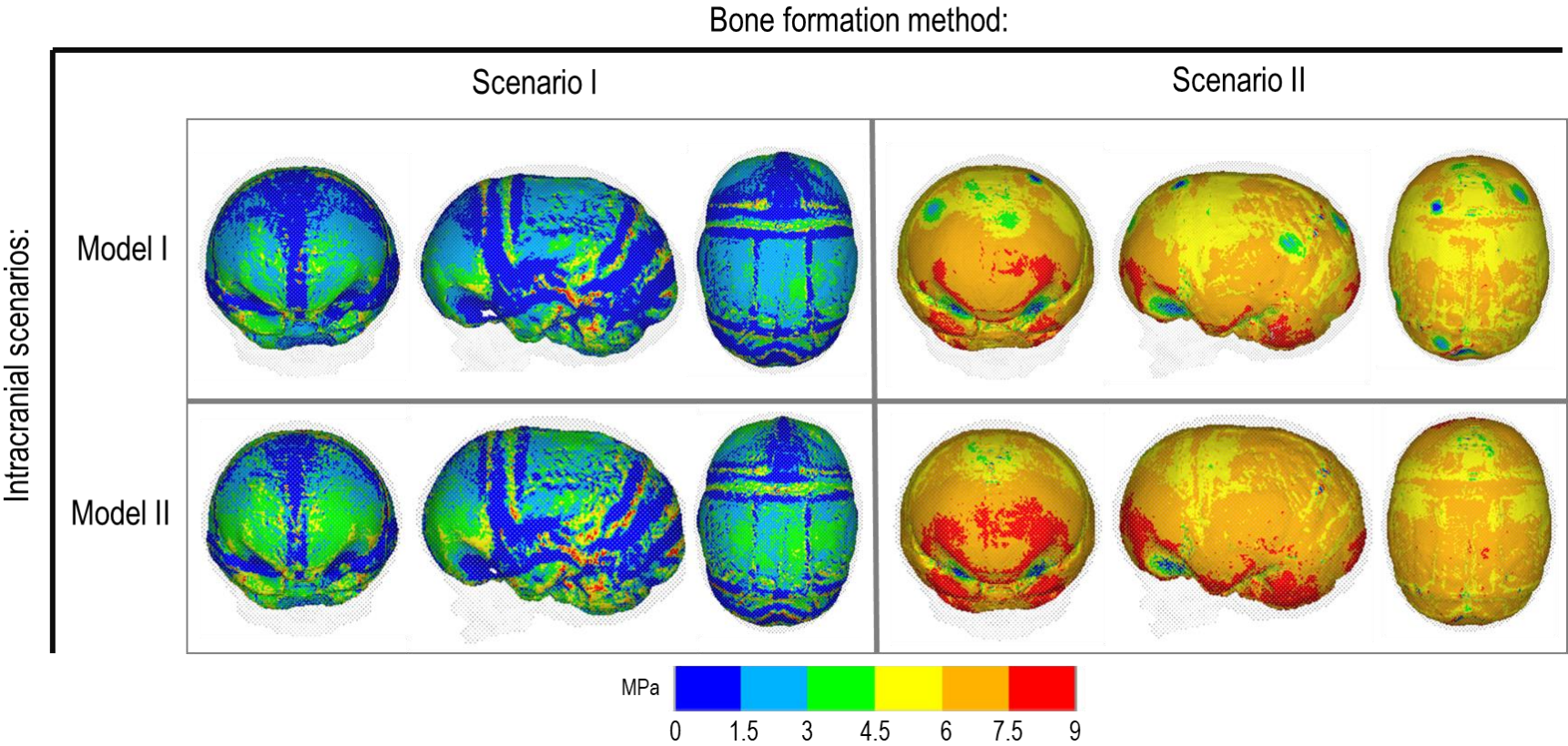
657 **Figure 5: Cross-section analysis of intracranial scenarios (Model I & II) against both bone formation methods (Scenario I &**  
658 **II) at 76 months of age. Showing sagittal, anterior and dorsal planes.**



659  
660  
661  
662  
663



664 **Figure 6: ICV pressure map at 76 months of age. Showing the dorsal, sagittal and anterior views.**



665

# Predicting and comparing three corrective techniques for sagittal craniosynostosis

Connor Cross<sup>1</sup>, Roman H Khonsari<sup>2</sup>, Dawid Larysz<sup>3</sup>, David Johnson<sup>4</sup>, Lars Kölby<sup>5</sup>,  
Mehran Moazen<sup>1</sup>

<sup>1</sup>Department of Mechanical Engineering, University College London, London, UK

<sup>2</sup>Department of Maxillofacial Surgery and Plastic Surgery, Necker – Enfants Malades University Hospital, Assistance Publique – Hôpitaux de Paris; School of Medicine, University of Paris; Paris, France

<sup>3</sup>Department of Head and Neck Surgery for Children and Adolescents. University of Warmia and Mazury in Olsztyn. Ul. Żołnierska 18a, 10-561 Olsztyn, Poland

<sup>4</sup>Oxford Craniofacial Unit, Oxford University Hospital, NHS foundation trust, Oxford, UK

<sup>5</sup>Department of Plastic Surgery, Sahlgrenska University Hospital, The Sahlgrenska Academy, University of Gothenburg, Gothenburg, Sweden

## Correspondence:

Mehran Moazen, Ph.D.

Email: [m.moazen@ucl.ac.uk](mailto:m.moazen@ucl.ac.uk)

**Keywords:** Biomechanics, Sagittal craniosynostosis, Spring assisted cranioplasty, Modified strip cranioplasty, Finite element method, Calvarial growth, Bone formation

## Abstract: 199 words

Sagittal synostosis is the most occurring form of craniosynostosis, resulting in calvarial deformation and possible long term neurocognitive deficits. Several surgical techniques have been developed to correct these issues. Debates as to the most optimal approach are still ongoing. Finite element method is a computational tool that's shown to assist with the management of craniosynostosis. The aim of this study was to compare and predict the outcomes of three reconstruction methods for sagittal craniosynostosis. Here, a generic finite element model was developed based on a patient at 4 months of age and was virtually reconstructed under all three different techniques. Calvarial growth was simulated to predict the skull morphology and the impact of different reconstruction techniques on the brain growth up to 60 months of age. Predicted morphology was then compared with *in vivo* and literature data. Our results show a promising resemblance to morphological outcomes at follow up.

Morphological characteristics between considered techniques were also captured in our predictions. Pressure outcomes across the brain highlight the potential impact that different techniques have on growth. This study lays the foundation for further investigation into additional reconstructive techniques for sagittal synostosis with the long term vision of optimizing the management of craniosynostosis.

## **1. Introduction**

Sagittal craniosynostosis is the result of the premature fusion of the sagittal suture, with an occurrence rate of 1 in every 10,000 live births [1-4]. It is the most common form of craniosynostosis, with several studies reporting a significant increase in its presents over the last 30 years [5, 6]. Raised intracranial pressure, potentially leading to cognitive impairment has been related to the calvarial deformation [7, 8, 3]. The first corrective techniques were developed in the late 19<sup>th</sup> century to restore the normative skull shape [9, 10]. In recent times, craniofacial centres have adopted a number of techniques. These range from strip craniotomy (removal of the fused suture) and total calvarial remodelling (reshaping of bone) to spring assisted cranioplasty (bone widening using springs) and helmet therapy (postoperative skull shaping) [11-15]. As a result, the most optimum method of treatment and their respective outcomes are still debated among craniofacial surgeons [16-20].

Finite element (FE) method is a powerful computational tool used to analyse a wide range of engineering solutions [21]. Recently, FE studies have investigated the management of craniosynostosis [22-26]. Advanced methods have accurately simulated calvarial growth and bone formation in developed models [27-32]. Such methods have the potential to investigate the biomechanics of craniosynostosis and predict various sagittal synostosis outcomes under a range of reconstructions. However, validating our approach with pre-existing data is critical for building confidence in our FE predictive results [33].

The aim of this study was to investigate the potential biomechanical differences between three corrective techniques used for the management of sagittal craniosynostosis i.e. two variations of spring-assisted cranioplasty (SAC) vs. modified strip craniotomy (MSC) using a generic FE approach. The primary intention for this research was to directly compare the spring vs. the strip techniques since from a biomechanical point of view the main difference between these techniques are the width of craniotomy and the presence or absence of the springs.

## **2. Materials and methods**

A preoperative generic 3D model of a sagittal craniosynostosis patient at 4 months of age was developed based on computed tomography (CT) data. This generic model was then virtually reconstructed based on two variations of spring-assisted cranioplasty (SAC) and the modified strip craniotomy (MSC). Post-operative calvarial growth was modelled using the FE method. Given the importance of validation of the computational models, results obtained from the SAC methods were compared versus a series of *in vivo* CT data while results obtained from the MSC technique were compared vs. published data in the literature. The overall morphology of the skull, spring displacement, the pattern of bone formation across the calvarial, and the level of contact pressure that each technique imposes on the growing brain (here, the intracranial volume) was investigated post-operatively. Note the generic preoperative model used in this study was described and validated in detail elsewhere [34].

**Surgical techniques:** *Spring-assisted cranioplasty (SAC):* The SAC procedure and parameters replicated in this study were based on the standard Gothenburg procedure, as detailed by Lauritzen et al., [10] and more recently by Satanin et al., [35]. A 1 mm wide craniotomy, extending from the anterior fontanelle to lambdoid suture was performed. Two holes were burred approximately 15 mm apart, across the craniotomy for spring placement (Figure 1A). These were performed 40 mm (anterior spring), 55 mm (middle spring – for 3 SAC) and 75 mm (posterior spring) from the coronal suture. The quantity of springs used can vary between two (i.e. 2 SAC) and three (i.e. 3 SAC). *In situ* spring displacement of approximately 5 mm occurs naturally (denoted as: ‘release’), allowing for mediolateral widening upon insertion of the springs (Figure 1B). These were then removed in a secondary procedure 5 months post-insertion (Figure 1C). After which, calvarial growth continued unaided (Figure 1D).

*Modified strip craniotomy (MSC):* For our comparative technique, we reconstructed the procedure described by Thomas et al., [13]. In brief, A 50 mm wide vertex craniotomy was created across the anteroposterior, extending from coronal to lambdoid.

**Image processing:** A previously described model was used for this study [34]. In short, CT data of a preoperative sagittal synostosis patient at 4 months of age was obtained from the Hôpital Necker – Enfants Malades Craniofacial Surgery Unit (Centre de Référence Maladies Rares Craniosténoses et Malformations Craniofaciales CRANIOST, Paris, France). Full ethical protocol for undertaking this study was approved by the institutional review board and committee from the Necker – Enfants Malades University Hospital. Informed consent was granted from the patient’s guardian. All patient information was anonymized prior to the



retrieval of CT data in accordance with the HIPAA (1996). Image resolution was measured at 0.625 x 0.625 mm. Full consent was granted by the child's guardians for the purposes of this study. The image processing package, Avizo (V9.2.0; Thermo Fisher Scientific, Mass, USA) was used for 3D model development. The calvarial bone, sutures, and intracranial volume (ICV i.e. all internal calvarial components) were all segmented in preparation for FE simulations. Calvarial bone was automatically highlighted using the Hounsfield scale method. Sutures and ICV were highlighted manually. The detailed 2 SAC, 3 SAC and MSC craniotomies, based on the techniques described above, were then replicated on the preoperative model prior to calvarial growth.

**Finite element analysis:** A quadratic tetrahedral mesh consisting of 4 million elements in total was selected after a mesh convergence study. Where 3,100,000 elements were used to mesh the bone, sutures, and craniotomy based on the von Mises strain and 900,000 elements were used to mesh the ICV based on the contact pressure. Mesh convergences was seen to have been achieved once both the strain and pressure values had plateaued by  $\pm 5\%$ . Alterations to individual element geometries were performed to reduce the initial penetration between elements and decrease the aspect ratio. The fully meshed model was then imported into the FE package, ANSYS (V19.0; Canonsburg, PA, USA), to simulate calvarial growth, bone formation and contact between the ICV-inner calvarial interface. All materials were defined as linear isotropic. Bone, ICV, suture and craniotomy properties were assigned an elastic modulus of 421MPa, 10MPa, 30MPa and 0.3MPa, respectively [32, 34, 36, 37]. Sensitivity tests were carried out which varied these stiffnesses initially (see: Supplementary Table S1 & S2) to achieve the target craniotomy widening (i.e. approx. 5 mm) seen after spring 'release'. Both the ICV and craniotomy Poisson's ratio was selected as 0.1. A Poisson ratio of 0.3 was selected for the bone and sutures.

**Boundary conditions:** A Hertzian frictional contact method was used to predict pressure changes across the ICV-inner calvarial interfaces, as previously implemented by Malde et al., [32]. To summarise, a penalty-based surface to surface contact was established with a normal contact stiffness of 50 N/mm, a penetration tolerance of 0.5 mm and a normal/tangential friction coefficient of 0.1 to reduce the level of penetration. These surfaces were initially in contact, which then allowed the freedom of movement in the normal/tangential direction during skull growth. All bone-suture, bone-craniotomy and craniotomy-suture interfaces were assumed to be in bonded contact, with no relative motion or separation authorised. Nodal constraints were placed around the foramen magnum and across the nasal ridge in all degrees of freedom to avoid rigid body motion. Thermal expansion analogy was used to model the ICV growth as previously described by Libby et al., [31]. Here, the ICV was increased from the initial preoperative volume (measuring 659 ml) to the target *in vivo* follow

up volume in five load-steps for both SAC (i.e.1240 ml) and six for MSC (i.e. 1376 ml). The predicted target volumes were correlated with values seen in the literature to estimate the age of the model at each load-step [38].

*Bone formation:* A previously described algorithm detailed by Marghoub et al., [28] was implemented to simulate the bone formation at the sutures and craniotomies during calvarial growth. In brief, elements were selected at a specified radius along the bone-suture/bone-craniotomy linings. The elastic modulus of these newly and previously selected elements was increased by 100 MPa for each month of growth. The elastic modulus of bone was also increased by 125 MPa for each month of growth. These changes in the elastic modulus of the bone/newly formed bone were estimated based on extrapolation of the bone properties that were measured during the development of normal mouse [37] to human (considering ICV growth). A radius of 0.2 mm for every month of calvarial growth was selected for the coronal, lambdoid and squamosal suture formation based on observations in literature [39, 40] and prior sensitivity studies [34] to predict the timing of closure. The metopic suture and anterior fontanelle were set to completely form by 24 months of age to represent the *in vivo* scenario [41, 42]. A sensitivity study was carried out to investigate the morphological effect of different rates for bone formation at the craniotomies (see: Supplementary Table S3 & Figure S1). Following these sensitivity tests, a rate of 10.8 mm per month of growth was specified for the rate of calvarial healing. After each load-step, the geometry of the skull, displacement across the springs length and forces were updated to the newly deformed shape and values, respectively, which was then used to estimate the morphology of the skull at the next step/age. No adaptive remeshing algorithm was used here, as the geometry was updated at each interval. This approach avoided element distortions that would have otherwise occurred due to the large deformations occurring.

*Spring mechanics:* To replicate the characteristics of the SAC, linear spring elements (i.e., COMBIN14) were positioned approximately 15 mm across the craniotomy at insertion (i.e. 5mm from the craniotomy into the parietal bone on either side plus the 5mm gap between equalling to a total of 15mm – see Figure 1A). These elements behave under Hookean law, where the outward force was directly proportional to the level of tension/compression [26, 43]. Here, a series of *in vitro* measurements were carried out to identify the force-length relationship of the springs (See Appendix S6). In short, an average force of 8 N was produced when crimping a wire initially measuring 100 mm to 15 mm (based on leg-to-leg

measurements – See: Figure 1A). These values were used to calculate the spring stiffness (K) at ‘release’ using Equation 1:

$$(1) K = f/dx$$

Where  $f$  represents the bilateral force and  $dx$  represents the change in spring displacement (here initially, 100 mm minus 15 mm). A sensitivity test was carried out to investigate the effect of altering the initial spring force values by updating the spring stiffness on the predicted morphology (see: Supplementary Table S4 & S5). During ‘release’ and calvarial growth, spring forces and spring leg distances values were automatically calculated and updated using Equation 2:

$$(2) f = K * dx$$

Upon removal, the modelled springs were given a fixed force of 0 N. The growth then continued unaided to the target follow up age. Note that the spring stiffness remained unchanged throughout all simulations.

*Simulation and measurements:* Both SAC and MSC techniques underwent calvarial growth up to the follow up ages of 36 and 60 months, respectively. Both predicted SAC calvarial morphologies were compared against a series of patient CT data sets undergoing the standard Gothenburg SAC procedure and retrieved from the Department of Plastic Surgery at the Sahlgrenska University Hospital (Gothenburg, Sweden). Full ethical protocols for undertaking this study were reviewed and approved by the institutional review board and committee at the Department of Plastic Surgery at the Sahlgrenska University Hospital. Informed consent was granted from all patient’s guardians. All patient CT information provided was anonymized in accordance with the Health Insurance Portability and Accountability Act of 1996 (HIPAA). CT data was grouped in accordance with the number of springs used for the treatment and classified as 2 SAC (n=10) and 3 SAC (n=8), respectively. The preoperative CT for both groups were taken at a mean age of  $4.9 \pm 1.3$  and  $4.1 \pm 0.7$  months, respectively. Post-operative CT was taken at  $10 \pm 1.3$  months of age, where the springs were removed. Follow up CT was taken at  $36 \pm 2.0$  months of age. Predicted MSC morphology was compared against reported CI outcomes of the same technique detailed by Thomas et al., [13] as CT data for this technique was unavailable for direct morphological comparisons. Measurements of the length (from glabella to opisthocranium), width (between the left and right euryons) and circumference were undertaken. The cephalic index (CI) was calculated by multiplying the width against the length and dividing by one hundred. 3D distance mapping was also used to observe predicted under- or over-estimation vs. the CT

data provided. Our predicted morphology was compared against a single CT skull that matched closest to the overall mean length/width measurements within both SAC groups. The predicted spring opening was measured during skull growth and compared against CT data at 9 months of age by manually measuring the leg-to-leg distance against each CT patient data using the aforementioned image processing software. Predictive bone formation was recorded throughout our simulations to observe differences in suture and craniotomy closure times between techniques. Contact pressure across the ICV surface was recorded to observe the effects each considered technique had on the brain (here ICV) growth.

### 3. Results

**Morphological comparisons:** Table 1 provides a summary of the *in vivo* CT and predicted measurements corresponding to each technique at different ages. At preoperative, the 4 months of age model used for the FE simulations measured a skull length, width, circumference, ICV and cephalic index of 137.2 mm, 108.1 mm, 430.6 mm, 659.9 ml and 78.7, respectively. The average age of patients who were treated with 2 SAC, 3 SAC (from our CT data) and MSC (from the literature [13]) were  $4.9 \pm 1.3$ ,  $4.1 \pm 0.7$  and 6 months (range: 3.1-9.5), respectively with corresponding CI of  $76.9 \pm 2.7$ ,  $74.3 \pm 3$  and  $65.7 \pm 4.7$ .

At the post-operative stage, the FE model predicted CI's of 78.5, 79.7 and 78.8 at 9 months of age and 74.6, 74.1 and 80.3 at 36 months of age for the 2 SAC, 3 SAC and MSC technique, respectively. At 12 months of age, CI of 81.1 was predicted for MSC. The *in vivo* CT and literature [13] CI measurements were  $79.9 \pm 2.9$ ,  $78.2 \pm 4.5$  and  $73.3 \pm 5.2$ , at 9-12 months of age, and  $76.4 \pm 2.5$ ,  $74.3 \pm 3.8$  and  $71.5 \pm 4.3$  at 36 months of age for the 2 SAC, 3 SAC and at 60 months of age for the MSC, respectively. Hence, while the FE model captured the post-operative relapse in the SAC techniques, it failed to capture the relapse in the MSC technique (Figure 2).

**Spring opening:** Increased spring opening from insertion (15.2 mm) to 'release' (19.5 mm) was predicted in both SAC techniques, which in turn lead to a 5 mm widening of the craniotomy (Figure 3). By 9 months of age, FE models under-predicted the spring opening data observed *in vivo* in the anterior (29.2 mm; 31.1 mm vs.  $45.5 \pm 10.5$  mm;  $39.0 \pm 8.5$  mm), central (31.9 mm vs.  $43.1 \pm 5.0$  mm) and posterior springs (29.2 mm; 31.3 mm vs.  $51.4 \pm 8.9$  mm;  $42.3 \pm 3.7$  mm).

3D displacement mapping results highlight the under- and over-prediction at several ages for both 2 SAC and 3 SAC techniques (Figure 4 & 5, respectively). Note that preoperative CT data is compared against the predictive release morphology. An under-prediction of the

anterior and posterior regions was evident from release to post-operative (i.e. 9 months) across both techniques. By follow up (i.e. 36 months), a good morphological match was observed, with minimal under-prediction across the mediolateral.

**Bone formation:** Predicted bone formations and overall calvarial morphologies are shown in Figure 6. At 9 months of age, both SAC techniques predicted complete closure of the craniotomy, while MSC showed large areas of patency. All sutures showed little formation by this age. By 36 months of age, bone was formed across all the sutures in all considered techniques, with some patency observed at the lambdoid suture in the SAC method. By this time, new bone was formed at the MSC craniotomy, with all sutures showing complete closure and narrowing compared to the SAC outcomes. Comparing the overall predicted morphology of the skull at 36 months of age between both SAC and MSC techniques highlighted the larger anteroposterior growth of the skull in the SAC technique in contrast to the larger dorsoventral growth of the skull in the MSC technique.

**Contact pressure:** Brain growth and contact pressure across the ICV at different ages are shown in Figure 7. When simulating spring release, pressure changes were negligible. At 9 months of age, greater pressure was observed across the ICV in both SAC vs. MSC. At 36 months of age, an even distribution of the pressure was observed in the SAC vs. MSC. Greater concentration of high pressure was observed at the anterior, mediolateral and across the anterior fontanelle in MSC while both SAC techniques highlighted minor elevated levels of pressure at the mediolateral sides of the skull in the temporal regions.

#### 4. Discussion

Many variations of sagittal craniosynostosis correction exist, ranging from invasive to non-invasive procedures [14]. Large debates over the optimal outcome between techniques are still ongoing. Since the mid-20<sup>th</sup> century, computational models using finite element (FE) method have been widely used to investigate the biomechanics of a range of clinical conditions and their managements [44-46]. FE shows promise in assisting with the management of various forms of craniosynostosis [33]. In this study, we attempted to illustrate the use of FE method in which the biomechanics of three corrective techniques were compared. Morphological outcomes were compared against our own CT data used for this study and literature data at various postoperative and follow up time points. Our results highlight the potential impact of the surgical techniques on the overall morphology of the skull, the pattern of bone formation across the craniotomies and other sutures as well as the

pressures that they may apply across the whole intracranial volume. The work here shows promising perspectives in optimizing the management of craniosynostosis.

**Morphological comparisons:** Our results under-predicted changes in skull length and width in predictive vs. *in vivo* data. This could have been attributed to predicted ICV measurements, particularly at postoperative time points. The simulations were run by increasing the ICV to an 'average' value at a specific age based on the literature and our previous studies [34, 38]. However, when comparing the FE results vs. the average ICV of the patients considered in this study at 9-12 months of age, there was a 20% difference between the two (based on the SAC technique). This could explain the large under-predictions in morphological outcomes at this age range. A closer match was achieved at 36 months, as this variation (between the *in silico* and *in vivo* ICVs) was seen to reduce to 1% (based on the SAC technique). This closer match in volume by 36 months may be attributed to the reduction in growth seen after the first year of life vs. our predicted linear growth in this study. One could argue that the preoperative CT data from our SAC cohort could have been used to develop a FE model for a true validation of the FE results. However, we considered (1) using a generic model to compare different surgical techniques (2) to keep a level of consistency regarding the preoperative morphology between our compared techniques shown here and thus, chose to utilize our previously validated FE model [34]. The CI was seen to vary slightly from the preoperative period to the time of spring removal in predictive and CT data (Figure 2). By 36 months, there was a reasonable match between the *in silico* and *in vivo* data. Although a more significant relapse was seen in predictive outcomes, it is interesting to see this postoperative pattern being accurately predicted. Further, the antero-posterior growth vector of the skull observed post-operatively in the SAC technique *in vivo* was also captured by the *in silico* FE results (Table 1).

Reported data for MSC by Thomas et al., [13] was limited for the present study. Nevertheless, a comparison of CI was undertaken to highlight the potentials as well as the limitations of our modelling approach. Greater changes were seen in reported *in vivo* data vs. our predicted data. Further, our predicted CI at 60 months of age overpredicted what was clinically observed in the study [13] (see Figure 2C). The differences between the *in vivo* and *in silico* results here could be due to a number of factors e.g. (1) the initial CI of the patient that we used to develop the FE models was considerably higher than the average preoperative CI of the patients considered in the study of Thomas et al., [13] (i.e. 78.7 vs. 65.7). The preoperative CI has indeed been shown to be clinically a major factor in determining the postoperative

outcomes [13]; (2) there could have been minor surgical technical details that have not been captured in the simulations performed here; (3) It is also possible that the ICV of the patients in the study of Thomas et al., [13] were lower than the 'average' values that were used in the FE simulations to model skull growth in the present study. Nevertheless, we believe that the virtual comparative nature of the assessments made between the different techniques considered here is interesting and valuable. Allowing our predictions to determine the growth under two extreme conditions (i.e. 5 mm vs. 50 mm craniotomy). Our predictions, considering their limitations, highlights that SAC technique can perhaps lead to a more antero-posterior growth of the skull whereas MSC technique used here can perhaps lead to a more dorsal-ventral growth of the skull. All techniques demonstrated an improvement in the CI before relapsing, although this was seen to be greater in the MSC predictions. This difference was attributed to the greater increase in length seen in SAC vs. MSC and a reduction in width. It could be argued that if further growth was undertaken beyond 60 months for MSC, this relapse would continue beyond the value seen in the SAC. Considering morphological measurements shown, our current analysis highlights improved outcomes in the MSC vs. SAC predictions. On the other hand, it must be noted that the MSC technique is no longer performed at the Oxford Craniofacial Unit given that the study of Thomas et al., [13, 47] highlighted that the total calvarial remodelling technique performed in this unit resulted in higher CI and better clinical outcomes for these patients.

**Spring opening:** Considering both SAC techniques, although our comparison of spring opening distance was restricted to a single time point, predictive results appeared to match in the low range of *in vivo* data at 9 months (Figure 3). However, reports from Windh et al., [48] and Lauritzen et al., [49] agree well with the distance measured upon release. Our spring predictions only gain an additional 11 mm in length from release to 9 months. Other centres have documented these changes in greater detail. Yang et al., [43] studied the spring opening and bi-temporal displacement of SAC patients during the entire 3 months of treatment. Spring opening was seen to increase rapidly from 7-10 mm to 23 mm in the first 2 hours after insertion. This rate of opening was seen to decrease to 4 mm after only 8 hours following insertion, after which the length was seen to plateau. Although these larger displacements were not seen in our predictions, it should be noted that a larger spring forces were used upon insertion (14 N vs. 8 N). Further, such levels of *in situ* craniotomy and spring widening observed in this work do not fully reflect the larger levels seen in other craniofacial centres under different operative parameters [26]. However, as our intention was to focus on a single

centres SAC conditions (i.e. Gothenburg, Sweden), such considerations were examined in a sensitivity analysis (See: Supplementary Table S4). Both 2 SAC and 3 SAC techniques show little change in opening spring length by 9 months, with all springs displacing by approximately 10 mm from 'release' to removal. Interestingly, incorporation of a middle spring for 3 SAC showed little effect on morphological outcomes, particularly that of biparietal widening. Nonetheless, these predictions, cross-referenced with our morphological measurements, may prove informative for surgeons in reducing the risk of damaging the sagittal sinus and/or lower risk of spring dislodgement as fewer distractors may be necessary to achieve the same morphological goals with regards to this study [50,51].

**Bone formation:** A previously developed approach to model bone formation detailed by Marghoub et al., [28] was adopted in this study. Given that the formation rate at the cranial sutures and craniotomies in humans could be different from what was used in our previous study, various sensitivity tests were carried out to justify the choice of this parameter (see Supplement Figure S1 & Table S3). Overall, we observed that the patterns of bone formation at different sutures and craniotomies appeared to match that of the *in vivo* observations from the literature [39-42] and the CT cohort used at 9 and 36 months of age. For example, our results showed a greater posterior/occipital narrowing at 36 months of age in both SAC models. Such a phenomenon was caused by the fusion of the craniotomy and the patency of the lambdoid sutures, allowing for angular changes across the parietal bone plates, a phenomenon also reported in the clinical study of Satanin et al., [35]. Further, considering the pattern of bone formation across the MSC technique, our model predicted initial bone formation across the craniotomy by 36 months of age. This is in line with observational studies of the same technique performed at a similar age [52,53]. A minor vertex bulging was evident by 36 months across the anterior-fontanel region. Such characteristics have been linked to ossification delays reported by Marucci et al., [54], who investigated the causes of 'copper beaten' appearances in previously treated MSC patients. Although our predictions display bone formation at the craniotomy by 36 months of age, large patency was seen at 9 months, which has resulted in a characteristic vertex bulging.

**Contact pressure:** Further to predicting morphological and ossification outcomes, this work highlights the changes in pressure across the, here, ICS. Our results highlight that the MSC technique perhaps constrains the growth of the ICS (as a whole) to a larger extent compared to the SAC techniques. This observation was most apparent by 36 months, where pressure was higher in isolated regions (Figure 7). This prediction suggests that improved



morphological outcomes, as seen in this work, may not correlate to unrestricted growth and thus, lower overall pressure. Whether this higher pressure has any neurofunctional impact on brain growth or not can not be commented based on our data at present and requires a much more detailed clinical investigation. Nonetheless, this study highlights the huge potentials of finite element methods in understanding the biomechanics of different management techniques have on brain growth.

**Limitations:** Despite promising resemblances between the *in silico* and *in vivo* results reported in this study, our study has several limitations. (1) Our simulations establish a bone-craniotomy & bone-suture lining method of formation. In reality, it is known that the dura mater possesses osteogenic properties which promote spontaneous ‘islands’ of bone across large calvarial defects [55]. Such advanced complexities and factors of ossification were not modelled in this study while these can be considered in future studies. Further, the values determined for replicating bone stiffness changes (i.e. 100 and 125MPa for each month) and constituting the stage of ‘closed’ for both sutures and craniotomy stated here is highly generic and may not represent the true changes in ossification postoperatively. (2) Our approach in predicting ICP pressure postoperatively aimed to compare the potential benefits between techniques and assess brain growth [56]. It has been suggested that different surgical techniques can result in different neuropsychological outcomes, but such relations are disputed [56, 57]. If at all, surgical outcome relates to neuropsychological outcome, our presented method predicts relevant skull size measures such as length, width and ICP and also predicts a more dynamic parameter, pressure, in the form of contact pressure mapping. Therefore, the presented method provides not only predictions of the morphological outcome but introduces a parameter with potential direct physiological significance. If in the future, we manage to determine the impact of the different outcome parameters on neuropsychological outcomes, FE models will add considerable value to surgical planning.

## 5. Conclusion

The current study is, to the best of our knowledge, the first comparative analysis in predicting various treatment outcomes for sagittal craniosynostosis using a FE approach. The discussed results show promising perspectives in accurately predicting post-operative morphology and characteristics seen *in vivo* and various reported scenarios. Further work aims to broaden the current number of techniques in this study and evaluated the biomechanical impact of these techniques accordingly.

## Disclosures

The authors declare that the research was conducted in the absence of any commercial or financial relationships that could be construed as a potential conflict of interest.

## Acknowledgements

This work was supported by the Rosetrees Trust [A1899]. The authors declare that no competing interests exist.

## References

1. Morriss-Kay GM, Wilkie AOM: Growth of the normal skull vault and its alteration in craniosynostosis: insights from human genetics and experimental studies. *J Anat* 207: 637-53 (2005).
2. Johnson D, Wilkie AOM: Craniosynostosis. *Eur J Hum Genet* 19(4): 369–376 (2011).
3. Mathijssen IMJ: Guideline for care of patients with the diagnoses of craniosynostosis: working group on craniosynostosis. *J Craniofac Surg* 26(6): 1735–1807 (2015).
4. Kalantar-Hormozi H, Abbaszadeh-Kasbi A, Sharifi G, Davai N, Kalantar-Hormozi A: Incidence of familial craniosynostosis among patients with nonsyndromic craniosynostosis. *J Craniofac Surg* 30(6): 514–517 (2019).
5. Rocco FD, Arnaud E, Renier D: Evolution in the frequency of nonsyndromic craniosynostosis. *J Neurosurg Pediatr* 4(1): 21–5 (2009).
6. Cornelissen M et al.: Increase of prevalence of craniosynostosis. *J Craniomaxillofac Surg* 44(9): 1273–1279 (2016).
7. Gault DT, Renier D, Marchac D, Jones BM: Intracranial pressure and intracranial volume in children with craniosynostosis. *Plast Reconstr Surg* 90(3): 377-381 (1992).
8. Lo LJ, Chen YR: Airway obstruction in severe syndromic craniosynostosis. *Ann Plast Surg* 43(3): 258-264 (1999).
9. Lane LC: Pioneer craniectomy for relief of mental imbecility due to premature sutural closure and microcephalus. *Jama* 18(2): 49-50 (1892).
10. Lauritzen C, Sugawara Y, Kocabalkan O, Olsson R: Spring mediated dynamic craniofacial reshaping: Case report. *Scand J Plast Reconstr Surg Hand Surg* 32(2): 331-338 (1998).

11. Kaiser G: Sagittal synostosis – it's clinical significance and the results of three different methods of craniectomy. Childs Nerv Syst 4(4): 223-230 (1988).
12. van Veelen MLC et al.,: Results of early surgery for sagittal suture synostosis: long term follow up and the occurrence of raised intracranial pressure. Childs Nerv Syst 29: 997-1005 (2013).
13. Thomas GPL et al.,: Long term morphology outcomes in nonsyndromic sagittal craniosynostosis: a comparison of 2 techniques. J Craniofac Surg 26(1): 19-25 (2015).
14. Simpson A, Wong AL, Bezuhly M: Surgical correction of nonsyndromic sagittal craniosynostosis concepts and controversies. Ann Plast Surg 78(1):103–110 (2017).
15. Delye HHK, Borstlap WA, van Lindert EJ: Endoscopy-assisted craniosynostosis surgery followed by helmet therapy. Surg Neurol Int 7(9): 59 (2018).
16. Fisher S et al.,: Comparison of intracranial volume and cephalic index after correction of sagittal synostosis with spring-assisted surgery or pi-plasty. J Craniofac Surg 27(2): 410-413 (2016).
17. Panchal Jet al.,: Sagittal craniosynostosis: outcome assessment for two methods and timing of intervention. Plast Reconstr Surg 103(6): 1574-1584 (1999).
18. Taylor JA, Maugans TA: Comparison of spring-mediated cranioplasty to minimally invasive strip craniectomy and barrel staving for early treatment of sagittal craniosynostosis. J Craniofac Surg 22(4): 1225-1229 (2011).
19. Gerety PA, Basta MN, Fischer JP, Taylor JA: Operative management of nonsyndromic sagittal synostosis: A head-to-head meta-analysis of outcomes comparing 3 techniques. J Craniofac Surg 26(4): 1251-1257 (2015).
20. Magge SNet al.,: A comparison of endoscopic strip craniectomy and pi craniectomy for treatment of sagittal craniosynostosis. J Neurosurg Pediatr 29: 708-714 (2019).
21. Fagan, M.J. "Finite element analysis: theory and practice". *Longman scientific & technical* (1992).

22. You J et al.,: The bone slot effect study of pi procedure for craniosynostosis correction plan based on finite element method. 3rd International Conference on Biomedical Engineering and Informatics: 605-608 (2010).
23. Wolański W, Larysz D, Gzik M, Kawlewska E: Modeling and biomechanical analysis of craniosynostosis correction with the use of finite element method. *Int J Numer Method Biomed Eng* 29(9): 916-925 (2013).
24. Borghi A et al.,: Spring-assisted cranioplasty: A patient specific computational model. *Med Eng Phys* 53: 58-65 (2018).
25. Dolack M et al.,: Computational morphogenesis of embryonic bone development: past, present, and future. In Niebur GL. [Ed.], *Mechanobiology – From Molecular Sensing to Disease*. Elsevier:. 197-217 (2020).
26. Borghi A et al.,: Assessment of spring cranioplasty biomechanics in sagittal craniosynostosis patients. *J Neurosurg Pediatr* 20(5): 400-409 (2017).
27. Lee C, Richtsmeier JT, Kraft RH :A computational analysis of bone formation in the cranial vault using a coupled reaction-diffusion-strain model. *J Mech Med Biol* 17(4): 1750073 (2017).
28. Marghoub A et al.,: Characterizing and modeling bone formation during mouse calvarial development. *Phys Rev Lett* 122(4): (2019).
29. Weickenmeier J, Fischer C, Carter D, Kuhl E, Goriely A: Dimensional, geometrical, and physical constraints in skull growth. *Phys Rev* 118(24): 248101-1-5 (2017).
30. Marghoub A et al.,: Predicting calvarial growth in normal and craniosynostosis mice using a computational approach. *J Anat* 232(3): 440-448 (2018).
31. Libby J et al.,: Modelling human skull growth: a validated computational model. *J R Soc Interface* 14(130): 20170202. 20170202 (2017).
32. Malde O et al.,: Predicting calvarial morphology in sagittal craniosynostosis. *Sci Rep.* 10(3): (2020).
33. Malde O, Libby J, Moazen M: An overview of modelling craniosynostosis using finite element method. *Mol Syndromol* 10(1-2): 74-82 (2019).

34. Cross C, Khonsari RH, Galiay L, Paternoster G, Johnson D, Ventikos Y, Moazen M: Using sensitivity analysis to develop a validated computational model of postoperative calvarial growth in sagittal craniosynostosis. *Front Cell Dev Biol.* 26(9): 621249 (2021).
35. Satanin L et al.,: Introduction of spring-assisted cranioplasty for scaphocephaly in Russia: first cases evaluated using detailed craniometry and principle component analysis. *J Plast Surg Hand Surg.* 53(3): 173-179 (2019).
36. Coats B, Margulies SS: Material properties of human infant skull and suture at high rates. *J Neurotrauma* 23(8): 1222-1232 (2006).
37. Moazen M et al.,: Mechanical properties of calvarial bones in a mouse model for craniosynostosis. *PLoS One* 12(10): e0125757 (2015).
38. Sgouros S, Golden JH, Hockley AD, Wake MJC, Natarajan K: Intracranial volume changes in childhood. *J Neurosurg* 91(4): 610-616 (1999).
39. Mitchell LA, Kitley CA, Armitage TL, Krasnokutsky MV, Rooks VJ: Normal sagittal and coronal suture widths by using CT imaging. *AJNR am J Neuroradiol* 32(10): 1801-1805 (2011).
40. Riahinezhad M, Hajizadeh M, Farghadani M: Normal cranial sutures width in an Iranian infant population. *JMSR* 5(3): 564-569 (2019).
41. Teager S, Constantine S, Lottering N, Anderson PJ: Physiological closure time of the metopic suture in south Australian infants from 3D CT scans. *Childs Nerv Syst.* 35(2): 329-335 (2018).
42. Pindrik J, Ye X, Ji B, Pendelton C, Ahn E: Anterior fontanelle closure and size in full-term children based on head computed tomography. *Clin Pediatr (Phila)* 53(12): 1149-1157 (2014).
43. Yang O et al.,: Analysis of the cephalometric changes in the first 3 months after spring-assisted cranioplasty for scaphocephaly. *J Plast Reconstr Aesthet Surg* 70(5): 673-685 (2016).
44. Huiskes R, Chao EY: A survey of finite element analysis in orthopedic biomechanics: the first decade. *J Biomech* 16(6): 385–409 (1983).

45. Herrera A et al.,: Applications of finite element simulation in orthopedic and trauma surgery. World J Orthop 3(4): 25-41 (2012).
46. Javidan M, Wang K, Moazen M: Biomechanical studies of human diaphyseal tibia fracture fixation. In Zhenxian C, Li J, Jin Z. (Ed), Computational Modelling of Biomechanics and Biotribology in the Musculoskeletal System. Elsevier (2021).
47. Thomas Get al.,: The incidence of raised intracranial pressure in nonsynodromic sagittal craniosynostosis following primary surgery. J Neurosurg Pediatr 15(4): 350-360 (2015).
48. Windh P, Davis C, Sanger C, Sahlin P, Lauritzen C: Spring-assisted cranioplasty vs pi-plasty for sagittal synostosis-A long term follow up study. J Craniofac Surg 19(1): 59-64 (2008).
49. Lauritzen C, David C, Ivarsson A, Sangar C, Hewitt T: The evolving of springs in craniofacial surgery: The first 100 clinical cases. Plast Reconstr Surg 121(2): 545-554 (2008).
50. Derderian CA: Discussion: Minimally invasive, spring-assisted correction of sagittal suture synostosis: technique, outcome, and complications in 83 cases. Plast Reconstr Surg 141 (2): 434-436 (2018).
51. Lin F et al.,: Delayed sagittal sinus tear. J Craniofac Surg 23 (5): 1382-1384 (2012).
52. Agrawal D, Steinbok P, Cochrane DD.: Reformation of the sagittal suture following surgery for isolated sagittal craniosynostosis. J Neurosurg 105(2): 115-117 (2006).
53. Kreppel M et al.,: Clinical evaluation of non-syndromic scaphocephaly surgically corrected with the procedure of total vertex craniotomy. J Craniomaxillofac Surg 46(9): 1465-1469 (2018).
54. Marruci D et al.,: Implications of a vertex bulge following modified strip craniectomy for sagittal synostosis. Plast Reconstr Surg 122(1): 217-224 (2008).
55. Gosain A et al.,: Osteogenesis in calvarial defects: contribution of the dura, the pericranium, and the surrounding bone in adult versus infant animals. Plast Reconstr Surg 112(2): 515-527 (2003).

56.Chieffo D et al.: Long term neuropsychological development in single-suture  
 craniosynostosis treated early. J Neurosurg Pediatr 5(3) 232-237 (2010).

57.Kljajić M, Giovanna M, Tarnow P, Sand P, Kölby L: The cognitive profile of children  
 with nonsynodromic craniosynostosis. Plast Reconstr Surg 143(5): 1037e-1052e  
 (2019).

**Figure 1:** Simulation workflow. All techniques were replicated at 4 months of age, when spring insertion [A] and ‘release’ [B] were replicated for SAC. Skull growth, calvarial healing and bone formation at sutures were replicated up to 9 months of age, when springs were removed [C]. Skull growth then continued up to 36 months of age [D].

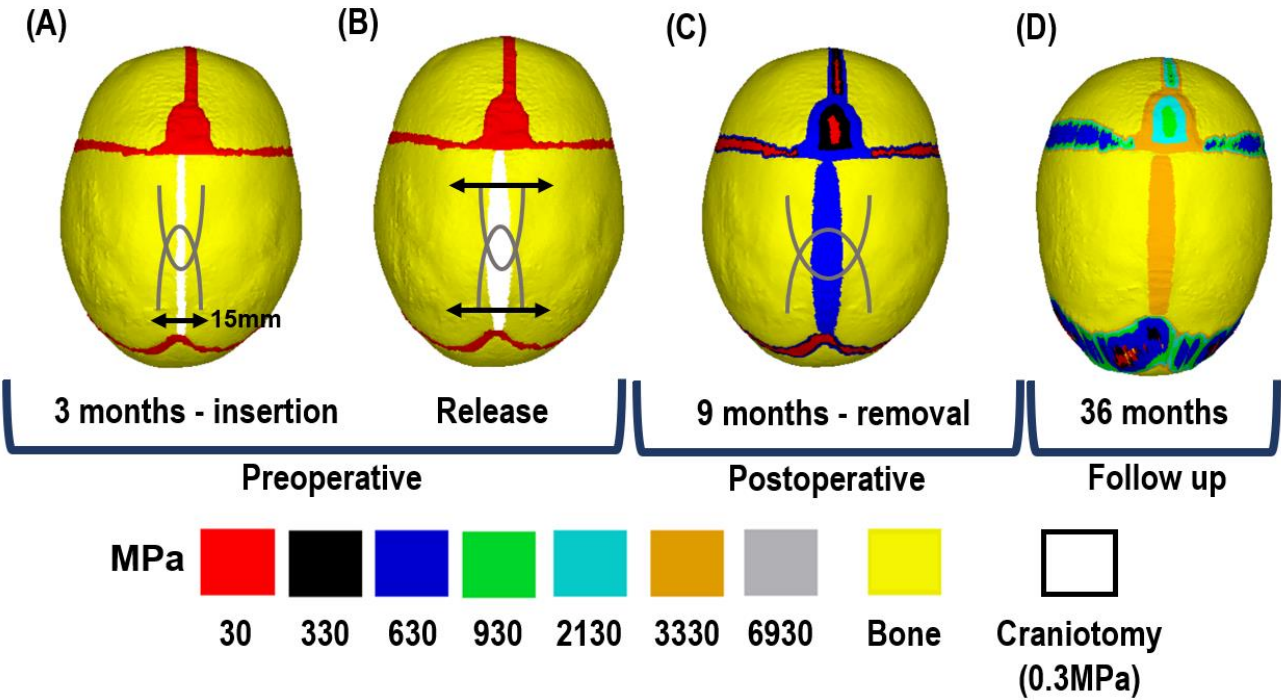


**Table 1:** Overview of predicted vs. *in vivo* measurements across all technique. Dashes indicate unavailable data. The preoperative FE model used for this study was at the age of 4 months with skull length, width, circumference, ICV and cephalic index of 137.2mm, 108.1mm, 430.6mm, 659.9ml, 78.7 respectively. NA at the preoperative stage for prediction data corresponds to the initial FE model that was the same model across all techniques that was then reconstructed to replicate each technique i.e. predicted the shape at different ages.

|                                | 2 SAC          |                 | 3 SAC          |                 | MSC [Thomas et al., 2015] |                 |        |
|--------------------------------|----------------|-----------------|----------------|-----------------|---------------------------|-----------------|--------|
|                                | clinical data  | prediction data | clinical data  | prediction data | clinical data             | prediction data |        |
| n:                             | 10             | 1               | 8              | 1               | 34                        | 1               |        |
| (%) male:                      | 80             | 1               | 50             | 1               | N/A                       | 1               |        |
| preoperative:                  |                |                 |                |                 |                           |                 |        |
| Age (months):                  | 4.9 ± 1.3      | N/A             | 4.1 ± 0.7      | N/A             | 6.0 ± 3.1-9.5             | N/A             |        |
| Mean length (mm):              | 148.5 ± 6.1    | N/A             | 150.5 ± 9.9    | N/A             | -                         | N/A             |        |
| Mean width (mm):               | 114.3 ± 5.7    | N/A             | 111.5 ± 5.6    | N/A             | -                         | N/A             |        |
| Mean circumference (mm):       | 455.3 ± 68.0   | N/A             | 457.2 ±27      | N/A             | -                         | N/A             |        |
| Mean intracranial volume (ml): | 800.9 ± 102.1  | N/A             | 800.8 ± 88.6   | N/A             | -                         | N/A             |        |
| Mean cephalic index:           | 76.9 ± 2.7     | N/A             | 74 ± 3.4       | N/A             | 65.7 ± 4.7                | N/A             |        |
| postoperative:                 |                |                 |                |                 |                           |                 |        |
| Age (months):                  | 10.9 ± 1.3     | 9.0             | 10.6 ± 0.3     | 9.0             | 12                        | 9.0             | 12.0   |
| Mean length (mm):              | 162.5 ± 8.0    | 143.3           | 165.2 ± 6.1    | 142.4           | -                         | 143.2           | 143.4  |
| Mean width (mm):               | 129.8 ± 5.0    | 112.5           | 129.1 ± 6.6    | 113.6           | -                         | 112.9           | 116.2  |
| Mean circumference (mm):       | 486.5 ± 59.4   | 397.3           | 429.0 ± 107.0  | 397.2           | -                         | 395.5           | 416.8  |
| Mean intracranial volume (ml): | 1089.2 ± 144.9 | 829.5           | 1131.2 ± 130.5 | 829.5           | -                         | 817.4           | 1007.0 |
| Mean cephalic index:           | 79.9 ± 2.9     | 78.5            | 78.2 ± 4.5     | 79.7            | 73.3 ± 5.2                | 78.8            | 81.1   |
| follow up:                     |                |                 |                |                 |                           |                 |        |
| Age (months):                  | 37.15 ± 2.0    | 36.0            | 37.6 ± 1.3     | 36.0            | 60                        | 36              | 60     |
| Mean length (mm):              | 176.9 ± 9.3    | 163.8           | 178.8 ± 8.8    | 163.4           | -                         | 155.8           | 155.1  |



|                                       |                |        |                |        |            |        |        |
|---------------------------------------|----------------|--------|----------------|--------|------------|--------|--------|
| <b>Mean width (mm):</b>               | 135.1 ± 5.4    | 122.3  | 132.7 ± 6.4    | 121.2  | -          | 122.3  | 124.7  |
| <b>Mean circumference (mm):</b>       | 512.4 ± 35.4   | 454.4  | 523.2 ± 37.0   | 453.3  | -          | 429.4  | 437.0  |
| <b>Mean intracranial volume (ml):</b> | 1245.0 ± 166.8 | 1261.0 | 1239.0 ± 133.8 | 1261.0 | -          | 1240.4 | 1376.9 |
| <b>Mean cephalic index:</b>           | 76.4 ± 2.5     | 74.6   | 74.3 ± 3.8     | 74.1   | 71.5 ± 4.3 | 78.4   | 80.3   |

628

629

630

631

632

633

634

635

636

637

638

639

640

641

642

643

644

645

646

647

648

649

650

651

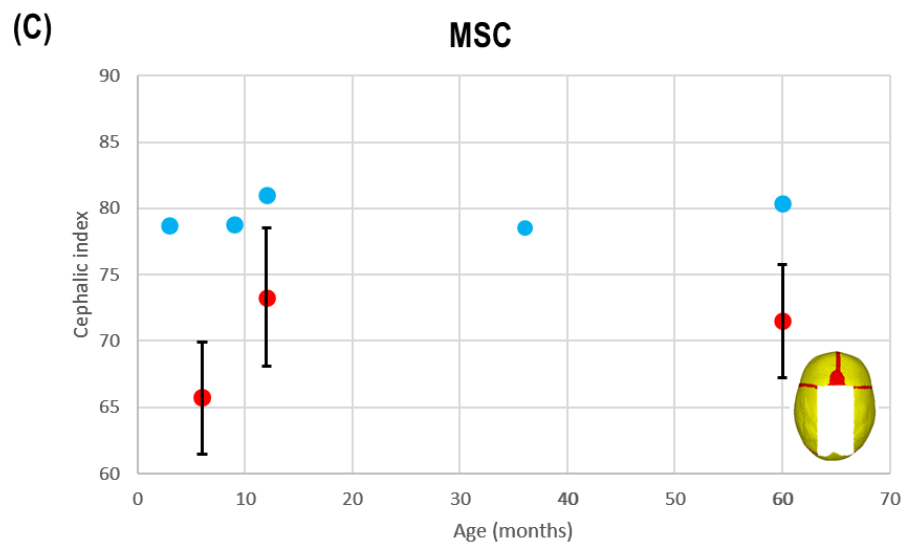
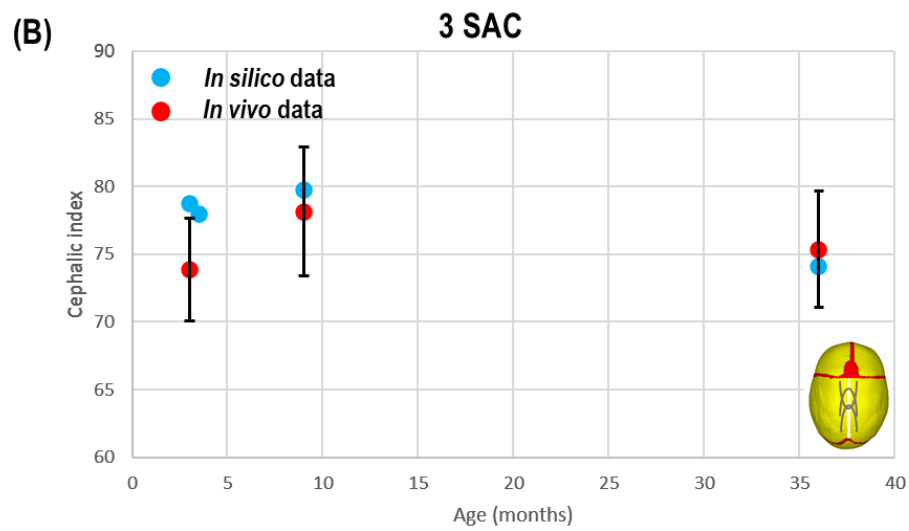
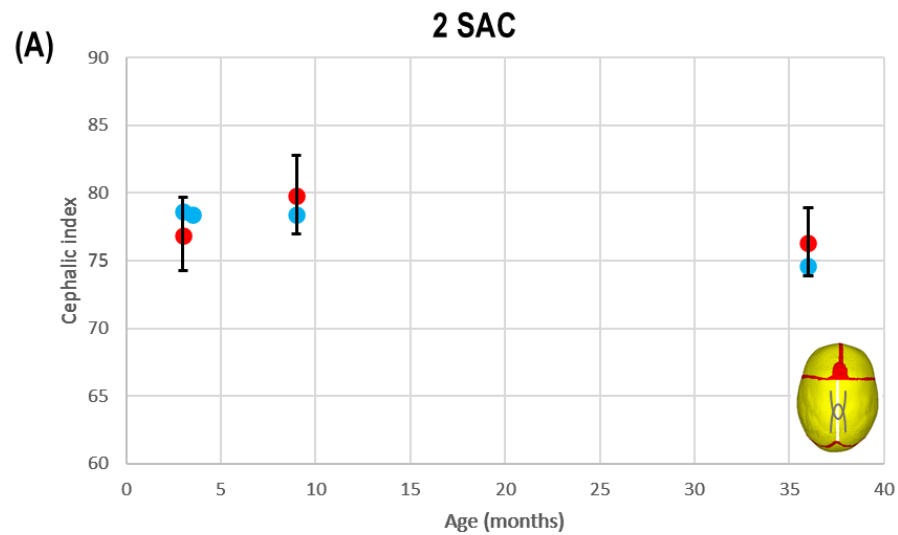
652

653

654

655

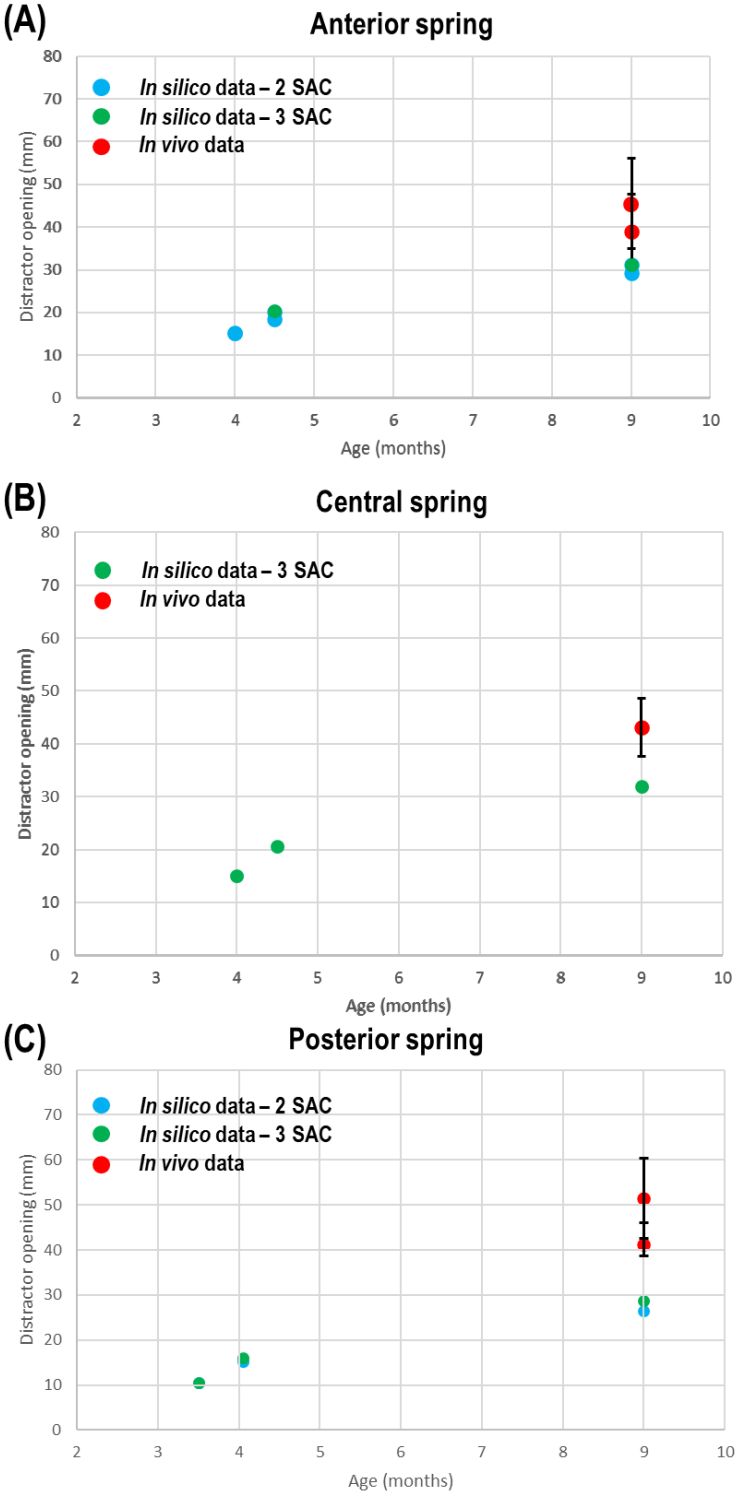
656 **Figure 2:** Predicted vs. *in vivo* cephalic index data with SD. Showing 2 SAC [A], 3 SAC [B] &  
657 MSC outcomes [C].



658

659

**Figure 3:** Predicted vs. *in vivo* spring opening data with SD. Showing anterior [A], central [B] & posterior [C] springs in both SAC techniques. Diagrams show regions where measurements were performed.



665 **Figure 4:** 2 SAC 3D distance plot at respective ages against mean *in vivo* CT skull.

666 **Release** **9 months**

667 **Figure 5:** 3 SAC 3D distance

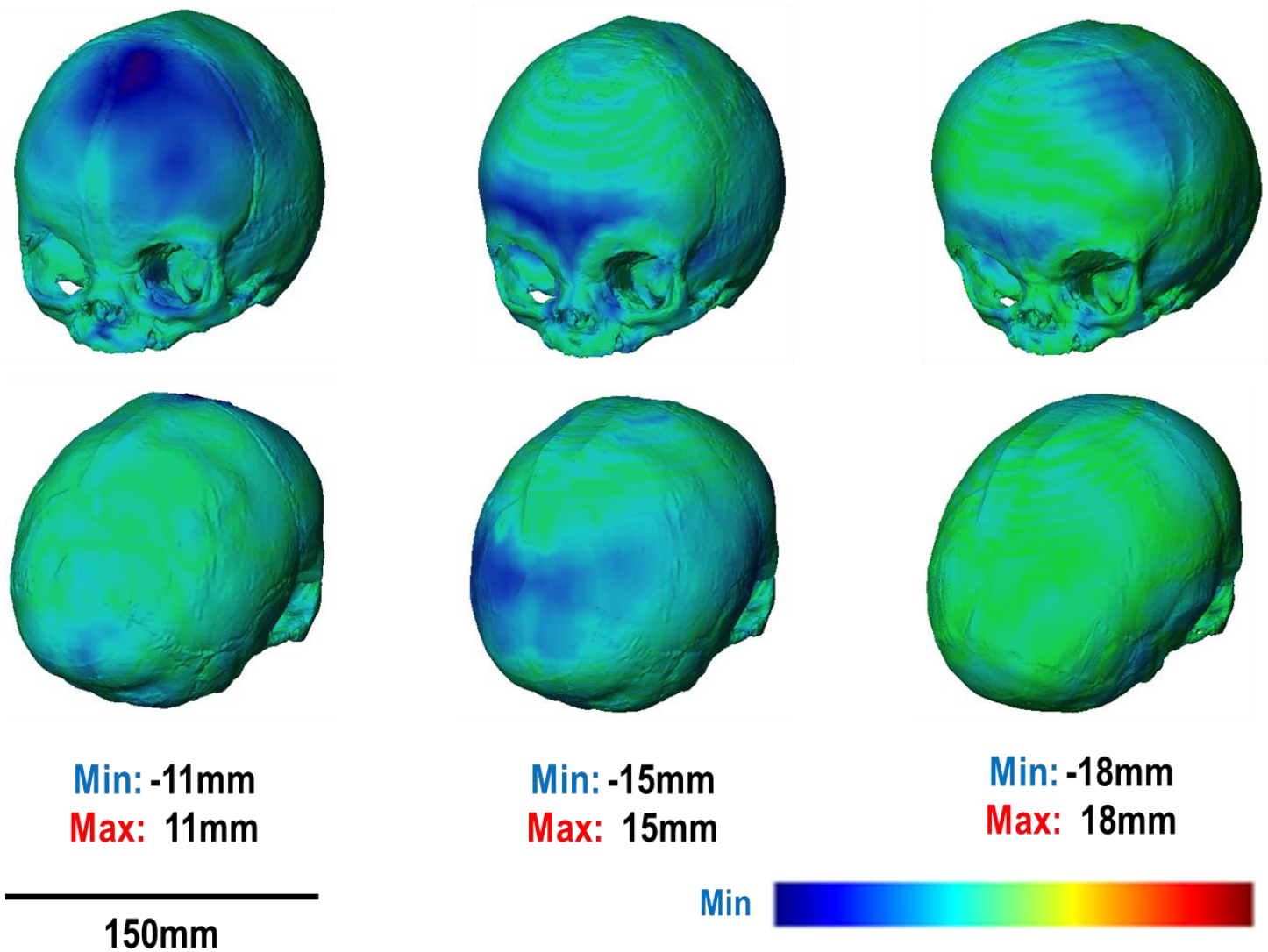
668 against

669 CT

**36 months**

plot at respective ages

mean *in vivo* skull.



670

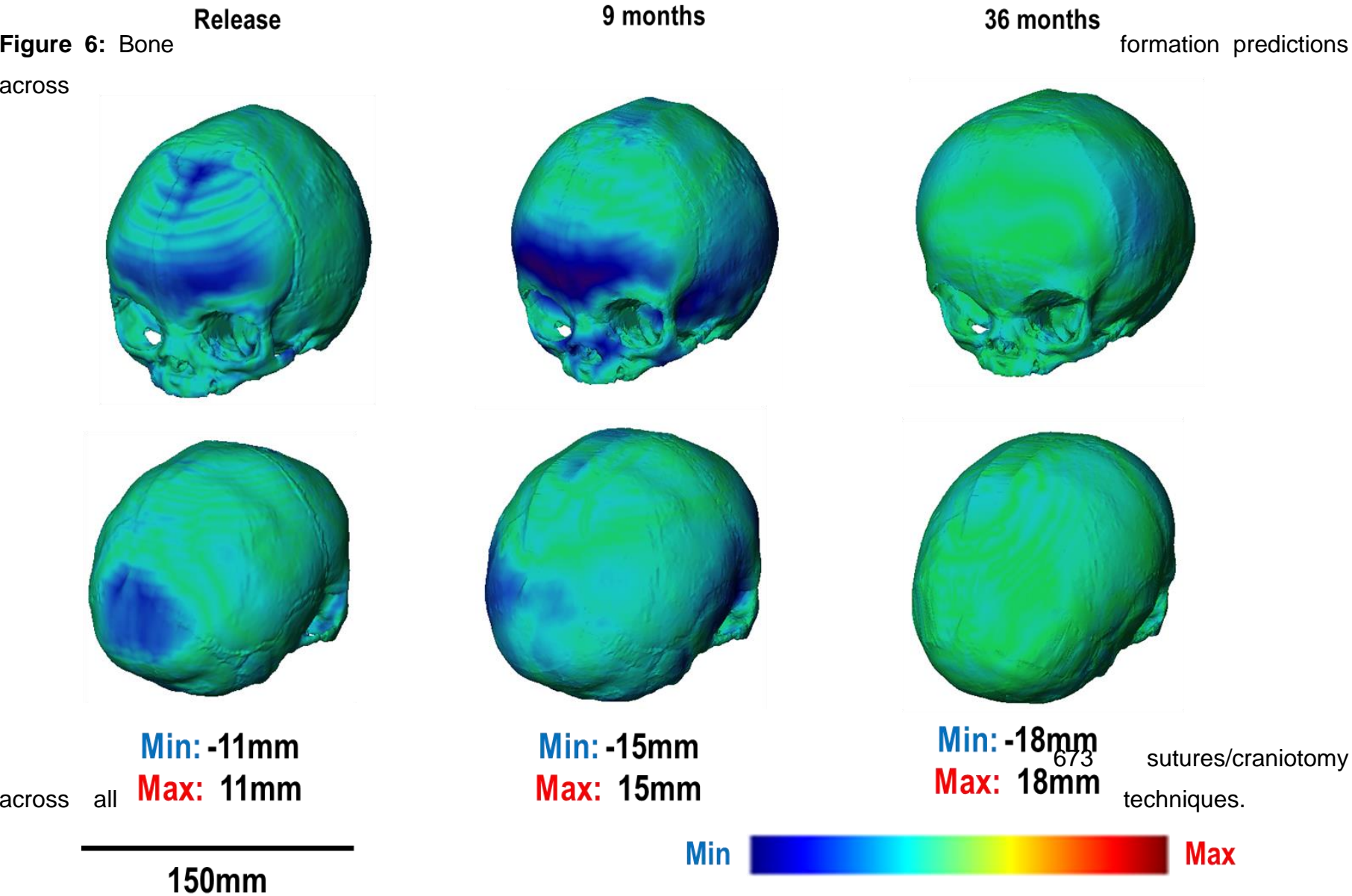
671

672

674

675

676



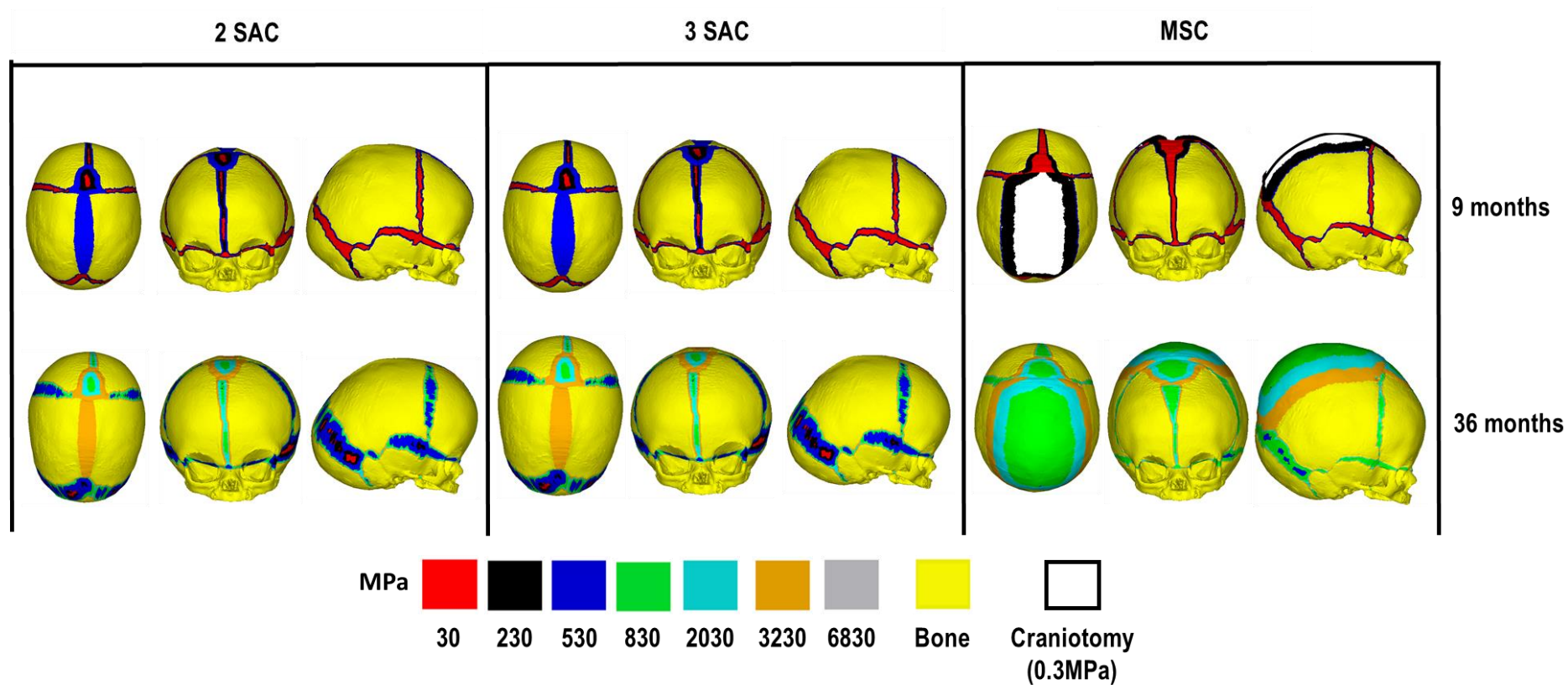
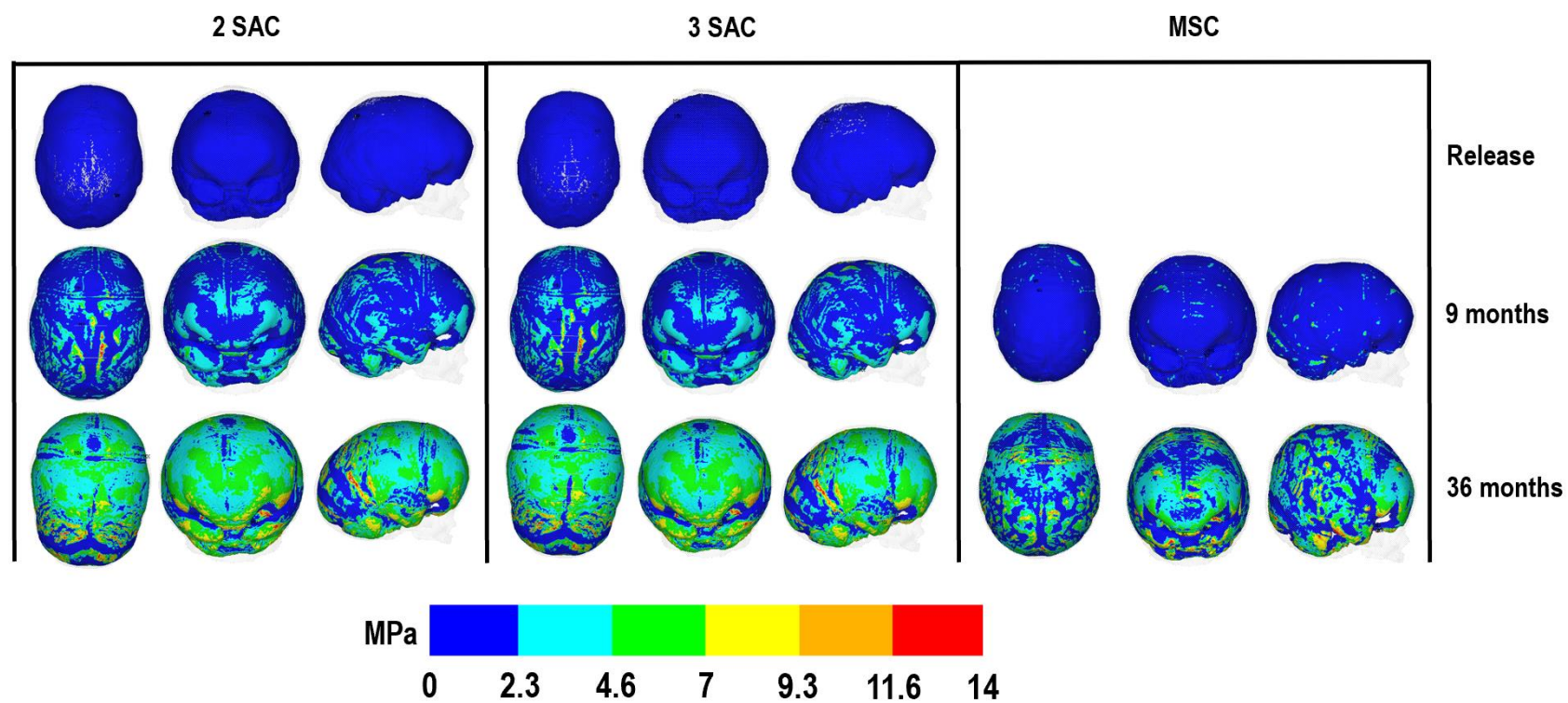


**Figure 7:** ICV pressure predictions across ICV-bone surface for all techniques.





683



# **A computational framework to predict calvarial growth: optimizing management of sagittal craniosynostosis**

Connor Cross<sup>1</sup>, Roman H Khonsari<sup>2</sup>, Giovanna Patermoster<sup>3</sup>, Eric Arnaud<sup>3</sup>, Dawid Larysz<sup>4</sup>, Lars Kölby<sup>5</sup>, David Johnson<sup>6</sup>, Yiannis Ventikos<sup>1</sup>, Mehran Moazen<sup>1</sup>

<sup>1</sup> Department of Mechanical Engineering, University College London, UK

<sup>2</sup> Department of Maxillofacial Surgery and Plastic Surgery, Necker – Enfants Malades Hospital, Assistance Publique – Hôpitaux de Paris, Paris, France

<sup>3</sup> Department of Neurosurgery, Craniofacial 16 surgery unit, Necker – Enfants Malades Hospital, Assistance Publique – Hôpitaux de Paris, Paris, France

<sup>4</sup> Department of Head and Neck Surgery for Children and Adolescents. University of Warmia and Mazury in Olsztyn, Poland

<sup>5</sup> Department of Plastic Surgery, Sahlgrenska University Hospital, University of Gothenburg, Gothenburg, Sweden

<sup>6</sup> Oxford Craniofacial Unit, Oxford University Hospital, Oxford, UK

## **Corresponding author:**

Mehran Moazen; Department of Mechanical Engineering, University College London, Torrington Place, London, WC1E 7JE, UK; T: +44 (0) 207 679 3862; E: M.Moazen@ucl.ac.uk

## **Abstract**

The neonate skull consists of several bony plates, connected by fibrous soft tissue called sutures. Premature fusion of sutures is a medical condition known as craniosynostosis. Sagittal synostosis, caused by premature fusion of the sagittal suture, is the most common form of this condition. The optimum management of this condition is an ongoing debate in the craniofacial community while aspects of the biomechanics and mechanobiology are not well understood. Here, we describe a computational framework that enables us to predict and compare the calvarial growth following different reconstruction techniques for the management of sagittal synostosis. Our results demonstrate how different reconstruction techniques interact with the increasing intracranial volume. The framework proposed here can be used to

inform optimum management of different forms of craniosynostosis, minimising the risk of functional consequences and secondary surgery.

Keywords: calvarial bones, sutures, skull growth, sagittal synostosis, finite element method biomechanics

## INTRODUCTION

The neonate skull consists of several bony plates, connected by fibrous soft tissues along their edges, called sutures [Opperman, 2000; Herring, 2008; Richtsmeier & Flaherty, 2013]. Sutures facilitate birth and accommodate rapid brain growth in the first year of life [Herring, 2008; Richtsmeier & Flaherty, 2013]. Premature fusion of sutures is a medical condition known as craniosynostosis [Herring, 2008; Richtsmeier & Flaherty, 2013; Johnson & Wilkie, 2011]. The most common form of this condition is sagittal synostosis (SS) caused by premature fusion of the sagittal suture, occurring in approximately 3 in every 10,000 births. This condition leads to bi-temporal narrowing and excessive anteroposterior growth of the skull with frontal and occipital bossing [Johnson & Wilkie, 2011; Mathijssen, 2015].

The management of SS involves surgical remodelling of the calvaria. The underlying aims of the surgery are to normalise the head shape and relieve the constraint on the growing brain, thus decreasing the potentially elevated intracranial pressure (ICP) [Mathijssen, 2015]. Several techniques have been developed and used over the years across the world for the management of SS [Mathijssen, 2015; Jane et al., 1978; Jimenez & Barone, 2012; Simpson et al., 2017]. These range from less invasive methods such as strip craniotomy and spring-mediated cranioplasty which are usually performed before 6 months of age, to more invasive approaches such as total vault remodelling which are usually performed at the age of about 12 months [Taylor & Maugans, 2011; van Veelen et al., 2016; Fischer et al., 2016; Gailey et al., 2021].

There is a growing number of clinical studies comparing the outcomes of different techniques for SS [Taylor & Maugans, 2011; van Veelen et al., 2016; Fischer et al., 2016; Gailey et al., 2021]. Nonetheless, our fundamental understanding of how different reconstruction methods interact with the growing brain is still limited. This is crucial as one of the key factors during early craniofacial development is the load arising from a growing brain. If this load is not accommodated by the reconstructed skull, it can constrain brain growth, leading to raised ICP and a possible risk of re-operation [Thomas et al., 2015]. Computational models are a promising tool to predict calvarial growth and optimise the management of craniosynostosis [Weickenmeier et al., 2017; Lee et al., 2017; Malde et al., 2018].

In a series of studies, we have previously developed a validated computational model based on the finite element method that enables us to predict the radial expansion of the calvaria as well as the bone formation at the cranial sutures in mice and humans [Marghoub et al., 2018; Marghoub et al., 2019; Libby et al., 2017; Malde et al., 2020; Cross et al., 2021a,b]. In this current work, (1) we present a computational framework that can be used to advance the treatment of various forms of craniosynostosis; (2) we inform and optimise the clinical management of sagittal craniosynostosis. We first virtually reconstructed the calvaria of a patient at 4 months of age, using 9 different techniques. Then we predicted the calvarial growth up to 76 months of age across all treatment options. Finally, we compared the overall morphology of the calvaria, level of contact pressure across the intracranial volume (ICV), and the pattern of bone formation between the considered techniques. To the best of our knowledge, the computational framework presented here is the first of its kind to predict the calvarial growth and the first steps toward the biomechanical optimisation of the clinical management of craniosynostosis. Both these elements are novel and constitute the main contributions of this study.

## MATERIALS AND METHODS

**Model development:** The overall computational methodology implemented here is illustrated in figure 1. Computed tomography (CT) images of a single preoperative sagittal craniosynostosis child skull at the age of 4 months were obtained from the Hôpital Necker – Enfants Malades Craniofacial Surgery Unit (Centre de Référence Maladies Rares Craniosténoses et Malformations Craniofaciales CRANIOST, Paris, France) for 3D model development. Full ethical protocol was approved by the institutional review board, committee, and the patients' guardians. The images had a voxel size of 0.625 mm across all axes.

The image processing software, Avizo (V9.2.0; Thermo Fisher Scientific, Mass, USA) was used for manual and automatic compartmentalisation of highlighted internal and external tissues. Here, the calvarial bones, sutures, and the complete intracranial volume (ICV) were segmented. The specifics of craniotomies performed across the model were based on the common clinical practices of the authors of this study. The model was then used to create a 3D mesh consisting of approximately four million quadratic tetrahedral elements suitable for finite element analysis using the ANSYS platform (ANSYS V19.0; Canonsburg, PA, USA).

**Boundary and interface conditions:** Isotropic material properties were assigned to all segmented components. The calvarial bones and sutures were assumed to have a linear elastic modulus of 421 MPa and 30 MPa, respectively [Coats & Margulies, 2006; Moazen et al., 2015], whereas the ICV and craniotomies elastic modulus was defined as 10 MPa and 0.3 MPa, values adopted from our previous sensitivity study [Cross et al., 2021a]. Appreciating fully the complexity and multiscale poroelastic features of the brain parenchyma, and related implications relating to skull loading [Gou et al., 2020].

The calvarial bones Poisson's ratio was 0.22, while the sutures were assumed to be 0.3. Both the craniotomy and ICV had a Poisson's ratio of 0.1. Techniques adopting bioabsorbable fixators (for a particular technique i.e. TCR1 – see simulation section) had an initial elastic modulus and Poisson's ratio of 2000 MPa and 0.1, respectively [Landes et al., 2006]. A sensitivity study analysing the impact of incorporating fixators on morphological shape predictions is presented in the supplemental Material [See: Supplementary figure S1]. To minimise rigid displacement, nodal constraints in all degrees of freedom across the nasal ridge and around the foramen magnum were maintained throughout all simulations. To simulate the rapidly growing brain, we expanded the ICV from the initial 4 months (659 ml) up to 76 months of age (1376 ml) using a linear thermal expansion analogy across six load steps. At each load step, the age was estimated by correlating the predicted volume against comparative age to volume literature data [Likus et al., 2014].

Establishing the brain growth across the model generated various levels of strain across the sutures and craniotomies, which were used to simulate the bone formation and differentiation of bone stiffness. Here, a two criteria system was parameterised: (1) Applicable elements must achieve a predetermined level of hydrostatic strain (i.e. summation of all principal strains and division by three) as a result of the growth; (2) Elements were required to be within a specified radial distance from the adjoining bone borders. Elements exclusively relative to the sutures were confined to both of these conditions, whilst elements representing the craniotomy followed only the former criteria. To represent the differentiation of bone stiffness, these elements would have their elastic moduli updated, which varied based on the relative changes in age. See our previous studies for a full detailed description of this approach [Cross et al., 2021a,b].

To account for the contact conditions across the ICV, a Hertzian contact algorithm was implemented between the inner-calvarial table and ICV interfaces. The penalty-based behaviour with a normal contact stiffness of 50 N/mm, a penetration tolerance of 0.5 mm and a friction coefficient of 0.1 allowed for minimal levels of interpenetration between surfaces [Malde et al., 2020; Cross et al., 2021a,b]. While initially in contact, normal/tangential separation was granted during simulated growth. Interfaces between the calvarial bones and sutures, calvarial bones and craniotomies, and suture and craniotomies maintained a 'bonded' contact, restricting all forms of separation.

***Simulated surgical techniques:*** Nine techniques were replicated across the model at various ages of intervention [see also: Gailey et al., 2021]. To represent an intervention age greater than the initial 4 months, growth was modelled across three load steps, with no correction having been performed, resulting in three additional models at 6, 9 and 12 months of age. The changes in morphology and contact pressure during the growth are highlighted in the Supplemental Material [See: Supplementary figure S2]. The techniques denoted as Renier's 'H', modified Renier's 'H', endoscopic, strip cranioplasty, and two variations of spring-assisted craniectomy

(SAC) which consisted of two or three springs, respectively (i.e. 2 SAC & 3 SAC) were replicated across the 4 months of age model. For comparison, the Renier's 'H' was also performed across the alternative 6 months of age model. The model at 12 months of age was further used for both total calvarial remodelling techniques (i.e. TCR 1 & TCR 2).

## RESULTS

First, we qualitatively assessed the pattern of bone formation across all techniques at 76 months of age (figure 2). Here, the timing of calvarial bone healing was defined as when no respective craniotomy (i.e. white) or suture (i.e. red) elements remained visible across the models. We found that rapid calvarial healing/bone formation at the craniotomies could be achieved by 5 months postoperatively for the SAC techniques, perhaps due to the shorter bilateral width. Followed by the endoscopic treatment at 9 months after surgery. The remaining techniques performed at 4 months of age achieved calvarial healing by 20 months after surgery. When postponing the timing of intervention (i.e. Renier's 'H' at 6 months), little difference in the level and rate of calvarial healing was observed vs. earlier intervention. However, evidence of delayed healing was obtained for both TCR methods; having healed by 24-36 months after surgery. Complete fusion of all sutures was predicted in the modified Renier's 'H', strip cranioplasty, and both SAC approaches by 76 months of age. Conversely, patency was still visible across the coronal and squamosal sutures in the Renier's 'H' and endoscopic methods at 76 months, respectively. Interestingly, this characteristic was not evident in the later performed Renier's 'H'. Delayed bone formation was predicted across the calvaria in TCR 2 as opposed to TCR 1 (perhaps attributed to the modelled bioabsorbable fixators in TCR 1).

To quantify the shape changes, we recorded cephalometric parameters for all approaches (figure 3). By 76 months of age, we predicted the largest overall length in both SAC techniques (figure 3-A), ranging from 175.2 mm to 173.1 mm, whilst the earlier performed Renier's H measured 163.3 mm, demonstrating the overall lowest length. Conversely, the greatest bitemporal widening (figure 3-B), measuring 131.7 mm, was achieved in the TCR 1 approach and the least, measuring 124.1 mm, was seen in the earlier Renier's H. Utilising these values, we calculated the cephalic index by multiplying the width against the length and dividing by one hundred (figure 3-C). Here, with a value of 79.1, the strip craniectomy predicted the overall best improvement with the caveat of a high vertex (see: figure 2). The worst cephalic index was seen in the 3 SAC predictions, valued at 72.7. We predicted that both total calvarial remodelling techniques, while achieving the second and third best cephalic index values, also showed a reduced level of pre to postoperative relapse in contrast to all earlier techniques. Further, the same response was also seen in the later performed Renier's H approach. It should be noted however that no technique was able to bring the cephalic index fully back to normal, seen within the normocephalic population at a value of greater than 80 [Gailey et al., 2021; Sgouros et al., 1999]. The

lowest circumference (figure 3-D) was achieved in the earlier Renier's H, whilst the greatest was seen in the 3 SAC.

Using pressure maps, we qualified the predicted contact pressure across the ICV at 76 months for all techniques (figure 4-A). To quantify these predictions, we subdivided the ICV component for all techniques into six regions of interest, with standard deviations highlighting the differences in pressure in these regions across the entire area (figure 4-B). The anterior, middle and posterior cerebral areas were divided between the left and right sides. We predicted that the TCR 2 approach leads to the lowest consistent pressure outcome across the anterior (Left:  $1.2 \pm 1.0$  MPa – Right:  $1.3 \pm 1.5$  MPa), middle (Left:  $1.3 \pm 1.2$  MPa – Right:  $1.4 \pm 1.2$  MPa) and posterior (Left:  $1.4 \pm 1.2$  MPa – Right:  $2.0 \pm 1.2$  MPa) regions of the ICV. In an earlier intervention, the modified Renier's 'H' approach estimated the overall greatest pressure values across the left ( $5.0 \pm 1.7$  MPa) and right ( $4.2 \pm 2.7$  MPa) anterior regions. Similar pressure findings were seen between the modified Renier's 'H' and the later performed Renier's 'H' procedure, which consistently produced the largest values across the middle left (modified Renier's:  $5.0 \pm 2.5$  MPa – Renier's H:  $5.0 \pm 2.1$  MPa), middle right (modified Renier's:  $5.2 \pm 2.1$  MPa – Renier's H:  $5.1 \pm 2.2$  MPa), posterior left (modified Renier's:  $4.8 \pm 3.5$  MPa – Renier's H:  $5.0 \pm 2.9$  MPa) and posterior right regions (modified Renier's:  $5.2 \pm 2.8$  MPa – Renier's H:  $5.5 \pm 2.3$  MPa). Interestingly, the number of simulated springs across both 2 SAC and 3 SAC techniques did not impact the overall pressure predictions, despite the small differences observed in the cephalometric measurements.

## DISCUSSION

Clinically, the target for SS correction is anteroposterior reduction accommodated by mediolateral and dorsal expansion. The computational framework proposed here showed that all techniques achieve this underlying objective yet with different morphological outcomes and relapses. The predicted morphologies and the contact pressure maps obtained across the calvaria highlighted that different reconstructive techniques constrain/facilitate the growth of the brain to a different extent.

Our results overall highlighted that the more invasive techniques (TCR 1 & 2) can potentially lead to a higher cephalic index compared to the less invasive techniques by 76 months of age. Further, the predicted contact pressure maps highlighted a lower level of pressure over the surface of the expanding brain for the two considered total calvarial remodelling techniques as opposed to the other considered techniques. Interestingly, our analysis of clinical CTs of over 100 scans corresponding to the techniques investigated in this study did not find a statistically significant difference in the morphological outcome of these techniques [Gailey et al., 2021]. However, it must be re-emphasised that the framework presented here does not take into account any clinical variables potentially differentiating the different cases [Gailey et al., 2021]

regarding the calvarial reconstruction techniques. This can be interpreted as both an advantage of the framework presented here and also as its key limitation.

Indeed, assumptions had to be made in the proposed computational framework. Many chemical and biological characteristics play a role in membranous bone formation during infancy [Opperman, 2000; Herring, 2008; Richtsmeier & Flaherty, 2013; Beederman et al., 2014] while a purely mechanical approach was considered here. Even within the considered approach, we have not incorporated a more detailed description of the hydrostatic loads caused by the normal skull and brain growth. Further, normal growth is most probably non-linear and anisotropic, versus the linear isotropic approach adopted here. Nonetheless, since this approach was uniformly applied to all techniques that were modelled, we were able to achieve a similar level of ICV volume size and shape changes up to 76 months of age [Gailey et al., 2021, Sgouros et al., 1999]. Hence, while we cannot be confident in the exact *absolute* values reported in this study, the relative comparisons provide invaluable insights for years to come.

Our previous studies have assessed the impacts that alternative material properties could have on the predicted calvarial growth [Cross et al., 2021a]. As such, these properties were brought forward to the current study, including the method of uniformly updating the elastic modulus of the bone. Whilst the effects of changing the elastic modulus of the calvarial bones were assessed, the current model lacks the consideration that viscoelastic properties could have on the manipulation of the bone morphology [Margulies & Thibault, 2000]. Such impacts have been assessed previously and are an important consideration for computational models when replicating the after-effects of surgery [Borghi et al., 2018; Borghi et al., 2020]. However, as we believe this only plays a role across a small time scale (perhaps within hours post-operatively), the former method of replicating the changes in bone properties was chosen (considering that we predicted the skull growth up to 76 months of age).

The assessment of cognitive outcomes pre-and post-operatively across differing techniques is typically conducted using dedicated questionnaires. Within the literature, there is still debate as to the optimum treatment option based on the outcomes of such questionnaires [Hashim et al., 2014; Care et al., 2019; Kljajic et al., 2019]. The contact pressure data obtained in our work is a surrogate to estimate to what extent different techniques constrain the growth of the brain parenchyma. The exact values predicted here must be treated with caution and require further investigations and validation, yet, they may prove informative for craniofacial surgeons in a comparative manner and provide a level of postoperative cognitive predictability when considering treatment options.

Clinically, the choice of a treatment option needs to be optimised based on a number of factors such as the experience of the team in performing a specific technique, the

necessity of blood transfusion [Meyer et al., 1993] and various associated costs. These factors were not considered in the computational framework proposed here. Further, more work is required to implement facial growth in the proposed approach. Orbital, mid-facial and palate deformations most probably play a role in calvarial morphometric outcomes [Ranly, 2000].

In summary, we believe the presented approach provides a sustainable way of assisting with preoperative sagittal craniosynostosis management and estimating the postoperative outcomes. The potential to examine the changes in biomechanical behaviour allows for the optimisation of morphological and cognitive characteristics in patients' years after surgery. This, in the long term, can reduce the level of complications and improve the overall quality of care.

This work was supported by the Rosetrees Trust through the PhD research project [A1899], PhD Plus project [PhD2021\100017].

## References:

Beederman, M., Farina, E.M., Reid, R.R. (2014). Molecular basis of cranial suture biology and disease: Osteoblastic and osteoclastic perspectives. *Genes Dis.* 1:1 120-125. doi: 10.1016/j.gendis.2014.07.004

Borghi, A., Rodrigues-Florez, N., Ruggiero, F., James, G., O'Hara, J., Ong, J. et al., (2020). A population-specific material model for sagittal craniosynostosis to predict surgical shape outcomes. *Biomech Model Mechanobiol.* 19:4 1319-1329. doi: 10.1007/s10237-019-01229-y

Borghi, A., Rodriguez-Florez, N., Rodgers, W., James, G., Hayward, R., Dunaway, D. et al., (2018). Spring assisted cranioplasty: a patient specific computational model. *Med Eng Phys.* 53 58-65. doi: 10.1016/j.medengphy.2018.01.001

Care, H., Kennedy-Williams, P., Cunliffe, A., Denly, S., Horton, J., Kearney, A. et al., (2019). Preliminary analysis from the craniofacial collaboration United Kingdom developmental outcomes in children with sagittal synostosis. *J Craniofac Surg.* 30:6 1740-1744. doi: 10.1097/SCS.0000000000005575

Coats, B., Margulies, S. (2006). Material properties of human infant skull and suture at high rates. *J Neurotrauma.* 23:8 1222-1232. doi: 10.1089/neu.2006.23.1222

Cross, C., Khonsari, R.H., Gailey, L., Paternoster, G., Johnson, D., Ventikos, Y. et al., (2021a). Using sensitivity analysis to develop a validated computational model of post-operative calvarial growth in sagittal craniosynostosis. *Front Cell Dev Biol.* 9. 621249. doi: 10.3389/fcell.2021.621249. eCollection 2021



Cross, C., Khonsari, R.H., Larysz, D., Johnson, L., Kölby, L., Moazen, M. (2021b). Predicting and comparing three corrective techniques for sagittal craniosynostosis. *Sci Rep.* 11. 21216. doi: <https://doi.org/10.1038/s41598-021-00642-7>

Fischer, S., Maltese, G., Tarnow, P., Wilkberg, E., Bernhardt, P., Kölby, L. (2016). Comparison of Intracranial Volume and Cephalic Index After Correction of Sagittal Synostosis With Spring-assisted Surgery or Pi-plasty. *J Craniofac Surg.* 27:2 410-413. doi: 10.1097/SCS.0000000000002519

Gailey, L., Hemmocq, C., Cross, C., Arnaud, D., Larysz, L., Kölby, L. et al., (2021). Management of sagittal craniosynostosis: Morphological comparison of 8 surgical techniques. *Br J Oral Maxillofac Surg.* doi: <https://doi.org/10.1016/j.bjoms.2021.09.017>

Gou, L., Vardakis, J.C., Chou, D., Ventikos, Y. (2020). A multiple-network poroelastic model for biological systems and application to subject-specific modelling of cerebral fluid transport. *Int J Eng Sci.* 147 103204. doi: <https://doi.org/10.1016/j.ijengsci.2019.103204>

Hashim, P., Patel, A., Yang, J., Travieso, R., Turner, J., Losee, J., (2014). The Effects of whole vault cranioplasty versus strip craniectomy on long term neuropsychological outcomes in sagittal craniosynostosis. *Plast Reconstr Surg.* 134:3 491-501. doi: 10.1097/PRS.0000000000000420

Herring, S.W. (2008). Mechanical influence on sutures development and patency. *Front Oral Biol.* 12:41 41–56. doi: 10.1159/0000115031

Jane, J.A., Edgerton, M.T., Futrell, J.W. (1978). Immediate correction of sagittal synostosis. *Journal of Neurosurgery.* 49:5 705-710. doi: <https://doi.org/10.3171/jns.1978.49.5.0705>

Jimenez, D.F., Barone, C.M., (2012). Endoscopic technique for sagittal synostosis. *Childs Nerv Syst: CnNS.* 28:9 1333-1339. doi: 10.1007/s00381-012-1768-y

Johnson, D., Wilkie, A.O.M. (2011). Craniosynostosis. *Eur J Hum Genet.* 19:4 369–376. doi: 10.1038/ejhg.2010.235

Kljajic, M., Maltese, G., Tarnow, P., Sand, P., Kölby, L. (2019). The cognitive profile of children with nonsyndromic craniosynostosis. *Plast Reconstr Surg.* 143:5 1037e-1052e. doi: 10.1097/PRS.00000000000005515

- Landes, C.A., Ballon, A., Roth, C. (2006). In-patient versus in vitro degradation of P(L/DL)LA and PLGA. *J Biomed Mater Res.* 76:6 403-411. doi: 10.1002/jbm.b.30388
- Lee, C., Richtsmeier, J.T., Kraft, R.H. (2017). A computational analysis of bone formation in the cranial vault using a coupled reaction-diffusion strain model. *Journal Mech Med Biol.* 17:4 1750073. doi: 10.1142/S0219519417500737
- Libby, J., Marghoub, A., Johnson, D., Khonsari, R.H., Fagan, M.J. (2017). Modelling human skull growth: a validated computational model. *J R Soc Interface.* 14:130 20170202. doi: 10.1098/rsif.2017.0202
- Likus, W., Bajor, K., Gruszczyńska, J., Baron, J., Markowski, M., Machnikowska-Sokołowska, D. et al., (2014). Cephalic index in the first three years of life: study of children with normal brain development based on computed tomography. *The Scientific World Journal.* 502836. doi: 10.1155/2014/502836
- Malde, O., Cross, C., Lim, C.L., Marghoub, A., Cunningham, M.L., Hopper, R.A. et al., (2020). Predicting calvarial morphology in sagittal craniosynostosis. *Sci Rep.* 10:3. doi: 10.1038/s41598-019-55224-5
- Malde, O., Libby, J., Moazen, M. (2019). An overview of modelling craniosynostosis using finite element method. *Mol Syndromol.* 10:1-2 74-82. doi: 10.1159/000490833
- Marghoub, A., Libby, J., Babbs, C., Pauws, E., Fagan, M.J., Moazen, M. (2018). Predicting calvarial growth in normal and craniosynostotic mice using a computational approach. *Jour Anat.* 232:3 440-448. doi: <https://doi.org/10.1111/joa.12764>
- Marghoub, A., Libby, J., Babbs, C., Ventikos, Y., Fagan, M.J., Moazen, M. (2019). Characterizing and modelling bone formation during mouse calvarial development. *Phys Rev Lett.* 122:4 048103. doi: <https://doi.org/10.1103/PhysRevLett.122.048103>
- Margulies, S.S., Thibault, K.L. (2000). Infant skull and suture properties: measurements and implications for mechanisms of pediatric brain injury. *J Biomech Eng.* 122:4 364-371. doi: 10.1115/1.1287160
- Mathijssen, I.M.J. (2015). Guideline for care of patients with the diagnoses of craniosynostosis: working group on craniosynostosis. *J Craniofac Surg.* 26:6 1735–1807
- Meyer, P., Renier, D., Arnaud, E., Jarreau, M.M., Charron, B., Buy, E. et al., (1993). Blood loss during repair of craniosynostosis. *Br J of Anaesth.* 71:6 854-857. doi: 10.1093/bja/71.6.854

Moazen, M., Peskett, E., Babbs, C., Pauws, E., Fagan, M. (2015). Mechanical properties of calvarial bones in a mouse model for craniosynostosis. *PloS One*. 10:5 1–13. doi: <https://doi.org/10.1371/journal.pone.0125757>

Opperman, L.A. (2000). Cranial sutures as intramembranous bone growth sites. *Dev Dyn*. 485 472–485. doi: 10.1002/1097-0177(2000)9999:9999

Ranly, D.M. (2000). Craniofacial growth. *Dent Clin North Am*. 44:3 457-470.

Richtsmeier, J.T., Flaherty, K. (2013). Hand in glove: brain and skull in development and dysmorphogenesis. *Acta Neuropathol*. 125:4 469–489. doi: 10.1007/s00401-013-1104-y

Sgouros, S., Goldin, J.H., Hockley, A.D., Wake, M.J.C., Natarajan, K. (1999). Intracranial volume change in childhood. *J Neurosurg*. 91 610-616. doi: 10.3171/jns.1999.91.4.0610

Simpson, A., Wong, A.L., Bezuhly, M. (2017). Surgical comparison of nonsyndromic sagittal craniosynostosis. Concepts and controversies. *Ann Plast Surg*. 78:1 103-110. doi: 10.1097/sap.0000000000000713

Taylor, J.A., Maugans, T.A. (2011). Comparison of spring-mediated cranioplasty to minimally invasive strip craniectomy and barrel staving for early treatment of sagittal craniosynostosis. *The J Craniofac Surg*. 22:4 1225-1229. doi: 10.1097/SCS.0b013e31821c0f10

Thomas, G.P.L., Johnson, D., Byren, J.C., Judge, A.D., Jayamohan, S.A., Magdun, P.G. et al., (2015). The incidence of raised intracranial pressure in nonsyndromic sagittal craniosynostosis following primary surgery. *J Neurosurg Pediatr*. 15:4 350-360. doi: 10.3171/2014.11.PEDS1426

van Veelen, M.C., Jippes, M., Carolina, J.C.A., de Rooi, J., Dirven, C.M.F., van Adrichem, L.N.A. et al., (2016). Volume measurements on three-dimensional photogrammetry after extended strip versus total cranial remodeling for sagittal synostosis: A comparative cohort study. *J Craniomaxillofac Surg*. 44:10 1713-1718. doi: <https://doi.org/10.1016/j.jcms.2016.07.029>

Weickenmeier, J., Fischer, C., Carter, D., Kuhl, E., Goriely, A. (2017). Dimensional, geometrical, and physical constraints in skull growth. *Phys Rev Lett*. 118:24 248101. doi: 10.1103/PhysRevLett.118.248101

## Figures:

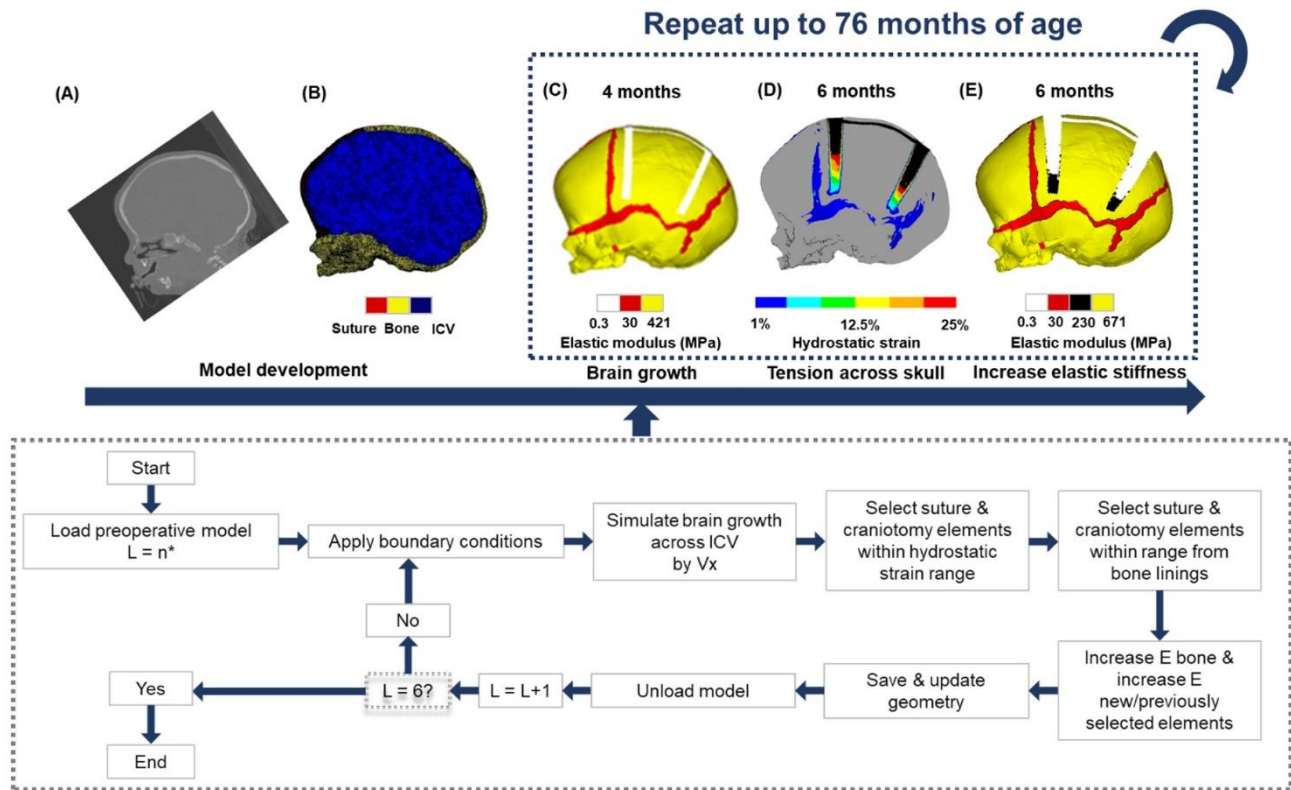
**Fig. 1:** Using CT -scan data at an initial preoperative age of 4 months (A), a 3D finite element model was developed (B). The chosen surgical technique at the appropriate age was performed (C). The intracranial volume was then expanded to a specified volume in 6 load steps (D). Elements across the sutures and craniotomies were then selected based on the level of hydrostatic strain and/or radii process from the bone lining, following the algorithm described in the flow chart. This process was repeated while updating the material properties and geometry of the model at each load step until the final load step has been reached (E). The intracranial volume at the final load step was equivalent to 76 months of age.

**Fig. 2:** Predicted bone formation across all replicated techniques at the postoperative age of 76 months. The material properties across the newly and previously selected elements were updated at each load step.

**Fig. 3:** Cephalometric measurements across all replicated approaches. The predicted length (A) and width (B) were used to calculate the cephalic index (C). The circumference (D) was measured in the transverse plane as shown within the diagram.

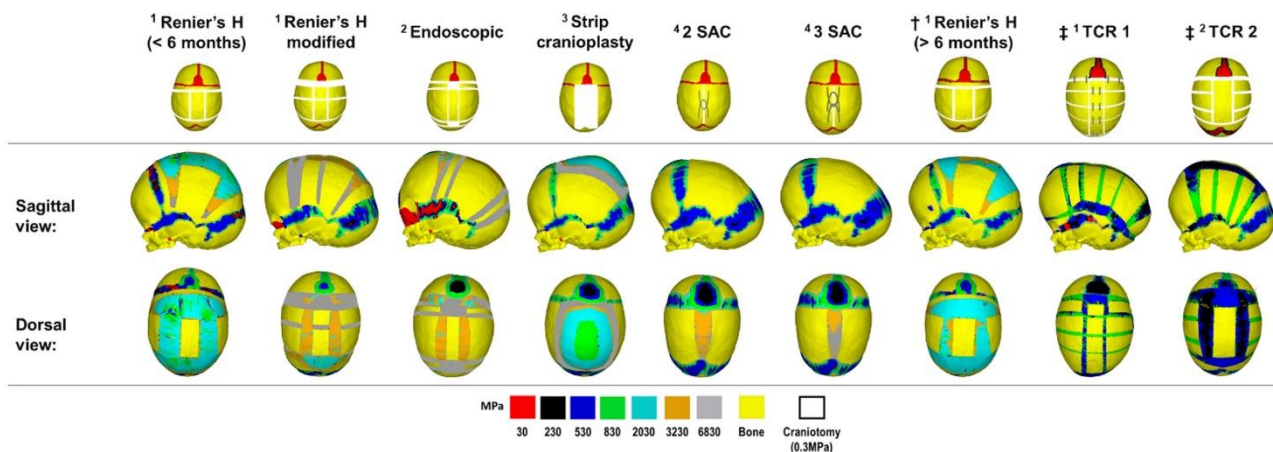
**Fig. 4:** The predicted contact pressure captured across the brain surface for all replicated techniques at 76 months (A). Contact pressure was quantified across different regions of the ICV for each replicated technique with standard deviations corresponding to the nodal distribution across the highlighted regions (B). All results were recorded at 76 months of age.

503  
504



\*: n varies based on the age at which chosen surgical technique is replicated.

505  
506  
507  
508  
509  
510  
511  
512  
513  
514  
515  
516  
517  
518  
519  
520  
521  
522  
523  
524  
525



<sup>1</sup> Adopted from the Department of Maxillofacial Surgery and Plastic Surgery, Necker – Enfants Malades University Hospital, Assistance Publique – Hôpitaux de Paris, School of Medicine (Paris, France)

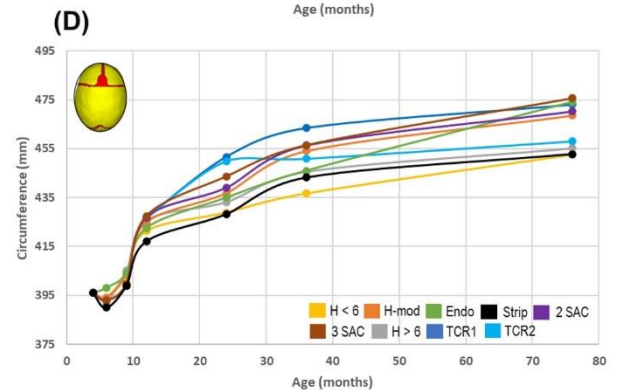
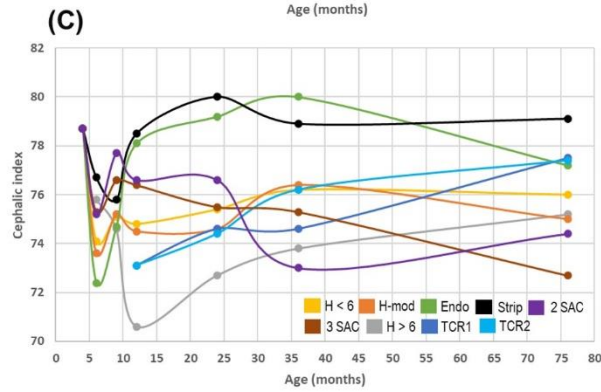
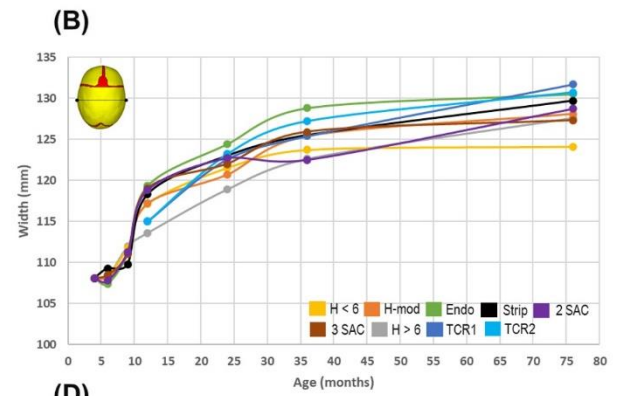
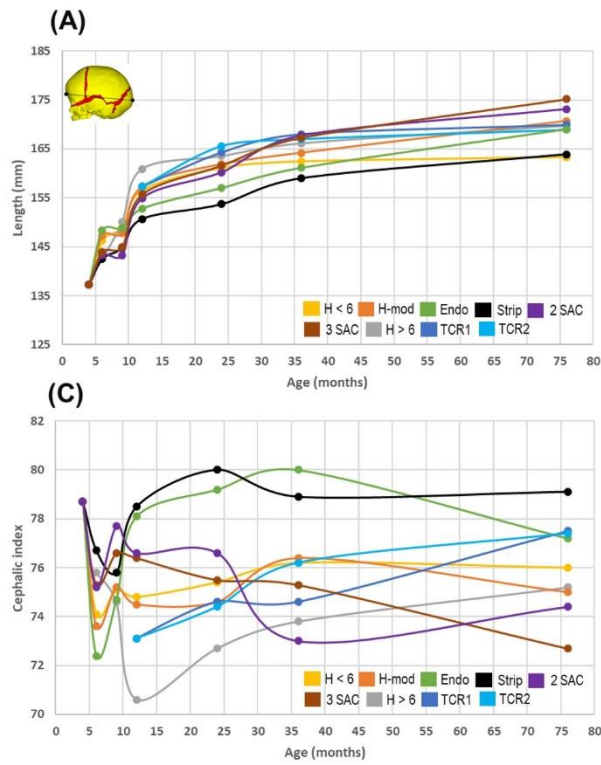
<sup>2</sup> Adopted from the Department of Head and Neck Surgery for Children and Adolescents, University of Warmia and Mazury (Olsztyn, Poland)

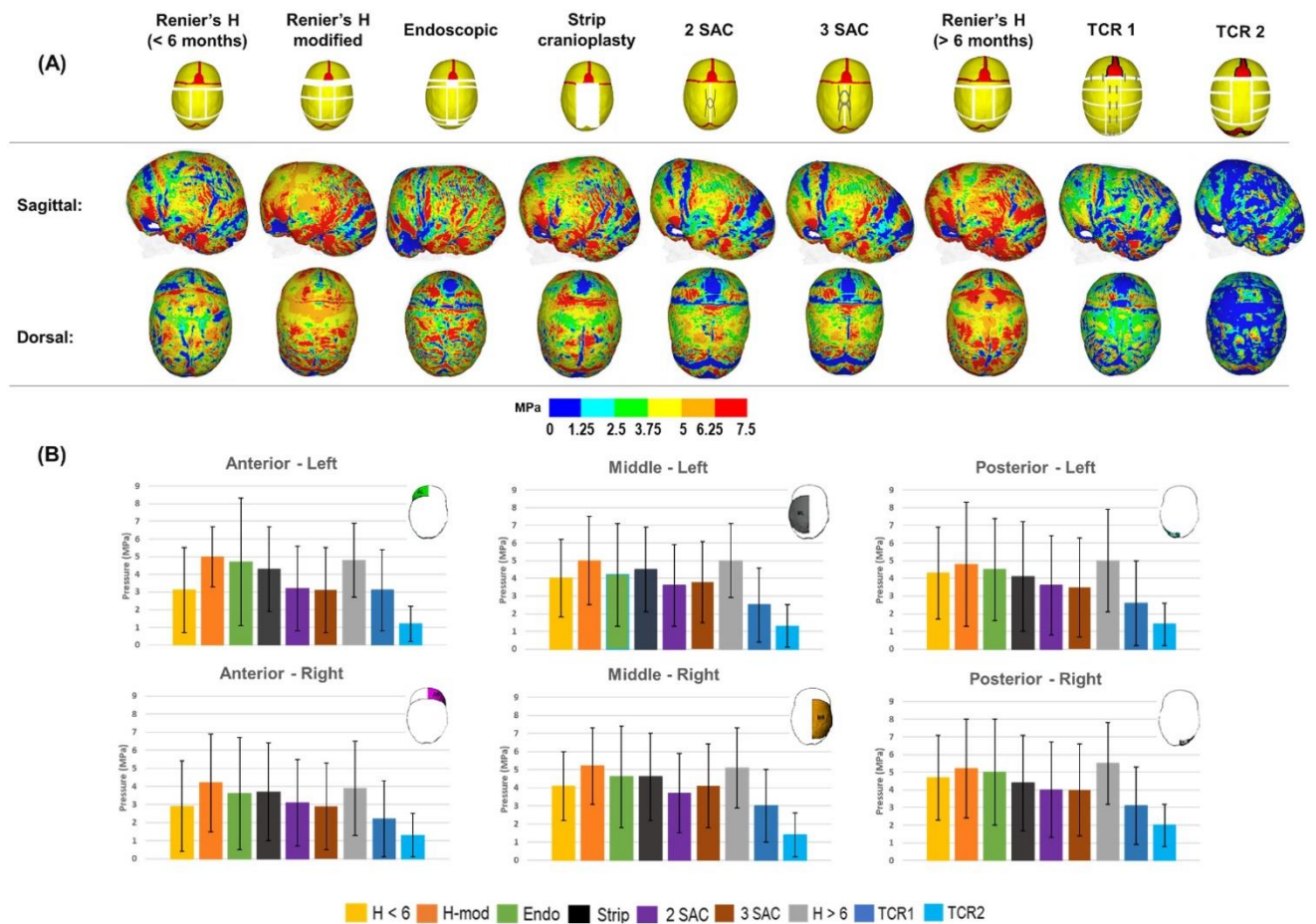
<sup>3</sup> Adopted from the Oxford Craniofacial Unit, Oxford University Hospital (Oxford, UK)

<sup>4</sup> Adopted from Department of Plastic Surgery, Sahlgrenska University Hospital (Gothenburg, Sweden)

†: Intervention at 6 months

‡: Intervention at 12 months







Supplement:

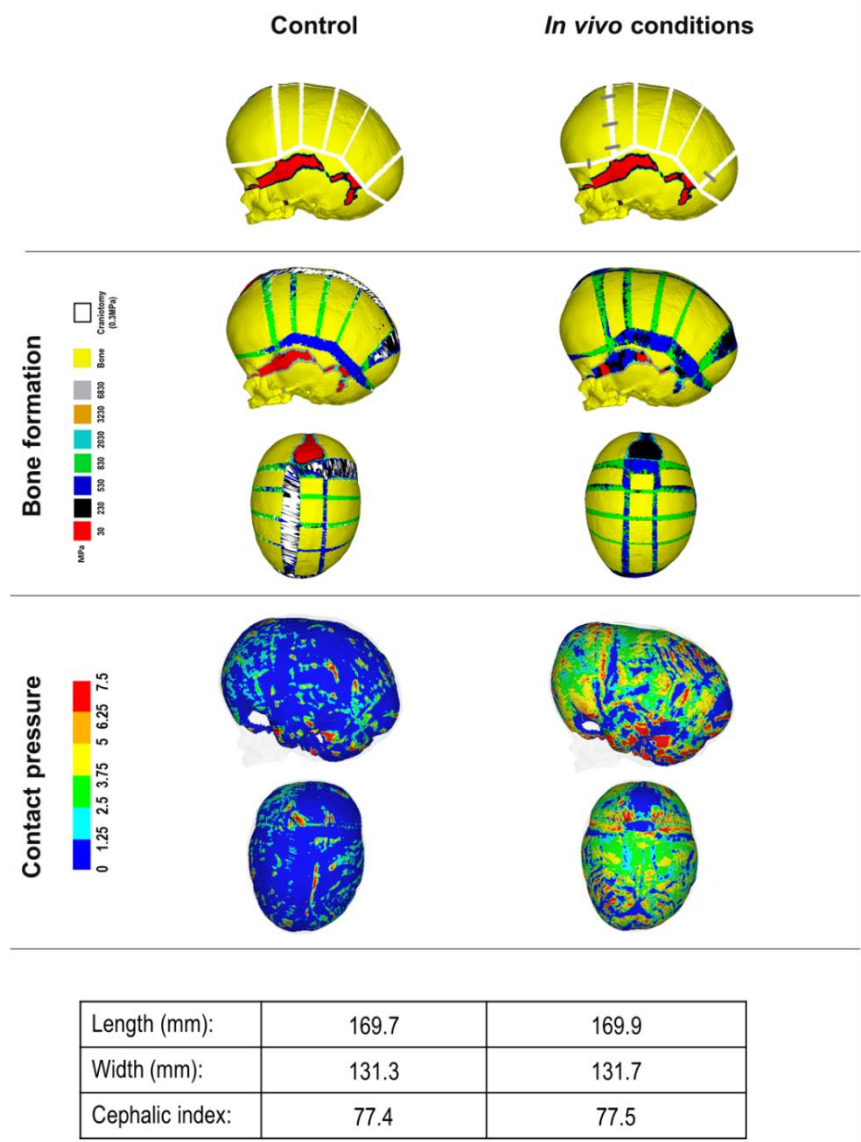


**Fig. S1:** Sensitivity results on the effects of simulating bioabsorbable fixators across the TCR 1 corrective technique at 12 months of age (Top row). We compared this with a control scenario, in which such fixators were absent. We specified the elastic modulus of the fixators as 2000 MPa. The fixators were then parameterised to be removed by 12 months after insertion, to represent the degradation of the fixators. Here, we captured a large change in the level of bone formation across the two approaches by 76 months of age (Middle row), in which a lack of fixators delayed the rate of formation across the temporal and anteroposterior craniotomies. We further observed a larger increase in the brain contact pressure (Bottom row) when fixators were present. Although large changes between these scenarios were captured, changes in cephalic measurements (See table) displayed little overall change.

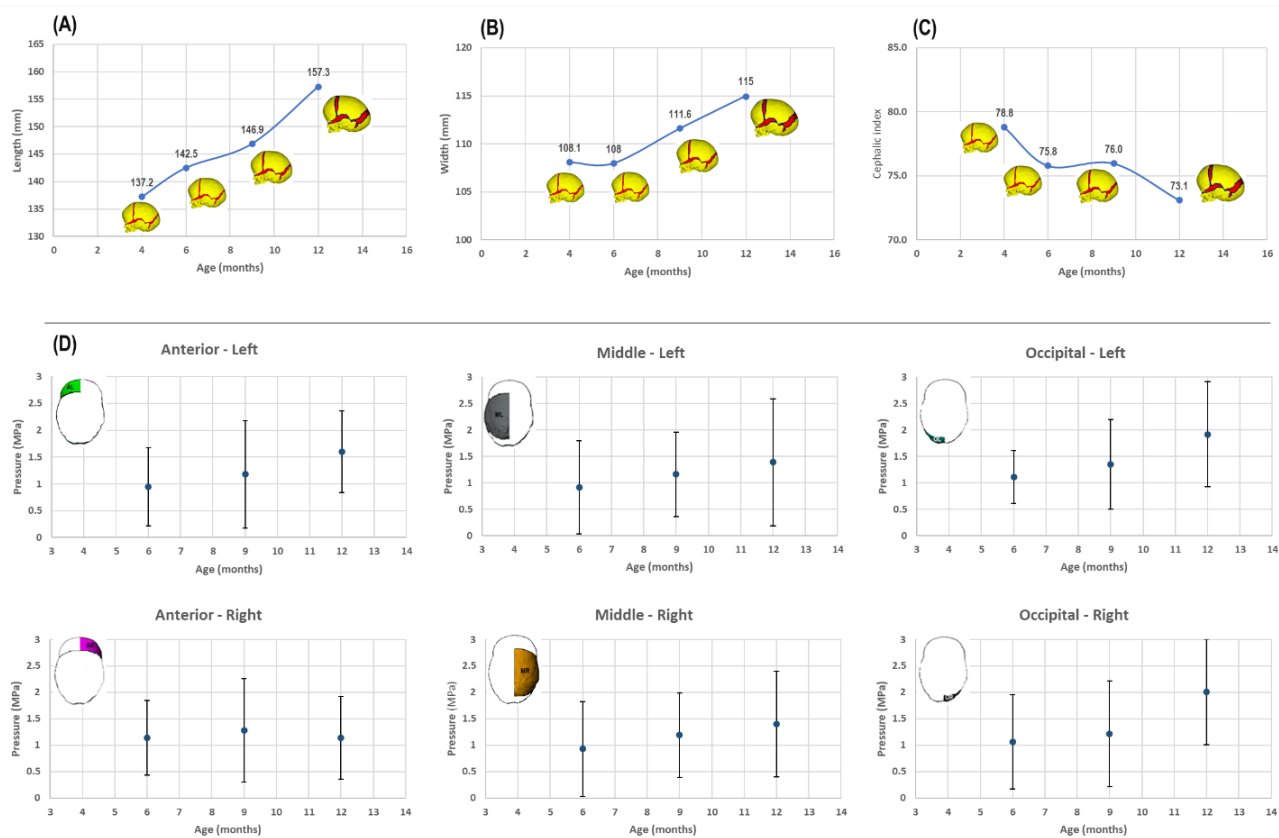


**Fig. S2:** Cephalometric measurements (Top row) under an unoperated condition up to 12 months of age, enabling us to replicate techniques later than the initial 4-month geometry. A greater length (A) was captured whilst a reduced width (B) was achieved, leading to a lower cephalic index with increasing age (C). Interestingly, the level of contact pressure was seen to be asymmetrical across the anterior regions, whilst the largest pressure levels were captured across the occipital area (D).

# A preliminary analysis of replicating the biomechanics of helmet therapy for sagittal craniosynostosis

Connor Cross<sup>1</sup>, Hans Delye<sup>2</sup>, Roman Hossein Khonsari<sup>3</sup>, Yiannis Ventikos<sup>1</sup>, Mehran Moazen<sup>1</sup>

<sup>1</sup> Department of Mechanical Engineering, University College London, London, UK

<sup>2</sup> Department of Neurosurgery, Radboudumc Nijmegen, The Netherlands

<sup>3</sup> Department of Maxillofacial Surgery and Plastic Surgery, Necker – Enfants Malades Hospital, Assistance Publique – Hôpitaux de Paris, France

## Corresponding author:

Mehran Moazen; Department of Mechanical Engineering, University College London, Torrington Place, London, WC1E 7JE, UK; T: +44 (0) 207 679 3862; E: [M.Moazen@ucl.ac.uk](mailto:M.Moazen@ucl.ac.uk)

## Summary

Sagittal craniosynostosis results in compensatory anteroposterior overgrowth, followed by bitemporal narrowing during infancy. There are many surgical options available to restore the aesthetic shape and minimise functional complications. The endoscopically assisted strip craniectomy approach followed by postoperative helmet therapy is a favoured and promising method, however, an understanding of the helmet's postoperative impacts on the growth from a mechanical perspective is limited. Here, we present a preliminary approach to represent the effects of postoperative helmet therapy using a computational approach. A previously developed four month old sagittal craniosynostosis 3D patient model was used. The strip craniectomy incisions were replicated across the segmented parietal bones. Areas across the calvarial were selected and constrained to represent the helmet placement after surgery. A linear expansion method was applied to the modelled intracranial volume to represent the calvarial growth, along with an algorithmic bone formation applied across the sutures and craniotomies. A contact behaviour was specified between the interface of the modelled intracranial volume, which could measure the level of contact pressure during simulated growth. Three variations of helmet therapy were investigated, where the timings of helmet removal alternated between two, five, and eight months after surgery. The simulated results suggest that the prolonging of helmet placement has a beneficial impact on the postoperative morphology while limiting the build-up of contact pressure across the modelled intracranial volume. The study here aims to inform surgeons of the mechanical aspects of helmet therapy while laying the foundations for further *in vitro* studies.

**Keywords:** Sagittal craniosynostosis, Helmet therapy, Finite element, Calvarial growth, Bone formation

## Introduction

Infant skull growth is most rapid during the first years of life, regulated by a complex interplay of different genes that control the proliferation-differentiation balance of cells present across the sutures and dura mater [1]. Craniosynostosis is caused by the premature fusion of one or more of these cranial sutures and occurs in approximately 1:1700 live births. [2-4]. The most common form, sagittal craniosynostosis, produces compensatory anteroposterior overgrowth and is represented as a distinct 'keel-shaped' skull [5]. If left untreated, defects associated with neurodevelopmental and social complications may arise [6,7].

The treatment of sagittal craniosynostosis (i.e. scaphocephaly) primarily aims to address the morphological abnormality and reestablish normal growth [8]. One such treatment is endoscopically assisted strip craniectomy (EAC) followed by helmet therapy. The goal of EAC is to remove the fused portion of the bone and attempt to normalize the skull shape as soon as possible, assisted by the patient-specific helmet which is placed a few days after surgery [9]. The helmet therapy then guides the multidirectional driving force of the expanding brain without being constrictive towards the overall growth.

There is a large body of evidence found in the literature that this treatment modality for craniosynostosis achieves good results, both financially and cosmetically [10-12]. However, it remains unclear as to what degree the early re-opening of the suture (i.e. suturectomy) or the postoperative helmet therapy affects the morphological or functional changes across the skull and brain. Furthermore, the duration of helmet therapy varies between craniofacial centres. Ethically, assessing the cosmetic outcomes of alternating helmet durations within a clinical environment would prove impractical.

The finite element (FE) method is a powerful computational tool used to analyse a wide range of engineering problems [13]. Using these detailed FE models, computational algorithms have been used to investigate the management of craniosynostosis. More advanced methods have been able to accurately simulate the calvarial growth and bone formation after different types of surgical treatment [14-19]. Such methods have the capability to investigate the biomechanics of craniosynostosis and simulate the outcomes of various surgical parameters, such as postoperative helmet therapy.

The aim of this study was to investigate the biomechanics behind EAC treatment while undergoing three different durations of postoperative helmet therapy using a generic FE approach. The study here presents a preliminary investigation into replicating the effects and simulating the outcomes of postoperative helmet therapy years after surgery. The long term goal of this work is to provide the foundation for further *in vitro* experimentation.

## Materials & methods

### CT data

A previously used 3D model of a preoperative sagittal craniosynostosis patient at 4 months of age was developed using computed tomography (CT) data obtained from the Hôpital Necker – Enfants Malades Craniofacial Surgery Unit (Centre de Référence Maladies Rares Craniosténoses et Malformations Craniofaciales CRANIOST, Paris, France). The full ethical protocol for undertaking this study was approved by the institutional review board and committee from the Necker – Enfants Malades University Hospital. Informed consent was granted by the patient's guardian.

### **Image processing & surgical technique**

Anatomical 3D rendering of the CT data was performed in the imaging processing software, Avizo (Thermo Fisher Scientific, Mass, United States). Segmentation of the calvarial bones, cranial sutures, and the intracranial volume (ICV i.e. all internal calvarial components) was performed and displayed in figure 1 (A-D). The calvarial bones were selected automatically using the Hounsfield scale method to differentiate between the hard and soft tissues. Both sutures and the ICV were segmented manually.

The EAC technique, as performed at the Radboudumc Centre of Expertise Craniofacial anomalies (Radboudumc Nijmegen, The Netherlands), was replicated across the 3D model under the surgical teams' guidance and the detailed report of Delye *et al.*, (2018). Figure 1 (E) depicts the replicated craniotomies performed across the 3D model. In short, an anteroposterior suturectomy, measuring a width of approximately 30 mm, was made across the fused sagittal suture to encourage dorsal growth. Four wedge-shaped craniotomies were made across the parietal bones and extended towards the squamosal sutures to promote bitemporal widening. These wedges measured approximately 15 mm wide at their bases.

### **Finite element analysis**

A total of 4 million quadratic tetrahedral elements were transposed across the complete 3D model. A requirement for the importation into the chosen FE program, ANSYS (V19.0; Canonsburg, PA, USA). The program allows for the material properties to be defined as well as the skull growth, bone formation, ICV contact pressure, and helmet therapy to be computationally simulated.

Material properties of the calvarial bones, cranial sutures, and the ICV were all defined as linear isotropic and assigned an elastic modulus of 421 MPa, 30 MPa, and 10 MPa, respectively [16-20]. The replicated craniotomies possessed an elastic modulus of 0.3 MPa, to represent the natural 'gaps' made *in situ* and minimise the level of resistance on the simulated growth [16]. Both the ICV and craniotomies Poisson's ratio was selected as 0.1. A Poisson ratio of 0.3 was selected for the calvarial bone and cranial sutures.

### **Boundary conditions**

To represent the skull growth, a previously adopted thermal expansion analogy was introduced across the ICV of the model [21]. This simulates the expansive growth of the ICV across five load steps, from the initial preoperative 4 months of age volume (measuring 659 ml) to the approximate target follow up volume seen at 36 months of

age (measuring 1240 ml). At each load step, the age of the model was approximated by correlating the predicted volumes against relevant literature data [22]. This, in turn, allowed for the applicable time of removing the helmet to be determined. As the morphology of the skull shape changes, the geometry of the model was updated at each load step to represent the new skull shape. To avoid rigid body displacement, constraints in all degrees of freedom were placed around the foramen magnum and nasal ridge of the model.

Representing the ossification and bone healing under a computational scenario is a challenging and highly limited function compared to the complex biological processes seen *in vivo*. Nevertheless, the bone formation across the cranial sutures and craniotomies during growth was simulated here and adopted from a previous study [18].

In summary, the rate and distance of formation across the cranial sutures were dictated by the level of strain (generated by the expansion of the ICV) followed by a predetermined radius extending from the adjoining bony borders (determined by the changes in age at each load step). The bone healing across the craniotomies maintained only the former parameter (i.e. level of strain), allowing for spontaneous bone growth away from the bony borders to be permitted.

Cranial suture and craniotomy elements that met their relevant conditions had their elastic moduli updated at each load step to represent the effects of osteoblast cell behaviour [23]. Further, the calvarial bone components' elastic modulus was also updated to represent the changes in bone malleability with age.

Estimating the loads across the intracranial space (here, the ICV) using a surface-to-surface contact analysis is a previously used novel method for observing and quantifying the pressure changes under simulated growth. Although highly informative, clinically, such information may not represent the true pressure distribution or absolute values post-surgery. Nonetheless, in the interests of this work, this method was introduced to the EAC technique for examination. In short, the level of pressure across the ICV surface was visually captured and quantified. Parameters to minimise the interpenetration between these surfaces during growth were previously established and discussed elsewhere [16-19].

## **Helmet therapy**

A simplistic approach to model the effects of helmet therapy was developed (Figure 1 F). While not represented as a physical geometry across the model, globally coordinated constraints across the anterior (Y-axis), posterior (Y-axis), and lower bitemporal (X-axis) regions restrict the growth in the applicable axis. Allowing for no relative movement to be granted throughout the simulations. A permissible 20 mm level of dorsal displacement (Z-axis) was granted during growth. This value was chosen based on the surgeon's guidance and from a sensitivity study which is discussed in the appendix (See: Supplementary figures S1 and Table S1). The potential impacts regarding the helmets' thickness and material properties were not considered here.

The effects of helmet therapy were introduced to the FE model at 4 months of age, along with the replicated EAC surgery, and remained during simulated growth until the

helmet was 'removed' (i.e. deletion of all helmet-related constraints). The timing of helmet removal alternated across three scenarios, at 2 months, 5 months, and 8 months after surgery, respectively. The most latter time point reflects the average duration for patients reported by Delye *et al.*, (2016). A control scenario, where only the EAC surgery was replicated across the model (i.e. No helmet introduced) was used as a comparative scenario.

## **Simulations and measurements**

All scenarios underwent calvarial growth up to the follow up age of 36 months. The predicted pattern of bone formation was captured at each load step during simulated calvarial growth. The cephalic length (glabella to opisthocranium), width (left and right euryons) and index (width divided by the length and multiplied by a hundred) were quantified during calvarial growth. The level of contact pressure across the ICV was captured and compared at each load step during simulated calvarial growth across all scenarios.

## **Results**

### **Pattern of bone formation & skull morphology**

The simulated patterns of bone formation and morphological shape across each helmet scenario are highlighted in figure 2. All helmeting scenarios and the single non-helmet scenario achieved craniotomy healing (here, defined as the initial white material no longer being present) by 20 months after surgery. All sutures, disregarding the anterior fontanelle, achieved a similar pattern of bone formation by the final load step of 36 months of age for all scenarios.

While the lack of a postoperative helmet did not impact the level or region of suture bone formation or bone healing during the simulated growth, a characteristic dorsal 'bulge' was evident by 36 months of age. This was seen to have corrected itself once the helmet had been introduced, regardless of the duration. Prolonging the helmet's removal (i.e. 8 months) was seen to encourage greater bitemporal widening in the long term when compared to the shorter durations (2 and 5 months).

Figure 3 and Table 1 quantify the changes in length, width and cephalic index across all helmeting scenarios up to the follow up age of 36 months. As each scenario utilised the same preoperative model, all represent identical length (137.2 mm), width (108.1 mm) and cephalic index (78.7) at 4 months of age. By 36 months of age, the greatest length was recorded in the 'No helmet' scenario (162.9 mm). The shortest was seen in the 8 months helmeting duration (146.6 mm). A difference of only 4 mm was seen across all simulated scenarios widths by 36 months. The highest was seen in the 8 months helmet duration (126.4 mm) whilst the lowest was in the 'No helmet' scenario (122.2 mm). These observations were reflected in the cephalic indexes, where the highest value was achieved by the 8 months duration helmet (86.2), while the lowest was recorded in the 'No helmet' scenario (75.0).

### **Contact pressure analysis**

Figure 4 presents the surface ICV contact pressure levels during growth for all helmet scenarios. The Initial pressure levels at 4 months of age were unobtainable for comparison here. Nonetheless, at 36 months of age, largely similar pressure patterns were captured across all scenarios involving the helmet, regardless of the duration of the placement. Areas of higher pressure were seen across the temporal, occipital, and dorsal regions for all helmet conditions while being slightly lower across the anterior region. The absence of the helmet resulted in a more plateaued level of pressure across the ICV.

## Discussion

Sagittal craniosynostosis results in over compensatory anteroposterior growth, ventrodorsal shortening, and bitemporal narrowing. The method of postoperative helmet therapy aims to help guide the skull growth vectors to address these morphological abnormalities after the initial surgery has been performed. The development of computational models and algorithms has the potential to optimise the management of this condition by answering key biomechanical-based questions. This study assesses the impacts that various durations of postoperative helmets could have on long term patient outcomes. Here, the morphological and contact pressure across the ICV was assessed at the follow up age of 36 months, with varied outcomes.

Due to the lack of standard post-EAC CT scans and the variability of the modelling approaches shown here, mostly regarding the duration of helmeting, the study suffers a lack of morphological or contact pressure validity. On the other hand, the generic FE model used here had been previously validated using patient-specific follow up data which could support a level of validity in this study [16]. The debate on optimising the method of correcting scaphocephaly is still a highly discussed topic within the literature [6,8]. With the advancements in computational modelling approaches, conclusions to such discussions could be addressed.

The method of replicating the calvarial growth and bone formation discussed here was adopted from a previous study [18], presenting a promising method of replicating the impacts that postoperative calvarial healing could have on surgical outcomes. However, the modelling approach lacks key biological considerations when compared to the true *in vivo* conditions [1,23]. In particular, a large level of cranial patency was seen 8 months after the replicated surgery. The regenerative abilities of bone during infancy, with rare exceptions, can achieve complete surgical healing weeks after surgery [24]. From a modelling point of view, however, it could be argued that the prolonging of calvarial healing in these simulations allows the model to continue to estimate the long term postoperative morphology, minimising the constrictions on the growth.

Helmet therapy after EAC has been reported to be a cost-effective method of correction while achieving the overall surgical goals for sagittal craniosynostosis. The technique adopted here is reported by Delye *et al.*, [10], where 10 months postoperative helmeting is the standard practice. Such reports detail overall improvement to the cephalic shape postoperative. Although they are overestimated, such observations were also captured in our simulations. Regarding the discussed method of replicating the helmet in our model, there is a clear distinction between the incorporation of the helmet and the postoperative duration. Most notably is the impact on the length which,



unlike the width measurements, showed the overall greatest change. This is an understandable response, due to the greater levels of constraints placed across the frontal and occipital bones vs. the temporal regions (Figure 1-F).

In reality, the average number of helmets produced throughout treatment is two [9]. This could grant a level of anteroposterior growth as the newly applied helmet forms the shape of the patient's skull. However, such a parameter is not considered here. This leads to almost zero give in skull lengthening throughout the simulated growth when the helmet is applied.

An alternative method to the helmet modelling approach shown here, which may address this issue, would be the rendering of a 3D solid helmet model, parameterised to fit and correct the generic FE model used here. However, due to the current computational costs of running these models, this prospect will be considered for future studies.

The study of simulating and comparing the level of contact pressure across the modelling ICV is a relatively new and novel approach for investigating the interaction between growing ICV and the overline calvarial bones across various surgical options [14,16,17]. Due to the lack of validity in this analysis, the simulations shown here must be interpreted with caution. It is hoped that such simulated results could assist with the interpretation of neurofunctional characteristics years after surgical intervention. Although the correlation between the ICV contact pressure shown here and the defective consequences of functional characteristics is unrealistic, a secondary function of these simulations is estimating the possible elevations of postoperative intracranial pressure [28,29]. Within the literature, the impacts on the morphological outcomes using the helmet therapy approaches have been previously recorded [25,26]. However, there is limited data which records the cognitive attainments after surgery [27].

## Conclusion

The work presented here provides a novel methodology for simulating the impacts three alternating durations of helmet therapy after EAC have on the skull morphology using the finite element method. Although the validation of these simulations could not be performed, these simulations showed that the duration of helmet therapy after EAC influenced the cephalic index at 36 months, with the highest value achieved by the 8 months duration helmet (86.2), while the lowest was recorded in the 'No helmet' scenario (75.0). This study provides critical information which could aid surgeons in understanding the postoperative outcomes of endoscopically assisted strip craniectomy accommodated with postoperative helmet therapy. Further studies aim to replicate the effects of helmet therapy under an *in vitro* approach.

## **Acknowledgements**

This work was supported by the Rosetrees Trust through the PhD research project [A1899] and PhD Plus project [PhD2021\100017] and Engineering and Physical Sciences Research Council (EP/W008092/1).

## **Conflict of interest statement**

The authors declare that the research was conducted in the absence of any commercial or financial relationships that could be construed as a potential conflict of interest.

## **Data availability**

The data used to support the findings of this study are included within the article and supplementary data.

## **Ethical approval**

No ethical approvals were required for the premise or experimentations that were undertaken during this study.

## References

1. Johnson D, Wilkie AOM. Craniosynostosis. *Eur J Hum Genet* 2011;19;369–76.
2. Morriss-Kay GM, Wilkie AOM. Growth of the normal skull vault and its alteration in craniosynostosis: insights from human genetics and experimental studies. *J Anat* 2005;207;637–53.
3. Cornelissen M, Otterlander BD, Rizopoulos D, Hulst RD, Molen AMD, Horst CD, Delye H, Veelen ML, Bonsel G, Mathijssen I. Increase in the prevalence of craniosynostosis. *J Craniomaxillofac Surg* 2016;44;1273–79.
4. Kalantar-Hormozi H, Abbaszadeh-Kasbi A, Sharif G, Davai N, Kalantar-Hormozi A. Incidence of familial craniosynostosis among patients with nonsyndromic craniosynostosis. *J Craniofac Surg* 2019;30;514–17.
5. Virchow R. Über den Cretinismus, namentlich in Franken, und über pathologische Schädelformen. *Verh Phys Med Gesell Würzburg* 1851;2:230–71.
6. Hashim PW, Patel A, Yang JF, Travieso R, Turner J, Losee JE, Pollack I, Jane J, Kanev P, Mayes L, Duncan C, Bridgett DJ, Persing JA. The effects of whole-vault cranioplasty versus strip craniectomy on long term neuropsychological outcomes in sagittal craniosynostosis. *Plast Reconstr Surg* 2014;134;491–501.
7. Sanger C, David L, Argenta L. Latest trends in minimally invasive synostosis surgery: a review. *Curr Opin Otolaryngol Head Neck Surg* 2014;22:316–21.
8. Kaiser G. Sagittal synostosis – its clinical significance and the results of three different methods of craniectomy. *Childs Nerv Syst* 1988;44;223–30.
9. Delye HHK, Arts S, Borstlap WA, Blok LM, Driessen JJ, Meulstee JW, Maal TJJ, Van Lindert EJ. Endoscopically assisted craniosynostosis surgery (EACS): the craniofacial team Nijmegen experience. *J Craniomaxillofac Surg* 2016;44;1029–36.
10. Delye HHK, Borstlap WA, Van Lindert EJ. Endoscopy-assisted craniosynostosis surgery followed by helmet therapy. *Surg Neurol Int* 2018;9.
11. Chan JWH, Stewart CL, Stalder MW, St Hilaire H, McBride L, Moses MH. Endoscope-assisted versus open repair of craniosynostosis: a comparison of perioperative cost and risk. *Journal Craniofac Surg* 2013;24;170–74.
12. Skolnick GB, Murthy S, Patel KB, Huang Z, Naidoo SD, Ju T, Smyth MD, Woo AS. Long term characterization of cranial defects after surgical correction for single-suture craniosynostosis. *Ann Plast Surg* 2019;82;679–85.
13. Fagan MJ. Finite element analysis: theory and practice. Longman Scientific & Technical, 1992.

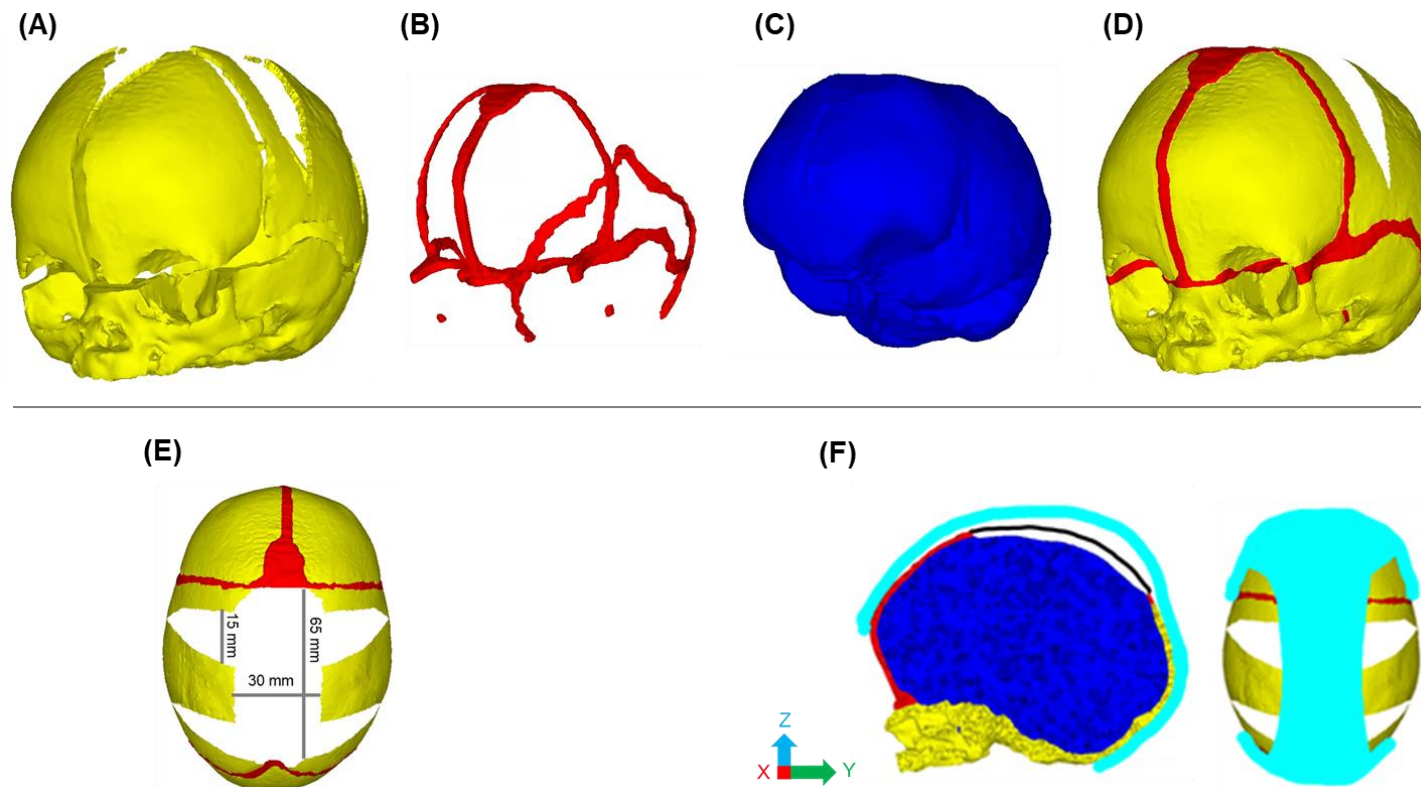
14. Malde O, Libby J, Moazen M. An overview of modelling craniosynostosis using finite element method. *Mol Syndromol* 2019;10;74–82.
15. Marghoub A, Libby J, Babbs C, Ventikos Y, Fagan MJ, Moazen M. Characterizing and modeling bone formation during mouse calvarial development. *Phys Rev Lett* 2019;122;048103.
16. Cross C, Khonsari RH, Galiay L, Paternoster G, Johnson D, Ventikos Y, Moazen M. Using sensitivity analysis to develop a validated computational model of postoperative calvarial growth in sagittal craniosynostosis. *Front Cell Dev Biol* 2021;9;621249.
17. Cross C, Khonsari RH, Larysz D, Johnson D, Kölby L, Moazen M. Predicting and comparing three corrective techniques for sagittal craniosynostosis. *Sci Rep* 2021;11;21216.
18. Cross C, Khonsari RH, Ventikos Y, Moazen M. Refining a tissue differentiation algorithm to predict calvarial growth following treatment of sagittal craniosynostosis (in press).
19. Malde O, Cross C, Lim CL, Marghoub A, Cunningham ML, Hopper RA, Moazen M. Predicting calvarial morphology in sagittal craniosynostosis. *Sci Rep* 2020;10;3.
20. Moazen M, Peskett E, Babbs C, Pauws E, Fagan MJ. Mechanical properties of calvarial bones in a mouse model for craniosynostosis. *PLoS One* 2015;12;e0125757.
21. Libby J, Marghoub A, Johnson D, Khonsari RH, Fagan MJ, Moazen M. Modelling human skull growth: a validated computational model. *J R Interface* 2017;14;20170202.
22. Sgouros S, Golden JH, Hockley AD, Wake MJC, Natarajan K. Intracranial volume changes in childhood. *J Neurosurg* 1999;91;610-16.
23. Weickenmeier J, Fischer C, Carter D, Kuhl E, Goriely A. Dimensional, geometrical, and physical constraints in skull growth. *Phys Rev Lett* 2017;118;248101.
24. Thenier-Villa J, Sanromán-Álvarez P, Miranda-Lloret P, Ramirez M. Incomplete reossification after craniosynostosis surgery—incidence and analysis of risk factors: a clinical-radiological assessment study. *J Neurosurg Pediatr* 2011;22;120-127.
25. Le MB, Patel K, Skolnick G, Naidoo S, Smyth M, Kane A, Woo AS. Assessing long term outcomes of open and endoscopic sagittal synostosis reconstruction using three-dimensional photography. *J Craniofac Surg* 2014;25;573-576.

- 494 26. Skolnick GB, Yu JL, Patel KB, David LR, Couture DE, Smyth MD, Woo AS.  
495 Comparison of 2 sagittal craniosynostosis repair techniques: spring-assisted  
496 surgery versus endoscope-assisted craniectomy with helmet molding therapy.  
497 Cleft Palate Craniofac J 2021;58;678-686.  
498
- 499 27. Care H, Kennedy-Williams P, Cunliffe A, Denly S, Horton J, Kearney A,  
500 Knapp M, O'Leary G, Piggott K, Pinckston M, Rooney N, Thomas S, Dalton L.  
501 Preliminary analysis from the craniofacial collaboration United Kingdom  
502 developmental outcomes in children with sagittal synostosis. J Craniofac Surg  
503 2019;30;1740-1744.  
504
- 505 28. Van De Beeten SDC, Mathijssen IMJ, Kamst NW, Veelen MC. Headache in  
506 postoperative isolated sagittal synostosis. Plast Reconstr Surg  
507 2019;143;798e-805e.  
508
- 509 29. Thomas GPL, Johnson D, Bryen JC, Judge AD, Jayamohan J, Magdum SA,  
510 Richards PG, Wall AS. The incidence of raised intracranial pressure in  
511 nonsynodromic sagittal craniosynostosis following primary surgery. J  
512 Neurosurg Pediatr 2015;15;350-354.  
513  
514  
515  
516  
517  
518

519 **Figures**

520

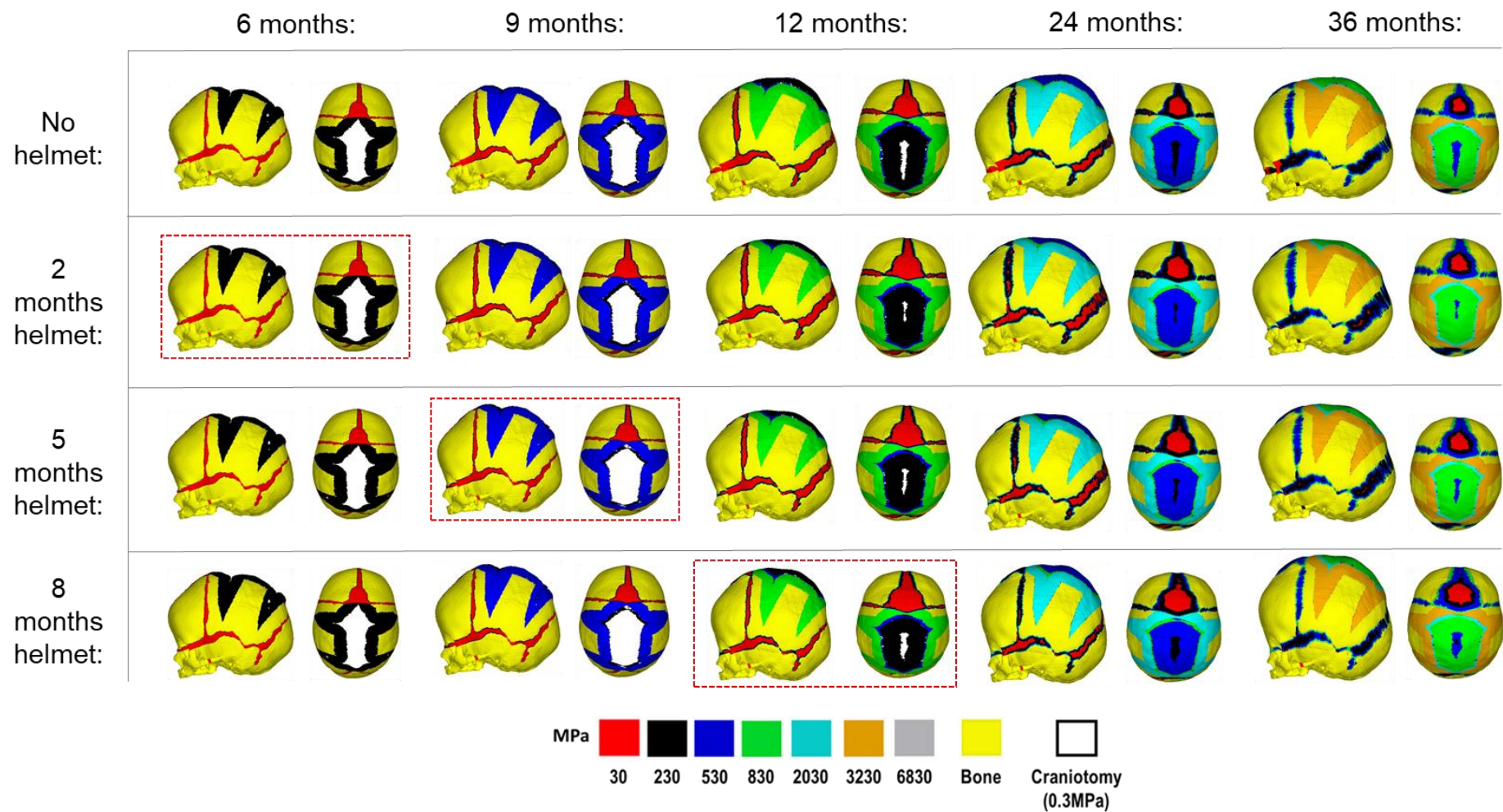
521 **Figure 1:** Process of 3D model development. CT imaging is used to segment the calvarial bones (A), sutures (B), and the ICV (C).  
522 All are incorporated to create the preoperative model at 4 months of age (D), adopted from Cross et al., [17]. The centre-specific  
523 craniotomies (marked in white) are replicated across the parietal bone (E). Constraints to represent the helmet therapy (light blue)  
524 are placed across the temporal, frontal, and parietal bones. While a level of vertex displacement is granted during simulated growth,  
525 quantified by a performed sensitivity test (F).



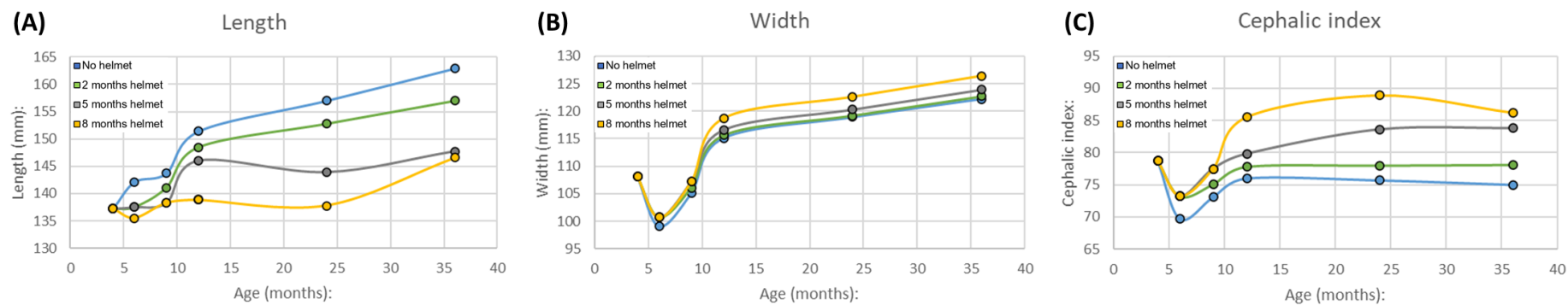
526

527

528 **Figure 2:** Simulated pattern of bone formation and skull shape with alternating durations of postoperative helmet treatment during  
 529 simulated growth. Red dashed boxes indicate the respective time points of helmet removal. Displaying sagittal and dorsal views.



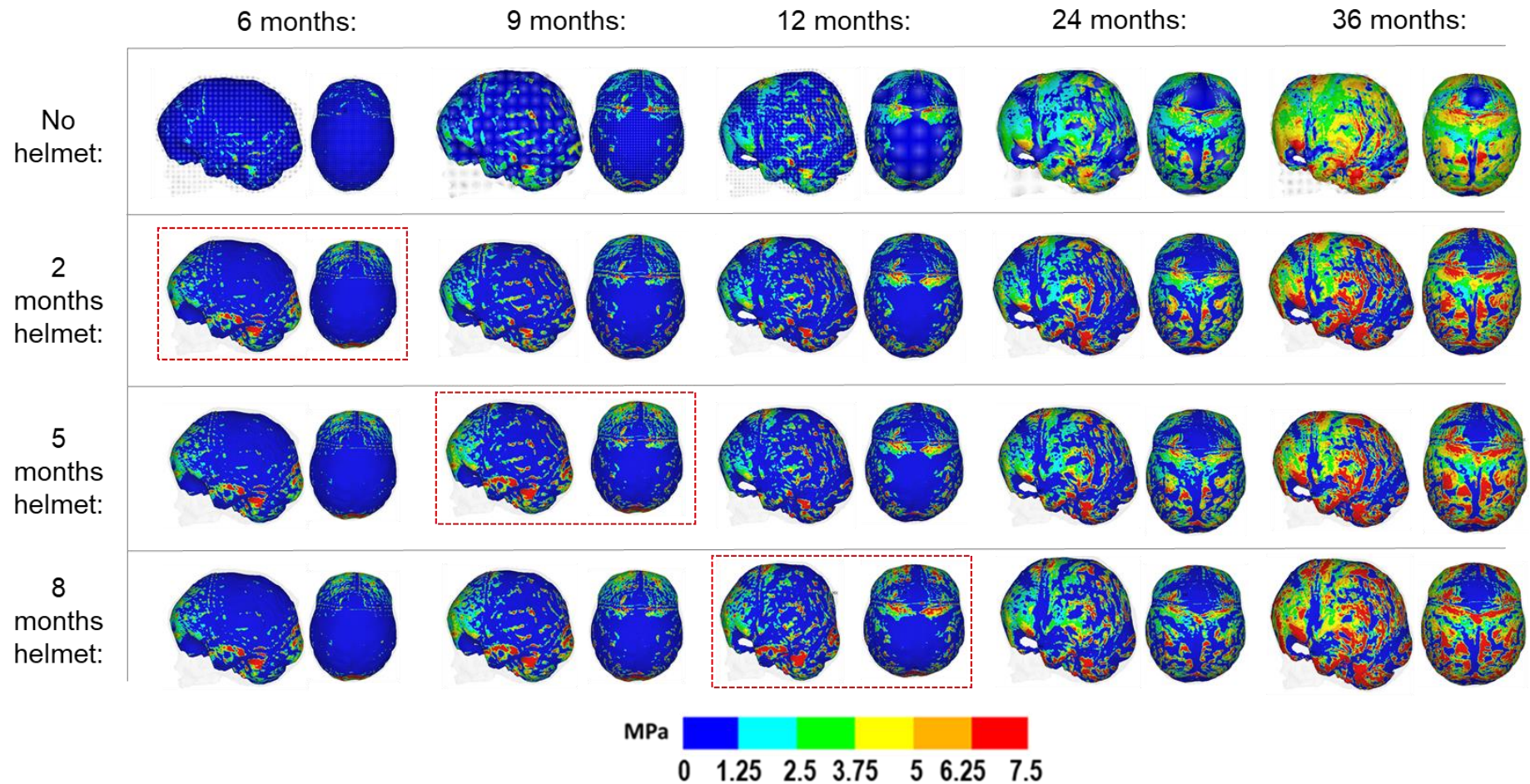
532 **Figure 3:** Cephalometric data of the simulated length (A), width (B), and cephalic index (C) from 4 months up to 36 months of age  
533 across alternating durations of postoperative helmet treatment.  
534  
535  
536



537  
538  
539  
540  
541  
542



543 **Figure 4:** Simulated pattern of contact pressure across the modelled ICV with alternating durations of post surgical helmet treatment  
 544 during simulated growth. Red dashed boxes indicate the respective time points of helmet removal. Displaying sagittal and dorsal  
 545 views.  
 546



548 **Tables**

549

550 **Table 1:** Quantitative data of all cephalometric data for all alternating helmet durations. Columns marked in grey indicate the  
 551 respective time points of helmet removal.

|                        |                 | 6 months: | 9 months: | 12 months: | 24 months: | 36 months: |
|------------------------|-----------------|-----------|-----------|------------|------------|------------|
| No<br>Helmet:          | Length (mm):    | 142.1     | 143.7     | 151.4      | 157.0      | 162.9      |
|                        | Width (mm):     | 99.1      | 105.1     | 115.1      | 118.9      | 122.2      |
|                        | Cephalic index: | 69.7      | 73.1      | 76.0       | 75.7       | 75.0       |
| 2<br>months<br>helmet: | Length (mm):    | 137.5     | 141.1     | 148.5      | 152.8      | 157        |
|                        | Width (mm):     | 100.7     | 106.1     | 115.6      | 119.2      | 122.7      |
|                        | Cephalic index: | 73.2      | 75.1      | 77.8       | 78         | 78.1       |
| 5<br>months<br>helmet: | Length (mm):    | 137.5     | 138.3     | 146        | 143.9      | 147.7      |
|                        | Width (mm):     | 100.7     | 107.2     | 116.6      | 120.3      | 123.9      |
|                        | Cephalic index: | 73.2      | 77.5      | 79.8       | 83.6       | 83.8       |
| 8<br>months<br>helmet: | Length (mm):    | 135.5     | 138.3     | 138.8      | 137.8      | 146.6      |
|                        | Width (mm):     | 100.7     | 107.2     | 118.7      | 122.6      | 126.4      |
|                        | Cephalic index: | 73.2      | 77.5      | 85.5       | 88.9       | 86.2       |

552

553

554

555

556

557

558 **Supplementary**

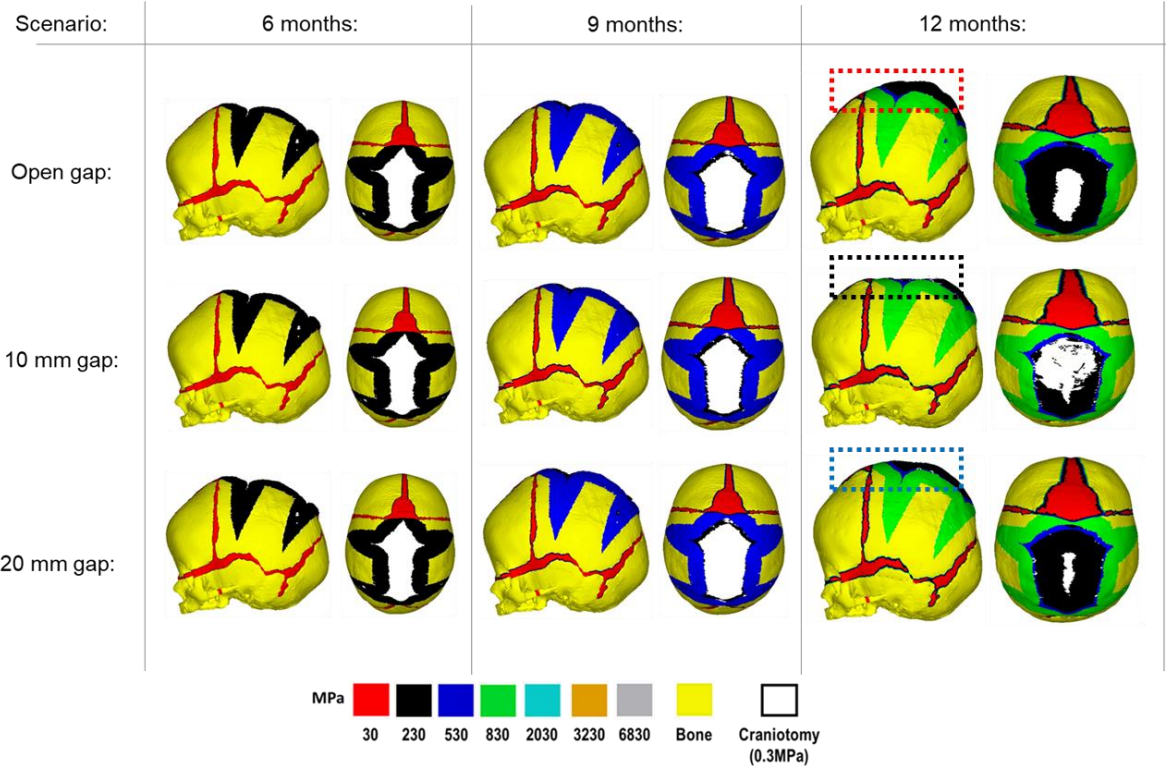
559

560 **Table S1:** A sensitivity study investigating the impacts on the morphology when altering the distance between the helmet strip and  
561 the modelled skull. The control scenario (i.e. Open gap) replicates the helmet constraints only across the anterior and posterior of the  
562 model. The first modelled helmet maintains the anterior and posterior constraints seen in the control, with a 10 mm displacement  
563 restriction applied to the dorsal growth of the model (i.e. 10 mm gap) before constraints are applied. The second modelled helmet  
564 carries over these parameters with the exception of increasing the allowable dorsal displacement (i.e. 20 mm gap). All scenarios  
565 underwent growth of the ICV from 4 months to 12 months of age. Results show the maximum dorsal height, measured from the  
566 foramen magnum to the most transverse dorsal point of the model.  
567

| Helmet: | Fig:  | Scenario: | Maximum dorsal height (mm): |           |           |            |
|---------|---|-----------|-----------------------------|-----------|-----------|------------|
|         |   |           | 4 months:                   | 6 months: | 9 months: | 12 months: |
| 1:      |    | Open gap  | 103.7                       | 108.9     | 117.8     | 130.5      |
| 2:      |   | 10 mm gap | 103.7                       | 108.2     | 113.6     | 114.7      |
| 3:      |  | 20 mm gap | 103.7                       | 108.2     | 117.8     | 123.9      |

568

569 **Figure S1:** The simulated pattern of bone formation captured across all sensitivity scenarios. All models presented incomplete  
 570 craniotomy healing by the 12 months of age mark. A greater level of dorsal bulging (red box) was seen in the 'open gap' scenario due  
 571 to the constraints applied to the anterior and posterior of the skull. Scenario '10 mm gap' predicts a severe flattening across the dorsal  
 572 (black box), accommodated by the greatest lack of calvarial healing. Caused by much of the skull reaching the allowable 10 mm gap  
 573 threshold. The '20 mm gap' parameter was used throughout all simulations in the main manuscript, as this addressed the dorsal  
 574 bulging and flattening (blue box) seen in the respective former scenarios.  
 575



576